IAEA-TECDOC-506

ATOMIC AND MOLECULAR DATA FOR RADIOTHERAPY

PROCEEDINGS OF AN ADVISORY GROUP MEETING
ORGANIZED BY THE
INTERNATIONAL ATOMIC ENERGY AGENCY
AND HELD IN VIENNA, 13–16 JUNE 1988

A TECHNICAL DOCUMENT ISSUED BY THE
INTERNATIONAL ATOMIC ENERGY AGENCY, VIENNA, 1989

The IAEA does not normally maintain stocks of reports in this series. However, microfiche copies of these reports can be obtained from

INIS Clearinghouse
International Atomic Energy Agency
Wagramerstrasse 5
P.O. Box 100
A-1400 Vienna, Austria

Orders should be accompanied by prepayment of Austrian Schillings 100,— in the form of a cheque or in the form of IAEA microfiche service coupons which may be ordered separately from the INIS Clearinghouse.

ATOMIC AND MOLECULAR DATA FOR RADIOTHERAPY
IAEA, VIENNA, 1989
IAEA-TECDOC-506
ISSN 1011–4289

Printed by the IAEA in Austria
May 1989

FOREWORD

Control of primary tumor remains one of the main challenges in cancer therapy and, in that respect, replacement of conventional X or γ rays by other types of radiation is a promising approach.

Responding to the development of accelerator therapy, the IAEA Nuclear Data Section has started a programme to tackle specific demands of physical data characterizing radiation interactions in atomic collision physics and in condensed-phase physics, typical for particle radiotherapy and clinical dosimetry. The required data include cross-sections for charged-particle interactions and basic radiation-physics quantities such as the stopping power and the ionization yield. The scientific expertise for performing compilation and evaluation of these data is available, though scattered in several groups throughout the world. However, those data are still fragmentary, discrepant and incomplete, even for a basic substance such as water. Furthermore, but for a few exceptional cases, the reliability of the available data has not been systematically evaluated.

In 1985 the IAEA Nuclear Data Section convened an Advisory Group Meeting on Nuclear and Atomic Data for Radiotherapy and related Radiobiology, at Rijswijk, the Netherlands. This meeting represents a milestone, since it reviewed for the first time the general needs for an improved understanding of the physical processes and data involved in radiotherapy and related radiobiology.

As a consequence of the Rijswijk meeting, the Agency has started a Coordinated Research Programme on Nuclear Data Needed for Neutron Therapy, and is currently contemplating to initiate a complementary Coordinated Research Programme on Atomic and Molecular Data Needed for Radiotherapy.

The atomic and molecular (A+M) data requirements for radiation research in general and radiotherapy in particular turned out to be much more complex than the nuclear data requirements. In fact, large sets of data or cross-sections for the interactions of photons, electrons, ions and other particles with atoms and molecules of human tissue elements are required.

It was therefore felt that, after the identification of the requirements at the Rijswijk meeting, a more thorough review of the status, availability and important gaps and deficiencies in A+M data for radiotherapy was needed, in order to focus the research under a potential future CRP to the most important outstanding problems in this field, complementary to the efforts under the CRP on nuclear data for neutron therapy. These considerations led IAEA/NDS to the proposal, endorsed by the INDC at its 16th Meeting in October 1987, to convene another Advisory Group Meeting devoted solely to review the atomic and molecular data needed for radiotherapy which was held in Vienna from 13 to 16 June 1988.

The meeting was convened with the objective to identify the important gaps and deficiencies in those atomic and molecular data which are most urgently needed specifically for radiotherapy and its human risk estimation. On the basis of this review the Agency sought specific advice from the participants on the scientific scope and programme of a planned new Coordinated Research Programme on Atomic and Molecular Data required for Radiotherapy.

The most important objectives of the meeting were to investigate the status, explore the availability, and identify the important gaps and

deficiencies in the atomic and molecular data most urgently needed for radiotherapy, with due account for data systematics and theoretical fittings. The following items as related to the atoms and molecules of human tissue were reviewed:

1. Cross sections differential in energy loss for electrons and other charged particles.
2. Secondary electron spectra, or differential ionization cross sections.
3. Total cross sections for ionization and excitation.
4. Subexcitation electrons (especially negative ion formation, thermalization, hydration of electrons etc).
5. Cross sections for charged-particle collisions in condensed matter.
6. Stopping power for low-energy electrons and ions.
7. Initial yields of atomic and molecular ions and their excited states and electron degradation spectra (for low-energy incident photons and electrons).
8. Rapid conversion of these initial ions and their excited states through thermal collisions with other atoms and molecules.
9. Track-structure quantities.
10. Other relevant data.

The meeting was chaired by M. Inokuti, USA, and H. Paretzke, Federal Republic of Germany. The presentation of review and contributed papers (18 and 1 post-meeting contribution) during the first half of the week was followed by the preparation of reports by the following three Working Groups:

Working Group A:	Scope of data needed: particles, energies and materials
Working Group B:	Cross sections for individual collision processes
Working Group C:	Data on consequences of multiple collisions

Dr. K. Okamoto of the Nuclear Data Section of the IAEA acted as scientific secretary for the Advisory Group Meeting. The Agency wishes to express its appreciation to Dr. M. Inokuti and Dr. H.G. Paretzke for acting as chairman and co-chairman and for preparing the summary and recommendations of the meeting.

EDITORIAL NOTE

CONTENTS

USE OF ATOMIC AND MOLECULAR DATA IN RADIATION THERAPY AND TRACK STRUCTURE ANALYSIS (Session I)

BASIC RADIATION PHYSICS QUANTITIES (Session II)

BACKGROUND INFORMATION (Session III)

INTRODUCTORY REMARKS*

M. INOKUTI *(Chairman)*
Argonne National Laboratory,
Argonne, Illinois,
United States of America

1. Introduction

The purpose of this meeting is to survey the current status of atomic and molecular data needed in radiation research and therapy and to identify areas appropriate for research in the near future. Although the general relevance of atomic and molecular data to radiation interactions with matter is widely understood, it is appropriate at the outset to consider needs for different atomic and molecular data that depend upon specific purposes.

In radiation therapy, the clinician must design methods of irradiation so that a desired dose may be delivered to a specified region of treatment, with a minimal dose delivered elsewhere. Here, a central problem is accurate dosimetry, which in turn hinges upon knowledge of certain basic physical data. Examples are stopping powers and total ionizations (W values) of human tissues and of materials used in dosimetry for various charged particles. The needs for improved data in this context are especially notable for low-energy ions resulting from neutron recoil, in view of the generally recognized difficulty of neutron dosimetry.

More generally in radiation research, one faces a more general and fundamental problem: What are the physical and chemical mechanisms leading to changes in matter caused by ionizing radiations? This problem not only is of great intellectual interest, but also is crucial to estimation of the risk from all radiations that are present in our environment. Some of these radiations come from natural sources and others from human activities such as nuclear-energy technology and use of radiations in industry and medicine.

---

*Work supported by the U.S. Department of Energy, Office of Health and Environmental Research, under Contract W-31-109-Eng-38.

Radiation doses relevant to the risk estimate are generally low, indeed much lower than those used in therapy. Biological effects at such very low doses are difficult to determine through direct observation. For this reason, the study of the mechanisms of radiation actions is especially important. When it is fully developed, knowledge of the mechanisms should permit us to predict low-dose effects generally and reliably.

The study of mechanisms necessarily requires a full description of physical and chemical processes that occur under radiation actions. Diverse atomic and molecular data are pertinent. Most of the obviously important topics have been identified in the program of this meeting. It is important to recognize that these topics are not at all independent of each other, but are in fact closely interrelated. For this reason, full communications among workers on different topics and in different places of the world are desirable and beneficial, and international collaborations among us are especially appropriate.

My views on technical aspects of our work were expressed at the Rijswijk meeting.[1] In what follows, I shall present several additional points.

2. Basic Physics and Data Physics

To clarify the special nature of the theme of the present meeting, it is appropriate to point out the sharp contrast between basic physics and what I call data physics. The meaning of basic physics is widely understood. It aims at elucidating principles of physics; the effective approach is to define an issue of some principle and to take data most crucial to the issue. A basic physicist, studying atomic collisions, may wish to determine the nature of a resonance or the threshold behavior of a specific cross section, for instance. In either theory or experiment, he focuses his efforts on specific ranges of variables such as the incident energy, the energy loss, or the scattering angle, and generates data most pertinent to the issue. Most often, the absolute value of a cross section is irrelevant. Indeed, in the

overwhelming majority of publications, cross-section values are presented over a narrow energy range and on a relative scale; sometimes a quantity such as the derivative of a cross section with respect to the incident energy is given.

Users of cross-section data in radiation research or other applications have different requirements. Almost all applications of the cross-section data require that the data be right, absolute, and comprehensive. Note the meanings of the three adjectives. The term "right" has been deliberately chosen in preference to "precise" or even "accurate." The idea is that the cross-section values for important processes must be roughly right, i.e., correct to the first significant figure. The meaning of "absolute" is obvious; it is the opposite of "relative." The term "comprehensive" concerns a wide range of variables such as the incident energy. I call these three the trinity of requirements for cross-section data.

It is a special challenge to meet these requirements. This challenge is shared by a considerable number of physicists who work on data physics. Perhaps the best recognized of them deal with fundamental physical constants.[2] Others write articles for handbooks and encyclopedias. All of these data physicists work hard to provide physical data for users in applications that include other branches of science such as chemistry, biology, and astronomy, as well as certain subfields of engineering, industry, and medicine.

3. Technical Issues

I suggest the following points for consideration at the present meeting, and throughout the planned research program.

First, the scope of study should be well considered. To be specific, the scope will be defined in terms of the kinds of data we consider and the materials we treat. There will be a general consensus that, for instance, cross sections for the interactions of electrons with molecules are relevant

to radiation research. However, opinions may differ as to which electron energies are most important, which specific processes, and which specific molecules.

Second, we shall survey data within the scope of study. The survey begins with collection of data in the literature, but the crucial part of the work is the critical evaluation of data reliability. For this purpose, one must apply a full knowledge of physics, both experimental and theoretical, and use the best judgement. Critical examination of experimental methods used to obtain data is extremely important. A classic example of such an undertaking is in the work by Kieffer and Dunn,[3] who examined cross sections for the ionization of atoms and molecules by electron collisions. At the same time, one should apply all the theoretical criteria to test the correctness of data. A related use of theory concerns the determination of analytical expressions suitable for data fitting, which is necessary for efficient storage of information as well as for the interpolation and extrapolation that are often necessary in applications. (Technical aspects of this topic were discussed earlier.[1])

Third, the critical evaluation of data reliability is not only necessary in the report of a survey, but is often extremely fruitful. Such evaluation naturally leads to the identification of topics for new research. When one finds that certain kinds of data are missing, one should consider the feasibility of their acquisition from either experiment or theory. Sometimes it will be appropriate to develop new concepts in theory for data testing or for data fitting.

Fourth, in the critical evaluation of data it is always important not only to do the best possible in the light of current knowledge but also to admit our ignorance candidly. Unless we firmly maintain professional integrity in this sense, our product will be of little value. The following two quotations from East and West are pertinent to this point.

To know one's ignorance is the best part of knowledge.

- Lao-Tsze, The Simple Way

I know nothing except the fact of my ignorance.

- Socrates, Diogenes Laertius

Finally, we should consider the appropriateness of modes of data dissemination. Presentation of data in tables and graphs has long been familiar to all scientists, and remains effective so long as the quantity and the variety of data are modest. However, newer ways of presenting data have risen with the wide use of computers. A large volume of data now may be stored in computer-readable forms such as disks and tapes, and may thus be accessible as a part of data bank. An example within the scope of our work is the data on secondary electrons resulting from ionizing collisions of a charged particle with a molecule. Here many variables are involved, e.g., the incident particle energy, the secondary-electron energy, and the angle of ejection, all of which are continuous. To present the cross-section data in a straightforward way and in full detail, one needs a three-dimensional array of figures. (One way to deal with this kind of data is to devise a suitable method of data fitting by an analytic expression, which should have a firm theoretical basis.) Once the data are accessible as part of a data bank, they are most conveniently available to a wide community of users through the tapes, disks, and computer networks that are now rapidly expanding.

4. Merits of Data Physics as a Topic of International Endeavor

The theme of the present meeting is a topic eminently suitable for international collaboration for the following reasons.

Studies on atomic and molecular data are examples of good small science, i.e., important areas for suitable study in countries with limited monetary resources. Yet, the studies are intellectually demanding and therefore provide excellent educational and training opportunities. In experimental studies of atomic and molecular data, one must have some background in many

subfields of physics and chemistry, such as electromagnetism, vacuum techniques, and surface science. In theoretical studies, one must have some background in scattering theory, atomic and molecular spectroscopy, and kinetic theory. Finally, the goal of the whole endeavor is clearly important to the need of all humans to learn how to use and live with ionizing radiations, which are and will remain an important element in life for years to come.

REFERENCES

1. M. Inokuti, Cross Sections for Inelastic Collisions of Fast Charged Particles with Atoms and Molecules, in Nuclear and Atomic Data for Radiotherapy and Related Radiobiology. Proceedings of an Advisory Group Meeting on Nuclear and Atomic Data for Radiotherapy and Related Radiobiology, organized by the International Atomic Energy Agency in cooperation with the Radiobiological Institute TNO and held in Rijswick, Netherlands, 16-20 September 1985. (International Atomic Energy Agency, Vienna, 1987) pp. 357-365.
2. E. R. Cohen and B. N. Taylor, Rev. Mod. Phys. 59, 1121 (1987).
3. L. J. Kieffer and G. H. Dunn, Rev. Mod. Phys. 38, 1 (1966).

SUMMARY OF THE MEETING

M. INOKUTI *(Chairman)*
Argonne National Laboratory,
Argonne, Illinois,
United States of America

The meeting, which was held in the IAEA headquarters on 13-16 July 1988, followed the customary format of earlier Advisory Group Meetings. On the first two days, prepared scientific papers were presented. These papers dealt with a wide range of topics, including virtually all the important issues within the theme of the meeting. The topics included (1) the uses of atomic and molecular data in radiation therapy and in track-structure analysis, (2) the current status of radiological and dosimetric data such as stopping powers and ionization yields for various radiations, and (3) a review of cross sections for individual elementary processes involved in radiation actions.

On the last two days, informal and extensive discussions were conducted concerning the needs of atomic and molecular data, for basic radiation research generally and for radiation therapy specifically. The general aims were to review the current status of knowledge, to recommend areas suitable for standard data compilation, and to identify urgent problems for new scientific studies. Three working groups treated different but closely related topics.

Full texts of the scientific papers and the reports of the three working groups are included in the present volume. Therefore, the following summary is brief and nontechnical.

Throughout the discussion there was a clear consensus that a large variety of atomic and molecular data should be compiled, critically evaluated for reliability, and then disseminated to the public. Such an enterprise will make a crucial contribution to the improvement of radiation therapy, as well as to the elucidation of health effects of ionizing radiations as a basis of radiation risk assessment in the nuclear energy industry, as well as in

medicine and other industries. Consensus was also developed for the types of atomic and molecular data that are most urgently needed. The needed data were defined in terms of two specifications, viz., first, particles and their energies, and second, materials of interest to radiation therapy.

Consequently, it is recommended that a coordinated research program be established by IAEA as soon as possible to foster compilation, critical assessment, and dissemination of atomic and molecular data needed in radiation therapy and related radiation research. The recommended program will produce a standard set of data that will be useful to those working on radiation therapy as well as on its scientific basis. The program will also provide its participants and colleagues an opportunity for reviewing results of current studies and for identifying appropriate areas of future research. Finally, the suitability of the program as an IAEA activity is clear in view of the importance of radiation therapy as an application of atomic energy research, and also in view of close scientific connections with other IAEA activities such as those on nuclear data needed in radiation therapy and on atomic and molecular data needed for fusion research.

The scientific level of the discussion was extremely high; indeed, some of the scientific papers included not only reviews of the current status of a subfield of research but also new data and hitherto unpublished ideas. As a consequence, the recommendations of the working groups are scientifically sound. This is the best result of the meeting.

On behalf of all the participants, I thank Dr. Okamoto, Dr. Schmidt, and others of the IAEA for all the efforts in hosting the meeting. We all learned much in our fields of science and renewed our conviction of the importance of these fields to human and societal needs.

Working Group A

SCOPE OF DATA NEEDED: PARTICLES, ENERGIES AND MATERIALS

Summary and Recommendations

Group Leader: **A. Wambersie** (Belgium)

Members: **P. Bauer** (Austria)
N. Getoff (Austria)
P. Olko (Federal Republic of Germany)
J.J. Schmidt (IAEA)

INTRODUCTION

Control of primary tumor remains one of the main challenges in cancer therapy and, in that respect, replacement of conventional x or γ rays by other types of radiation is a promising approach.

Some of the new beams, typically high-energy protons or helim ions, improve the physical selectivity of the irradiations. These low-LET (linear energy transfer) beams produce bilogical effects that are not very different from those produced by photons. Other types of beams have been introduced in therapy aim at improving the differential effect between tumors and normal tissues. These other beams consist primarily of high-LET radiations, most usually fast neutrons. In addition, some heavy-ion therapy programs have been initiated.

In the present document, boron neutron capture therapy is not considered. Although much information has become available during the last few years (especially concerning synthesis of new boronated compounds), this technique is too different from the conventional beam therapy to be discussed here.

Likewise, pion therapy is not considered in the present document. However, data for some of the secondary particles in pion nuclear reactions (e.g. n,α) will be treated here.

BEAM THERAPY

Proton Beams

The clinical benefit resulting from the better selectivity of the proton beams compared to photons, became evident first for radioresistant tumors located close to critical normal radiosensitive structures. Among them, uveal melamona is the most current type of tumor treated with proton beams (more than 3000 patients have been treated to date). Chordomas and chondrosarcomas of the base of the skull, as well as paraspinal tumors and arteriovenous malformations (AVM), also are good indications for proton beams, and take full advantage of their high selectivity.

However, more recently, some proton beam therapy programs aim at treating a larger proportion of tumors, even deep-seated ones. For example, the LOMA-LINDA program with four treatment rooms, connected to a 250-MeV synchrotron, will have a capacity in 1989 to treat about 1000 patients a year.

Table 1 lists the proton therapy programs, both current and planned. This list is likely to increase in the near future. By the end of 1987, more than 6000 patients had been treated by proton beams in nine centers throughout the world (i.e., Harvard 4139, Moscow 1359, SIN-Switzerland 262).

A proton energy of about 70 MeV is sufficient for proton beam therapy of uveal melanoma. For deep-seated tumors, an energy up to 250 MeV is necessary.

Fast-Neutron Beams

Fast-neutron therapy is being developed in several countries, and the amount of clinical information available is increasing steadily.

High-energy, hospital-based cyclotrons now allow therapy with physical selectivity similar to that currently achieved with modern electron linear accelerators, as far as beam penetration, collimation, beam arrangement, and positioning, are concerned. With these cyclotrons,

the role of fast neutrons in cancer therapy can be fully assessed, and the previous handicaps related to the poor dose distributions with low-energy neutron sources are being progressively eliminated.

Table 2 presents some characteristics of the neutron facilities used for patient treatment. More than 15,000 patients have been treated so far with fast neutrons, either by neutron irradiation only or in combination with other treatments. In some centers, the follow-up period now exceeds seventeen years.

The superiority of fast neutron therapy over conventional therapy is now established for some types and sites of tumors such as locally extended salivary gland tumors and prostatic adenocarsinomas or slowly growing sarcomas. For other tumors, the superiority of fast neutrons has not yet been universally recognized; further studies, conducted under strict statistical and dosimetric conditions, are needed to identify the indications and contra-indications of neutrons.

From the current data, it can be concluded that 10-20% of the radiotherapy patients could be better treated with high-LET radiation. This conclusion implies that ideally a ratio of one high-LET machine to ten low-LET machine is needed for therapy centers.

Selection of the patients for high- vs. low-LET irradiation remains a major problem, and much effort is being directed toward the development of individual prediction tests.

To obtain neutron beams suitable for therapy, the energy of the incident particles should be at least about 40-50 MeV for deuterons (to induce d+Be reactions) and about 35-45 MeV for protons (to induce p+Be reactions). Today at three facilities neutrons produced by 65 MeV proton on Beryllium [p(65)+Be] are used. Consequently, atomic and molecular data are required for those deuterons and protons, and for all secondary particles generated by them.

Heavy-Ion Beams

Heavy-ion beams combine a high physical selectivity (similar to that of a proton beams) and the radiobiological properties of high-LET

Table 1. The Proton Therapy Facilities World-Wide

Location	First treatment	Number of patients treated	REMARKS (Date at which the number of patients was reported)
Berkely, CA, USA[a]	1955	30	closed 1957
Uppsala, Sweden	1957	73	closed 1976; the cyclotron is being rebuilt
Harvard, MA, USA	1961	4139	(Dec. 1987)
Moscow, USSR	1965	1359	(Oct. 1987)
Dubna, USSR	1967	80	(1977)
Gatchina, USSR	1975	457	(Oct. 1987)
Chiba, Japan	1979	≃ 30	closed 1986
Tsukuba, Japan	1983	67	(1987)
PSI/SIN, Switzerland[b]	1984	429	(May 1988)

Proton therapy facilities in preparation:

Loma-Linda, CA, USA	Synchrotron under construction
Clatterbridge, UK[c]	Proton beam line under construction
Louvain-La-Neuve, Belgium[d]	"
Orsay, France	Proton beam line being tested
N.A.C., South Africa	200 MeV proton beam line in preparation
PSI/SIN, Switzerland	250 MeV proton machine in preparation

(a) He ions used from 1957, closed Dec. 1986, 1297 patients treated.

(b) At present Paul Scherrer Institute; formerly Swiss Institute for Nuclear Research. Protons are used for the treatment of uveal melanoma ("OPTIS program").

(c) A 62 MeV proton beam line on a cyclotron used for routine fast neutron.

(d) A 90 MeV proton beam line on a cyclotron used for routine fast neutron therapy.

Table 2. Characteristics of the fast neutron therapy facilities in the world.

Summary of relevant data, including depth dose characteristics and penumbra width, for a field size of approximately 10 cm x 10cm (From ICRU Clinical Neutron Dosimetry Part I, in press).

Facility	Reaction	SSD (cm)	Z_{50}* (cm)	P_{20}^{80}** (cm)
Chicago	d(8.0)+D	100	9.8	2.2
Hamburg	d(0.5)+T	80	8.8	2.4
Heidelberg	d(0.2)+T	100	10.6	2.7
Münster	d(0.2)+T	100	10.5	2.7
Krakow	d(12.5)+Be	91	7.7	2.0
Dresden	d(13.5)+Be	100	7.9	2.3
Tokyo	d(14.0)+Be	125	8.3	2.3
Essen	d(14.3)+Be	125	8.1	2.4
Ghent	d(14.5)+Be	125	8.7	2.6
Edinburgh	d(15)+be	125	8.9	2.3
Hammersmith	d(16)+Be	117	8.7	2.2
Pretoria	d(16)+Be	135	8.6	2.1
Chiba-shi	d(30)+be	175	11.7	1.7
Riyadh	p(26)+Be	125	10.3	2.4
Orléans	p(34)+be	169	12.8	1.9
Houston	p(42)+Be	125	14.0	2.0
Cleveland	p(43)+Be	125	13.5	2.2
UCLA	p(46)+Be	150	13.1	1.7
Seattle	p(50)+be	150	14.8	1.4
Clatterbridge	p(62)+Be	150	16.2	1.6
Louvain	p(65)+Be	162.5	17.6	1.7
Fermilab	p(66)+Be	190	16.6	2.0
	^{60}CO gamma rays	80	11.6	1.6
	8 MV x rays	100	17.1	0.8

* Depth in water at which the total (n+γ) absorbed dose is reduced to half its maximum value.

** Distance off-axis between 80% and 20% of the central axis total - (n+γ) absorbed dose at a depth of 10 cm in the phantom.

radiations (which are proven to be superior for some well-defined groups of patients). However, the technical complexity and the cost of the installation will limit the development of heavy-ion therapy. Future development of technology could help to solve this problem.

The only clinical data at present available are those from the BEVALAC in Berkeley where about 100 patients were treated with Ne ions. The best results were obtained for the same localizations (e.g. salivary gland, prostate, and sarcomas) as with fast neutrons. Several other heavy-ion therapy programs are in preparation or planned: Berkeley (i.e. continuation of the present program), Chiba (Japan), Darmstadt (FRG), and EULIMA (Oakland).

The energies required to obtain a sufficient beam penetration are typically:

- for carbon ions: 400 MeV/amu
- for neon ions: 620 MeV/amu
- for argon ions: 860 MeV/amu.

Required accuracy

For photon therapy, a dose accuracy of better than ±5% and possibly as high as ±3-5% is required. This requirement is due to the steepness of the dose-effect relations for local tumor control and normal-tissue complications. For fast neutrons all the available clinical or radiological data indicate that these dose-effect relations are as steep as those observed for photons, and that consequently at least the same degree of accuracy has to be achieved.

Furthermore, because of a reduced differential effect at high LETs, high physical selectivity (i.e., sufficient beam penetration, efficient collimation system, accurate potioning, and others) is also required.

Materials of interest as target and kinds of data needed:

The materials of interest fal into three categories: (1) the elements and constituents of the human tissues, (2) materials of detectors and dosimeters, and (3) other materials used to shape and guide the beam.

For the ions used as projectiles, the first quantity of interest is the stopping power from the impinging energy down to zero. If fast neutrons are used for irradition, the interactions with the atomic nuclei of the tissues yield energetic recoil nuclei. For these recoils, the stopping powers have to be known. It is difficult to measure stopping powers of real tissue materials; therefore, it has been customary to estimate it from data on constituent atoms and in gas phase. To assess the accuracy of such estimates, it is important to, study first the influence of the chemical binding on the stopping cross section. Second, the electronic structure of an ion penetrating a solid generally differs from that of the solid material. In addition, physical interactions are different: for instance, charge-changing collisions, which contribute to the stopping process, occur with different probabilities; consequently, the mean number of electrons bound to the projectile can be different.

Thus, the influence of the chemical bond and of the projectile charge on the stopping power has to be known. This information is important because highly precise knowledge of the stopping power is needed in order to shape the delivered dose in such a way that the tumor is exposed to a high dose but the healthy tissue around it is spared to the maximum extent possible. This precise information is especially needed for the heavy ion and neutron fluxes where the high LET tends to diminish differences between the radiosensitivity of tumore cells and normal cells. The energy-loss data are also needed for compound materials, i.e., separate data are needed for different tissues and bones.

Electron emission data are needed for two purposes. First, the liberated electrons are the source of the charge that is collected in the dosimeters and detectors used for the delivery and monitoring of the dose. For dosimetry, two groups of materials are of particular interest: (1) solids, which constitute chamber or counter walls, and (2) gases filling these detectors. Several sets of data are required: stopping powers, gas-to-wall conversion factors, and rates of recombination of charge carriers in gases. Commonly used wall materials such as aluminum, A-150 and other plastics, as well as tissue-substitute gas mixtures (methane- and propane-based) should be studied in the entire energy range of ions and neutrons. The energy spectra of charged particles, produced in the wall and gas materials, are important for the interpretation of the detector signals and should be assessed by calculations and measurements, e.g. with low-pressure proportional counters.

Second, the electrons cause most of the chemical and biological damage inside the human body. In order to maximize the killing of cells in the tumor and to minimize the effects on the healthy tissue, it is necessary to understand how the biological effectiveness (BE) of a radiation field depends on the local density and energy spectra of the electrons produced in the target. It has been shown that for neutrons of different energies the BE can vary greatly because of different energy spectra of recoil nuclei, which act like heavy-ion radiation.

For protons and heavier ions, very complicated behavior of the BE as a function of the LET has also been observed. For heavy ions produced as neutron recoils or as primary radiation from an accelerator, the distribution of the emitted electrons in space and time needs to be determined with high precision. Necessary information includes a description of particle tracks formed by the primary events, i.e. primary excitations and the electron emission and the development of tracks by collisions of these electrons with other target molecules inside the biological cell. To understand the biological action of these electrons, the electron interactions with biomolecules such as DNA, proteins, water, and nuclear membranes should also be studied extensively. Although the repair process is of biochemical and biological nature (and thus beyond the scope of the present discussion), the induction of breaks, i.e., the disruption of chemical bonds in DNA by the electron impact, is clearly a physico-chemical problem, which should be treated in context. Only if one knows the dependence of the induction of severe biological damages, e.g. of double-strand breaks, on track structure, can one fully understand the variation in BE for different radiations.

Working Group B

CROSS-SECTIONS FOR INDIVIDUAL COLLISION PROCESSES

Summary and Recommendations

Group Leader: **L.H. Toburen** (United States of America)

Members: **Y. Hatano** (Japan)
Z. Herman (Czechoslovakia)
T.D. Märk (Austria)
S. Trajmar (United States of America)
J.J. Smith (IAEA)

INTRODUCTION

As mentioned earlier, for optimizing the effects of radiation on tumor cells and minimizing the effects on healthy tissue, as well as for adequate dosimetry in radiation therapy, a wide range of atomic and molecular data are needed. These data are used in appropriate models to assess physical and dosimetric quantities for evaluating probabilities of cell survival and killing under radiation therapy treatment conditions.

Cross sections for the interactions (e.g., excitation, ionization, charge transfer) for primary and recoil ions are needed in various atomic, molecular, and condensed-phase materials. Additional data are needed for the subsequent interactions of secondary electrons and photons in the absorbing medium, and ultimately, detailed information is needed on the interactions of ions, excited states, and dissociation products in transferring excitation energy to biomolecules. Atomic and molecular data concerning gaseous H_2O, H_2, O_2, N_2, CO, CO_2, CH_4, and larger hydrocarbons are needed for understanding the fundamental processes of energy deposition in biological cells and energy transfer in gases used in dosimetry.

Data on the interactions of ions and electrons with macromolecules (such as DNA and proteins) and their constituents are needed for the understanding of damages in cells. In order to apply our better knowledge of atomic and molecular data in gases to those in tissue, further information is required for interactions of charged particles and photons in condensed phases, including data for molecular clusters, liquids, and solids. The study of interaction cross sections for

molecular clusters is considered particularly important for providing guidance on the application and modification of gas-phase data to tissue conditions relevant to radiation biology and radition therapy. In order to improve the dosimetry of charged particles and neutrons, data are also needed on the ranges and stopping powers of charged particles in the wall materials of dosimeters.

IONIZATION CROSS SECTIONS FOR FAST IONS

A primary mechanism for energy loss by fast charged particles is ionization of the atomic and molecular constitutents of the medium. Knowledge of the cross sections for the production of secondary electrons of given kinetic energy ε and emission angle θ is fundamental in that these cross sections are indispensable for the analysis of further processes of excitation and ionization by secondary electrons.

There has been a good deal of work on the measurement of secondary-electron spectra (differential in electron emission energy and angle) for bare ions such as protons, alpha particles, and electrons. There are few data, however, for heavy ions that carry bound electrons. Collision of those heavy ions are the most difficult to treat theoretically. Electron spectra arising from multiply ionized targets are only beginning to be obtained.

Since electron emission is the most important initial stage for absorption of energy by the medium, it is crucial that data on this process be reviewed and critically evaluated; additional data also need to be generated. Badly needed data include those for heavier ions, as well as carbon and oxygen ions of a few keV to a few MeV, which are particularly important in neutron dosimetry. Heavier and faster ions should be studied also for the interpretation of radiation biology experiments, now being carried out at Darmstadt, Federal Republic of Germany and Berkeley, U.S.A.

DOUBLE DIFFERENTIAL CROSS SECTIONS: AVAILABILITY AND NEEDS

Electron impact

Data on electron-impact double-differential cross sections are available for a wide range of atoms and simple molecules. Several laboratories have been involved in such studies including Joint Institute for Laboratory Astrophysics (JILA, University of Colorado), University of Nebraska, Indiana University, University of Michigan, and Tokyo Institute of Technology. There is need for review and critical evaluation of these data before they can be used in track-structure calculations. It is also recommended that new studies be initiated on more complex molecular targets such as larger hydrocarbons and biomolecules.

Proton impact

Considerable data have been accumulated on proton-impact ionization of simple gases. Energy ranges from a few keV to several MeV have been investigated and theoretical methods have been developed to extrapolate data to much higher energies, i.e., hundreds of MeV, which are relevant to radiation therapy. These data have been provided by several laboratories including Pacific Northwest Laboratory, University of Nebraska, Hahn-Meitner Institut, and Tokyo Institute of Technology. These data should be critically evaluated and made widely available in a computer-readable form. Efforts toward this end are particularly important because of the large quantity of the data and to the need of the data in track-structure analysis.

Heavy ions and neutral particles

Only limited data are available for neutral-particle impact, and these data are for particles at very low energies, i.e., lower than a few hundred keV. There are virtually no data available for fast heavy ions. In view of the inadequacy of present theoretical techniques for heavy ions that carry bound electrons, it is recommended that emphasis be placed on experimental studies in this topic in general, and especially on the interactions of heavy ions with H_2O and hydrocarbon molecules.

CHARGE-TRANSFER CROSS SECTION

Considerable data are available on charge transfer between light ions such as H^+ and He^+ with simple atoms and molecules. These data have been reviewed by the fusion-research community in many publications including the Oak Ridge National Laboratory compendia,[1-3] compilations by the Institute of Plasma Physics, Nagoya,[4] by Japan Atomic Energy Research Institute (JAERI),[5] and by the Joint Institute for Laboratory Astrophysics.[6] The data base on charge-transfer reactions of H^+, C^{q+}, O^{q+}, where q = 1 - 6, CO^+, and Fe^{q+} with C, O, O_2, CO, and lower hydrocarbons has also been reviewed by Janev et al.[7] For heavier ions, data are widely scattered and often fragmentary. It is recommended that an effort be devoted to an extensive survey of the literature and to a compilation of all the available cross section data for fast heavy ions.

TOTAL IONIZATION CROSS SECTIONS

Considerable data are available on the total ionization cross sections for electron and proton impact. The proton-impact ionization cross sections have recently been reviewed by Rudd et al.[8] Electron-impact ionization has been the subject of several data base reviews, primarily by the fusion energy research community. Data on ionization processes, including total and partial cross sections, have been reviewed, and recommended data have been given for atoms and ions along with numerical fits for H through O by Bell et al.,[9] F through Ni and C through U by Lennon et al.[10] Similar data for molecules, including partial and dissociative ionization cross sections, have been reviewed for diatomic molecules (H_2O, O_2, N_2, CO, and NO) and polyatomic (H_2O, CO_2, NO_2, CH_4) molecules, for energies below 500 eV, by Lennon et al.[11] In addition, data for CH_n (n = 2 - 4) have been reviewed by Ehrhardt and Langer.[12]

ELECTRON- AND ION-INDUCED EXCITATION AND DISSOCIATION

Considerable data are available on electron-impact excitation and dissociation of atoms and simple molecules relevant to fusion. Data have been compiled on electron-impact excitation and dissociation of CO, O_2, CO_2, H_2O, and CH_n (n = 2 - 4), for energies from 5-500 eV, by Janev et al.[7] Data on C, N, O, Al, and Fe atoms and ions excited by

Table 3. Summary of Data Currently Available

Material	Reactions	Energy range
H_2O, CO, CO_2, CH_4 He, Ne, Ar	Electron-impact double-differential ionization cross sections	100 - 500 eV
H_2O, CH_4, CH_3NH_2 $(CH_3)_2NH_2$, C_2H_2, C_2H_4, C_2H_6, He, Ne, Ar, TeF_6, SF_6	Proton-impact double-differential ionization cross sections	300 - 2000 keV
H_2O, Ar, He	He^{2+} and He^{+} impact double-differential ionization cross sections	300 - 2000 keV
	H^{o} impact double-differential ionization cross sections	
C, O, O_2, CO CH_n (n = 2 - 4)	Charge transfer for H^{+}, He^{n+}, C^{8+}, O^{8+}, CO_{+}	keV - MeV
CO, CO_2, H_2O, CH_n (n = 2 - 4)	Electron-impact excitation and dissociation	
H through U atoms H_2, O_2, N_2, CO, NO H_2O, CO_2, NO_2, CH_4	Electron-impact total ionization	

electrons have been reviewed by Janev and Katsonis.[13] Very little data exist for comparable studies of proton or other ion impact. Such studies should be encouraged.

SUMMARY: Table 3 presents a summary of currently available data.
Table 4 presents a summary of data needed.

ELECTRON COLLISON PROCESSES

Interactions of any radiation (e.g., neutrons, charged particles, high-energy photons) with matter eventually generate electrons with energies ranging from thermal to very high. A large fraction of the primary energy is thus converted to electron kinetic energy. The interactions of these electrons with matter are fundamental to the processes leading to radiation damage.

Table 4. Summary of Data Needed

Material	Reactions	Energy range
H_2O, CH_4, N_2, CO, CO_2, C_3H_8 macromolecules, clusters	Double-differential ionization cross sections C^{n+}, O^{n+}, N^{n+} (n=1-5)	1 keV - 10 MeV
	C^{n+}, Ge^{n+}, Fe^{n+}, U^{n+} (n equal to the corresponding equilibrium value)	1 MeV/u - 1000 MeV/u
H_2O, CH_4, N_2 CO, CO_2, C_3H_8 macromolecules, clusters	Total ionization cross sections C^{n+}, O^{n+}, N^{n+} (n = 1 - 5)	1 keV - 10 MeV
H_2O, CH_4, N_2 CO_2, C_3H_8 macromolecules	Charge transfer cross sections C^{n+}, O^{n+}, N^{n+}	1 kev - 10 MeV
Cn-hydrocarbons n = 7 - 20	Photoionization and photoabsorption	Threshold to 10keV
N-containing molecules	"	
S-containing molecules	"	
Polymers, DNA, proteins ice, clusters, liquid H_2O	"	
Water clusters - H_2O ions and ion fragments	Ion-cluster interactions	0 - 10 eV

At high impact energies (i.e., at energies far exceeding the ionization threshold) cross-section data are readily available or can be calculated reliably for simpler targets. Also, the energy-loss distribution for high impact energies is more similar for gas-phase and condensed-phase targets than it is for low impact energies. At low impact energies, cross sections are generally more difficult to measure or to calculate. Also, there are often significant differences in the energy-loss distribution between the gas and condensed phases.

The most effective way to generate consistent sets of cross sections for the many processes and species required in radiotherapy seems to be a coordinated experimental and theoretical approach.

To characterize electron interactions, the following kinds of data are needed:

- Total scattering cross sections
- Elastic scattering cross sections
- Excitation cross sections
- Dissociation cross sections
- Electron attachment cross sections
- Total, partial, and differential ionization cross sections

Gas Phases

For some of the gases species of interest in radiotherapy, the cross sections are available (see Table 5 and quoted compilations). For other gases, the cross sections are not known at all or known only roughly (See Table 6).

Clusters

From the point of view of radiotherapy, condensed phase is the primary medium. Direct studies on electron collisiions at low energies in this phase have been sparse. Other recent developments paved the way for bridging the gap between gas and condensed phase; it became feasible to study electron collisions with clusters ranging from dimers to those containing millions of monomeric species. Since this is a new field, very little information is presently available. Work in this direction should be encouraged so that the general trends in the movement from gas to condensed phase can be established.

Condensed phase

An important recent development is the application of electron-beam scattering techniques (developed for gas-phase studies) to condensed targets. The feasibility of such studies has been demonstrated, most notably at University of Sherbrook, Canada. Current results show that, in addition to scattering by single centers, the excitation of intermolecular and collective modes, coherent and incoherent multiple

Table 5. Data Available On Electron Collision Processes[a]

Process	Species	Energy range[b]
Gas phase:		
Total scattering	H_2, N_2, O_2, H_2O, CO_2, CH_4, Ar	1 - 1000 eV
Elastic scattering	H_2, N_2, O_2, H_2O, CO_2, CH_4, Ar	1 - 1000
Excitation	H_2, N_2, O_2, Ar	Threshold-100
Dissociation	H_2, N_2, O_2, H_2O, CO_2, CH_4, Ar	Threshold-100
Attachment	H_2, N_2, O_2, H_2O, CO_2, CH_4, C_3H_8	Threshold-100
Total ionization	H_2, N_2, O_2, H_2O, CO_2, CH_4, Ar	Threshold-100
Partial ionization	H_2, H_2O, CO_2, CH_4	Threshold-100
Differential ionization	H_2, N_2, O_2, H_2O, CO_2, CH_4, Ar	Threshold-100
Condensed phase:		
Total scattering	solid H_2O	1 - 20
Elastic scattering	solid H_2O	1 - 18
Vibration excitation	solid H_2O	1 - 18
Electronic excitation	solid H_2O	1 - 18

a Data on any of the molecules are not complete, and are often fragmentary.

b The given energy range merely indicates a general idea. A precise energy range differs for each molecule.

Table 6. Data Needed On Electron Collision Processes[a]

Process	Species	Energy range[b]
Gas phase:		
Total scattering	C_3H8	1 - 1000 eV
Excitation	H_2O, CH_4, CO_2, C_3H_8	Threshold-1000
Dissociation	C_3H_8	Threshold-1000
Total ionization	C_3H_8	Threshold-10000
Partial ionization	N_2, O_2, C_3H_8	Threshold-10000
Differential ionization	C_3H_8	Threshold-10000
Condensed phase:		
Data required for all target species for all processes mentioned.		

a There are some data available on the molecules cited, but are in general incomplete or unreliable.

b The given energy range merely indicates a general idea. A precise energy range depends on specific applications.

scattering, and distortion of the gas phase species are important. Further work in this area should be encouraged.

Representative sources of data

Gas phase

See Refs. 14-18.

Clusters

See Refs. 19-20.

Condensed phase

See Ref. 21.

PHOTOABSORPTION AND PHOTOIONIZATION CROSS SECTIONS

Photoabsorption cross sections, σ_t, and photoionization cross sections, σ_i, are of great importance in radiation research. Oscillator-strength distributions or differential oscillator strength values, df/dE, are proportional to the σ_t values. The ionization efficiency or the quantum yield of ionization, $\eta(E) = \sigma_i/\sigma_t$, are also of great importance in radiation research where E is the photon energy.

The experimental data on which these cross-section values are based must be correct, absolute, and comprehensive. However, this requirement has not been met in general because of experimental difficulties, including that few suitable photon sources and window materials exist in the wavelength region of vacuum ultraviolet and soft x-rays. Instead, fast-electron energy-loss spectroscopy has been used as a substitute for optical spectroscopy. Also, the use of synchrotron radiation in this wavelength region is most promising.

The σ_t values have been already measured for various molecules in the wavelength region at least longer than the near UV region, whereas the values in the wavelength region shorter than the LiF cutoff at 105 nm are very few. When the Thomas-Kuhn-Reiche sum is compared with the sum of the σ_t values for a molecule in the wavelength region longer than

Table 7. Availability of σ_t and σ_i values for atoms and molecules to radiation therapy.

Atoms and Molecules	Data Availability[a] σ_t or df/dE[b]	σ_i	Comments
He, Ne, Ar, Kr, Xe	A	A	
H_2, N_2, O_2, CO, NO	B	B	
H_2O, CH_4, CH_3, HF	C	C	
C_2H_6, C_3H_8, Cn-Hydrocarbons (n:2-6)	C	D	
C_n-Hydrocarbons (n: 7-20)	O	O	
O-Containing molecules (CH_3OH, C_2H_5OH, CH_3OCH_3, $CH_3OC_2H_5$)	C	C	
N-Containing molecules	O	O	
S-Containing molecules	O	O	
Polymers, DNA, proteins	D	O	
Si, LiF, CaF_2, Graphite	B	-	
Mg, Al, Cu	B	-	
ice	C	O	
Clusters	O	O	Threshold behavior is known.
Liquids	O	O	Often the ionization potential and the electron solvation energy are known. η or σ_i is very important, but unknown.

[a] A: most accurate and more comprehensive
B: less accurate and comprehensive
C: relative data
D: least accurate comprehensive
O: no data available

[b] E: $E_{threshold}$ (5~20 eV) - 10 keV

105 nm, which corresponds to about the ionization potential of most molecules, it is found that the sum of the measured oscillator strength values corresponds to less than a few percent of the total number of electrons in the molecule. Thus, the absorption by any molecule is strongest in the far ultraviolet and soft x-ray regions.

Table 7 shows an availability of σ_t and σ_i values for atoms and molecules of interest to radiation therapy.

Partial ionization cross sections and optical emission or dissociation cross sections have been also measured for some molecules, but these measurements are not included in Table 7 because they are not yet so comprehensive.

RAPID CONVERSION OF INITIAL IONS AND EXCITED NEUTRALS THROUGH COLLISIONS WITH OTHER MOLECULES

The following processes are important in the physico-chemical stage of radiolysis in which ions and excited neutrals (formed in primary events including excitation by secondary electrons) change their chemical identify in near-thermal collisions with other molecules. These processes link the physics of initial processes with the chemistry of subsequent events, consequently, their understanding is of basic importance.

Ion-Molecule Processes

- Chemical reactions of both positive and negative ions [total reaction cross sections or rate constants, branching ratios, the dependence on collision energy (thermal to several eV)]

- Chemical reactions of positive or negative cluster ions (total cross sections, branching ratios)

- Charge-transfer processes (total cross sections, and the dependence on energy)

- Recombination of ions with electrons and ions of opposite charge (total cross sections or rate constants, and the energy dependence)

Table 8. Data availability for rapid conversion processes

	σ_{tot}
ion-molecule reactions	absolute data on total cross sections with about ±20% accuracy, relative data plentiful; less information on negative ion reactions.
Cluster-ion reactions	fragmentary to non-existent
recombination	information on some systems available, otherwise incomplete need for further studies
Penning ionization	absolute data for some processes only, more information on relative cross sections, need for further studies urgent
excitation energy transfer	information ranges from accurate for some systems to fragmentary, depending on systems studied

Neutral-Neutral Processes

- Penning ionization, including chemi-ionization (total cross sections, branching ratios, partial cross sections for ionization as opposed to neutral-species production, and energy dependence)

- Excitation energy transfer leading to neutral excited species (cross sections or rate data)

In addition, data on energetics of reactants and products of the processes in question should be compiled. They include heats of formation, proton affinities, and electron affinities.

Scope of Materials

Atoms: He, Ar

Simple molecules: H_2, N_2, O_2, NO, H_2O, CO_2

Larger molecules: alkanes (suitable for a simulation of polyethylene)

Elements: Mg, Al, Si

clusters: $(H_2O)_n$, $(O_2)_n$, $(N_2)_n$, $(CO_2)_n$

Particular emphasis should be given to reactions of water and species produced from it. Planned work should concern collisions of ions and excited species with parent molecules and other molecules.

Data Availability and the Present Status

Systematic compilation of data for radiation-research purposes has not been carried out. Compilations carried out for other purposes offer partial summaries of data for several of the processes.

Sporadic data in the literature exist on many of these processes, with the exception of the reactions of clusters where experimental and theoretical work is necessary. The data status of total cross sections for ion-molecules and netral-neutral processes is given in Table 8.

REFERENCES

1. C.F. Barnett, J.A. Roy, E. Ricci, M.I. Wilker, E.W. McDaniel, E.W. Thomas, H.B. Gilbody, Atomic Data for Controlled Fusion Research, Report ORNL-5206 and 5207, Oak Ridge National Laboratory, Oak Ridge, Tennessee 37830, USA, (1977).

2. C.F. Barnett, Collision of H, H_2, He and Li Atoms and Ions with Atoms and Molecules, Atomic Data for Controlled Fusion Research, Vol. I, Report ORNL-6086/VI, Oak Ridge National Laboratory, Oak Ridge, Tennessee 37830, USA, to be published.

3. R.A. Phaneuf, R.K. Janev, M.S. Pindzola (Editors), Collisions of Carbon and Oxygen Ions with Electrons, H, H_2, and He, Atomic Data for Controlled Fusion Research, Vol. V, Report ORNL-6090/V5, Oak Ridge National Laboratory, Oak Ridge, Tennessee 37830, USA, (1987).

4. K. Okuno, Charge Changing Cross Sections for Heavy-Particle Collisions in the Energy Range from 0.1 eV to 10 MeV. II. Incidence of C, N, O, and their Ions, Report IPPJ-AM-10, Institute for Plasma Physics, Nagoya University, Nagoya, Japan, (1978).

5. Y. Nakai, T. Shirai, T. Tabata, R. Ito, At. Data Nucl. Data Tables, 37 (1987) 69.

6. R.K. Janev, J.W. Gallagher, B.H. Bransden, Evaluated Theoretical Cross Section-Data for Charge Exchange of Multiply Charged Ions with Atoms, Report 25, Joint Institute for Laboratory Astrophysics, University of Colorado, Boulder, U.S.A., (1984).

7. R.K. Janev, M.F.A. Harrison, H.W. Drawin, Atomic and Molecular Data Base for Fusion Plasma Edge Studies, submitted to Nuclear Fusion.

8. M.E. Rudd, Y.-K. Kim, D.H. Madison, and J.W. Gallagher, Rev. Mod. Phys. 57 (1985) 965.

9. K.L. Bell, H.B. Gilbody, J.G. Hughes, A.E. Kingston, and F.J. Smith, J. Phys. Chem. Ref. Data 12 (1983) 891.

10. M.A. Lennon et al., to appear in J. Phys. Chem. Ref. Data.

11. M.A. Lennon et al., to appear as a report of the Culham Laboratory.

12. G. Ehrhardt and W. Langer, Princeton Plasma Physics Laboratory Report No. PPL-2477 (1987).

13. R.K. Janev and K. Katsonis, Nucl. Fusion Special Topic 1493 (1987).

14. L.G. Christophorou (Editor), ELectron and Ion Swarms, (Academic Press, 1981).

15. L.G. Christophorou (Editor), Electron Molecule Collisions and Their Applications, Vol. I and II (Academic Press, 1984).

16. S. Trajmar, D.F. Register, and A. Chutjian, Phys. Rep. 97 (1984) 219.

17. L.C. Pitchford, B.V. McKoy, A. Chutjian, and S. Trajmar (Editors), Swarm Studies and Electron Molecule Collisions, (Springer Verlag, New York, 1987).

18. T.D. Märk and G.H. Dunn (Editors), ELectron Impact Ionization, (Springer Verlag, Vienna, 1985).

19. T.D. Märk and A.W. Castleman, Adv. Atom. Molec. Phys. 20 (1985) 65.

20. T.D. Märk , Int. J. Mass Spectrom. 79 (1987) 1.

21. M. Michaud and L. Sache, Phy. Rev. A 36 (1987) 4672; ibid (1987) 4684.

Working Group C

DATA ON CONSEQUENCES OF MULTIPLE COLLISIONS

Summary and Recommendations

Group Leader:	**H. Paul**	(Austria)
Members:	**I.G. Kaplan**	(Union of Soviet Socialist Republics)
	G. Kraft	(Federal Republic of Germany)
	P. Pihet	(Belgium)
	D. Srdoč	(Yugoslavia)
	E. Waibel	(Federal Republic of Germany)

STOPPING POWERS

Stopping powers in elemental materials and in various compounds are widely used in radiation research to characterize tracks left by charged particles in matter. Stopping powers represent the average energy lost per unit pathlength by primary charged particles such as protons or heavy ions. They are used to calculate the range of the ions in matter and their LET. For indirectly ionizing particles (photons, neutrons), stopping powers are necessary to describe the slowing down of the secondary charged particles released in matter. For practical dosimetry with gas-cavity detectors (e.g., ionization chambers and proportional counters), stopping powers represent the basic atomic data needed to convert the energy imparted to the gas into the dose absorbed in the wall material. For this application, the uncertainty in stopping powers and stopping power ratios between the gas and wall materials influences the uncertainty of the determination of the total absorbed dose or the kerma.

Stopping power tables or fits to experimental data may be found for different ions in a large variety of elemental materials and for wide energy ranges.[1,2] Stopping powers of tissues, tissue substitutes, counting gases, or other materials related to radiation research are often derived by using the Bragg addivity rule. This approach is useful in general regarding, for example, the large data set needed in neutron dosimetry for protons, deuterons, alpha particles, as well as C, N, O, Be, and B ions released with initial energies from several hundred keV up to 60 MeV. However, the Bragg rule is known to be only a first

approximation because of chemical binding effects, especially for materials with low-Z constituents, for solid compounds, and for particles at low energies near and below the stopping power maximum (Waibel, this meeting; Paul et al., this meeting). Critical compilations of evaluated stopping powers for particles and materials of interest to radiation research are therefore needed.

Stopping powers for electrons, from 10 keV up to 1000 MeV, were compiled in an ICRU Report.[3] ICRU compilations are in progress for protons (1 keV to 1 GeV) and for alpha particles (10 keV to 100 MeV) by M.J. Berger and his report committee, and for heavier ions by P. Sigmund and his report committee. Summaries of data and issues related to the Bragg rule for protons and alpha particles have been published by Thwaites [4-7]. Stopping powers for protons and for alpha particles (400 keV/amu to 100 MeV/amu) for materials used in dosimetry with ionization chambers and proportional counters were calculated by Makarewicz, Burger, and Bichsel[8] using the mean excitation energy values recommended for the same compounds in ICRU Report 37. However, very few stopping powers have been measured experimentally to test compiled values, especially for low-energy electrons, protons, and alpha particles near and below the stopping-power maximum. Some experimental values have been obtained for low-energy electrons[9] and for low-energy protons (i.e., 40-200 keV, by Fukuda,[10] and 1-100 keV by Waibel and Willems[11]) in methane-based tissue-substitute gas. Fewer experimental data have been obtained for solid compounds such as tissue substitute plastics.

For gas-cavity detectors used in neutron dosimetry, gas-to-wall dose conversion factors are derived from average stopping power ratios for the secondary charged particles produced by neutron interactions in the wall and entering the cavity. Overall uncertainties of these dose conversion factors are therefore due to uncertainties about the stopping powers data used and to uncertainties about the secondary charged particle spectra, i.e., on the energy distribution of those particles and their relative contribution to the total absorbed dose. These uncertainties lead to serious problems especially at the high neutron energies used for therapy, and the overall uncertainty achievable on the total absorbed dose generally depends on the neutron energy. To meet the uncertainty limit of ±5% required in neutron dosimetry for therapy, an overall uncertainty of ±2% is necessary for the dose conversion factors. This problem is less important for "TE wall-TE gas" detectors because of the

similarity in the wall and gas compositions. However, it becomes much more critical for nonhydrogenous ionization chambers and proportional counters, walled with carbon, aluminum, or oxygen compounds and filled with different gases, which are now attracting increasing interest in neutron dosimetry. Dose conversion factors are available[12,13] for neutron energies up to 14 MeV, and are also being compiled by the ICRU for a future report. Very few data, however, are available for proportional counters filled with propane-based TE gas used in microdosimetry, and at higher neutron energies, i.e., 5-60 MeV (Pihet and Menzel, this meeting).

Materials for which stopping powers are needed

Gases: H_2O, H_2, O_2, CO_2, Ar, Air
N_2, CO_2, CH_4, C_3H_8
$TE(CH_4)$, $TE(C_3H_8)$ (for these TE gases commonly used in dosimetry and in microdosimetry, the application of the Bragg's rule for the N_2, CO_2, CH_4, C_3H_8 gas constituents is found to be a good approximation)

Solids: Pure elements: C, Mg, Al, Si, P, Ca, Fe

Compounds: for solid-state detectors: LiF, CaF
tissue substitutes: A-150 TE plastic, perspex, polyethylene, nylon
oxygen compounds: e.g., Al_2O_3

Liquids: H_2O and hydrocarbons

Charged particles and energy ranges

The following list includes primary charged particles as well as secondary particles produced by photon and neutron interactions.

Electrons: Needed from 50 eV to 1000 MeV (partially covered by ICRU Report 37)

Need further investigations: - from 50 eV to 10 keV
- experimental tests of the ICRU 37 values are required

Protons: Needed from 1 keV to 400 MeV needed (to be covered by a forthcoming ICRU report)

Need further investigations:
- comparison of gas and condensed phase for identical compounds
- for TE gases or constituents, near and below the maximum stopping power (especially for propane-based TE gases)
- measurements for solid tissue substitutes

α-particles: Needed from 10 keV to 400 MeV/u (mainly from neutron interactions) (to be covered by a forthcoming ICRU report)

Need further investigations:
- for TE gases or constituents, near and below the maximum stopping power
- measurements for solid tissue substitutes

Heavy ions: Needed for neutron secondaries: C, N, O. Be, B from 100 keV to 20 Mev

Heavy ions for therapy: C to Ar up to 800 MeV per nucleon

(covered by H.H. Andersen and J.F. Ziegler, and by the ICRU work led by P. Sigmund)

Need further investigations:
- phase effects
- more precise data for C and O resulting as recoils from neutrons
- in the high energy region for the heavy ions foreseen for therapeutic applications

General recommendations

In addition to the requirements listed above, the following recommendations are presented:

1. A critique of the Bragg additivity rule for compounds requires additional theoretical and experimental work including determination of influence of both chemical binding and phase.

2. The concept of "effective charge" to determine the stopping powers for heavy ions is subject to limitations and needs further study.

3. There may be some values to comparing stopping powers of tissue substitutes with those for real tissues.

4. At high energies, the projected range is well approximated by the range calculated from stopping power; however, more accurate evaluations are required for low-energy particles (protons, alpha particles, and especially electrons); in particular, the determination of the range of subexcitation electrons is encouraged.

5. Accurate experimental determination of the stopping power for protons and alpha particles of A-150 TE plastic is encouraged to reduce the uncertainty on the stopping-power ratios and on the resulting dose conversion factors for neutrons; more investigations are also needed for the materials of nonhydrogenous ionization chambers and proportional counters used for the dosimetry of neutrons with an energy above 14 MeV.

INITIAL YIELDS OF IONS

Initial yields of ions and excited states, as well as electron degradation spectra are another kind of important atomic and molecular data. Knowledge of these quantities is essential for investigation of charged-particle track structure in condensed matter. This subject area is currently of great interest since progress in radiation research is becoming increasingly dependent on the study of elementary interaction processes of particles with the biological matter such as DNA and proteins at very small scales (down to a few nanometers). This type of investigation requires detailed theoretical studies (e.g. in the spirit of Spencer and Fano) applied to photons and electrons at low energies, as well as studies that include new dimensions such as the time-dependent effects of irradiation. Emphasis is also being placed on the effect of complex compounds, as opposed to chemically pure substances, and on the phase effect.

Knowledge of the ionization yield in gases and the average energy to produce an ion pair (the W value) have been of interest for a long time in radiation research because of the extensive use of gas-cavity chambers for dosimetry in radiotherapy (Waibel, this meeting; Srdoc, this meeting). The W value is needed to convert the ionization yield by

charged particles in the gas into energy loss. Low-pressure proportional counters operate as cavity chambers with low-pressure gases. They measure primarily the spectra of ionization yields by impinging charged particles or by secondary particles released in the counter wall and entering the cavity. The measured ionization yield spectra constitute only an approximation of the energy deposition spectra because each single ionization yield cannot be converted with an adequate W value. A rigorous conversion can only be done by theoretical calculations. The comparison of experimental ionization yield spectra with theoretically calculated spectra (e.g., by using the computer program of Caswell and Coyne) has already been used to investigate energy deposition spectra for neutrons frm several keV up to 60 MeV. This procedure is useful although limited by the available nuclear cross section data. It requires precise W values for different secondary particles over wide energy ranges and their slowing down spectra. In proportional counters, most of the secondary particles have ranges larger than the simulated diameter, and therefore differential ionization values (commonly denoted by w) are also needed. Ionization chambers and proportional counters allow precise determination of integral quantities such as the kerma. In practice, the W values need to be evaluated. As it is the case for stopping power, the uncertainty in the W values directly influences the overall uncertainty in the measured kerma (as discussed by Pihet and Menzel at this meeting).

Microdosimetry describes the spatial distributions of energy deposition in very samll sites. It is, however, experimentally limited to a dimension of the sensitive volume on the order of 1μm. To provide a better understanding of interaction processes at smaller scales, microdosimetry is being extended to sites with nanometer dimensions, although only theoretical calculations based on track simulations can currently be used (Olko, this meeting). Such experimental studies would provide an important source of data for intercomparison with track structure analysis (Paretzke, this meeting). In particular, for the experimental determination of the radial dose distributions, the dependence of W on the ionization and excitation cross section ratio as a function of the radial distance needs to be determined accurately. The applicability of the W-value concept, as an average quantity, to sites as small as a few nanometers needs to be carefully examined.

Research is required on the applicability of an additivity rule to derive W values for complex substances from the W values for their

constituents. Available experimental data show that this procedure is critical and imply large uncertainties for W values not only for condensed-phase materials but also for gases. As an example, very few W values for propane-based TE gases used in proportional counters are available; the extrapolation of the W values for methame-based TE gases to other mixtures is probably a poor approximation, especially in view of the uncertainty level of ±2% required, e.g., for obtaining average W_n values in neutron dosimetry for therapy.

The energy losses of any charged particles in matter are the final results of many collision processes and are therefore stochastic. The resulting fluctuations in the energy losses are called straggling, and have been a subject of study for many years. Data on straggling are much less extensive than those on the mean energy loss, viz., the stopping power. Neverthelss, a review of the straggling data will be highly valuable.

The statistical fluctuations of the number of ions produced by a fixed kind of radiation (e.g., a charged particle of given energy) are likewise an important subject of study. These fluctuations are commonly characterized by the Fano factor. Data on this quantity are not yet extensive, but deserve full documentation, because the Fano factor represents a key index of stochastic aspects of radiation-energy absorption, which are discussed more extensively in later paragraphs concerning track structures and microdosimetry.

Gases for which W values are needed

Gases: H_2O, H_2, O_2, Ar, air
N_2, CO_2, CH_4, C_3H_8
Methane-based TE gas, propane-based TE gas

Charged particles and energy ranges

The following includes primary charged particles as well as secondary particles from photon and neutron interactions.

Electrons: Needed from 50 eV to 100 MeV (covered from threshold up to several hundred eV by ICRU Report[14] 31 and by Combecher[15]; from 30 eV to 2 keV for CH_4, CO_2, N_2, Ar, and TE(CH_4) by Smith and Booz;[16] from 20 eV to 5 keV for air, CH_4 and N_2 by Waibel and Grosswendt;[17] and for methane-based tissue-substitute gas and CO_2 by Waibel at this meeting)

Need further investigations:
- data needed in the intermediate energy region above 5 keV and above several MeV
- extension to C_3H_8 and propane-based gases

Protons: Needed from 1 keV to 250 MeV (partially covered by ICRU Report[14] 31, and by Goodman and Coyne;[18] for CH_4, N_2, CO_2, and methane-based TE gases from 1 keV to 100 keV by Sidenius,[19] by Huber,[20], and by Waibel and Willems,[21] from 1.2 to 3.5 MeV by Thomas and Burke[22])

Need further investigations:
- further precise measurements at intermediate energies above 100 keV to 1 MeV
- data needed in the high-energy energy region
- extension to C_3H_8 and propane-based TE gases (at all energies)

α-particles: Needed from 10 keV to 100 MeV (partially covered up to 10 MeV by ICRU Report[14] 31; for methane-based TE gases up to 10 MeV by Goodman and Coyne,[18] from 15 keV to 375 keV by Nguyen et al.,[23] for propane-based TE gases from 25 keV to 375 keV by Posny et al.,[24])

Need further investigations:
- extension to C_3H_8 and propane-based TE gases (at all energies); precise data are needed in particular for calibration of proportional counters from 500 keV to 2 MeV and for 5.3-5.7 MeV
- further data needed in the high-energy region

Heavy ions: Needed for neutron secondaries: C, N, N, O, Be, B from 100 keV to 20 MeV

Heavy ions for therapy: C, Ne, ... Ar up to 800 MeV per nucleon (partially covered by ICRU Report 31, and by Goodman and Coyne,[18], more recent but scarce data available at low energy for TE(CH_4) and constituents by Nguyen et al.[23], by Huber et al.[20], and for TE(C_3H_8 by Posny et al.[24])

Need further investigations:
- extension to C_3H_8 and $Te(C_3H_8)$ gases (at all energies)
- further data needed in the high energy region

General recommendations

In addition to the requirements listed above, the following recommendations are presented:

1. Data on propane-based TE gases mixture are urgently needed in view of the increasing number of applications of proportional-counter measurements for therapy applications; some data are available in internal reports by Burger et al.[25] and Srdoc.[26] A critical compilation of these data will markedly assist users.

2. The precise values obtained by Thomas and Burke[22] for protons around 1 MeV show a discontinuous trend compared with other data at lower energies. Complementary measurements are encouraged to explain this shape.

3. At high energies, differential w values require experimental investigations. Because of the large contribution of recoil protons to the total absorbed dose for fast neutron therapy beams, the w values for protons above several MeV need to be determined with high accuracy (i.e., better than 1%).

4. Average W values for neutrons (W_n) were compiled by Goodman and Coyne[18], by Rubach and Bichsel[12], and Burger and Makarewicz[13] for neutron energies up to 14 MeV. Further investigations are required at higher neutron energies, and results should be adapted to analyses of proportional counters including the influence of the wall material, which determines the secondary charged particle spectra (e.g., for nonhydrogenous counters).

5. Comparative evaluations of track-structure calculations for different charged particles by different computer codes are needed including detailed investigations of the ratio of ionized- and excited-state yields, G-values for ionizations in the condensed phase, and electron degradation spectra.

TRACK STRUCTURE QUANTITIES

Yields of ions and excited states, and the electron degradation spectra, as discussed in the previous sections, contribute to modeling studies of biological effects. However, knowledge of these quantities alone is insufficient to explain the basic mechanisms of radiation action. In particular, the unrestricted LET for different kinds of charged particles has limited applicability for characterizing the effects produced by these particles. More detailed information is generally needed on the spatial distribution of energy transfers to critical biological structures. Obtaining this information is the object of studies in the area of track-structure analysis. Quantities under this category include also microdosimetric spectra, radial dose distributions, and other track structures related to the energy transferred at small sites (down to a few nanometers). Indeed, full characterization of track structures presents an open field for investigation (as pointed out by Paretzke at this meeting).

A comprehensive description of microdosimetric quantities, methods, and current results is given in ICRU Report[27] 36. Recent progress and advanced ideas in the application of the microdosimetric concepts in radiobiology, radiation protection, and radiotherapy were presented at the last Congress of Radiation Research.[28-31] During the past years, considerable results have been achieved by accurate measurement of microdosimetric spectra for various radiations, mainly photons and neutrons over wide energy ranges. Since more experimental and theoretical results are becoming available, their critical reviews and compilations will be highly valuable for users.

REFERENCES

1. J.F. Ziegler, J.P. Biersack, and U. Littmark, The Stopping and Range of Ions in Solids, (Pergamon, New York, 1985).

2. J.F. Janni, At. Data Nucl. Data Tables 27 (1982) 147.

3. International Commission on Radiation Units and Measurements, Stopping Powers for Electrons and Positrons, ICRU Report 37, (Washington, D.C., 1984).

4. D.I. Thwaites, Radiat. Res. 95 (1983) 495.

5. D.I. Thwaites, Nucl. Instr. Meth. B12 (1985) 84.

6. D.I. Thwaites, Radiat. Prot. Dosim. 13 (1985) 65.

7. D.I. Thwaites, Nucl. Instr. Meth. B27 (1987) 293.

8. M. Makarewicz, G. Burger, and H. Bichsel, Phys. Med. Biol. 31 (1986) 281.

9. B. Grosswendt and E. Waibel, Nucl. Instr. Meth. 197 (1982) 401.

10. A. Fukuda, Phys. Med. Biol. 25 (1980) 877.

11. E. Waibel and G. Willems, Phys. Med. Biol. 32 (1987) 365.

12. A. Rubach and H. Bichsel, Phys. Med. Biol. 27 (1982) 893.

13. G. Burger and M. Makarewicz, in Nuclear and Atomic Data for Radiotherapy and Related Radiobiology, STI/PUB/741 (International Atomic Energy Agency, Vienna, 1987), p. 225.

14. International Commission on Radiation Units and Measurements, Average Energy Required to Produce an Ion Pair ICRU Report 31, (Washington, D.C., 1979).

15. D. Combecher, Radiat. Res. 84 (1980) 189.

16. B.G.R. Smith and J. Booz, in Proceedings of the Sixth Symposium on Microdosimetry, edited by J. Booz and H.G. Ebert, (Harwood Academic Publishers, Inc., London, 1978), p. 759.

17. E. Waibel and B. Grosswendt, in Proceedings of the Eighth Symposium on Microdosimetry, edited by J. Booz and H.G. Ebert, (Commission of the European Communities, 1983), p. 301.

18. L.J. Goodman and J.J. Coyne, Radiat. Res. 82 (1980) 13.

19. G. Sidenius, Radiat. Eff. 39 (1978) 213

20. R. Huber, D. Combecher, and G. Burger, Radiat. Res. 101 (1985) 237.

21. E. Waibel and G. Willems, Radiat. Prot. Dosim. 13 (1985) 79.

22. J. Thomas and M. Burke, Phys. Med. Biol. 30 (1985) 1201.

23. V.D. Nguyen, M. Chemtob, J. Chary, F. Posny, and N. Parmentier, Phys. Med. Biol. 25 (1980) 509.

24. F. Posney, J. Chary, and V.D. Nguyen, Phys. Med. Biol. 32 (1987) 509.

25. G. Burger, unpublished report of Institut für Strahlenschutz, Gesellschaft für Strahlen- und Umweltforschung.

26. D. Srdoc, unpublished report of Radiological Research Laboratory, Columbia University.

27. International Commission on Radiation Units and Measurements, Microdosimetry, ICRU Report 36, (Washington, D.C., 1983).

28. J. Booz and L.E. Feinendegen, in Radiation Research. Proceedings of the 8th International Congress of Radiation Research, Edinburgh, July 1987, edited by E.M. Fielden, J.F. Fowler, J.H. Hendry, and D. Scott, (Taylor & Francis, London, 1987) Vol. 2, p. 331.

29. A.M. Kellerer, ibid. p. 338.

30. H.G. Menzel, ibid. p. 345.

31. A. Wambersie, ibid. p. 351.

USE OF ATOMIC AND MOLECULAR DATA IN RADIATION THERAPY AND TRACK STRUCTURE ANALYSIS

(Session I)

NEED FOR IMPROVING THE ACCURACY IN DOSE DELIVERY IN RADIO- AND NEUTRON THERAPY
Importance of atomic and molecular data

A. WAMBERSIE*, J. VAN DAM**, G. HANKS***,
B.J. MIJNHEER+, J.J. BATTERMANN++

* Cliniques universitaires Saint-Luc,
Université catholique de Louvain,
Brussels, Belgium

** Universitaire Ziekenhuis Saint-Rafaël,
Leuven, Belgium

*** Fox Chase Cancer Center,
American Oncologic Hospital,
Philadelphia, Pennsylvania,
United States of America

\+ The Netherlands Cancer Institute
(Antoni van Leeuwenhoekhuis),
Amsterdam, Netherlands

++ Instituut voor Radiotherapie,
Rijksuniversiteit Utrecht,
Utrecht, Netherlands

Abstract

In photon therapy, an accuracy of 3 5 % in absorbed dose delivery to the dose specification point is required It corresponds to one relative standard deviation, combining types A and B uncertainties (i e random and systematic, respectively) This requirement results from the steepness and the separation of the dose-response curves observed for tumour control and normal tissue complications For both types of effects, the available clinical data are reviewed Besides the accuracy requirement in dose level, the problem of dose distribution (or "geometry problem") is considered, and the possible consequences of an inaccuracy in patient/beam positioning are discussed Examples taken from the "Patterns of care study" are presented, i e for prostatic adenocarcinoma and Hodgkin's disease In fast neutron therapy, the required accuracy is at least as high as that required with photons As a matter of fact, the same steepness of the dose-response curves is observed for tumour control and normal tissue complications. In addition, the physical selectivity is more critical with neutrons since a general reduction of the differential effect between cell populations has been observed after high-LET compared to low-LET radiation The rationale for using protons and other heavy charged particles is presented Additional basic physical data are needed for improving the accuracy in dose level as well as in physical selectivity, especially for neutrons and heavy charged particles They are needed in order to evaluate more accurately the kerma and absorbed dose in different human and biological tissues, to determine the response of different detectors, and also to optimize the beam collimation systems and thus improve the physical selectivity of the irradiation

1 INTRODUCTION

The outcome of radiation therapy - or the clinical result - is closely related to the dose that has been delivered to the target volume and the normal tissues The problem of accuracy in dose delivery can be approached from different points of view

From a first point of view, one can distinguish the prescription and the execution of a treatment In other words, a treatment can be wrong because the initial prescription was wrong (e g selection of the target volume, of its limits, of the dose level, of the fractionation scheme, etc) A treatment can also be wrong because its execution was not correctly done

The prescription of the treatment is essentially a medical problem, while of course for its execution, there is a team responsibility including radiotherapists, physicists, technicians As already advocated [7], a plea for a full collaboration between these different groups of persons is probably much better than long discussions about the respective responsibilities of the different members of the team

From another point of view, for both the prescription and the execution of the treatment, one can distinguish the problems related to dose level and those related to dose distribution

The first ones include the prescription of the target absorbed dose and the accuracy in its delivery, the second ones (which will be called "geometrical problems") include the selection of the target volume, the field sizes, the beam arrangement, the patient positioning, etc In the present report, the following points will be discussed successively

- the target aborbed dose level its prescription and the accuracy required in its delivery,
- the difficult problems of "geometry" in a radiotherapy treatment,
- some specific problems raised by the introduction as treatment modality of fast neutrons or other types of non-conventional radiations

II ABSORBED DOSE LEVEL

II 1 The dose prescription

The optimum dose level is always a compromise between the maximum possible cure rate and the acceptable complication rate It is often defined as the dose level corresponding to the maximum percentage of uncomplicated local tumour control

The relationship between the dose and the probability for uncomplicated tumour control is derived from the dose-effect curves for local tumour control and normal tissue complications (Fig 1) A "bell-shaped" curve is usually obtained its maximum corresponds to the optimum target absorbed dose level [18] [39]

The knowledge of the optimal target absorbed dose to be delivered for a given tumour type or site can only result from the accumulation of clinical experience In practice, in many situations, the dose actually delivered is not optimal because the relevant information is not available or not adequately used The consequences are of course a

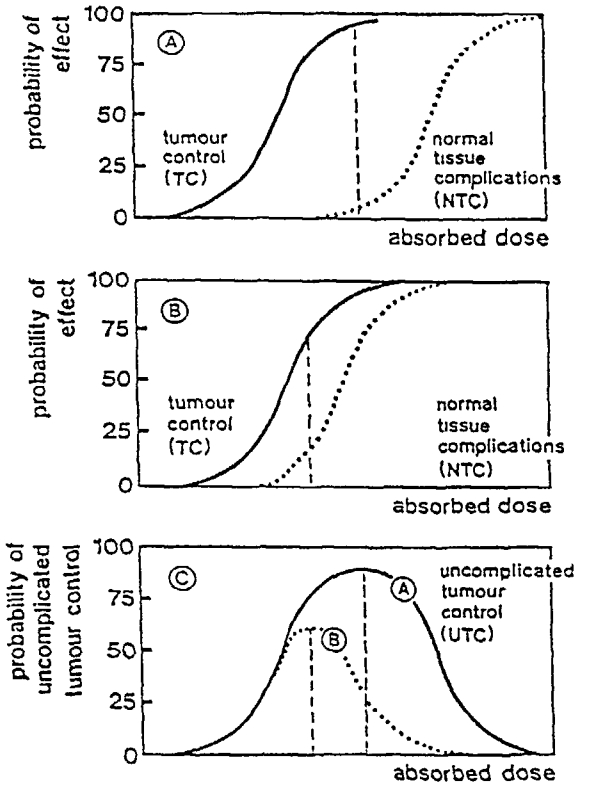

FIG 1

Hypothetical dose-effect relationships for local tumour control and normal tissue complications, and resulting uncomplicated tumour control curves

The dose-effect curves are assumed to have the same sigmoidal shape and steepness

A Favourable situation a high local tumour control rate can be achieved without inducing a high complication rate

B Less favourable situation dose levels which could achieve a tumour control rate in excess of 50 % would induce a high complication rate

C Uncomplicated tumour control $P_{UTC} = P_{TC} \times (1-P_{NTC})$ for situations A and B The optimal dose values are indicated by dashed lines

(modified from Holthusen [18], Withers and Peters [39]

TABLE I

Radiotherapy of prostatic adenocarcinoma (1973-1975) Relation between absorbed dose and infield recurrence rate (at 4 years) All T stages pooled T-0, 1, 2, 3, 4, N-0, M-0 The doses are specified at the centre of the prostate		
Absorbed dose (Gy)	Number of patients	Recurrence rate
< 55	31	24 %
55-59,99	65	20 %
60-64,99	93	16 %
65-69,99	195	11 %
≥ 70	190	10 %
Total	574	
Significance whole curve p = 0 05 Significance linear trend p = 0 01		

from Hanks, 1985 [13]

TABLE II

Radiotherapy of prostatic adenocarcinoma (1973-1975) Relation between absorbed dose and infield recurrence rate Stages T-0, 1, N-0, X, M-0 (same presentation as Table I)		
Absorbed dose (Gy)	Number of patients	Recurrence rate
< 55	8	0 %
55-59,99	24	8 %
60-64,99	30	7 %
65-69,99	75	3 %
≥ 70	65	6 %
Total	202	
Significance whole curve p = N S Significance linear trend p = N S		

from Hanks, 1985 [13]

lack of tumor control or, on the other hand, unnecessary complications which could have been avoided

One way of obtaining information on the optimum dose level is to perform systemic retrospective studies on large patient series Such investigations were performed, at a large scale, in the United States within the frame of the "Patterns of Care Study" [24] [25] [26] The example of prostate cancer is particularly illustrative

A total number of 2026 patients, with prostate adenocarcinoma, were treated between 1956 and 1979 in 7 major U S institutions (Stanford

University, Mallinckrodt Institute, M D Anderson Hospital, University of Arizona, Medical College of Wisconsin, Virginia Mason Clinic, Massachusetts General Hospital) For this study, the average annual access of patients with prostatic cancer varied between 11 and 36 per year and per institution

Among these 2026 patients, the study of Hanks [13] analyzed 574 patients treated between 1973 and 1975, which provides a "two-year time window" Table I presents the distribution of patients according to the dose level The doses indicated have been recalculated by the physics team which performed the survey, they correspond to the

TABLE III.

Radiotherapy of prostatic adenocarcinoma (1973-1975) Relation between absorbed dose and infield recurrence rate Stages T-2, N-0, X, (same presentation as Table I)		
Absorbed dose (Gy)	Number of patients	Recurrence rate
< 55	10	40 %
55-59,99	17	18 %
60-64,99	17	12 %
65-69,99	51	12 %
≥ 70	41	10 %
Total	136	
Significance whole curve p = 0 06 Significance linear trend p < 0 05		

from Hanks, 1985 [13]

TABLE IV

Radiotherapy of prostatic adenocarcinoma (1973-1975) Relation between absorbed dose and infield recurrence rate Stages T-3, N-0, X, (same presentation as Table I)		
Absorbed dose (Gy)	Number of patients	Recurrence rate
< 55	8	38 %
55-59,99	14	36 %
60-64,99	29	21 %
65-69,99	53	11 %
≥ 70	61	10 %
Total	165	
Significance whole curve p < 0 01 Significance linear trend p < 0 01		

from Hanks, 1985 [13]

absorbed dose at the center of the prostate (which is close to the "specification point" defined in ICRU Report 29 [21] The local control rate increases with dose level, up to approximately 65 Gy, and then tends to level off

In Tables II - V, the different "T" groups are analysed separately For small tumours (T_0,T_1), local control is higher than 92 % and, consequently, no dose-response curve can be derived On the other hand, a significant dose-response relation is observed for T_2 and T_3 tumours For T_4 tumours, which are fixed or invade adjacent organs, no dose/response relation can be obtained below 70 Gy, a dose at least as high as 70 Gy seems necessary to obtain optimal local control (Table V)

From these data, and the complications observed, an optimal dose level can be derived for each T group (Table VI), it increases with T stage (or with the tumour volume or extent) due to the increased number of cancer cells which have to be killed

As far as complications are concerned, 3 5 % were observed for doses below 70 Gy and 7 % (twice as much) for doses above 70 Gy (in this study only severe complications are considered, for which there was a hospital admission for diagnosis or management)

TABLE V.

Radiotherapy of prostatic adenocarcinoma (1973-1975)
Relation between absorbed dose and infield recurrence rate
Stages T-4, N-0, X,
(same presentation as Table I)

Absorbed dose (Gy)	Number of patients	Recurrence rate
< 55	11	36 %
55-59,99	10	10 %
60-64,99	17	29 %
65-69,99	16	38 %
≥ 70	23	13 %
Total	77	
Significance whole curve	N S	
Significance linear trend	N S	

from Hanks, 1985 [13]

Taking into account the "optimum" dose levels derived from Tables II-V, it can be seen (retrospectively) that for some patients the prescribed dose was too low and for others too high In particular (Table VII), 167 patients with T_0, T_1, T_2 and T_3 tumours received more than 70 Gy, which induced 12 complications (with the "optimum dose", only 6 complications would have been expected) On the other hand, local failure would probably have been avoided in 28 out of the 151 (18 %) patients who received less than the optimum dose

TABLE VI.

Radiotherapy of prostatic adenocarcinoma (1973-1975)
Optimum dose level according to T stage

Stage	Number of patients	Optimum absorbed dose (Gy) minimum	maximum
T-0, T-1	202	?	60
T-2	133	60	< 64,99
T-3	163	65	< 69,99
T-4	76	≥ 70	?

from Hanks, 1985 [13]

A more recent study on 313 patients with T1 tumours of the prostate confirmed that, for limited primary tumours, the optimum target dose is less than 70 Gy, and lies between 60-65 Gy [16] There was indeed no dose-response relation for in-field recurrence above 60 Gy, the failure rate at 5 years remaining 12 % As far as major complications are concerned, they ranged from 0 % at 60 Gy to 17 % at or above 70 Gy

These studies demonstrate that, in current radiotherapy practice, the actually prescribed target absorbed doses are not always optimal, and it is one of the aims of the Quality Assurance Programs to improve the situation Information on the optimal dose to be delivered in the different patient series can be derived from two methods prospective trials and retrospective studies

The merits of prospective trials are recognized they answer specific questions and compare the respective value of 2 (or more) treatment

TABLE VII

CANCER OF THE PROSTATE DOSE-OPTIMIZATION BY T STAGE COMPLICATION RATES RESULTING FROM INAPPROPRIATE DOSE DELIVERY	
Number of patients with T0,T1, T2,and T3 tumours who received a dose ≥ 70 Gy *	167
Complications observed **	12
Complications expected if appropriate dose level could have been given ***	6
Avoidable complications	6

* complication rate above 70 Gy = 7 %
** severe complications (see text)
*** complication rate below 70 Gy = 3 5 %

From Hanks [13]

modalities They are the only way to eliminate a possible bias in the patient recruitment On the other hand, their limitations have to be kept in mind one trial can answer only one (or few) specific question(s) and the conclusions are derived on a small fraction of the patient population, because of the strict rules of exclusion

Retrospective studies, such as the "Patterns of Care Study" mentioned above, implying a review of large amounts of patient records, can provide important and basic data concerning a large proportion of the patient population Especially, they can provide information on the complete dose-response relation, which for obvious ethical reasons, can not be obtained from prospective trials However, these studies provide only (statistically significant) correlations, for which it is sometimes difficult to identify and to separate the influence of different possible factors

In the discussion above, the optimum dose is prescribed taking into account the outcome of groups of patients, the groups being defined by tumour extent, histology, etc However, within a given group, the variability in tumour response is well recognized This gives full value to individual predictive tests, such as those developed by Brock et al [4] Predictive tests could help to select the optimum dose and best treatment modality for an individual patient For example, the test could foresee a relative radioresistance to conventional photon treatment and orientate the patient to another treatment modality, e g fast neutrons

II 2 Accuracy required in dose delivery

II 2 1 Historical review

In 1969, WAMBERSIE et al [37] and in 1971, HERRING and COMPTON [17] made an estimation of the degree of accuracy required in the dose delivered in radiotherapy They concluded that changes in the dose of 10 % either way can significantly change the probability of tumour control or normal tissue complication, and therefore the uncertainty associated with dose delivery should be less than ± 5 %

Continuing in the same direction, the ICRU in its Report 24 [20] made the following recommendation "the available evidence for certain types of tumor points to the need for an accuracy of ± 5 % in the delivery of an absorbed dose to a target volume if the eradication of the primary tumor is sought" Additional clinical evidence accumulated since 1976, and reviewed in the next paragraphs, has strenghtened this recommendation, which in fact has been taken over by several authors, as well as by national and international organizations It must be recognized that this ± 5 % accuracy requirement was selected as a "reasonable compromize" between

what should be ideal and what could be reached in practice In that respect, the ICRU Report 24 also recalls that "some clinicians have requested even closer limits such as ± 2 %, but at the present time it is virtually impossible to achieve such a standard"

More recently, Mijnheer et al [27] proposed for the combined uncertainty of type A and B (random and systematic, respectively) a requirement of 3 5 % (one relative standard deviation) in the absorbed dose delivery to the dose specification point For the determination of the absorbed dose to other points in the treatment volume other uncertainties have to be added, e g in the correction procedures for the irregular patient surface contours and in the off-axis absorbed dose determinations The uncertainties in the dose calculation algorithms also have to be added for more complicated treatment techniques At these points a 5 % (one standard deviation) dose accuracy requirement therefore seems more appropriate, according to these authors

The accuracy required in dose delivery is derived from the difference in dose which can be detected clinically, i e from the dose-effect curves for local tumour control or normal tissue complications These curves are generally sigmoid in shape (Fig 1), their slope and relative position may differ from one situation to another

The clinical data from which the dose-effect curves are derived should ideally be obtained from homogeneous groups of patients differing only by the level of the administered dose This is certainly not the case in all reported series (historical series, modifications in techniques, etc) In addition, clinical studies generally assume that each radiation beam adequately traverses the desired target volume during every session and that the total absorbed dose at the dose specification point is equal to the prescribed dose This is unfortunately not always the case, and in a good standard radiotherapy centre, where a quality assurance program is regularly applied, the setting of patients is generally considered as the weakest point of the chain and largely contributes to the uncertainty in the dose level but also to distortion of the dose distribution [7] A quantitative approach for evaluating this type of uncertainty has been proposed recently by Goitein [10] and will be considered in section III

Although, in principle, the required accuracy should be derived from human data, in practice however, taking into account the difficulties discussed above, useful information can also be derived from theoretical models and from in vitro or animal experiments, where all parameters can be better controlled However, one has to recognize the difficulties when extrapolating data from models or animal experiments to clinical situations

II 2 2 Dose-effect relationships for local tumour control

Steep dose-effect curves for local tumour control are derived from cellular models In the example presented in Table VIII [39] assuming an initial number of clonogenic cells of 8×10^7 and a $D_{o(eff)}$ of 3 5 Gy for a fractionated irradiation, the tumour control probability ranges from 50 % at 65 Gy to about 5 % and 85 % at dose levels of 60 Gy and 70 Gy respectively (i e for dose variations of less than ± 10 %) This is of course an extreme situation where the radiosensitivity of the cell population is assumed to be homogeneous Steep dose-effect curves are also observed when irradiating experimental tumours For example, for mammalian carcinoma in C3H mouse, irradiated with a single fraction in anoxic conditions, tumour control rate increases from 20 % to 80 %, when increasing the absorbed dose from 5 Gy to 6 Gy [31]

As far as clinical observations are concerned, it is probably the merit of Shukovsky [29] to have drawn the attention to the steepness of the dose-effect curve for local control of T2 and T_3 supraglottic squamous cell carcinoma On the other hand, for T_1 lesions, no variation of the tumour control level with dose was observed above 60 Gy, but the cure rate was high (> 80 %) and a variation of the

TABLE VIII

VARIATION OF TUMOUR CONTROL PROBABILITY COMPUTED AS A FUNCTION OF ABSORBED DOSE *

Absorbed dose (Gy)	Tumour control probability (%)
50	0 0000
55	0 0006
60	5 54
65	50 00
70	84 70
75	96 10
80	99 05
100	99 997

* Based on an initial clonogenic cell number of 8×10^7 and $D_{0(eff)}$ for fractionated irradiation of 3 5 Gy, giving a 50 % tumour control probability at 65 Gy (From Withers and Peters [39])

response with dose was no longer expected (see Fig 1) Although a reevaluation of these data [32] resulted in a less steep curve (see Table IX), Stewart and Jackson [30] came to similar conclusions for T3 larynx tumours when increasing the absorbed dose from 52 5 Gy to 55 and 57 5 Gy (i e a 5 % or 10 % difference), the local control rate increased from 35 % to 45 % and 70 %, respectively In the same review for T_2 tumours, a 5 % increase in dose (from 52 5 to 55 Gy) slightly improved the (already high) local control rate from 65 % to 80 % As can be expected, for T1 tumours, the dose-effect relation leveled off at 52 5 - 57 5 Gy, where the local control rate was as high as 95 %

TABLE IX.

RELATIVE STEEPNESS OF THE DOSE-EFFECT CURVE FOR LOCAL TUMOUR CONTROL

The steepness is expressed as the relative increase in absorbed dose (in %) producing a change in tumour control probability from 50 to 75 %

Site of tumour	Steepness (%)
Supraglottic larynx T_2 and T_3 (Shukovsky)	5
Larynx T3 (Stewart and Jackson)	6
Supraglottic larynx all stages (Hjelm-Hansen et al)	11
Larynx all stages (Hjelm-Hansen et al.)	12
Bladder T_{4B} (Battermann et al.)	13
Epidermoid carcinoma head and neck (Cohen)	13
Supraglottic larynx T_1 and T_2 (Ghossein et al.)	13
Skin and lip (Strandqvist)	17
Supraglottic larynx T_2 and T_3, revised analysis of the Shukovsky date (Thames et al.)	17
Nasopharynx T_1 and T_2 (Tokars and Griem)	18
Nasopharynx (Moench and Philips)	19
Lymphoma (Fuks and Kaplan)	21
Retromolar trigone/anterior faucial pillar T1 and T2 (Thames et al)	21
Bladder all stage (Morisson)	26
Base of tongue T_1 and T_2 (Thames et al)	31
Tonsillar fossa T_3 and T_4 (Thames et al)	32
Hodgkin (Kaplan)	46
Base of tongue T_3 and T_4 (Thames et al)	50

From Mijnheer, Battermann and Wambersie [27]

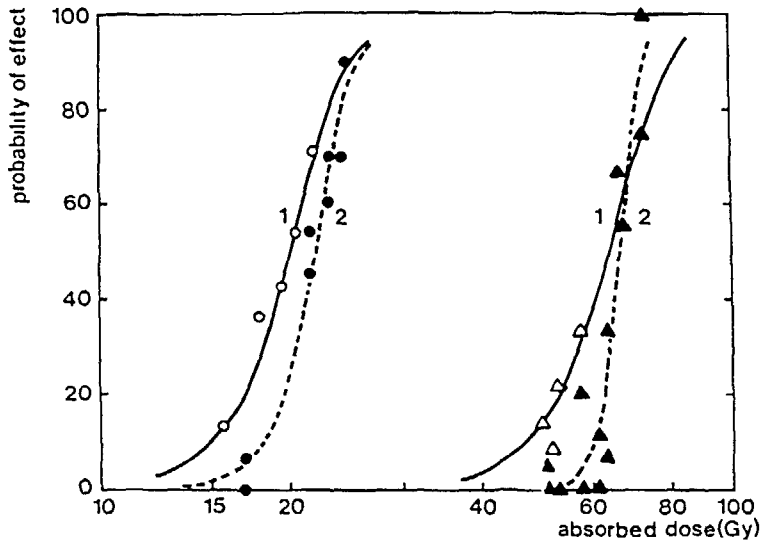

FIG 2

Treatment of bladder tumours (T4B) with photons (triangles) and fast neutrons (circles)

The dose-effect relationships for tumour control (1) (open symbols) and for skin and intestinal damage (2) (closed symbols) are indicated As the curves for skin and intestinal damage are almost identical, just one curve is shown The curves have been computed adopting the equation

$$p = \exp (a + bD) / [1 + \exp (a + bD)]$$

where P is the probability for an effect and D the absorbed dose

(modified from Battermann et al , [1])

Even for Hodgkin disease, Kaplan [22] has shown a rather steep dose-response relation the local cure rate increases from 22 % to 40 %, 65 % and 95 % when the dose increases from 5 to 10, 20 and 40 Gy respectively

Figure 2 presents the data reported more recently by Battermann et al. [1] for T4B bladder tumours A very steep dose-effect curve is observed both for photons and fast neutrons (see below)

The data available at present are summarized in Table IX where the relative slope of the dose-effect curves is expressed as the difference in dose (in percent) producing a change in tumour control probability from 50 to 75 %, which corresponds to the current clinical range Thus, a small value for the relative steepness is related to a steep dose-effect curve The figures range between 5 and 50 %, but are smaller than 20 % for the small head and neck tumours The data presented in Table IX indicate the influence of the absorbed dose level only, all other parameters being kept constant The table does not refer to situations where the irradiation techniques and thus the resulting dose distributions differ, as often occurs, when data obtained using different techniques or data from different centres are compared

The level of accuracy required in radiotherapy can also be derived from the evaluation of the minimum dose variation which can be detected clinically In that respect the data obtained at the Institut Gustave Roussy on tonsillar carcinoma [9] indicate that a difference in dose of 10 % can be detected from the observation of tumour regression In that randomized clinical trial published in 1967, photons and electrons were compared, but for several reasons which were discussed [37], the dose delivered per week was 10 % lower in the electron group than in the photon group This difference in "nominal target absorbed dose" resulted in a faster tumor regression in the photon group relative to the patients irradiated with electrons As no RBE effect could be invoked to explain this observation, it could be concluded that a difference in target absorbed dose of 10 % is clinically detectable Because the group of patients was randomized, tumour regression could be assumed to be a relevant parameter to calculate the efficiency of the treatment However, for the same "nominal target absorbed dose", the dose distribution was different for photon and electron irradiation, which could also influence tumour regression

Although the importance of accuracy in target dose delivery is well recognized, the role of precision remains a subject of debate Recently, using mathematical modelling, Boyer and Schultheiss [3]

concluded that the cure rate of early stage patients increases by about 2 % per 1 % improvement of precision in dose delivery

II 2 3 Dose-effect relationships for normal tissue tolerance

As far as normal tissue reactions are concerned, there is a lot of experimental evidence that here also steep dose-effect curves are observed As an example, for intestinal tolerance in mice (Fig 6), the survival at 6 days after a single fraction irradiation decreases from 75 % to 50 % when the dose is increased by 14 9 % (Table XVI) The dose-effect curve is even steeper after 10 fraction irradiation, and the survival of the animals at 5 5 days is reduced from 75 % to 50 % when the absorbed dose is increased by 9 4 % [12]

There is also clinical evidence that steep dose-effect curves exist for normal tissue tolerance The first ones were reported by Herring and Compton [17] from the analysis of the data of Fletcher for laryngeal oedema and sigmoiditis and of the data of Phillips and Buschke for myelitis

Table X summarises the clinical data at present available They are presented in a similar way as the tumour data in Table IX, but the relative increase in dose (in %) producing an increase in normal tissue complications (NTC) from 25 % to 50 % is quoted (as a matter of fact this range corresponds better to the current clinical situation) The quoted steepness increases from 2 to 17 % depending on the tissue and irradiation conditions

Similarly as for tumour control (see section II 2 2), the required accuracy can also be derived from the assessment of the difference in dose which can be detected clinically from normal tissue reactions Wambersie et al [38] found for early skin reactions after high-energy electron irradiation that, on adjacent fields in the same patient, a difference in dose of 10 % could be detected in 80 % of the cases and a difference in dose of 20 % could be detected in 90 % of the cases (in the dose range corresponding to erythema and dry desquamation) In symmetrically irradiated supraclavicular fields, differences in dose of about 5 % could be detected clinically Similar conclusions were reached by Turesson and Notter [33] The effect of a dose difference of 6 to 7 % could be detected to a significant level by reflectance determination for skin erythema, but not for pigmentation

TABLE X.

RELATIVE STEEPNESS OF THE DOSE-EFFECT CURVE FOR NORMAL TISSUE REACTION

The steepness is expressed as the relative increase in absorbed dose (in %) producing a change in the probability for normal tissue reaction from 25 % to 50 %

Normal tissue reaction	Steepness (%)
Major chronic complications of the larynx (Harwood and Tierie)	2
Peripheral neuropathy (Stoll and Andrew)	3
Late skin damage (Battermann et al.)	4
Late intestinal damage (Battermann et al.)	4
Brachial plexus (Svensson et al.)	5
Radiation pneumonitis (van Dijk et al.)	6
Skin reaction (Turesson and Notter)	7
Major complications of the intestine and bladder (Morrison)	9
Skin and lip (Strandqvist)	10
Myelitis (Phillips and Buschke)	15
Major and non major complications of the larynx (Ghossein et al.)	17

From Mijnheer, Battermann and Wambersie [27]

III. GEOMETRICAL PROBLEMS

As far as geometry problems are concerned, we have to distinguish the prescription of the treatment and its execution

- the treatment prescription includes the adequate delineation of the target volume taking into account the tumour type and extent, as well as tissues at risk in the vicinity;

- the treatment execution includes the patient positioning (and immobilisation) and beam positioning with respect to the patient, according to the planned beam arrangement,

- the selection of the beam quality (photons/electrons), beam energy and arrangement (number, size, orientation) can be considered as part of the prescription and/or execution (the border between prescription and execution should not be too rigid).

When a recurrence or a complication is observed, there is a tendency to incriminate the dosimetry (dose level) with the implicit assumption that the beams were correctly positioned. It is often difficult to evaluate a posteriori the influence of a geometrical error When detected, it is immediately corrected and the only permanent documents are the portal films and eventually the records of the machine parameters. These are only a small part of the successive steps involved in a correct positioning

III. 1 Random errors in patient positioning

During patient positioning "random" and/or "systematic" errors can be introduced The possible consequences of random errors have been thoroughly analyzed by Goitein [10] [11], they can result in distortion of the dose distribution which in turn could influence the local control rate or complication rate. The distinction between random errors and systematic errors is not always easy Some examples in patient positioning, and their consequences, will be presented.

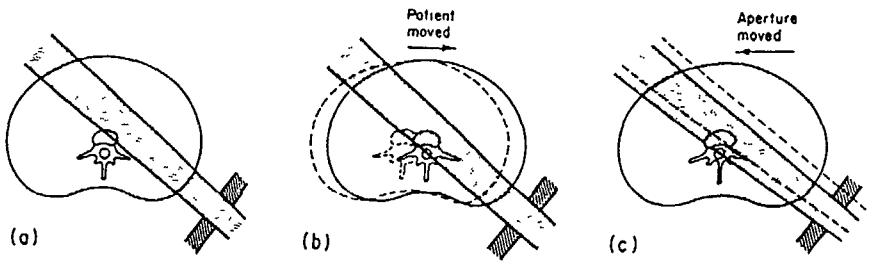

FIG. 3.

(a) A single posterior oblique field designed to avoid the cord while treating a central target (b) A possible alignment error in which the patient is displaced laterally relative to the intended position (shown with dashed lines) The cord is then at the geometric edge of the beam (c) Calculationally equivalent situation to that shown in (b) in which a aperture is considered to have been displaced laterally to the patient.

From Goitein [10]

III. 1 1. Distortion of the dose distribution

Distortion of the dose distribution due to positioning errors is illustrated in Fig. 3, for a single posterior-oblique field [10]. The relative position of the beam with respect to the target volume can be altered either by a wrong position of the patient, a wrong position of the beam or both. Assuming a given uncertainty in the relative positioning, one can identify (Fig. 4) :

- a tissue volume which remains always within the geometrical limits of the fields;

- volumes which are always outside the field limits;

- a transition zone Its width depends of course on the uncertainty which was estimated to be 1 cm in the example discussed by Goitein [10].

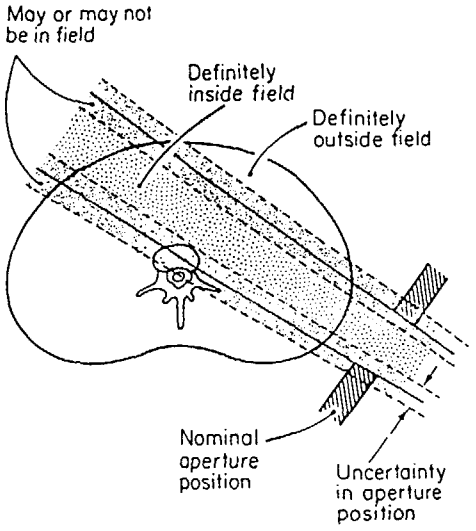

FIG. 4.

Schematic representation in two dimensions of the zone of uncertainty near the geometric edge of the aperture. Points inside that zone are (at the confidence level implied by the thickness of the zone selected) likely always to be "inside" the field. Points outside are likely always to be "outside" the field. Points within the crosshatched zone may or may not be within the field.

From Goitein [10]

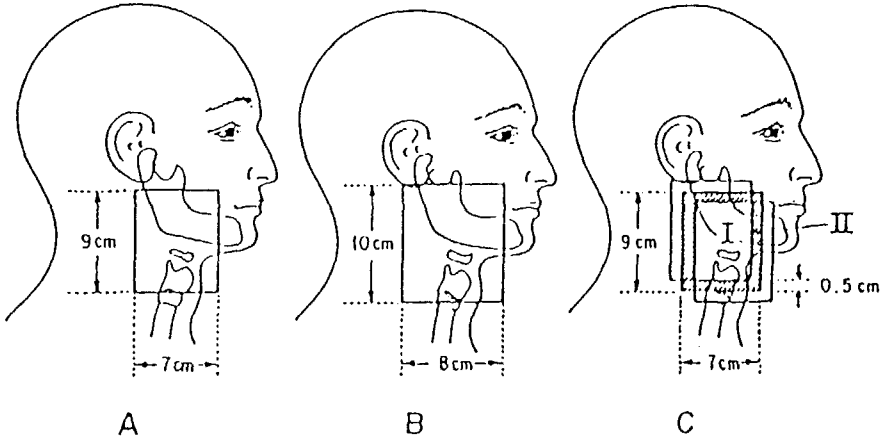

FIG. 5.

Treatment fields considered typical for treatment of squamous-cell carcinoma of the suppraglottis.

A. The tight field used with good immobilization.

B. The loose field used with less careful immobilization. The volume of this field is (10 x 8) / (9 x 7) = 27 % larger than that of the tight field.

C. A region of reduced dose (II) within the margins of a 9 cm x 7 cm field due to random ± 5 mm immobilization error.

From Goitein and Busse [11]

In simple cases (single beam, parallel opposed beams) it is relatively easy to imagine the consequences of positiong errors. However, for more complicated (and not infrequent) beam arrangements (3 or more fields), the "intuitive approach" is difficult and could be misleading. Therefore, in addition to the dose distribution currently computed assuming the "ideal" positioning, Goitein proposes to compute also the dose distributions in the extreme cases (Fig. 4). This additional workload is justified in a number of cases.

III.1.2. Loss in local control rate

Goitein and Busse [11] have evaluated the consequences of an inaccuracy in positioning with regard to local control rate for the particular case of squamous-cell carcinoma of the head and neck area. It was assumed that the target volume can be adequately covered by 2 parallel opposed fields, 9 cm x 7 cm in size; the inaccuracy in positioning was estimated to be 5 mm (Fig. 5).

TABLE XI.

IRRADIATION OF SUPRAGLOTTIC DISEASE			
	Field size (cm x cm)	Tumour control probability 66 Gy Dose level	74 Gy Dose level
Standard setup	9 x 7	59 %	95 %
Enlarged field	10 x 8	44 %	90 %
Dose in margin			
18 % low	9 x 7	47 %	85 %
50 % low	9 x 7	19 %	31 %

From Goitein and Busse [11]

TABLE XII

IRRADIATION OF HODGKIN'S DISEASE		
	Field size (cm x cm)	Tumour control probability 44 Gy Dose level
Standard setup	30 x 12	98 7 %
Enlarged field	32 x 14	98 3 %
Dose in margin		
18 % low	30 x 12	98 4 %
50 % low	30 x 12	96 5 %

From Goitein and Busse [11]

Two alternatives can be considered First, if the therapist is aware of the limitations of his positioning technique, he will compensate by enlarging the field size In the chosen example, a 9 cm x 7 cm field is then replaced by a 10 cm x 8 cm field, i e a 27 % increase of the beam section (or volume of irradiated tissue) The normal tissue tolerance decreases with the size of the irradiated volume, in the present conditions, the decrease in dose can normally be expected to be 3 % In turn the consequence of a 3 % reduction in dose, on the tumour control rate, can be evaluated from the dose-effect relationship (or its slope) at the considered dose level (Table XI) For example, using the data of Shukovsky [29], at 74 Gy a 3 % dose reduction will reduce the tumour control rate from 95 % to 90 %, at 66 Gy (steeper part of the dose-effect relation), it will reduce the control rate from 59 % to 44 %

In the second alternative, it is assumed that no action is taken to compensate for the inaccuracy in positioning (5 mm at each of the 4 field edges) There will be a decrease in dose at the border or the target volume, the consequences of which are evaluated The marginal recurrence rate was calculated (Table XI) for different assumptions on the number of cancer cells present and on the dose reduction in the peripheral strip

A similar evaluation has been performed for Hodgkin patients The consequences of inaccurate positioning were found less dramatic (Table XII) than for head and neck, this could be explained, at least partly, by an apparently shallower dose-effect curve for tumour control This can be due to the heterogeneity in the tumour group (e g histology) and does not exclude the existence of a steeper dose-effect curve for some subgroups of Hodgkin patients The rather large field size used in the treatment of Hodgkin's disease could also be an explanation

III 1 3 The different factors producing random errors in patient positioning.

The relative importance of some factors which could lead to random errors has been investigated by Blanco et al [2] using multiple

verification films A first study was performed on lung carcinoma Statistical analysis was performed on the film documents taken in routine conditions during radiotherapy treatment Among the factors involved when a positioning error was detected, tumour extent and patient's general and psychological condition, were found most frequently Field complexity (e g shielding blocks) was also found to increase the error rate, as well as irradiation in prone position as compared to supine position

On the other hand, the error rate was not dependent on the moment at which the control was made (beginning, middle or end of the therapy course), which implies the constancy of the treatment quality all over the treatment

III 1 4 Random errors in transition from simulation to treatment and treatment-to-treatment variations

Huizenga et al [19] reported the results of a study on the accuracy in radiation field alignment for treatments of head and neck tumours For this analysis 138 verification films were compared to 55 simulation films in 22 patients

When going from simulation films to verification films at the treatment machine, the distance between the corresponding points at the field edges was found to be 5 mm on the average, with a standard deviation of 5 mm (these figures are consistent with the inaccuracy estimated by Goitein and Busse [11] (see above) From an analysis of a series of verification films taken every three sessions, variations are as large as the errors due to the transition from the simulation to the treatment situation Variations of the patient's position within the cast was clearly one of the error sources

III 2 Systematic errors in patient positioning

Up to now only "random positioning errors" were considered The consequences of a systematic error in the positioning and/or in the appreciation of the disease extent are even more dramatic, they are discussed in this section

TABLE XIII

Radiotherapy of Hodgkin's disease (1973-1974)
Infield or marginal recurrence rate for 5 selected North American Centres

Facility	Number of patients	Relative rate of infield recurrence at 3 years *
A	48	2 89
B	43	0 49
C	33	0 62
D	42	0 00
E	45	0 92
	$p \leq 0\ 00006$	

* corrected for stage, and expressed as the ratio of observed to expected infield recurrences Values greater than 1 0 reflect increased recurrence rate, values smaller than 1 0 fewer than expected

From Kinzie et al , [23]

A clear illustration of the role of the geometry problems in the outcome of a radiation treatment has been provided in the "Patterns of Care Study" [15] [23] The geometry problems are particularly important when complex irradiation techniques have to be applied, as for example for patients with Hodgkin's disease [14]

The records of 200 patients treated for Hodgkin's disease were reviewed, which corresponded to a total number of 990 involved lymph node areas These patients were treated in 5 U S centres (referred to as centres A, B, C, D and E, in Table XIII), "selected" on the base of their large recruitment and experience

TABLE XIV.

Radiotherapy of Hodgkin's disease (1973-1974)
Frequency of inadequate portal margins by facility

Facility	Number of patients	Patients with inadequate margins
A	54	34 (63 %)
B	50	12 (24 %)
C	37	12 (33 %)
D	50	8 (16 %)
E	41	11 (24 %)
Total	232	77

From Kinzie et al [23]

TABLE XV

Radiotherapy of Hodgkin's disease (1973-1974)
Effect of inadequate portal margins on infield (or marginal) recurrence

	Number of patients	Recurrence rate (%)
Adequate margins	115	8 %
Inadequate margins	66	32 %

From Kinzie et al [23]

The infield recurrence rate was evaluated for each centre For centres B, C, D and E, it was lower than the average value over the U S centres (this average value is referred to, in Table XIII, as the "expected" value) On the other hand, the infield recurrence rate of centre A is about 3 times as high as the expected value

In order to explain this observation, the portal films were reviewed and a higher proportion of inadequate margins was observed in centre A (63 % compared to 16-33 % for the other centres, see Table XIV) In addition, the importance of inadequate margins on portal films is illustrated by the fact that the infield recurrence rate is 4 times higher for patients with inadequate margins (32 % and 8 % respectively, see Table XV)

When patients were treated with combined chemotherapy and radiation therapy, the survey did not show any increased infield or marginal recurrence rate, even with inadequate portal margins This indicates that MOPP chemotherapy can compensate for technically inadequate radiation therapy (which is obviously not the goal of chemotherapy)

This study illustrates how, in the presence of an infield recurrence, one has to check first the field size, and the patient positioning (i e retrospectively the portal films) before invoking a tumour radioresistance, a wrong selection of the prescribed dose or a dosimetric error As a matter of fact, there was no dose-response relation between 30 and 50 Gy (in that dose range, the local control rate was higher than 94 %)

IV ACCURACY REQUIRED IN THERAPY WITH FAST NEUTRONS AND OTHER TYPES OF NON-CONVENTIONAL RADIATION

Fast neutrons is the most widely used type of non-conventional radiation and will be considered first The required accuracy in dose delivery depends on the steepness of the dose-effect curves, and on their separation between tumour control and normal tissue damage They will be compared for neutron and photon irradiations

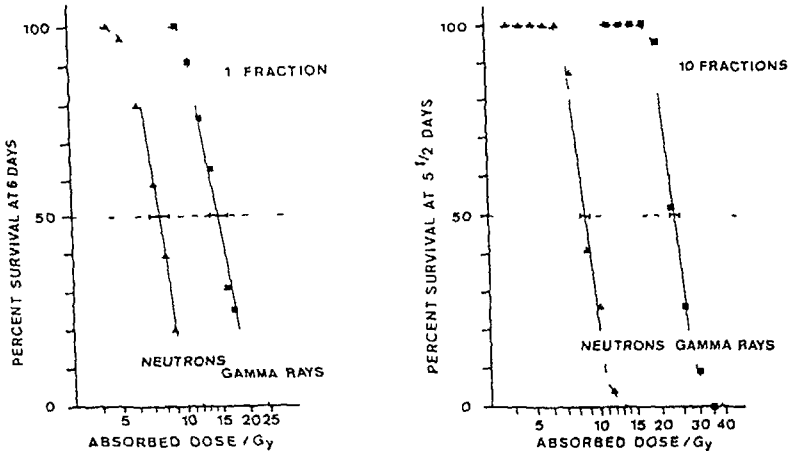

FIG 6

Dose-effect relationships for intestinal tolerance in mice after abdominal irradiation with ^{60}Co gamma rays and d(50)+Be neutrons Intestinal tolerance is assessed from the survival of the animals scored 6 days after a single fraction irradiation (left) or after 10 fraction irradiation (right) In this latter case, the successive fractions are separated by 3 5 h and the survival is scored at 5 5 days after the mid-point of the irradiation (i e after the fifth fraction) (modified from Gueulette [12]

IV 1 Comparison of the steepness of dose-effect curves after photon and neutron irradiation

Dose-effect curves for normal tissue and tumour response in vivo after photon and neutron irradiation in animals have been reported by different authors In Fig 6, as an example, dose-effect curves are presented for early intestinal tolerance in mice after single and fractionated irradiation with ^{60}Co gamma rays and d(50)+Be neutrons [1]

[1] According to the ICRU terminology, d(50)+Be signifies neutrons produced by deuterons with an energy of 50 MeV impinging on a thick beryllium target

TABLE XVI

Comparison of the relative gradient of the dose-effect curves Δ50/75 for intestinal tolerance in mice after abdominal irradiation with photons and neutrons for single and fractionated irradiation

Fractionation	Δ50/75*	(95% confidence interval)
Single fraction	14 9	(12 3-19 2)
10 fractions	9 4	(7 6-12 2)

*Δ50/75 is expressed as the relative increase in absorbed dose (in %) producing a change in survival from 75 to 50 % The relative gradients Δ50/75 are not significantly different after photon and neutron irradiation, and only one value is given for both radiation qualities

From Mijnheer, Battermann and A Wambersie [27]

The data have been analysed using the logistic model [6] which gave a good fit to the curves The resulting values for the relative steepness of the curves for photon and neutron irradiation are not significantly different A similar conclusion can be drawn for the bone marrow syndrome [12] and for late spinal cord damage [34] The steepness is, however, significantly different between single and fractionated irradiation This is illustrated in Table XVI which shows that the relative steepness (the reciprocal of Δ 50/75) for intestinal tolerance is higher for fractionated irradiation than for single fraction irradiation A similar observation was made for other biological systems [8] [28]

The steepness of the dose-effect curves for tumour control and normal tissue damage after neutron and photon irradiation in patients has been compared, as an example, for the curves presented in Fig 2 The relative gradients of these curves are presented in Table XVII For the

effect on the tumour, no difference in relative gradient can be observed after photon or neutron irradiation However, for late normal tissue damage the lower Δ50/25 value observed for photons relative to that for neutrons might indicate that the photon dose-effect curve is somewhat steeper compared to the neutron dose-effect curve, although not statistically significant Clinical data are not always available in the ranges of effect compared in Table IX and Table X tumour control can be smaller than 50 % whereas a probability for normal tissue damage of 25 % is unacceptable for the complications mentioned in Table X

For instance, in Fig 2, no tumour control probability larger than about 40 % has been observed in the photon series, and consequently Δ 75/50 has to be estimated For the analysis of the curves presented in figures 6 and 2, the logistic model described by Cox [6] was used, giving the relationship between the probability P for tumour control or normal tissue damage and the absorbed dose D by the formula

$$P = \exp(a+bD) / [1 + \exp(a+bD)] \qquad (1)$$

The values of the parameters a and b were determined from the clinical data and can be found elsewhere [1] The absolute steepness of the curve represented by Eqn (1) can now be given in a quantitative way For instance, at the P = 50 % effect level, the absolute steepness is given by b/4 In order to compare the steepness of corresponding neutron and photon dose-effect curves, the absolute steepness b/4, for the neutron dose-effect curve, has to be divided by the RBE at the 50 % effect level The steepness of the curves presented in Fig 2 and calculated in this way, is also given in Table XVII By applying the absolute steepness at the 50% dose level, the same conclusions are obtained as using the relative gradient approach at two different levels of effect

From the animal and patient data it can then be concluded that for the effects on the tumour and the early injury to normal tissue no significant difference in relative steepness is observed between photons and neutrons For some of the late normal tissue data, the dose-effect

TABLE XVII.

Comparison of the relative gradient and the absolute steepness of the dose-effect curves after photon and neutron irradiation of T4B bladder tumours

Clinical effect	Δ75/50 or Δ50/25	$b/4$	Δ75/50 or Δ50/25	$(b/4) \times (1/RBE)$
	Photons		Neutrons	
Serious skin and intestinal damage	4 ± 1	0 10 ± 0 03	10 ± 3	0 05 ± 0 02
Bladder tumour control	13 ± 9	0 03 ± 0 03	11 ± 3	0 04 ± 0 01

Δ75/50 and Δ50/25 are the relative gradients expressed as the increase in absorbed dose (in %) producing a change in tumour control probability from 50 to 75 % or a change in the probability for normal tissue damage from 25 to 50 %, respectively

The absolute steepness at the 50 % effect level of the clinical effect is given by $b/4$ (in Gy^{-1}) for the photon curve and by $(b/4) \times (1/RBE)$ (in Gy^{-1}) for the neutron curve, with the RBE corresponding to the 50 % effect level The dose-effect data have been fitted by the formula $P = \exp(a+bD) / [1 + \exp(a+bD)]$

From Mijnheer, Battermann and Wambersie [27]

curve seems somewhat steeper for photons relative to neutron, although within the statistical uncertainty

IV 2 Fast neutrons and a reduction of the differential effect

Historically, fast neutrons were introduced in therapy because of the existence of hypoxic cells and the reduction in OER with increasing LET However, high-LET radiations exhibit other differences in their biological properties, when compared to low-LET radiations [36]

- a reduction of the differences in radiosensitivity from cell line to cell line (i e "intrinsic radiosensitivity"),
- a reduction of the differences in radiosensitivity related to the position of the cell in the mitotic cycle (Fig 7),
- less repair phenomena, and as a consequence less importance of differences in repair phenomena and less differences between the responses of the cell populations to different fractionation schemes

These observations can be summarized by saying that all cell populations, in all conditions, tend to respond in a more similar way when exposed to neutrons compared to photons A reduction in OER is always an advantage, since the normal tissues are well oxygenated On the other hand, a reduction in the differences of intrinsic radiosensitivity, or a reduction in the differences of radiosensitivity related to cell position in the mitotic cycle, or a general reduction in the repair phenomena could bring an advantage or a disadvantage depending on the characteristics of the tumour and of the normal tissue(s) at risk for a particular patient This raises the important problem of patient selection

As a consequence, with high-LET radiation, there is a need for a high physical selectivity, which proceeds from the reduced difference in radiosensitivity When large differences in radiosensitivity are observed between the cancer and normal cell populations, a poor physical selectivity is of limited consequence In typical cases, such as seminomas or lymphomas, the dose prescribed to the target volume is

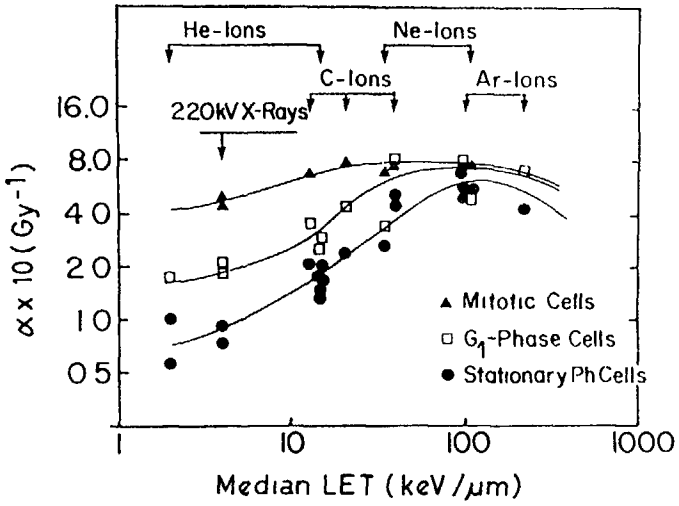

FIG 7

Single-hit inactivation coefficients (α) for homogeneous populations of mitotic, G1-phase, and stationary phase Chinese hamster cells irradiated with 220 kV X-rays and various charged-particle beams, as a function of median LET (in keV/μm)

(modified from Chapman [5])

well below the tolerance dose, and irradiation of a few additional cm3 of normal tissue would be of little clinical importance (in chemotherapy, there is obviously no physical selectivity at all, and the potential therapeutic gain depends only on a biological selectivity) In contrast, when the differences in radiosensitivity are reduced with high-LET radiation, the therapeutic efficiency mainly rests on a high level of physical selectivity, sparing a few cm3 of normal tissues then becomes really important

IV 3 Other types of non-conventional radiation

IV 3 1 Proton beams

The rationale for introducing proton beams in therapy is the improved physical selectivity On the other hand, the biological effects

produced by protons are similar to those produced by photons, and no benefit has to be expected as far as the differential effect is concerned

The superiority of proton beams compared to photons (or electrons) is obvious for the irradiation of radioresistant tumours located close to radiosensitive structures (e g uveal melanomas, chordomas or chondro-sarcomas of the base of the skull, paraspinal tumours) There is however a recent trend for irradiating a larger proportion of patients with protons As a matter of fact, since an improved physical selectivity is in itself always a benefit, all photon patients are "in principle" potential candidates for proton beam therapy [35]

IV 3 2 Helium ion beams

For the present discussion, helium ion beams can be considered as being similar to the proton beams For the energies involved, they are low-LET radiations and they allow to achieve similar dose distributions

IV 3 3 Heavy ion beams

Heavy ions combine the advantages of high-LET radiation for the treatment of some tumour types and an excellent physical selectivity Heavy ion beams exhibit similar depth dose curves as proton or helium ion beams (i e a Bragg peak which has to be spread out adequately to cover the target volume)

However, much higher energies have to be used (about 500 MeV per nucleon for O, C or Ne ions), which implies a considerable increase in the cost and complexity of the accelerator So far, only one heavy ion therapy program has been carried out, at the BEVALAC in Berkeley, and limited clinical experience is available at present There is another project of heavy ion therapy at the NIRS in Japan, and 2 projects in Europe at the GSI in Darmstadt (Fed Rep of Germany), and the EULIMA project (European Light Ion Medical Accelerator)

V CONCLUSION

There is an increasing amount of clinical evidence indicating that a high degree of accuracy in dose delivery is essential for the success of radiotherapy In general, the highest possible accuracy should be aimed at It applies to the dose level as well as the dose distribution (physical selectivity)

As far as the dose level in photon therapy is concerned, a requirement for an accuracy of 3 5 % has been proposed (i e one relative standard deviation, combining types A and B uncertainties) for the dose at the specification point At other points in the target volume a 5 % (one standard deviation) dose accuracy requirement is more appropriate It should be noted that the 3 5 % and 5 % criteria for the accuracy in dose delivery serve only as simple guidelines for daily clinical practice In many cases larger values are acceptable but in a few special cases an even smaller value should be aimed at if very steep complication curves are involved From a practical point of view it is, however, difficult to conceive several levels of accuracy in the same radiotherapy department

The radiobiological and clinical data obtained with fast neutrons indicate that the dose response curves for tumour control and normal tissue complications are as steep for high-LET radiation as those observed with low-LET radiation The same accuracy in dose delivery should then be aimed at

As far as the physical selectivity is concerned, it is more important with high-LET than with low-LET radiation, since the (biological) differential effect between cell populations is, in general, reduced with high-LET radiation

Heavy charged particles are needed especially in those clinical situations where the physical selectivity is essential, i e typically radioresistant tumours close to critical normal structures

The accuracy in dose delivery in radiation therapy results from a chain of successive procedures In order to keep the final accuracy within the required limits, each step of the chain has to be as accurate as possible

TABLE XVIII

PHYSICAL DATA NEEDED IN HEAVY PARTICLE THERAPY

Materials
1 Human tissues N, O, C, H, (Ca), (A150 plastic)
2 Detector materials gas, solid state
3 Collimation/shielding Pb, W, Fe
Particles and energy ranges
Neutrons up to 65-70 MeV
Protons up to 250 MeV
Helium ions up to 650 MeV
Heavy ions C, O, Si, Ar, Ne, up to 500-900 MeV per nucleon

The clinical and technical problems related to dose delivery are at one end of the chain, and the acquisition of basic physical data (i e atomic and molecular data) are at the other end

Basic physical data are needed in order

1) to evaluate the kerma, and the absorbed dose in the different human (and biological) tissues,

2) to determine the response of the different detectors (kerma and absorbed dose in the detector materials),

3) to optimize the collimation systems and thus improve the physical selectivity,

A list of materials, and of particle types and energy ranges, for which atomic and molecular data are needed is proposed in Table XVIII

REFERENCES

1 J J Battermann, A A M Hart & K Breur, Dose-effect relations for tumour control and complication rate after fast neutron therapy for pelvic tumours, Brit J Radiol 54 (1981) 899-904

2 S Blanco, M A Lopez-Bote & M Desco, Quality assurance in radiation therapy Systematic evaluation of errors during the treatment execution, Radiotherapy and Oncology 8 (1987) 253-263

3 A L Boyer & T Schultheiss, Effects of dosimetric and clinical uncertainty on complication-free local tumor control, Radiotherapy and Oncology 11 (1988) 65-71

4 W A Brock, M H Maor & L J Peters, Predictors of tumor response to radiotherapy *Proc Symp* at Lawrence Berkeley Lab , Univ California, Berkeley, California, May 1-3, Radiation Research, 104 (1985) 290-296

5 J D Chapman, Biophysical models of mammalian cell inactivation by radiation In R E Meyn and H R Withers (Eds) Radiation Biology in Cancer Research, Raven Press, New-York, 21-32, 1988

6 D R Cox, Analysis of binary data Methuen monographs series, Methuen, London, 1970

7 A Dutreix, When and how can we improve precision in radiotherapy ?, Radiotherapy and Oncology, 2 (1984) 275-292

8 J J Fischer and J E Moulder, The steepness of the dose-response curve in radiation therapy Radiology 117 (1975) 179-184,

9 R Flamant, E P Malaise, A Dutreix, J Dutreix, M Hayem, P Lazar, B Pierquin & M Tubiana, Un essai therapeutique clinique sur l'irradiation des cancers amygdaliens par faisceaux de photons ou d'électrons de 20 MeV, Eur J Cancer, 3 (1967) 169-181

10 M Goitein, Calculation of the uncertainty in the dose delivered during radiation therapy, Med Phys 12 (1985) 608-612

11 M Goitein & J Busse, Immobilization error some theoretical considerations, Radiology, 117 (1975) 407-412

12 J Gueulette, Efficacité Biologique Relative (EBR) des neutrons rapides pour la tolerance de la muqueuse intestinale chez la souris, These de Doctorat de l' Universite Paul Sabatier de Toulouse, France (1982)

13 G E Hanks, Optimizing the radiation treatment and outcome of prostate cancer, Int J Radiat Oncol Biol Phys 11 (1985) 1235-1245

14 G E Hanks, J J Diamond & S Kramer, The need for complex technology in radiation oncology Cancer (Supplement) 55 (1985) 2198-2201

15 G E Hanks, J J Kinzie, R L White, D F Herring & S Kramer, Patterns of care outcome studies results of the national practice in Hodgkin's disease, Cancer, 51 (1983) 569-573

16 G E Hanks, J M Krall, K L Martz, J J Diamond & S Kramer, The outcome of treatment of 313 patients with T-1 (UICC) prostate cancer treated with external beam irradiation (In preparation, personal communication)

17 D F Herring & D M J Compton, The degree of precision required in the radiation dose delivered in cancer therapy in Computers in Radiotherapy (Glasgow, Scotland, September 1970) Brit J Radiol Special Report n° 5, British Institute of Radiology, (1971) 51-58

18 H Holthusen, Erfahrungen uber die Vertrachlichkeitsgrenze fur Roentgenstrahlen und deren Nutzanwendung zur Verhutung von Schaden,
Strahlentherapie, 57 (1936) 254-269

19 H Huizenga, P C Levendag, P M Z R De Porre & A G Visser, Accuracy in radiation field alignment in head and neck cancer A prospective study, Radiotherapy and Oncology 11 (1988) 181-189

20 International Commission on Radiation Units and Measurements,
Determination of absorbed dose in a patient irradiated by beams of X or gamma rays in radiotherapy procedures
ICRU Report 24, Woodmont Avenue 7910, Washington DC, 20014, USA (1976)

21 International Commission on Radiation Units and Measurements,
Dose specification for reporting external beam therapy with photons and electrons
ICRU Report 29, Woodmont Avenue 7910, Washington D C , 20014, USA (1978)

22 H S Kaplan, Evidence for a tumoricidal dose level in the radiotherapy of Hodgkin's disease, Cancer Research 26 (1966) 1221-1224

23 J J Kinzie, G E Hanks, C J Maclean, S Kramer, Patterns of care study Hodgkin's disease relapse rates and adequacy of portals, Cancer, 52 (1983) 2223-2226

24 S Kramer, The patterns of care study A nationwide evaluation of the practice of radiation therapy in cancer management, Int J Radiat Oncol Biol Phys 1 (1973) 1231-1236

25 S Kramer, The study of patterns of cancer care in radiation therapy, Cancer, 39 (1977) 780-787

26 S A Leibel, G E Hanks & S Kramer, Patterns of care outcome studies Results of the national pratice in adenocarcinoma of the prostate, Int J Radiat Oncol Biol Phys 10 (1984) 401-409

27 B J Mijnheer, J J Battermann & A Wambersie, What degree of accuracy is required and can be achieved in photon and neutron therapy ?, Radiotherapy and Oncology 8 (1987) 237-253

28 J V Moore, J H Hendry & R D Hunter, Dose-incidence curves for tumour control and nomal tissue injury, in relation to the response of clonogenic cells Radiotherapy and Oncology, 1 (1983) 143-157

29 L J Shukovsky, Dose, time, volume relationships in squamous cell carcinoma of the supraglottic larynx Am J Roentgenol 108 (1970), 27-29

30 J G Stewart & A W Jackson, The steepness of the dose response curve both for tumor cure and normal tissue injury, Laryngoscope, 85 (1975) 1107-1111

31 H D Suit, Radiation Biology, A basis for radiotherapy in Textbook of radiotherapy, G H Fletcher Ed 75-121, Lea and Febiger, Philadelphia, USA (1973)

32 H D Thames Jr , L J Peters, W Spanos & G H Fletcher, Dose response of squamous cell carcinomas of the upper respiratory and digestive tracts, Brit J Cancer, 41 (Suppl) (1980) 35-38

33 I Turesson & G Notter, Skin reaction as a biological parameter for control of different dose schedules and gap correction Acta Radiol Oncology, 15 (1976) 162-175

34 A J Van der Kogel, Late effects of radiation on the spinal cord Thesis University of Amsterdam The Netherlands, 1979

35 A Wambersie, Is there any future for high-LET radiations ?
Strahlentherapie, 1988 (in press)

36 A Wambersie, G Barendsen & N Breteau, Overview and prospects of the application of fast neutrons in cancer therapy J Eur Radiother 5 (1984) 248-264

37 A Wambersie, J. Dutreix & A Dutreix, Précision dosimétrique requise en radiothérapie Conséquences concernant le choix et les performances exigées des détecteurs, J Belge de Radiologie, 52 (1969) 94-104

38 A Wambersie, H. Zreik, M Prignot & J C Van Dorpe, Variation of RBE as a function of depth in a high energy electron beam in the first millimeters of the irradiated tissues determined by the observation of skin reactions on patients (a clinical trial), Strahlentherapie, 148 (1974) 279-287

39 H Withers & L J Peters, Basic principles of radiotherapy - Biologic aspects of radiation therapy in Textbook of radiotherapy (Third Edition), G.H Fletcher Ed 103-180, Lea and Febiger, Philadelphia, USA (1980)

PARAMETERS CHARACTERIZING CHARGED PARTICLE TRACK STRUCTURES*

H.G. PARETZKE
Institut für Strahlenschutz,
Gesellschaft für Strahlen- und
Umweltforschung mbH München,
Neuherberg, Federal Republic of Germany

Abstract

It is well-known in radiation research that a profound knowledge of the spatial distribution of localized new chemical species produced in matter upon radiation interaction, i.e. the track structure, represents an indispensable prerequisite for the understanding of physical, chemical and biological actions of ionizing radiation. This can easily be shown by the fact that the same dose absorbed from different radiation fields can have different types and/or magnitudes of effects. Charged particle track structures evidently are characterized by joint probability functions describing the locations and types of new species at a given time; they thus represent the initial boundary condition for all subsequent reactions in the affected sector of the irradiated matter and describe it fully at later stages. However, such full descriptions are too complicated in a mathematical sense and, thus, coarser classification quantities have been searched for and introduced. Although major scientific activities are required to improve our knowledge on

a) processes of energy transfer from radiation to matter,
b) chemical modifications of target molecules by the absorbed energy,
c) non-homogeneous biochemical reactions in particle track at early times,
d) identification of parameters characterizing track structures regarding their similarities and dissimilarities with respect to the subsequent reactions,

* Work supported by the Commission of the European Communities under Contract BI6-0011-D(B).

this paper discusses only the specific research needs to improve the scarce present knowledge on parameters characterizing charged particle track structures in matter.

---

1. Introduction

Scientific interest in radiation research can be divided into two subgroups, namely a) research into changes of the physical properties of the penetrating radiation and, b), research into the physical, chemical or biological changes produced in the irradiated matter. Unfortunately and in spite of its large practical importance, the status of knowledge in the latter field of research, i.e. in the target related area, is far less advanced than that in the radiation field related area. There are several reasons for this striking difference in knowledge.

First, many radiation field related processe depend only on two rather macroscopic target parameters, namely the electron density and (the logarithms of) the mean excitation potential; details of the chemical structure and the physical phase state of the target have mostly only minor effects on these types of problems. Properties of molecular changes in the irradiated medium, however, depend rather sensitively on a large number of physical and chemical parameters of the target medium.

Secondly, today it is rather easy to measure changes in radiation field properties introduced by interaction with matter (e.g. with semiconductors), and this can often be done even for single field particles. On the contrary, the short lifetime of early chemical species produced by radiation interaction with matter and the small interspecies distances in condensed matter make track structures left behind in the wake of penetrating radiations rather inaccessible to experimental observation.

Thirdly, there exist clear concepts, quantities, etc. which can be used to unambiguously describe radiation fields and their changes (e.g. the charge, mass, energy, direction of charged particles, the energy spectrum of photon fields, etc.). Equivalent concepts and useful quantities characterizing the structures of charged particlesin a target, i.e. the net effect on the medium of the fast disturbance by the penetration, however, are still missing and only first attempts to overcome this severe drawback can be reported below.

This paper does not deal with three other aspects of charged particle track formation, namely

- with the cross sections describing the probality per unit path segment for particular energy and momentum transfer interactions, since this is topic of other papers at this meeting, and
- with the probabilities, that certain energy and momentum transfers to a target molecule introduce there a certain primary chemical change, i.e. a new chemical species, and
- with those various fast and slow chemical reactions of these primary species with each other and the target matrix which then lead to the formation or expression of a "final" radiation effect, yield, cell mutation, light flash, etc.

However, it should clearly be mentioned, that profound knowledge also on these aspects is an indispensable prerequisite for any mechanistic understanding of radiation effects, and that our present state of the art there is also very unsatisfactory.

2. The Need for Characterization

As has been pointed out by Fano[1] it should be the natural aim of track structure theory to describe and predict the spatial distribution of localized events produced by radiation interaction with a minimum of detailed analysis and of assumptions concerning preliminary physical processes. This should be done by using joint probability functions of

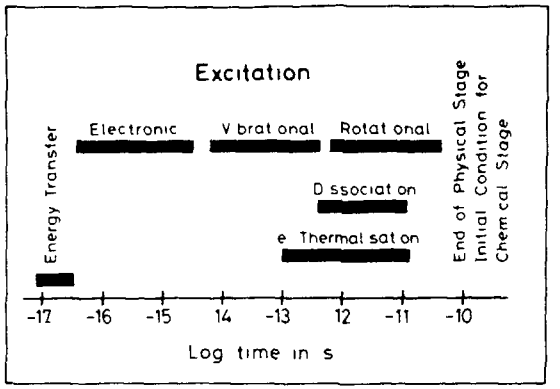

Fig 1 Time sequence of process occurring during the physical stage of track formation

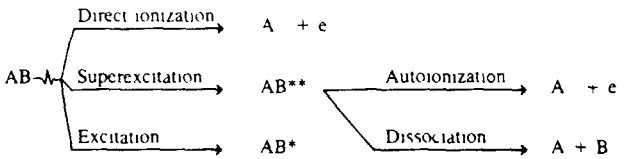

Fig 2 Time sequence of proscesses leading to the formation of new chemical species

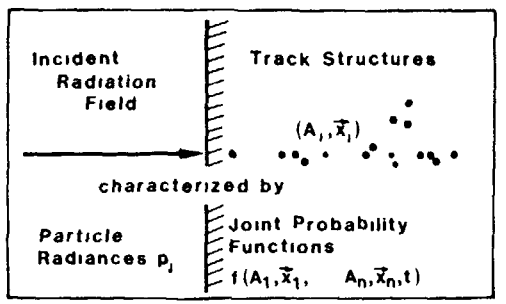

Fig 3 Track structures represent the changes left in a target by an incident radiation field

time describing the probability per unit time to find a certain new chemical species of type A_1 at location $\vec{x}_1$, and at the same time another species A_2 at $\vec{x}_2$, and A_n at $\vec{x}_n$. In this context, a primary event may be defined as a new chemical species of reasonably long lifetime (say, $\geq 10^{-11}$ sec.) (Fig 1) produced as a consequence of an energy transfer from the radiation field to the target molecule (Fig. 2) Such a joint probability function represents and fully characterizes a charged particle track, i e. the ensemble of relevant molecular changes in the irradiated medium, in a similar way as the incident radiation field is characterized by the energies, masses, directions, etc. of all directly and indirectly ionizing particles making up a radiation field (Fig. 3).

It is not meaningful and practicable to describe each single particle in an incident field separately and therefore quantities as e.g. energy spectrum, parameters describing the direction of particles, radiances, etc have been introduced to characterize a field. Concepts and quantities describing the important properties also of the tracks left behind in a target are necessary since it is in general one of the most basic tasks in research to identify the relevant and essential parameters in the usually rather large vectors of descriptors which can be attached to any object, process, etc Such identification then leads to the necessary reduction and concentration of information without which understanding and perception of the essentials cannot be achieved. However, utmost care is in order to not loose essential information by wrong classification. Wrong classification in turn might very effectively inhibit any scientific understanding of a scientific problem Adequate classification requires, in an iterative scientific process, that, first, descriptors for the objects of interest are established, which represent appropriate measures of the objects regarding the intented analysis Then, secondly, the similarities and dissimilarities of these objects must be quantified and they must be ordered according to them

The main problem, in general and also here, is the selection of those quantities/descriptors This selection is necessary to be able to com-

pare effects of different radiation fields in an optimum way, design adaquate measurement devices which are sensitive to the relevant properties of a radiation field, to identify the important parts of the track structure, etc., etc. Various preliminary concepts and parameters used for classification of radiation track structures will be discussed below.

3. Classification by Dosimetry Concepts

Dosimetric concepts belong to the oldest ways of characterization of charged particle tracks in matter. Already in 1937 L.H. Gray[2] assumed that "the most natural unit of radiation dosimetry is the absolute increase of energy of the absorbing medium". Since then the absorbed dose has been the central parameter in radiation research, because it is "devised to provide a physical measure to correlate with actual or potential effects"[3]. However, from our present point of view it has become evident that dose often does not provide a too meaningful base for correlation, and the use and - even more so the frequent misuse of the quantitiy "dose" - might be one of the main reasons for the fact that our understanding of radiation effects is not more advanced inspite of several decades of intense research.

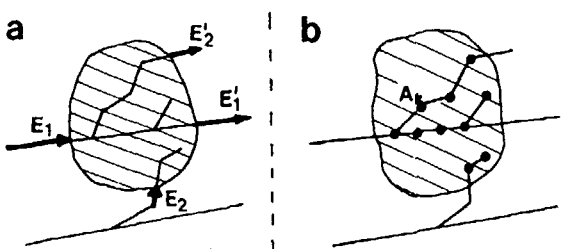

Fig. 4: Definitions of "energy imparted" and "dose".

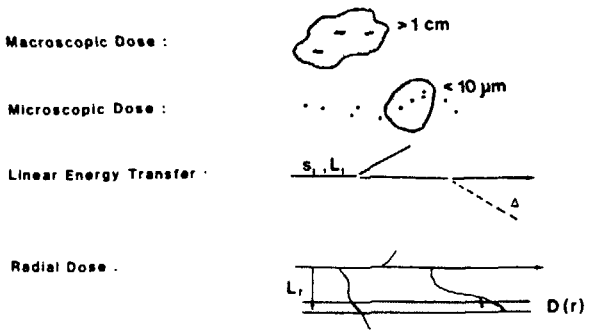

Fig. 5: Some concepts using essentially the parameter "dose" for characterization of charged particle track structures.

The quantity dose can be defined in two ways, which are depicted in fig. 4. The ICRU[3] has defined it as the quotient of $d\bar{\varepsilon}$ by dm, where $\bar{\varepsilon}$ is the mean energy imparted by ionizing radiation to a mass element m, and the energy imparted is defined as the difference between the sum of the energies (excluding the rest energies) of all ionizing particles that enter the mass element and the sum of those which leave the mass element. Evidently, the imparted energy is also the sum of the energies needed to produce all activations (excitations, ionizations, etc.) in the mass element considered.

There are several types of dosimetric concepts (fig. 5), all of which use the quantity" energy deposited/transferred" to a certain mass element, volume or at a certain location as the important parameter to characterize charged particle track structures.

The dose in macroscopic targets is just the total energy deposited by irradiation within a certain volume (typical ≥ 1 cm^3) divided by the mass of that element; it can be measured, e.g. by its corresponding increase in temperature. No additional information can be obtained from this parameter e.g. on the number of ionizations produced or on their spatial density. In radiation research dose is no useful parameter in particular at low doses, since it does not describe the number of primary events in small sites properly.

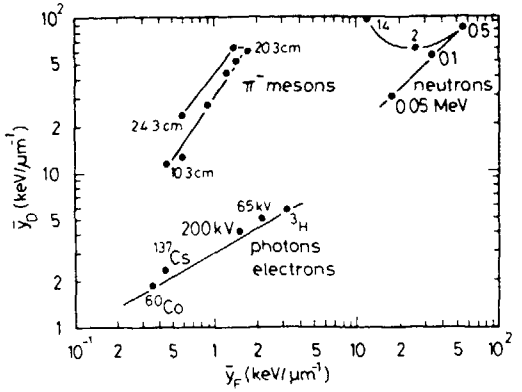

Fig. 6: Dose- and frequency means of microdosimetric linear energy spectra in 1 µm-diameter sites for various radiation fields[4].

Microdosimetric concepts are a refinement of the macroscopic dose concept, and they do describe the number of primary events in small sites properly. They are concerned with a parameterization of track structures essentially by the statistical distributions of energy imparted to very small (typical dimensions ≤ 100 µm³) volumes of interest[4-5]. These distributions show large differences for sparsely ionizing radiations (e.g. X-rays) and for densily ionizing radiations (e.g. alphaparticles). Thus parameterization of track structures can be done in microdosimetric concepts, e.g., by considering the first two moments of such distributions (fig. 6). For the interpretation of radiation action, however, additional non-dosimetric track structure information is necessary.

Higher densities of events along charged particle tracks often show a higher efficiency of producing serious biological effects at the same macro- or micro-dose value than particles with lower ionzation density, or the opposite may be the case. Therefore, concepts have been introduced to classify track structures according to the linear stopping power[7] of the respective charged particles. At the same linear stopping power L, however, fast ions can emit more energic electrons from target atoms which can carry and deposit considerable fractions of the energy transferred at larger distances from the ion path, and, thus, lead to a "dilution" of the energy and event density along the ion path. To account for this effect, related concepts of energy-restricted stopping power[7] L_Δ, radius restricted stopping power[7] L_r, and radial dose profiles[8,9] $D(r) \sim -\frac{dL_r}{dr}$, have been introduced to characterize the important aspect of track structures. One common problem for all of these L-concepts is their concentration on first moments (mean values) of energy/event-density distributions, which is likely to be an information reduction on a too early stage since a particular track and the related particular response of the irradiated matter do not "know" about the "average" track and "average" response.

Further problems in all those concepts are mainly due to

a) the failure of the so-called optical approximation at low electron energies and for larger energy transfers,
b) the neglectance of spatial correlations between primary activations regarding the subsequent reactions,
c) the use of only one or two moments (e.g. mean value) of in fact stochastic distributions (e.g. fig. 6).

Because of these problems dosimetric concepts may be useful for measurements in radiation fields but are alone only of limited usefulness for the interpretation and mechanistical understanding of radiobiological data. They may be useful to determine the various amounts of directly and indirectly ionizing particles impinging on a target of the same radiation field. However, they provide not an useful basis for an intercomparison of effects of different radiation fields and for interpretation of radiation action.

4. Classification Concepts based on Track Entities

As has already been mentioned in the introduction that adequate theories describing charged particle track structures themselves or their

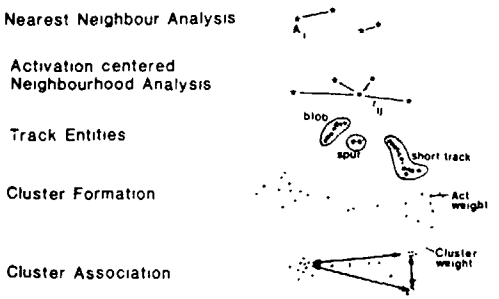

Fig. 7: Some classification concepts based on activations (new track species).

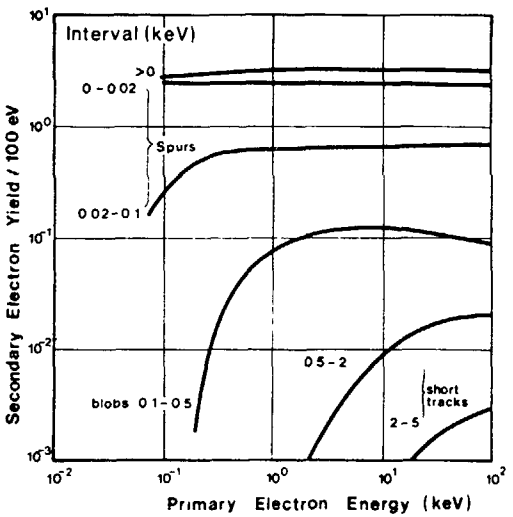

Fig. 8: Yields of track entities for electrons in water.

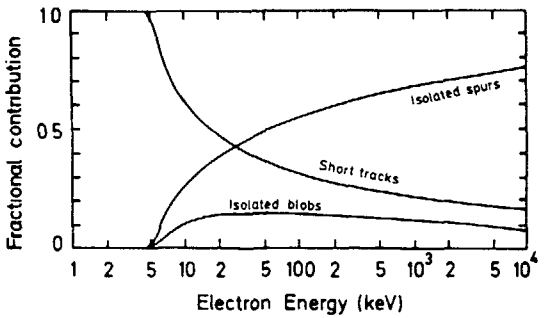

Fig. 9: Fractions of short tracks, blobs and spurs in the tracks of fast electrons.

relevant parameters are still lacking. However, there are several promising approaches (fig. 7) to overcome these problems which might be worth mentioning.

A very useful concept is the "track entity"-concept introduced by Mozumder and Magee[10], which results in a classification according to regions of energy transfers:

≤ 0.1 keV : blobs
0.1-0.5 keV : spurs
0.5-5 keV : short tracks
≥ 5 keV : branch tracks.

In these different entities a different number of new species will be produced and thus react with each other in different ways leading to locally different chemical and biological consequences. The yield of such entities for slow and fast electrons is shown in fig. 8.

The respective fractions for the various entities in fast electron track structures demonstrates fig. 9; evidently keV-electrons mainly produce short tracks, whereas faster electrons increasingly produce isolated spurs (because of the predominance of glancing collisions).

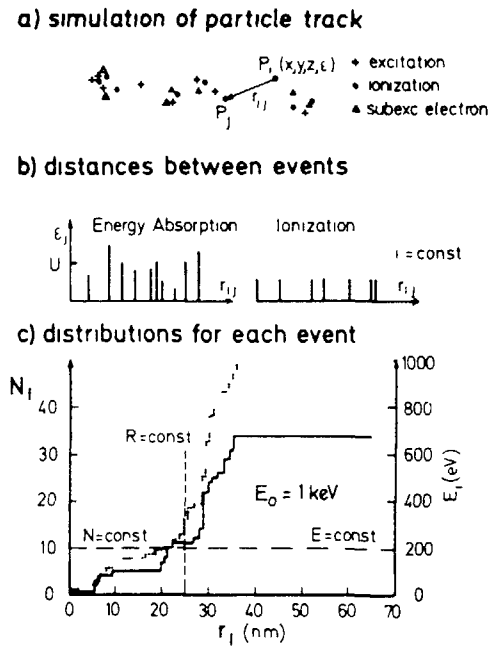

Fig. 10: Principles of cluster- and neighbourhood-analysis in charged particle track structures.

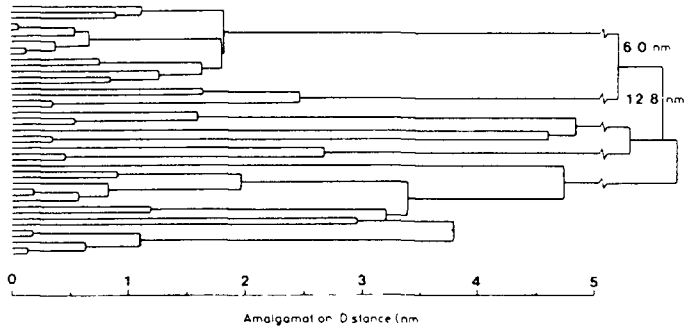

Fig. 11: Cluster-Dendrogramm of 1-keV electron track with the k-means algorithm.

Although this radiation chemical concept is rather old and somewhat crude, it has promising aspects regarding the additional implicit consideration of fast chemical and biological reactions, and it is worth developing further with the help of new information from detailed history track structure simulations.

With such simulation programs one tries to calculate the types and locations of new species in charged particles tracks (fig. 10), which then can be evaluated according to those aspects of neighbourhood- and cluster-analysis, which tentatively are considered important, such analysis might turn out to lead to a better understanding of radiation effects and identification of important parameters characterizing track structures then did dosimetric concepts. An example of such a promising attempt is given in fig. 11, where the k-means algorithm was used to form clusters in a 1 keV-electron track[12].

5. Conclusions and Outlook

The identification of important parameters for adequate classification of track structures of charged particles is still an open and interesting problem in radiation research. With the recent development of Monte Carlo track structue programs simulating in great detail the processes occuring during the primary physical stage and subsequent chemical reaction processes it can be hoped that some progress in this field can be reached soon. Such progress is likely to result from application of new cluster alogorithms with weight assignment (regarding the severity of direct or indirect consequences) to primary and secondary chemical species and from methods employed in similar problems in related scientific fields as e.g. fuzzy set theory[13], artificial intelligence[14] and pattern recognition[15].

Until better results are obtained in this identification process of important parameters characterizing charged particle track structures in radiaion biology and therapy, one might consider

a) to apply spectrometric measurement techniques (e.g. low pressure proportional counters) to obtain physical information on a local, possibly moderated, mixed radiation field, then
b) to avoid any possibly inappropriate classification by dosimetric concepts at this stage, but
c) use track structure programs to calculate the spatial distribution of new chemical species including subsequent chemical and biological reactions in the target of interest from the radiation field measured above, and
d) only then try tentative, event based cluster algorithms and other new techniques mentioned above to identify those important parameters of these charged particle tracks structures which predominantly determine the outcome of this irradiation and thus might be used as relevant quantities in radiation "quality" theories and might be measured in adequately tuned measurement devices.

REFERENCES

[1] U. Fano, G.E. Adams, D.K. Bewley, and J.W. Boag (Eds.), in "Charged Particle Tracks in Solids and Liquids", Series No. 8, Institute of Physics Conference, London, 1970, p. 1.

[2] L.H. Gray, Br. J. Radiol., 10 (1937) 600 ff and 721.

[3] International Commission on Radiation Units and Measurements (1980), Report 33 "Radiation Quantities and Units", Washington, D.C.

[4] International Commission on Radiation Units and Measurements (1983), Report 36 "Microdosimetry", Bethesda, MD.

[5] H.H. Rossi, Radiat. Res. 10 (1959) 522-531.

[6] A.M. Kellerer and H.H. Rossi, Current Topics of Radiat. Res. Quart. 8 (1972) 85-158.

[7] International Commission on Radiation Units and Measurements (1970), Report 16 "Linear Energy Transfer", Bethesda, MD.

[8] R. Katz, S.C. Sharma, and M. Homayoonfar, in "Topics in Radiation Dosimetry-Radiation Dosimetry Supplement 1", F.H. Attix (Ed.), Academic Press, New York, 1972, p. 317.

[9] J.J. Butts and R. Katz, Radiat. Res. 30 (1967) 855

[10] A. Mozumder and J.L. Magee, Radiat. Res. 28 (1966) 203.

[11] A. Mozumder, in "Advances in Radiation Chemistry", Vol. 1, M. Bruton and J.L. Magee (Eds.), Wiley, 1969, p. 1.

[12] H.G. Paretzke, in "Kinetics of Nonhomogeneous Processes", G. Freeman (Ed.), Wiley, New York (1987) p. 89.

[13] J. Kacprzyk and R.R. Yager (Eds.), "Management Decision Support Systems Using Fuzzy Sets and Possibility Theory", Verlag TÜV Rheinland, Köln, 1958.

[14] C.H. Chen (Ed.), "Pattern Recognition and Artificial Intelligence", Academic Press, New York, 1976.

[15] H. Haken (Ed.), "Pattern Formation by Dynamic Systems and Pattern Recognition", Springer-Verlag, Berlin, 1979.

80

COMPUTER EXPERIMENT AND RADIATION DATA FOR LIQUID WATER AND WATER VAPOR IRRADIATED BY FAST ELECTRONS

I.G. KAPLAN
L.Ya. Karpov Institute of Physical Chemistry,
Moscow, Union of Soviet Socialist Republics

Abstract

The radiation data obtained in computer simulation of the irradiation process by fast electrons of the water in liquid and gase phases are presented. Among them are yields of excited and ionized states, ranges and stopping power, yields of primary (at $t \sim 10^{-11}$s) radiolysis products. The specific features of liquid phase and its influence on radiation data are discussed.

1. INTRODUCTION

To a considerable degree, and in some cases almost entirely, the effect the different types of radiation (such as neutrons, heavy ions, decay fragments, gamma quanta, and X-rays) produce in a medium is the effect produced by fast electrons. In this talk I am going to discuss the results of computer experiments in which we simulated the irradiation of water (which is one of the main components of biological systems) by fast electrons.

There is a number of radiation data which cannot be measured experimentally, and the only way they can be found is in computer experiments based on the Monte Carlo method. Among them the yields of excited and ionized states; the spectrum of ejected secondary electrons, including Auger electrons; the yield of collective excitations in the condensed phase, and a number of other data. On other hand, in order to make such an experiment we must supply the computer with reliable data on cross-sections of the interaction between electrons and the medium.

One of the directions of research in our laboratory is the study of the influence the specific features of the condensed state have on the radiation yields, mass stopping power, and other radiation data[1-3]. The model traditionally used in radiobiology is the model of tissue-equivalent gas, which simulates the liquid state as a gas with equivalent density. Later in this talk I will show that this approximation is too crude to be used in calculations of the radiation-chemical (and subsequent biological) transformations. At the same time in calculations of the ranges and stopping powers of fast electron the tissue-equivalent approximation does not lead to large discrepancies.

Since at electron energies below 1 keV the data on the stopping powers contradict each other[4-8] and data on the ranges very scarce, we have calculated the stopping power and ranges using the Monte Carlo method. Of course, as was justly noted in Refs.[4,9], the knowledge of the stopping powers is only the first step in determining the distribution of absorbed energy in the medium. In our previous works[2,3] we have shown that in calculations of the primary excitation and ionization yields it is crucial to make allowance for the influence of secondary electrons, and that this is the main reason why the optical approximation[10,11] fails.

In conclusion of my talk I will present the data on the primary radiation yields of intermediate products of liquid water radiolysis, obtained on the basis of calculated excitation and ionization yields and scheme of the decay and evolution excited and ionization states in liquid water. These data are necessary for the study of the mechanism of biological effects produced by fast electrons.

2. THE METHOD OF CALCULATION AND THE USED CROSS-SECTIONS

When we calculate the processes of energy absorption by a charged particle in a condensed medium the first thing we must

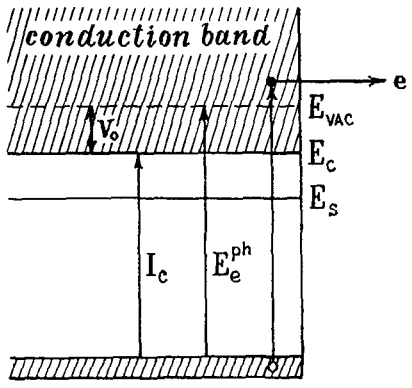

$$I_c = E_e^{ph} - V_o$$

H_2O

$$I_c = 10.06 - 1.3 = 8.76 \text{ eV}$$

$$I_g = I_c + V_o + P_+ = 12.8 \text{ eV}$$

Fig.1 Scheme of energy levels in a dielectric. I_c is the ionization potential in the condensed state, E_e^{ph} is the photoemission threshold, V_o is the bottom energy of the conductivity band counted off the vacuum level, E_s is the energy level of a solvated electron.

do is to take into account the special features the condensed phase has compared to the gaseous phase. One of them is the lowering of the ionization potential I_c. In the condensed phase the ionization occurs when an electrons gets into the conductivity band (Fig.I). The ionization potential I_c then equals the energy corresponding to the bottom of the conductivity band and is related to the ionization potential in the gaseous phase I_g as

$$I_c = I_g + P_r + V_o \qquad (1)$$

where P_+ is the energy needed for rearrangement of the medium after one of its molecules is ionized, V_o is the bottom energy of the conductivity band counted off the energy an electron has in vacuum (it is usually negative; e.g. for water V_o=-1.3 eV). I_c is simply related to the photoemission threshold E_e^{ph}:

$$I_c = E_e^{ph} + V_o \qquad (2)$$

Experiment[12] gives E_e^{ph} = 10.06 eV, which yields I_c= 8.76 eV. Such a considerable lowering of the ionization potential (ΔI = 3.8 eV) results in a substantial increase of the ionization yield in the liquid phase.

Still greater changes occur in the distribution of oscillator strengths[13] (Fig.2). The discrete peaks at low energies one

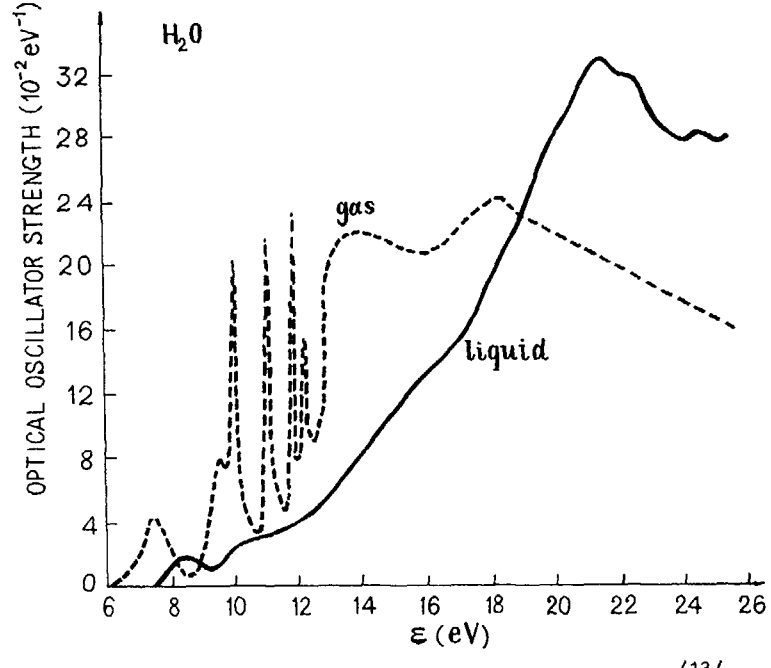

Fig.2 Distribution of oscillator strengths in water [13]: _____ liquid water, -------- water vapor.

observes in the gaseous phase transform into a continuous distribution with a wide absorption peak around 21 eV. The latter peak is usually attributed to collective plasmon-type excitations (for details see review[1]).

The probability of energy losses by a charged particle in a condensed medium is described by the energy loss function, which equals the imaginary part of the inverse permittivity: $\mathrm{Im}[-1/\varepsilon(\omega)]$. It is this function that determines the distribution of oscillator strengths in the liquid phase:

$$F(\omega) = \frac{2\omega Z}{\pi \omega_{pl}^2} \mathrm{Im}\left[-\frac{1}{\varepsilon(\omega)}\right] \qquad (3)$$

where $\omega_{pl} = (4\pi N_e e^2/m)^{1/2}$ is plasmon frequency, N_e is the number of electrons in a unit volume of the medium, m and e are electron mass and charge, and Z is the number of electrons in a molecule. The values of the energy loss function in our calculations were taken from reflection experiments[14]. For the differential cross-section we used the Born approximation

$$\frac{d\sigma}{d\omega} = \frac{4\pi a_0^2 Ry}{E_0} \frac{F(\omega)}{\hbar\omega} \ln\frac{E_0}{\hbar\omega}, \qquad (4)$$

where E_0 is the incident electron energy, a_0 is the Bohr radius, and Ry = 13.65 eV is Rydberg energy. The excitation probability for the nth transition was then found by integrating cross-section (4) over the widths of the peaks. The excitation cross-sections for the gaseous phase were calculated according to Bethe's formula[1,15] with the oscillator strengths of Ref. 13. For the ionization cross-section, both for the liquid and the gaseous phases we have taken the semiempirical Jain-Khare cross-section [16] (details see in Ref. /2/).

The type of collision: ionization or excitation - was determined beforehand. The calculations require the knowledge of total cross-sections of ionization σ_{ion} and excitation σ_{ex}. For the gaseous phase, at $E_0 \leqslant 100$ eV σ_{tot} and σ_{ion} were extracted from the experimental curves obtained in Ref. /17/ ($\sigma_{ex} = \sigma_{tot} - \sigma_{ion}$); at $E_0 > 100$ eV the cross-sections were calculated using the semiempirical formulae of Ref. /15/ with coefficients from Ref. /18/. For the liquid phase σ_{ion} and σ_{ex} were found using the energy loss function [13] and ionization cross-section [16].

In Ref. /3/ we have also made allowance for an additional channel of ionization which is due to the Auger effect. Since with ionization of a K-electron in water an Auger electron is ejected with practically unit probability, to a good approximation the cross-section of Auger electron ejection can be taken equal to the cross-section of K-shell ionization in an oxygen atom [19]. The spectrum of Auger electrons consists of several lines around 500 eV. Since the most intensive of these lines corresponds to 500 eV [20], we considered this to be the energy of all ejected Auger electrons.

Using the Monte Carlo algorithm we (in collaboration with V.Ya.Sukhonosov) have also calculated the average energy losses $\overline{\Delta E}(E_0)$ of an electron with energy E_0 in a single scattering event and total ranges. The obtained values of $\overline{\Delta E}(E_0)$ equivalent with those calculated according to the formula

$$\overline{\Delta E}(E_0) = \frac{1}{\sigma_{in}} \left[\sum_k \varepsilon_k \sigma_k(E_0) + \int_{I}^{E_0} \varepsilon \frac{d\sigma(E_0,\varepsilon)}{d\varepsilon} d\varepsilon\right], \qquad (5)$$

where σ_{in} is the total cross-section of inelastic scattering, σ_k is the excitation cross-section of a state with energy ε_k, $d\sigma/d\varepsilon$ is the differential ionization cross-section, and is the lost energy. The ratio of $\overline{\Delta E}(E_0)$ and the average free path length of

an electron with energy E_0, $\bar{\ell}_{in}(E_0)$, gives us the stopping power of the medium S. Since $\bar{\ell}_{in}(E_0) = I/n\sigma_{in}$, where n is the number of molecules in a unit volume, we get the well-known formula - definition for the stopping power:

$$S = n \left[\sum_k \varepsilon_k \sigma_k(E_0) + \int_{I_1}^{E_0} \varepsilon \frac{d\sigma(E_0,\varepsilon)}{d\varepsilon} d\varepsilon \right] \qquad (6)$$

In order to find the ranges we need to know the cross-section of elastic scattering. For electrons with $E_0 > 200$ eV the differential cross-section was calculated according to the formula /21/

$$\frac{d\sigma_{el}}{d\theta} = \frac{Z^2}{4v^4(\alpha^2 + \sin\frac{\theta}{2})^2}, \qquad (7)$$

where θ is the scattering angle, Z = 10 is the number of electrons in an H_2O molecule, v is the velocity of the incident electron, and $\alpha = 0.373\ Z^{1/3}\ v^{-1}$ is the screening parameter. The total cross-section of elastic scattering was found by integrating (7) over θ, which yields

$$\sigma_{el} = \frac{\pi Z^2}{v^4} \frac{1}{\alpha^2(1+\alpha^2)} \qquad (8)$$

For electrons with $E_0 \leq 200$ eV the differential cross-section of elastic scattering was extracted from experimental data presented as a table in Ref. 22. We assumed that the elastic scattering cross-section is the same in liquid and in vapor; the difference in the phase state was taken into account in processes of inelastic scattering. In calculations of the ranges we tracked down the motion of each electron through the medium as long as its energy was above 15 eV. Below 15 eV the elastic scattering becomes dominant and the calculation time sharply increases.

3. RESULTS OF CALCULATION AND THEIR DISCUSSION

A. Yields of excited states and ionizations in liquid water.

The results of Monte Carlo calculations for different radiation characteristics are presented in Tables 1-6. As it follows from the data presented in Tables 1 and 3, the yields of excited states and the spectrum of ejected electrons are practically independent of the incident electron energy. This results in that the yield per 100 eV of absorbed energy of radiolysis products is also independent of E_0. In Ref. 2 we have shown that the so-called optical approximation /10,11/ cannot be used even for qualitativ estimates of the yields of excited states. According to this approximation, the yield of the nth excited state should be proportional to the ratio f_n/E_n, where f_n is the optical oscillator strength and E_n is the excitation energy. The optical approximation works well only for fast electrons, but since the secondary electron spectrum is dominated by slow electrons the predictions of the optical approximation badly disagree with reality. For instance, using the optical approximation the authors of Ref. 14 predicted that in the liquid phase at the initial moment practically all the energy should be concentrated in the form of plasmon excitations since the energy loss function is maximum around the peak of collective absorption. They however didn't take into account the degradation of primary electron energy on the production of secondary electrons, and shifting the spectrum of the latter toward smaller energies. In reality, according to Table 1, the yield of collective plasmontype excitations for $E_0 = 10$ keV is $g_{pl} = 1.06$, which is only two times greater than the yield of the first excited state, and the energy spent on excitation of collective states is only 22.7% of E_0. However, according to the optical approximation, $g_{pl}^{opt}/g_1^{opt} \approx 44$.

Table 1

Yield per 100 eV of absorbed energy of excited states produced in liquid water by the primary electron with energy E_0 /3/

Electron-excited state	Excitation energy /13/	Oscillator strength /13/	E_0, keV		
			1	5	10
A^1B_1	8.4	0.018	0.535	0.542	0.545
B^1A_1	10.1	0.039	0.256	0.258	0.256
Ry(A + B)	11.26	0.0089	0.039	0.038	0.038
Ry(C + D)	11.93	0.0536	0.187	0.191	0.184
Diffusion bands	14.1	0.103	0.209	0.202	0.200
Collective excitations	21.4	2.03	1.200	1.066	1.060
Total yield of excitations					

Table 2

Distribution of the energy of an electron with E_0 = 10 keV in liquid water /3/

	Number	Energy carried, percents of E_0
Subexcitation electrons ($\varepsilon < 8.4$ eV)	264	6
Delta electrons	188	54.2
Auger electrons ($\varepsilon \approx 500$ eV)	0.9	4.5
All ejected electrons	453	64.7
Excited states	228	35.3

This shows how important it is to take into account the secondary electrons when considering the distribution of the fast electron energy in the medium.

Table 2 shows that though the energy spent on production of Auger electrons is 4.5% of E_0, their fraction in the spectrum of ejected electrons is very small being only 0.9/453 = 0.002. About 2/3 of the primary electron energy is spent on ionization, and 1/3 of it is spent on excitation of electron states of the medium.

In Table 3 we present the values of the spectral density of ejected electrons. More then a half of them are subexcitation electrons. In order to write down the analytical approximation for the spectrum of subexcitation electrons we have to divide the latter into two energy groups. Then

$$n(\varepsilon) = 0.2 \exp(-4.38\, \varepsilon / I_0) \qquad \text{for } 0 < \varepsilon \leq 1.3 \text{ eV}$$

$$n(\varepsilon) = 1.16\ 10^{-2} + \frac{13.34\ 10^{-2}}{(1 + \varepsilon / I_0)^3} \qquad \text{for } 1.3 < \varepsilon < 8.4 \text{ eV}$$

Table 3

Spectral density of ejected electrons /3/

$n_i = \Delta N_i / N_o \Delta E_i$ (eV^{-1})

Initial electron energy, keV	1	5	10
Energy range, eV			
0-0.3	0.191	0.187	0.186
0.3-0.5	0.174	0.169	0.172
0.5-0.7	0.160	0.157	0.154
0.7-0.9	0.144	0.138	0.138
0.9-1.1	0.126	0.126	0.125
1.1-1.3	0.116	0.113	0.112
1.3-1.7	0.102	0.100	0.099
1.7-2.1	0.088	0.086	0.085
2.1-2.6	0.074	0.074	0.074
2.6-3.8	0.059	0.059	0.058
3.8-5.3	0.045	0.044	0.045
5.3-8.4	0.045	0.045	0.045
8.4-10.06	0.026	0.026	0.026
10.06-14.1	0.019	0.019	0.019
14.1-20	0.012	0.013	0.013
20-50	0.004	0.004	0.005
50-100	0.001	$9.67\ 10^{-4}$	0.001
100-490	-	$8.48\ 10^{-5}$	-
100-500	$8.82\ 10^{-5}$	-	$8.48\ 10^{-5}$
490-510	-	$9.25\ 10^{-5}$	-
510-10^3	$2.53\ 10^{-6}$	$5.66\ 10^{-6}$	$5.88\ 10^{-6}$
10^3-5 10^3		$3.94\ 10^{-7}$	$4.14\ 10^{-7}$
5 10^3-10^4			$1.94\ 10^{-8}$
Total number of ejected electrons N_o	43	225	453

In the second energy range the qualitative behaviour of the energy dependence coincides with the one obtained by Platzman /23/.

B. The role of the phase state.

The phase state has the most essential effect on the yields of excitations and ionizations. The reasons for this were discussed in the beginning of sect. 2 (the lowering of the ionization potential in the condensed phase (Fig. I) and the changes in the distribution of oscillator strengths (Fig. 2) . As it follows from Table 4, in the condensed phase the fraction of ionizations relative to that of excitations becomes much greater than it is in the gaseous phase: in the latter case the yield of ionizations is slightly smaller than the excitation yield, but in the condensed phase the ionization yield becomes two times greater than the yield of excitations. If further we take into account that within about 10^{-16} sec collective states decay with ionization and that the produced electrons, whose energy is 21.4 - 8.76 = 12.64 eV, also additionally ionize the medium, the ratio of ionization and excitation events becomes greater than 4. The average energy required to produce a pair of ions, which in a gas equals W_i = 29.5 eV, in liquid water, with account of plasmon decay, equals W_i = 16.6 eV. I want to underline this fact: the W-value reduces twice when we go from gas to liquid. It is very important and must be taken into account when radiobiological effects are considered.

Let us now discuss how the stopping power and the pathlengths depend on the phase state. The results presented below were obtained in collaboration with V.Ya.Sukhonosov.

As I mentioned earlier in sect. 2, within the Monte Carlo method the stopping power can be calculated as a ratio of average energy losses $\overline{\Delta E}$ in a single event of inelastic scattering and the average free pathlength $\overline{\ell}_{in}$ between two subsequent events.

According to Table 5, $\overline{\Delta E}$ in the liquid phase is greater than it is in the gaseous phase within the whole energy range considered in the calculations, and the difference in $\overline{\Delta E}$ becomes greater with lowering of the energy. This can be explained by the shifting of energy levels in the liquid phase toward higher energies together with appearance of an additional channel of energy losses on collective excitations with energy at the maximum about 21.4 eV. With increase of electron energy a greater part of absorbed energy is spent on ionization. And since the spectrum of ejected electrons depends very little on the phase state of the medium /2/, the difference in average energy losses in water and in vapor must become smaller, in agreement with the data of Table 5.

Whereas the average energy losses increase monotonically with increase of electron energy, the average free pathlength $\bar{\ell}_{in}$ has a minimum, in agreement with the behaviour of the total cross-section of inelastic interaction σ_{in}. For liquid water the minimum is located at 40 eV; for water vapor the minimum is shifted toward higher energies and is around 100 eV.

The results of calculations for the mass stopping power $S_\rho = \frac{1}{\rho} S$ are presented in Figure 3. For comparison we also presented the curves for mass stopping power in water and in water vapor obtained in Ref. 7. At high energies and down up to E = 200 eV the values of S_ρ for water and for vapor are the same. At $E < 200$ eV, according to our calculations, the value of S_ρ for liquid water is essentially higher than it is for vapor which disagrees with results of Ref. 7 according to which the two curves for the stopping power are close to each other.

Our results on the phase state dependence of S_ρ at energies $E < 200$ eV are qualitatively different from those of Ref. 8, althow at higher energies our results agree with those of Ref. 8, as with those of Ref. 7. The reason for this is apparently due to

Table 4

Phase state dependence of radiation yields and average energy spent on production of an ion pair for an electron beam with E_0 = 10 keV

	g_i	g_{ex}	g_i/g_{ex}	$g_{tot} = g_i + g_{ex}$	W_i, eV
Vapor /2/	3.39	3.82	0.9	7.21	29.5
Liquid /3/:					
primary yield	4.52	2.28	2	6.8	22.1
yield with account of plasmon decay	6.04	1.43	4.2	7.47	16.6

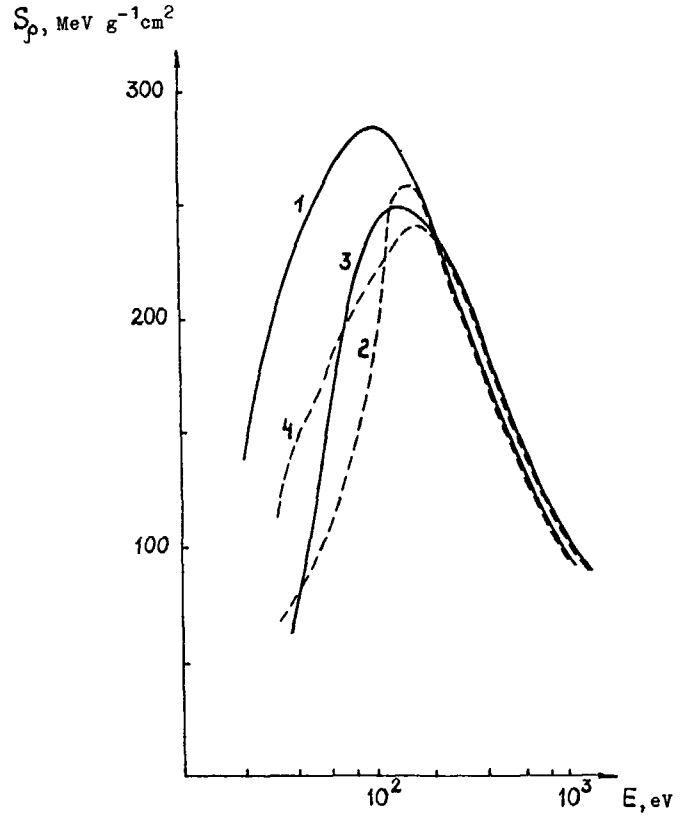

Fig.3 Mass stopping power curves for liquid water (———) and water vapor (-------). I and 2, our calculations, 3 and 4, Ref./7/

the inaccuracy at low energies of modified Bethe's formula used in Ref. 8. Since the theoretical predictions for the cross-sections at low energies are unreliable, in our calculations we used the corresponding experimental cross-sections (see The Method of Calculation). At energies where Bethe's formula for S_ρ is sufficiently accurate the calculations give equal values of S_ρ for the two phases, despite the significant difference in $\bar{I}$. On the

Table 5

Average energy losses $\overline{\Delta E}$ and average free pathlength $\bar{l}_{in}$ (in 10^{14} g/nm^2) for electrons with energy E_o in water and in water vapor

Phase state	E_o, eV	20	40	60	80	100	200	400	600	800	10^3
Water	$\overline{\Delta E}$, eV	8.05	11.29	14.53	18.11	19.84	25.36	28.40	31.64	30.57	32.85
	$\bar{l}_{in}$	0.61	0.48	0.56	0.64	0.72	1.05	1.72	2.38	2.93	3.55
Vapor	$\overline{\Delta E}$, eV	6.88	8.83	11.17	15.36	18.12	23.84	27.88	30.58	29.42	31.23
	$\bar{l}_{in}$	1.57	1.08	1.03	1.00	0.96	1.01	1.61	2.27	2.83	3.31

Table 6

Average ionization ranges of electrons in water and in water vapor (in 10^{14} g/nm^2)

Phase state	E_o, eV	50	100	200	400	600	800	10^3
Liquid water	R_x	0.71	1.24	1.34	6.29	12.03	18.77	26.93
	R_y	0.10	0.24	1.19	4.74	9.20	14.33	20.84
	R	0.78	1.40	2.51	10.78	20.67	32.26	46.70
Vapor	R_x	1.78	2.16	3.59	6.71	12.32	18.75	26.31
	R_y	0.83	0.98	1.39	5.17	9.37	14.29	20.24
	R	2.42	2.98	4.72	11.62	21.19	32.26	45.33
	R_{95}^{exp} [25]		3,6	6,27	12,67	21,33		40,67

other hand, at energies where the values of S_ρ become different Bethe's approach even modified is no longer accurate. One is puzzled by the large difference between effective excitation potentials in the solid and the liquid phases ($\Delta I_{eff.}$ = 12.1 eV), whereas for the gaseous and the liquid phase this difference is much smaller (ΔI_{eff} = 3.5 eV). The distribution of oscillator strengths is qualitatively different in liquid water compared to what it is in vapor (Fig.2), and changes little as we pass from liquid water to ice. The energy loss functions for liquid water [13,14] and ice [24] are also very much alike.

In Table 6 we present the calculated values of the ranges for water and water vapor. We calculated the following characteristic ranges of an electron: the total range R, which equals the actual path length of electron in the medium; the projective range R_x, which equals the projection of the vector $\vec{R}$ connecting the beginning and the end of electron's trajectory onto the initial direction of motion X; perpendicular ranges R_y and R_z, which are the projections of vector $\vec{R}$ onto the corresponding axes. Since the medium is isotropic we have $R_y = R_z$. For comparison, in the last line of Table 6 we present the experimental values of range R_{95}^{exp} obtained in Ref.25 for air and reevaluated by us for water vapor.

The problem of comparing the calculated and the experimental ranges is not so simple. Actually, there are several reasons why such a comparison may turn out to be incorrect. When comparing calculations with experiment, one usually compares the total path length R with R_{95}^{exp} (see e.g. Ref. 25). However, all experimentally measured ranges are projective, since they are found by measuring the absorption in a layer with fixed thickness; so the compared theoretical ranges must also be projective. In Monte Carlo calculations one obtains average pathlengths, and one should compare the projective pathlength R_x^{theor} to R_{50}^{exp}, since it is R_{50}^{exp} that corresponds to the average pathlength (see Ref. 26). Furthermore, one should bear in mind that, if not stated otherwise, the calculated ranges are ionization ranges and don't include the path lengths of subexcitation electrons. The pathlength of a subexcitation electron until its thermalization can be very large; in water it is of order of 10 nm [27]. Compare this value with the ionization pathlength of an electron with E_o = 100 eV, which according to Table 6 is only 1.4 nm. Thus, one should also take into account to what degree the measured ranges include those of subexcitation electrons.

As it follows from Table 6, for electrons with $E_o \geqslant 400$ eV the difference between ranges in liquid water and in vapor with the same density is very small and is about 3%. With lowering of electron energy the ranges in liquid water becomes much smaller than it is in vapor. For electrons with $E_o \geqslant 400$ eV the total pathlength

R exceeds the projective range R_x by about 42%. This agrees well with the experimental estimates of Williams (see Ref. 28), according to which $(R - R_x)/R \simeq 40\%$. At electron energies between 50 and 200 eV the deviation of electron's trajectory from its initial direction becomes smaller owing to the smaller number of inelastic scattering events (at such energies elastic scattering is not yet dominant). Let us also note that within the whole calculated energy range there holds an approximate equation $R_x + R_y \simeq R$.

C. Yields of Primary Radiolysis Products in Liquid Water.

By considering the further evolution of excited and ionized states and using the obtained values of their yields (Table I and 4) we are able to find the radiation-chemical yields of primary radiolysis products[3].

We considered the following decay scheme of excited states[29]:

$$H_2O\ (I) \longrightarrow OH + H \qquad (10)$$

$$H_2O\ (II\text{-}V) \longrightarrow \begin{cases} OH + H \\ O + H_2 \end{cases} \qquad (11)$$

In reaction (II) oxygen is produced in the singlet excited state (the ground state of the oxygen atom is triplet). We also took into account the fact that the energy of all excited state, starting from state II, exceeds the first ionization potential, i.e. that all of them belong to the class of superexcitation states introduced by Platzman[30,1]. In such states there is competition between dissociation and ionization. Since in the liquid phase a pair of radicals produced with dissociation for some time after its formation is surrounded by neighbouring molecules, it prevents for the radicals to escape into the volume and favours their recombination. We accounted for this "cage" effect using the diffusion gradient method of Bagdasaryan[31].

Table 7

Yield per 100 eV of absorbed energy of ionization and primary products by the time $t \leqslant 10^{-12}$ s

Product	H_2O^+	H_3O^+	H	H_2	OH	O
Present calculations	6.57	4.8[a)]	0.84	0.62	6.82	0.03
Results of Ref.[33]	6.3	6.3	2.1	0.3	8.4	0.3
Experiment[35,36]	-	4.8	0.7	0.45	5.9	-

a) Experimental value

We then considered the competition between the reaction with formation of an oxonium ion

$$H_2O^+ + H_2O \longrightarrow H_3O^+ + OH \qquad (12)$$

and the ion-electron recombination

$$H_2O^+ + e \longrightarrow H_2O^* \qquad (13)$$

With account of the energy spent on rearrangement of the medium the excitation energy of the neutral molecule produced in reaction (13) equals 6.26 eV. This is smaller than the energy of the first electron-excitation state, which in the liquid phase equals 8.4 eV.

Such a vibrationally excited molecule has three possible decay channels:

$$H_2O^* + H_2O \longrightarrow \begin{cases} 2H_2O \\ H_2 + 2OH \\ H + OH + H_2O \end{cases} \qquad (14)$$

The results of our calculations, in which we considered decay schemes (10) - (14) and used the values of the yields presented in Tables I and 4, are shown in Table 7. The value of the yield of ionized states, $G_i = 6.57$, is greater then the one presented in Table 4 owing to our taking into account the additional channel of ionizations due to the decay of superexcitation states. For the yield of solvated electrons, $G_s = 4.8$, we have taken its experimental value. As one can see, our results are in satisfactory agreement with experiment. The fact that G_i is much greater than G_s indicates that the recombination reaction (13) is quite efficient, which agrees with the scheme of radiolysis presented in Ref. 32 and disagrees with the approach of Refs. 33,34.

REFERENCES

1. I.G.Kaplan and A.M.Miterev. Adv. Chem.Phys. 68, 255(1987).

2. I.G.Kaplan, A.M.Miterev and V.Ya.Sukhonosov. Radiat. Phys. Chem. 27, 83(1986).

3. I.G.Kaplan, A.M.Miterev and V.Ya.Sukhonosov. Khimiya Vysokikh Energii. 22, No 2 (1989).

4. M.Inokuti. In: Applied Atomic Collision Physics, v.4, p.179, ed. S.Dutz, Ac.Pr., Orlando, 1983.

5. M.J.Berger. In: Nuclear and Atomic Data for Radiotherapy and Related Radiobiology. Proc. Advisory Group Meeting, Rijsmijk, 16-20 September 1985, IAEA, Vienna, 1987, p.323.

6. J.E.Turner, H.G.Paretzke, R.N.Hamm, H.A.Wright and R.H.Ritchie. Radiat. Res. 92, 47(1982).

7. H.G.Paretzke, J.E.Turner, R.N.Hamm, H.A.Wright and R.H.Ritchie. J. Chem. Phys. 84, 3182(1986).

8. J.A.LaVerne and A.Mazumder. J. Phys. Chem. 90, 3242(1986).

9. M.Inokuti and M.J.Berger Nucl. Instr. and Meth. B27, 249(1987).

10. R.L.Platzman. In: Radiation Research (Ed. by G.Silini), p.20, North-Holland, Amsterdam, 1967.

11. I.Santar and J.Bednar. Int. J. Radiat, Phys. Chem. 1, 133(1969).

12. P.Delahay and K.Von Burg. Chem. Phys. Lett. 83, 250(1981).

13. G.J.Kutcher and A.E.S.Green. Radiat. Res. 67, 408(1976).

14. J.M.Heller, R.N.Hamm, R.D.Birkhoff and L.R.Painter. J.Chem. Phys. 60, 3483(1974).

15. M.Inokuti. Revs. Mod. Phys. 43, 297(1971).

16. D.K.Jain and S.P.Khare, J. Phys. B. Atom. Molec. Phys. 9, 1429(1976).

17. H.G.Paretzke and M.J.Berger. In: Proc. of 6th Symp on Microdosimetry, p.749, Harwood Publ., Brussels, 1978.

18. G.D.Zeiss, W.J.Meath, L.C.F.McDonald and D.J.Dawson. Radiat. Res. 63, 64(1975).

19. J.Durup and R.L.Platzman. Int. J. Radiat. Phys. Chem. 7, 121(1975).

20. H.Siegbahn, L.Asplund and P.Kelve. Chem. Phys. Lett. 35, 330(1975).

21. N.Mott and H.Massey. The Theory of Atomic Collisions; Oxford, 1965.

22. A.Danjo and H.Nishimura. J. Phys. Soc. Jpn. 54, 1224(1985).

23. R.Platzman Radiat. Res. 2, 1(1955).

24. J.Daniels. Opt. Commun. 3, 240(1971).

25. A.Cole. Radiat, Rec. 38, 7(1969).

26. H.Bethe and J.Ashkin. In: Experimental Nuclear Physics (ed. E.Segre), Wiley, N.Y. 1953 v.1, part 2.

27. V.V.Konovalov, A.M.Raitsimring and Yu.D.Tsvetkov. Chem. Phys. 93, 163(1985).

28. D.E.Lee. Action of Radiation on Living Cells, Cambridge, University Press, 1946.

29. C.R.Claydon, G.A.Segal and H.S.Taylor. J. Chem. Phys. 54, 3799(1971).

30. R.Platzman Radiat. Res. 17, 419(1962).

31. Kh.S.Bagdasaryan, Uspekhi Khimii 53, 1073(1984).

32. L.T.Bugaenko, V.M.Byakov and S.A.Kabakchi. Khimiya Vysokikh Energii 19, 291(1985).

33. J.E.Turner, J.L.Magee, H.A.Wright, A.Chatterjee, R.N.Hamm and R.H.Ritchie, Radiat. Res. 96, 437(1983).

34. G.V.Buxton. In: Study of Electron Pulse Radiolysis, 1982, p.241.

35. C.D.Jonah and J.R.Miller. J. Phys. Chem. 81, 1974(1977).

36. C.D.Jonah, M.S.Matheson, J.R.Miller and E.J.Hart. J. Phys. Chem. 80, 1267(1976).

ATOMIC DATA REQUIRED IN ACCURATE MEASUREMENTS OF KERMA FOR NEUTRONS WITH LOW PRESSURE PROPORTIONAL COUNTERS

P. PIHET, H.G. MENZEL
Fachrichtung Biophysik und Physikalische
Grundlagen der Medizin,
Boris Rajewsky-Institut,
Universität des Saarlandes,
Homburg (Saar), Federal Republic of Germany

Abstract

The accuracy achievable in neutron dosimetry for radiation therapy critically depends on the knowledge of the kerma factors for the tissue components and the detector materials Gas filled cavity chambers allow to achieve relatively accurate measurements of kerma for the chamber wall material Ionisation chambers and proportional counters measure with high precision the charge from ionisation produced in the gas by the charged particles released in neutron interactions with the wall and with the gas However, the overall uncertainty of the kerma measurement depends on the quality of the basic physical data required in the application of the cavity chamber principles, in particular, W-values, stopping powers and stopping power ratios for the charged particles released and their energy dependence

The paper summarizes the experience gained in evaluating atomic data to be used in cavity chamber principles for neutron kerma measurements with tissue-equivalent and non hydrogenous proportional counters Proportional counters with walls made of A-150 TE plastic, graphite, Al, Mg, Fe, Zr and ZrO have been used to measure neutron kerma factors by several groups Different mixtures such as methane based TE gas, propane based TE gas or CO_2 were used as counting gases It is shown that the spectral information provided by the proportional counters can be used to assess quantities such as the gas-to-wall absorbed dose conversion factor An attempt is made to assess the uncertainties in kerma measurements due to the uncertainties of basic atomic data

1. INTRODUCTION

Accurate determination of kerma for penetrating radiation in different materials are required in dosimetry for radiation therapy (Menzel, 1987). The kerma (K) is determined by cross sections and the charged particle spectra. The complexity of nuclear processes and the difficulty to calculate theoretically kerma for light nuclei, especially for neutrons in the high energy region, emphasizes the interest of direct measurements of the kerma. Experimental determination of the kerma is based on absorbed dose measurement because the absorbed dose is a good approximation of

the kerma under condition of charged particle equilibrium Absolute measurements of kerma may be achieved with high accuracy by using calorimetry However this method is of limited applicability For routine applications and dosimetric investigations, gas cavity detectors are widely used due to their high precision and to several practical advantages such as their use in various types of phantom and the possibility to vary the composition of the wall material These detectors include ionisation chambers and small proportional counters However, the determination of absorbed dose or of kerma with gas cavity chambers requires the precise knowledge of basic physical data For new treatment modalities actually used or planned (e g fast neutrons, pions, protons, heavy ions) these data are not always available with the required accuracy

In neutron therapy, radiobiological and clinical studies have led to the requirement of an accuracy level of ± 5 % for the determination of the absorbed dose delivered for a treatment (Wambersie, 1984) Whereas this requirement can be met for neutron therapy beams below 14 MeV (Mijnheer, 1987), considerable improvement in neutron dosimetry is needed at the higher neutron energies (up to 65 MeV) These are used by the more recently installed therapy facilities because of the better balistic properties of the beams in order to be comparable to high energy photon therapy beams There are two major problems in neutron dosimetry above 20 MeV Neutron cross section data for light nuclei at high energy are scarce and inaccurate, or even discordant, which limits considerably the applicability of theoretical calculations of the energy transferred (Brenner, 1987) Secondly, different tissue substitutes used for building cavity detectors are losing their quality of being "tissue-equivalent" (TE) at high neutron energies due to the replacement of oxygen in tissue by carbon in TE material mainly because of the need for electrical conductivity of the detector wall In the neutron energy range above approximately 15 MeV, kerma to carbon and oxygen is mainly determined by nuclear interactions (non-elastic) processes the energy dependence of which is very nuclide specific The difference to the composition of real tissues explains the poor accuracy of the order of ±10% for total absorbed dose in tissue actually achievable for high energy neutrons The severity of the problem is increased by changes in the composition of different tissues

The kerma is the total energy transferred by indirectly ionizing particles to charged particles In principle, the differences in the composition of e g TE gases, TE substitutes, phantom materials or real tissues can be accounted provided the kerma in their elemental constituents are known The relatively large uncertainties in theoretical calculations at high neutron energies have motivated efforts of several groups to perform measurements of kerma for neutrons by using proportional counters walled with A-150 TE plastic and with pure graphite (Menzel et al , 1984, De Luca et al , 1985, Menzel, 1987, Wuu and Milavickas, 1987, Dietze et al , in preparation) Low pressure proportional counters have the advantage of a relatively low frequency of primary interactions with the gas due to the low mass of the gas They provide a pulse height spectrum which is related to the physical properties of the charged particles For instance, the spectra allow the relative contribution of these particles to the total kerma in the wall material to be evaluated However proportional counters operate as cavity chambers, i e they primarily measure ionisation yield in the gas which needs to be converted into energy loss in order to derive the integral quantities absorbed dose and kerma In addition, in general the counting gas and the wall do not have identical compositions, gas-to-wall dose conversion factors are needed to convert the energy imparted to the gas into absorbed dose in the wall material The overall uncertainty for kerma therefore depends directly on the uncertainties for basic atomic and molecular data, mainly stopping power (STP) and average energy required to produce an ion pair (W) This problem is particularly critical for non hydrogenous counters due to the larger differences between gas and wall composition

The present paper reports on detailed calculations of the dose conversion factors and the average W-values for neutrons to apply for kerma measurements with tissue-equivalent proportional counters (TEPC) and with carbon walled proportional counters (CPC) using the characteristics of the experimental ionisation yield spectra and different atomic data tables for STP and W Kerma factors in A-150 TE plastic and in carbon, and kerma ratios for monoenergetic neutrons from 5 to 60 MeV determined with TEPC's and CPC's were presented previously (Menzel et al , 1984, Menzel et al , in press, Dietze et al , in preparation) These results are revised according to the present calculations and the overall uncertainty in kerma measurements is discussed with particular emphasis on the influence of the uncertainties in atomic data used The application of these calculations to neutron therapy beams is discussed

2 NEUTRON FIELDS

The kerma measurements reported here for monoenergetic neutrons of 5, 13 9, 15, 17 and 19 MeV were carried out at the Physikalisch-Technische Bundesanstalt (PTB) in Braunschweig, Federal Republic of Germany The neutrons were produced by the $T(d,n)^4He$ reaction at the low scattering area of the accelerator facility for fast neutron dosimetry Details on the physical properties of the beams, the experimental method and the results of kerma measurements in A-150 TE plastic and in carbon may be found elsewhere (Menzel et al , 1984,Dietze et al , in preparation) Other measurements for monoenergetic neutrons were performed at the Swiss Institute for Nuclear Research (SIN) in Villigen Neutrons were produced by the $^9Be(p,n)^9B$ reaction (thin target) with energies of 27 8, 39 7 and 60 3 MeV Preliminary results of these measurements were presented recently (Menzel et al , in press)

Kerma measurements with TEPC's and CPC's were also performed at several European Neutron Therapy Facilities within an intercomparison program carried out by the EORTC (European Organization for Research on Treatment of Cancer) Heavy Particle Therapy Group (Pihet et al , 1987) Some results are reported here for d(0 25)+T ($\bar{E}_n$=14 MeV) and p(62)+Be ($\bar{E}_n$=27 MeV) neutron therapy beams used at the Generator Karin of the Institut fur Nuclearmedizin in the DKFZ Heidelberg (F R G) (Hover at al 1981) and at the MRC Cyclotron Unit in Clatterbridge Hospital (United Kingdom) (Bonnett et al , 1988) respectively, results are also reported for the collimated d(14)+Be (E_n=$\bar{5}$ 6 MeV) neutron beams developed at PTB Braunschweig (F R G) as reference standard beam for neutron dosimetry for therapy (Dietze et al , 1984)

For the neutron fields produced at PTB, the neutron fluence were known with high accuracy which allow to determine the kerma per unit fluence (K/ϕ), or kerma factor, in A-150 TE plastic and in carbon At the other facilities, the spectral fluence in was not available and the results are therefore reported in terms of kerma ratio between carbon and A-150 TE plastic

3 CAVITY THEORY APPLIED TO LOW PRESSURE PROPORTIONAL COUNTERS

Principles of neutron dosimetry using gas cavity chambers were described in details by Caswell (1966) and by Rubach and Bichsel (1982) The most relevant quantities are the average W-value for neutrons (W_n) to convert ionisation yield into energy imparted to the gas, the gas-to-wall dose conversion factor ($(r_{m\,g})_n$) to account for difference in the composition of the wall and the gas, and the kerma ratio ($(K/K_w)_n$) to express the absorbed dose determined in the wall material into another medium These quantities are averaged over all secondary charged particles released by neutron interactions in the detector wall and surrounding matenal, and in the gas (average values are formally referred under the subscript 'n') This is due to the impossibility to indentify experimentally the energy imparted by each single charged particle Therefore average quantities (absorbed dose or kerma with ionisation chambers) or statistical distributions (ionisation yield spectra with proportional counters) may only be measured

Neutron interactions release secondaries as different as electrons, protons, alpha particles and heavy ions over wide scale of initial energy, i e with large differences in ranges By using gas cavity detectors, this is taken into account by differentiating the secondaries produced by neutron interactions with the gas ("insiders", "starters") and with the wall and surrounding material ("crossers", "stoppers") Neutron dosimetry presents a particular problem as the relative contribution to the total absorbed dose of interactions with gas and with wall critically depends on neutron energy and on the mass of the gas For secondaries emitted in the material surrounding the cavity, the problem is complicated by two basic processes (a) the emission of the secondaries and their initial energy spectra, and (b) the slowing-down of these secondaries in the surrounding material before entering the cavity

The $(r_{m\,g})_n$ are derived for crossers from their stopping power ratio and for insiders from their kerma ratio (gas-to-wall) For stoppers and starters, a precise determination of $(r_{m\,g})_n$ can in principle only be derived by energy deposition calculations such as with the Caswell and Coyne code (1981) Compared to ionisation chambers, low pressure proportional counters approach more closely the ideal case of a "Bragg-Gray cavity" due to the very small mass of gas, i e the majonty of the particles are 'crossers" This statement represents a relatively good approximation for neutron energy above 10 MeV and a considerable simplification since, for an infinitesimal cavity, the dose conversion factor $(r_{m\,g})_n$ depends only on the slowing down spectrum of the charged particles entering the cavity, and on their stopping power ratios (Rubach and Bichsel, 1982) The calculation may be simplified by deriving the average gas-to-wall stopping power ratio for each charged particle component weighted by their relative contribution to the total kerma (Makarewicz et al , 1986) This method, however, requires to evaluate the average energy of the secondaries from their energy distributions At neutron energies above 14 MeV, large uncertainties in the nuclear cross section data present important problems to calculate the initial and slowing-down charged particle spectra (Buhler et al , 1986, Brenner et al , 1987) At neutron energies below approximately 10 MeV, the dose contribution of neutron interactions in the gas may not be neglected Additional assumptions can be made on the basis of energy deposition calculations to approximate $(r_{m\,g})_n$ and its uncertainty

Proportional counters determine the distributions of energy imparted (ε) by the secondary charged particles ionising the gas in the cavity which volume has a mean chord length ($\bar{l}$) of the order of 1 μm The measured pulse height spectra are usually calibrated in lineal energy ($y=\varepsilon/\bar{l}$ in keV/μm) by using the spectrum of single charged particles of known lineal energy (y_c, 'c' standing for calibration) (Dietze et al , 1984) The linear relationship established between y and the pulse height produced by a single energy deposition event implies that the average energy W required to produce an ion pair is assumed to be constant ($=W_c$) independently of the type and the velocity of the charged particle traversing the cavity Since for neutron induced events different charged particles can be responsible for the same pulse heigth, it is not possible to convert the experimental pulse heigth spectra into energy deposition spectra with appropriate W values for each channel so that energy deposition spectra can only be approximated by "ionisation yield spectra" (Caswell and Coyne,.1981) The absorbed dose is determined by the integral of the ionisation yield spectrum provided the ratio of the average W_n- and W_c-value is known for each neutron field

The overall uncertainty for kerma measurements with cavity chambers is predominantly influenced by the uncertainties on $(r_{m\,g})_n$ and W_n (Rubach and Bichsel, 1982, Menzel et al , 1984) For the investigations reported here, TEPC's, walled with A-150 TE plastic (10 1% H, 77 6 % C, 3 5% N, 5 2% O, 1 7% F, 1 8% Ca) and CPC's were used, all counters were filled both with TE gas (10 3% H, 56 9% C, 3 5% N, 29 3% O) TE chambers are usually built to achieve identical wall and gas composition implying a $(r_{m\,g})_n$ value close to unity For TEPC's, the influence of the differences in gas and wall composition depends on neutron energy, namely, whereas at intermediate energies the counter can be considered in first approximation as homogeneous, this approximation is not valid at high neutron energies due to differences in C and O contents For CPC's, the differences in gas and wall composition play an more important role, for instance $(r_{m\,g})_n$ may deviate up to more than 20 % from unity for carbon chamber Due to the smaller contribution of protons to the total absorbed dose in a CPC, $(r_{m\,g})_n$ more critically depends on neutron energy

4 EXPERIMENTAL AND CALCULATION PROCEDURES

4 1 Proportional counters

All measurements reported here were performed with spherical proportional counters from Far West Technology (Goleta, USA) The counters have an inner diameter of 12 7 mm and their walls are made of A-150 TE plastic or of pure graphite, with the same thickness of 2 54 mm Propane and methane based TE gases are commonly used in experimental microdosimetry because of their good counting gas properties The propane based TE gas mixture is often preferred due to the higher gas gain achievable (Srdoc, 1970) Both TEPC and CPC were filled with this gas mixture at a pressure of 4 4 kPa which corresponds to a diameter of 0 1 mg/cm^2 (1 µm at unit density) The counters were exposed in free air and with additional polyethylene and carbon build up cap thicknesses depending on neutron energy

For precise kerma measurements the calibration procedure of the proportional counters requires a critical evaluation (Dietze et al , 1984) Three independent methods may be used The calibration of the pulse height in units of lineal energy (y in keV/µm) is achieved by using the pulse height spectrum of collimated monoenergetic alpha particles produced by a ^{244}Cm built-in source ("single event calibration") This method is however associated with a considerable uncertainty mainly due to the uncertainties in effective energy and path length of the alpha particles crossing the cavity (Schrewe et al , in press), in addition, for absorbed dose measurements, the accurate knowledge of the mass of the gas is required This last problem may be overcome by performing a "multiple event calibration" or calibration in absorbed dose using a reference standard photon source The third method is useful for neutron measurements and independent of the two others The sharp cut off ("edges") of the pulse height for protons and alpha particles released by neutron

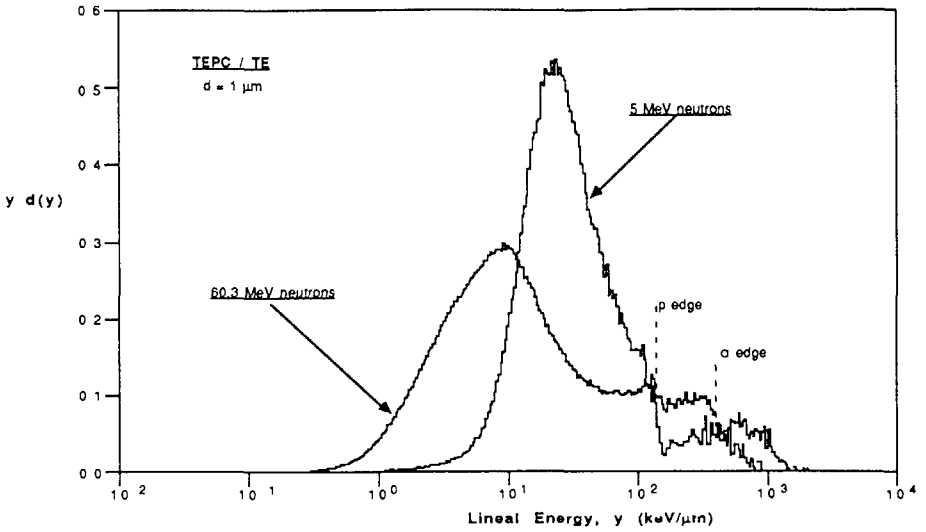

Figure 1 Ionisation yield spectra measured with a proportional counter with A 150 TE plastic wall and filled with propane based TE gas for 5 MeV (PTB Braunschweig) and for 60 3 MeV (SIN Villigen) monoenergetic neutrons Ionisation yield spectra are presented in terms of dose distribution of lineal energy Maximum ionisation yield by protons and by alpha particles ("edges) are indicated

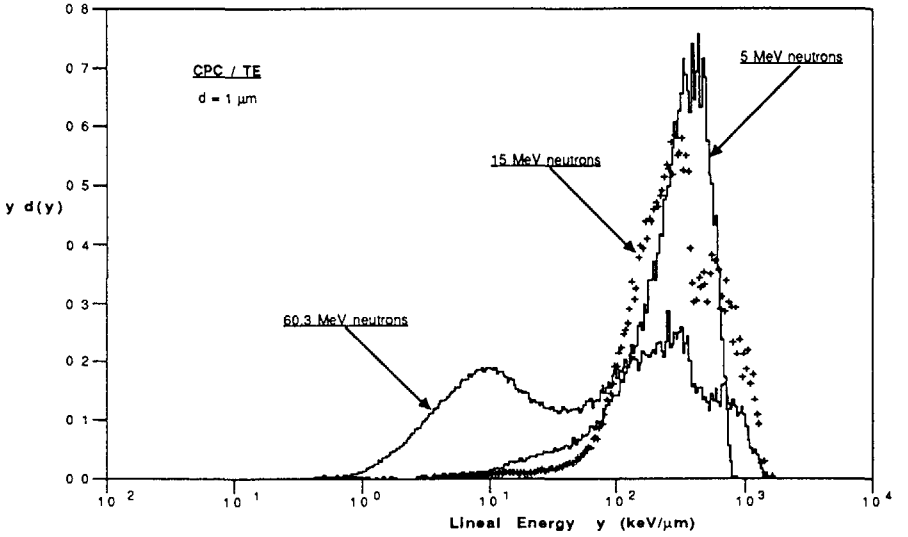

Figure 2 Ionisation yield spectra measured with a proportional counter walled with pure graphite and filled with propane based TE gas for 5 MeV and 15 MeV neutrons (PTB Braunschweig) and for 60 3 MeV neutrons (SIN Villigen) The total kerma is predominantly due to carbon recoils at 5 MeV to alpha particles Be and C ions at 15 MeV At 60 3 MeV protons produced by the (n p) reaction in carbon also contribute a large fraction to total kerma

Table 1 Maximum energy deposited by protons and alpha particles in the cavity of a proportional counter filled with propane based TE gas for different simulated diameters. The values are derived from the range curves in the energy region of the maximum stopping power Maximum lineal energies are found at 130 keV and 700 keV for the energy of protons and alpha particles entering the cavity.

Charged particle	Maximum theoretical lineal energy (keV/µm) d = 1 µm	d = 2 µm	d = 5 µm
protons	144 9 (134) †	134 8 (127)	108 8 (109)
alpha	400 (356)	395 (349)	354 (330)

† calculated after Ziegler (1977) values in brackets are calculated using the SPAR code (Armstrong and Chandler 1973)

interactions is used as internal calibration value (Figure 1 and 2) The "edge" technique reduces the overall uncertainty on the total absorbed dose provided accurate value for the maximum energy loss by the particles in the cavity are known which requires accurate stopping power data in the energy region of the Bragg-maximum Maximum lineal energy for protons in cavities filled with propane based TE gas were determined using the Andersen and Ziegler fitting formulae (1977) and applying the Bragg additivity rule for the gas mixture (Table 1) The accuracy of this procedure was confirmed experimentally for methane based TE gas (Waibel et al , 1987)

Each method of calibration requires the knowledge of the corresponding W value for the radiation used (Table 2) For the alpha particles emitted by the internal source of calibration, differential w-values are needed, they were evaluated to be 29 36 eV and 26 70 eV for methane based and propane based TE gas respectively

4 2 Experimental ionisation yield spectra

Although ionisation yield spectra only approximate energy deposition spectra, they are conventionally represented in terms of lineal energy y (ICRU Report 33, 1983) A semi-logarithmic representation for the frequency and dose distributions of lineal energy is used because of the large dynamic range needed for fast neutrons, from 0 01 to more than 1000 keV/µm The distributions are obtained after redistribution of 4 pulse heigth subspectra measured simultaneously with different gain settings A compact microcomputer based measurement system was developed in the Homburg Laboratory in order to perform the necessary operations which lead to the final distributions the control of the linearity of each amplification line, of the monitors and of the overlaps between the different subspectra, the extrapolation to low lineal energies below the experimental threshold, the internal edge calibration and the redistribution on a logarithmic scale in y The neutron and gamma components are derived from the dose distribution of lineal energy y d(y) by comparing the measured spectrum to the distribution for high energy gamma rays and by fitting the high energy proton component which overlaps largely the gamma component below 1 KeV/µm especially for neutrons of energies higher than 30 MeV

In experimental microdosimetry, the frequency and dose distributions y f(y) and y d(y) are often normalized to unity The integral over the dose distribution is therefore the unit dose and the aera under the curve in a fixed y interval gives directly the relative contribution to the total absorbed dose (d_i) of the events in this interval The pure neutron distribution may be unfolded in good approximation into its main

Table 2 W-values for different charged particles used for the calibration of proportional counters (PC) and the analysis of lineal energy spectra for neutrons measured with TEPC's and CPC's W-values for electrons are used for the evaluation of the gamma dose component in the neutron fields. W-values for 5 3 MeV alpha particles are applicable to alpha particles emitted by internal calibration sources (see text for differential w values) W-values for 130 keV protons and 700 keV alpha particles are applicable for protons and alpha particles with maximum energy deposition in the cavity (proton and alpha "edge's"), these edges may be used for internal calibration of lineal energy spectra for neutrons.

Charged particle	Methane based TE gas (†) W ± ΔW		Propane based TE gas (††) W ± ΔW	
electrons	29 2 ± <0 58	(1)	26 1 ± <0 52	(1)
protons (125 keV)	30 09 ± 1 61	(2)	27 9 ± 1 05	(3)
alpha (5 3 MeV)	30 77 ± 0 14	(4)	27 98 ± 1 76	(5)
alpha (700 keV)	34 25 ± 1 03	(6)	29 21 ± 1 03	(3)(6)

(†) 64 4 % CH_4 32 4 % CO_2 3 2 % N_2 (††) 55 % CH_8 39 6 % CO_2 5 4 % N_2

(1) Combecher 1980 (3) Posny et al 1987 (5) ICRU Report 31 1979
(2) Nguyen et al 1980 (4) Thomas and Burke 1985 (6) Bichsel and Rubach 1982

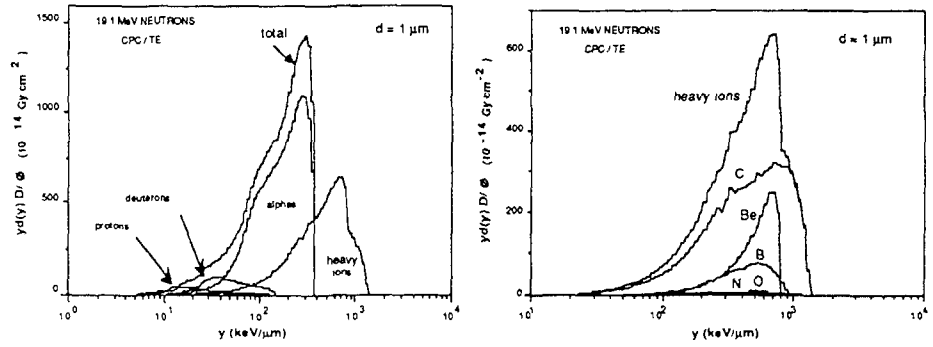

Figure 3 Theoretical ionization yield spectra calculated for 19 MeV neutrons using the Caswell and Coyne code for a carbon proportional counter filled with propane based TE gas The figure on the right expands the heavy ion component

charged particle components, protons, alpha particle and heavy ions. In some practical cases, these contributions may be more easily assessed by defining fixed y intervals and by neglecting the overlapping regions. This assumption has been found adequate for the present calculations if y intervals up to 150 keV/µm for protons (proton edge), from 150 to 400 keV/µm for alpha particles and above 400 keV/µm for heavy ions are used (Figure 1 and 2) (Bühler et al., 1985). Using the same procedure, the frequency distribution y.f(y) can be used to evaluate the mean lineal energy ($\bar{y}_{F,i}$) of protons and alpha particles entering the cavity. This method is too uncertain to be applicable for heavy ions.

4 3 Calculated energy loss and ionisation yield spectra:

Energy loss distributions were calculated for monoenergetic neutrons up to 19 MeV using the analytical code by Caswell et al. (1981) which uses nuclear input data evaluated from the Evaluated Nuclear Data File Version B (ENDF/B, Brookhaven National Laboratory, Upton, New-York). The energy deposition spectra were calculated in 1 µm spheres for the wall materials, A-150 TE plastic or carbon, and the TE gas used. Ionisation yield spectra were derived from the energy deposition spectra applying the energy dependence of W values for the different charged particles.

Although influenced by significant uncertainties in nuclear cross secton data and reaction kinematics at high neutron energies, the calculation of ionisation spectra provide useful informations (Bühler et al.,1985). For each wall material they provide the relative contribution of the different reaction channels and charged particle components to the total kerma or the total ionisation yield; in particular they indicate the contribution of different heavy ion species which cannot be distinguished in the experimental spectra (Figure 3). For each charged particle component, the contribution of interactions with the wall and with the gas can be discriminated allowing to account for deviations from the ideal Bragg-Gray chamber in the calculation of the $(r_{m,g})_n$ and W_n factors especially at neutron energies below 14 MeV for which theoretical calculations have relatively low uncertainties (Table 3).

In the present report, for neutron energies from 14 to 19 MeV, the calculated spectra for TEPC's and CPC's indicate that for 1 µm spheres more than 90% of the secondaries are crossers (Table 3); no correction was applied at these energies for interactions with the gas. The calculated spectra were used to estimate approximately

Table 3. Fractions of energy deposited by the secondary charged particles for monoenergetic neutrons in the cavity of A-150 TEPC's and CPC's filled with propane-based TE gas (simulated diameter = 1 µm). The values are derived from the ion yield spectra calculated using the analytical computer code of Caswell and Coyne taking into account the fluence spectra for each neutron field (see text).

A. TEPC / TE

	Percentage of energy deposition per ion per event type				Percentage of total *energy deposition*	Neutron *energy*
Ion type	Insiders	Starters	Stoppers	Crossers	per ion type	(MeV)
p	0 02	0 29	0 69	99 0	91 9	
α	0	4 70	0 82	94 5	0 41	5 25
Be B,C,N,O	1 10	23 6	9 51	65 8	7 71	[1]
All	0 08	2 11	1 37	96 4		
p	0	0 08	0 24	99 7	66 7	
α	0 001	1 58	0 61	97 8	24 2	19
Be B C,N,O	0 68	16 3	3 70	79 3	9 10	[2]
All	0 06	1 92	0 65	97 4		

B. CPC / TE

	Percentage of energy deposition per ion per event type				Percentage of total energy deposition	Neutron energy
Ion type	Insiders	Starters	Stoppers	Crossers	per ion type	(MeV)
p	0 91	99 1	0	0	2 30	
α	0	100	0	0	0 39	5 25
Be B,C,N O	1 40	19 7	11 8	67 1	97 3	[1]
All	1 38	21 9	11 5	65 2		
p	0 49	27 1	0 50	71 9	5 29	
α	0	1 06	0 80	98 1	70 7	19
Be B C,N,O	0 96	13 9	6 10	79 0	24 0	[2]
All	0 24	4 61	2 06	93 1		

[1] (Ti-T), GSF München [2] (Ti-T), PTB Braunschweig

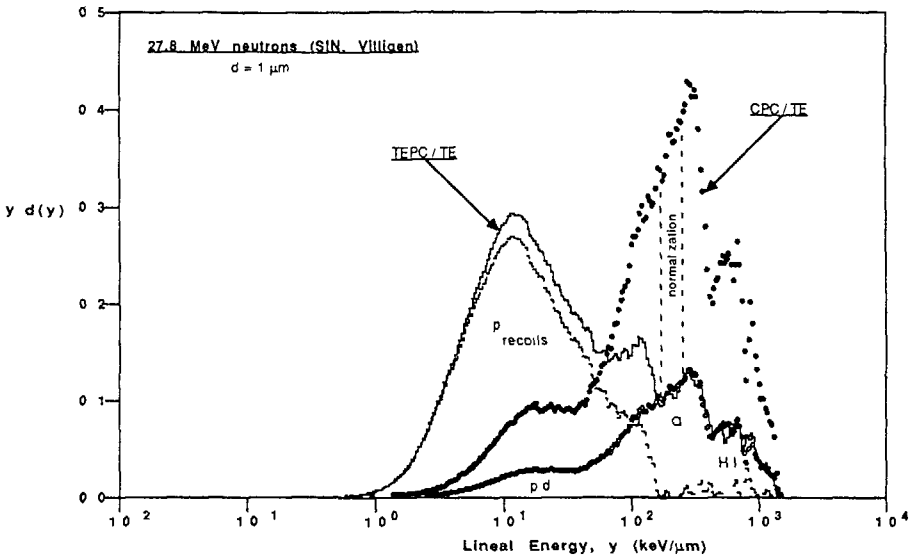

Figure 4 Twin TE and carbon proportional counter technique illustrated for 27 8 MeV neutrons The method is based on the assumption that for a TEPC walled with A 150 plastic the dose fraction above the proton edge is only due to carbon interactions (77 6 % by weigth in A-150) The CPC spectrum is forced to coincide to the TEPC curve above 150 keV/µm The recoil proton component in the TEPC response is derived by substracting the normalized CPC curve from the TEPC spectrum The CPC distribution may be unfolded into three main components protons and deuterons alpha particles and heavy ions (C Be and B)

the relative contribution of the different heavy ion species (Figure 3) For neutron energies from 27 8 to 60 3 MeV, the results of the calculations for 19 MeV were used For 5 MeV neutrons, the calculated ionisation yield spectra for CPC's were used to estimate the contribution of insiders and starters to account for the determination of $(r_{m\,g})_n$, the contribution of N and O ions released by neutron interactions with the gas were taken into account to derive W_n The comparison of the energy loss spectra and ionisation yield spectra enables the theoretical evaluation of the product $(W_n/W_c)\,(r_{m\,g})_n$ (Wuu et al , 1987)

4 4 Twin A-150 — Carbon proportional counter measurements

Although the present calculations of W_n and $(r_{m\,g})_n$ include simplifying assumptions either by using theoretical or experimental spectra for TEPC's and CPC's, the procedure is considerably improved by the combination of the two counters exposed in identical conditions to various neutron fields (Figure 4) For fast neutrons, ionisation yield spectra measured with the TEPC and the CPC show that

the CPC response may be used to approximate the TEPC spectrum above 150 keV/µm and that the small oxygen, nitrogen, calcium and fluorine contributions may be approximated by carbon interactions, this approximation has been supported by the theoretical approach Using this procedure, the contribution of recoil protons in the TEPC spectra can be separated, and the "CPC component" can be unfolded into its main contributions, i e protons, alpha particles, and C, Be and B released ions Using the same separation procedure, the corresponding frequency distributions (Figure 5) have been used to estimate the effective energy of the protons and the alpha particles entering the cavity ($E_{eff\,i}$) from their mean lineal energies ($y_{F,i}$) using the empirical formula described in ICRU Report 33 (1983) The correlation between the effective energy of recoil protons calculated by this method and their average initial energy (equal to $E_n/2$) is illustrated on Figure 6 This method is particularly useful for alpha particles because the very complex reaction channels for alpha particle production prevent any theoretical assessment For heavy ions, the effective energy is assumed to be the mean initial energy as calculated from the nuclear reaction equation using the neutron energy and the Q-value of each reaction

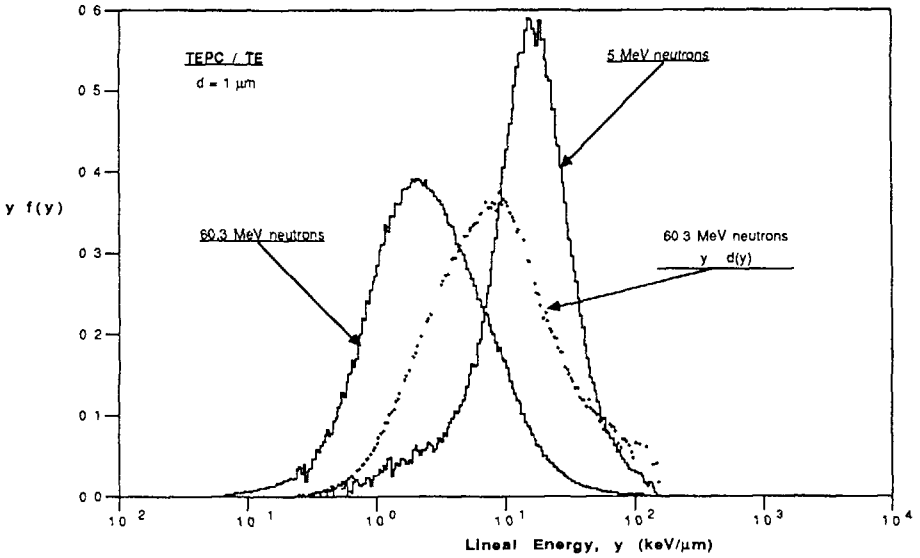

Figure 5 Ionisation yield spectra for the recoil protons produced by elastic scattering in the A 150 TE plastic wall of a proportional counter by 5 MeV and 60 3 MeV neutrons The recoil proton component is obtained from the total dose distribution of lineal energy y d(y) after substracting the alpha particle and the heavy ion components (see Fig 4) The frequency distributions y f(y) are derived from the dose distributions the frequency and dose distributions for recoil protons from 60 3 MeV neutrons are compared

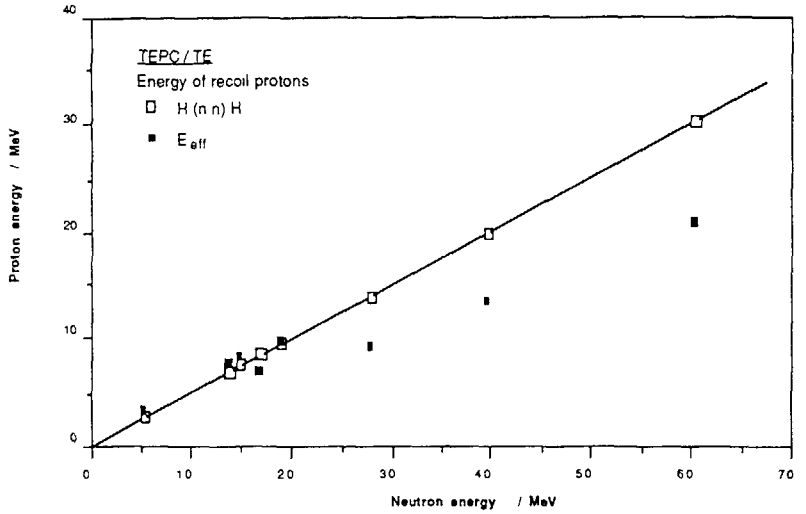

Figure 6 Comparison of the mean initial energy of recoil protons produced by elastic scattering in the wall of a TEPC and the effective energy of the slowing down recoil protons entering the cavity as derived from their mean lineal energy (see text)

4 5 Neutron dose conversion factors

General principles of the method used here were described by Makarewicz et al (1986) The $(r_{m,g})_n$ are derived from the contribution of the different charged particles to the total kerma and from their respective gas-to-wall stopping power ratios This method was adapted to be used for non-hydrogenous proportional counter filled with TE gas by Buhler et al (1986), the relative kerma contributions of different charged particles were derived from the experimental y d(y) distributions The same procedure was used here for the CPC measurements to evaluate the contribution of alpha particles, C, Be and B ions The procedure has been improved for TEPC measurements by separating the recoil proton component and by using the shape of the CPC spectrum for the other species as described above (N and O contributions were neglected) The determination of the mean energy of the charged particles entering the cavity is more difficult The average initial energy may be assessed in good approximation for particles released in elastic scattering processes and in nuclear reactions However, depending on the neutron energy, an evaluation is difficult due to the complexity of inelastic and non-elastic processes especially for alpha particles induced by neutron interactions with carbon In addition, the slowing down spectra differ significantly from the initial spectra at high neutron energy due to the material thickness needed to achieve charged particle equilibrium, for 60 MeV neutrons, the maximum build up in TE material was reached at about 15 mm

In summary dose conversion factors for TEPC and CPC measurements were calculated using the relation

$$(r_{m\ g})_n = \Sigma d_{cr,i}(s_{m,g})_i + d_{in}[K_m/K_g]_n$$

where subscript 'i' stands for the charged particle components, d is their relative contribution to the total kerma, the subscripts 'cr' and 'in' stand for crossers and insiders respectively Insiders were only accounted for 5 MeV neutrons and for CPC measurements, the approximation to add together the contribution of starters and insiders was adopted $s_{m,g}$ were calculated for the mean effective energy of the charged particles entering the cavity using the relations

— for protons and alpha particles $E_{eff,i} = \bar{y}_{F\ i}[R(E_{eff,i}) + d_s]$

— for ion recoils $E_{eff,i} = (m_n + M_i)E_n/(m_n M_i)$

— for the rest energy of ions released in nuclear reactions

$$E_{eff\ i} = E_n - \{2m_n m_x M E_n/(m_x+M_i)^2 + [(M_i Q + E_n(M_i - m_n)]/(m_x+M_i)\}$$

where R is the range of the particle of energy $E_{eff\ i}$ calculated as the integral of the inverse stopping power, d_s is the simulated diameter, the subscript 'x' stands for proton or alpha particle released in a given nuclear reaction with corresponding Q-value As can be seen from the above relation, $E_{eff\ i}$ for heavy ions have been assumed to be their average initial energy and for the nuclear reactions $^{12}C(n,p)^{12}B$ and $^{12}C(n,\alpha)^{9}Be$ This constitutes a large simplification the consequances of which on the uncertainty in the calculation of $(r_{m,g})_n$ are discussed later

Stopping power values were calculated using the fitting formulae of Andersen and Ziegler (1977) for proton and alpha particles including different parameters for the gas and the condense phases for alpha particles Stopping power (condense phase) for heavy ions were calculated from the codes given by Ziegler, Biersack and Littmark (1985) Stopping power in TE gas mixtures and in A-150 TE plastic were derived using the Bragg-Kleeman additivity rule For the simulated diameter of 1 μm used, the contribution of insiders and starters were neglected for neutron fields above 5 MeV For 5 MeV neutrons, corrections were applied using the kerma values tabulated by Caswell and Coyne (1980)

4 6 Average W-values for neutrons

Using the combination of TEPC and CPC spectra as described above, average W_n values were calculated with the relation

$$W_n^{-1} = \Sigma d_{cr,i}\ w_i^{-1} + \Sigma d_{in,i}\ W_i^{-1}$$

where W values for the charged particle component 'i' was obtained for the effective energy $E_{eff,i}$ calculated as in section 4 5 For crossers, the differential w values were calculated using the relations (Schrewe et al , in press)

$$R(E_i) - R(E_f) = d_s$$

$$w^{-1}(E_i, E_f) = (E_i/\Delta E) [W^{-1}(E_i) - W^{-1}(E_f)] + W^{-1}(E_f)$$

As for the calculation of $(r_{m\,g})_n$, interactions with the gas were accounted only for 5 MeV neutrons and for CPC measurements by adding the contributions of insiders and starters and accounting for N and O ion contributions

Experimental data for W-values in propane based TE gas mixture are very scarce (Huber et al , 1985, Posny et al 1987) Some data are available for propane, however, the application of the Bragg additivity rule for W values in gas mixtures is known to be a poor approximation Althougn there is no experimental evidence that ratios of W values are not affected by the difference in the composition of the two gas mixtures, W-values in methane based TE gas were used since only the ratios W_n/W_c are required for the present application The consequences of this assumption are discussed later W_i values were obtained using the functions given by Bichsel and Rubach (1982) For protons above 1 MeV, the values obtained by Thomas and Burke (1985) were used Above 5 MeV a constant value of 29 6 eV was adopted, the differential w value was assumed to be identical

5 RESULTS AND DISCUSSION

51 TEPC AND CPC MEASUREMENTS

Dose distributions of lineal energy for monoenergetic neutrons measured with TEPC's allow to distinguish the different charged particle components (proton, alpha particles and heavy ions) and to determine their contribution to the total kerma which can be easily visualized by the aerea under the curve, the total integral being normalized to unit dose (Figure 1, 2 and 4) The spectra obtained with CPC's illustrate the complexity of neutron interactions with carbon depending on the neutron energy and the threshold of different nuclear reactions (Figure 2) For 5 MeV neutrons, the total kerma is mainly due to carbon recoils released in the wall, the cut off of the distribution is due to their low mean energy (average initial energy 750 keV) At 15 MeV, a peak due to alpha particle can be seen together with a increase of the heavy ion component mainly attributed to Be ions released in $^{12}C(n,\alpha)^{9}Be$ reaction At higher neutron energies, the alpha and heavy ion components appear clearly but the broadness of the peaks illustrates the complexity of different processes leading to the release of alpha particles (Menzel, 1987) Measurements at neutron energy above 20 MeV indicate a significant contribution of protons produced by the (n,p) reaction in carbon around 10 keV/µm

Theoretical calculation of ionisation yield spectra in 1 µm spheres surrounded by A-150 TE plastic or by carbon were performed for 5, 13 9, 15, 17 and 19 MeV neutrons (Table 3, Figure 3) The neutron spectral fluence values were available for these neutron fields (Menzel et al ,1984) For TEPC's the calculated spectra show the predominant contribution of recoil protons, the CPC spectra are dominated by carbon recoils and, above 5 MeV, by alpha particles Above 5 MeV, more than 90 % of the total kerma for TEPC's and CPC's is due to crossers for 1 µm spheres, interactions with the gas do not exceed 2 5 % for TEPC's and 6 5 % for CPC's. For 5 MeV neutrons, more than 20 % of the absorbed dose is due to interactions with the gas for CPC's, they were taken into account in the calculations of the dose conversion factors The small contribution fo N and O ions to the total kerma for TEPC spectra supports the validity of the assumption that events above the proton edge are mainly due to carbon interactions in A-150 plastic

The combination of TEPC and CPC measurements, illustrated in Figure 4, considerably improve the unfolding of the TEPC spectrum into its charged particle components. This method allows a precise determination of the recoil proton component and consequantly allows to determine in good approximation the mean energy of the recoil protons entering the cavity (Figure 5 and 6) including their slowing down in the chamber wall and surrounding material For the other secondaries, in particular for alpha particles, the pragmatic approach to use fixed lineal energy intervals could be improved by a more accurate approximation of the heavy ion and proton peaks but would require further analysis Within the limits of applicability of these assumptions, the present method has the advantage to derive the effective energy of the particles entering the cavity from their experimental ionisation yield distributions

The physical properties of the neutron beams used for therapy are generally not well known (e g spectral fluence, low energy contamination) This limits further progress in neutron dosimetry for the high energy beams actually used for routine clinical applications At earlier neutron therapy facilities, d(14)+Be neutron beams and 14 MeV neutron beams produced by D+T generators were often used, the actual tendency is to use neutron beams produced using the p+Be reaction at energies up to 65 MeV for the better balistic properties of the beams A microdosimetric intercomparison was recently performed at several European facilities in order to compare the differences in radiation quality between the different neutron beams used (Pihet et al , 1987) The neutron therapy beams are often described in terms of their mean neutron energy The concept of mean energy, especially for broad neutron spectra produced by the d+Be and p+Be reactions, is very limited due to the complexity of neutron interactions and their energy dependence as illustrated in Figures 7 and 8 In d(14)+Be neutron beams (average energy equal to 5 6 MeV), neutrons below and above 5 MeV contribute almost equally to the total fluence

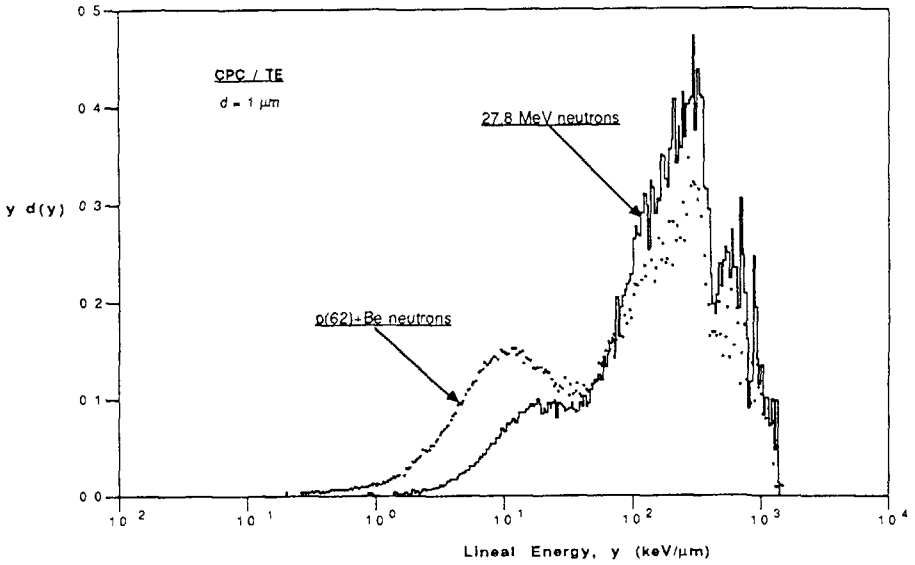

Figure 7 Comparison of ionisation yield spectra measured with CPC s in the same conditions for 27 8 MeV monoenergetic neutrons (SIN, Villigen) and for p(62)+Be neutron therapy beams with broad *neutron spectra* (MRC Cyclotron, Clatterbridge)

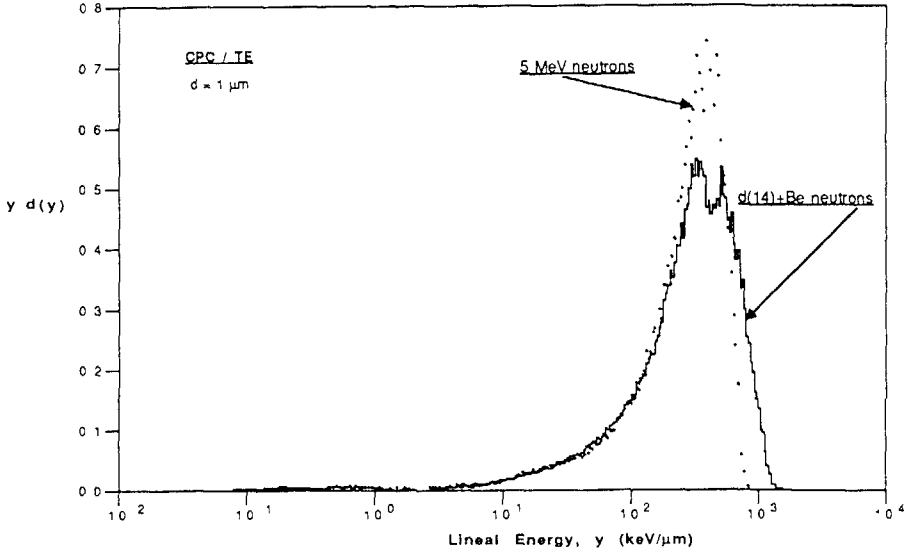

Figure 8 Comparison of ionisation yield spectra measured with CPC's in the same conditions for 5 MeV monoenergetic neutrons (PTB Braunschweig) and for d(14)+Be collimated neutron beams with broad neutron spectra used as reference standard for dosimetry in neutron therapy (PTB, Braunschweig)

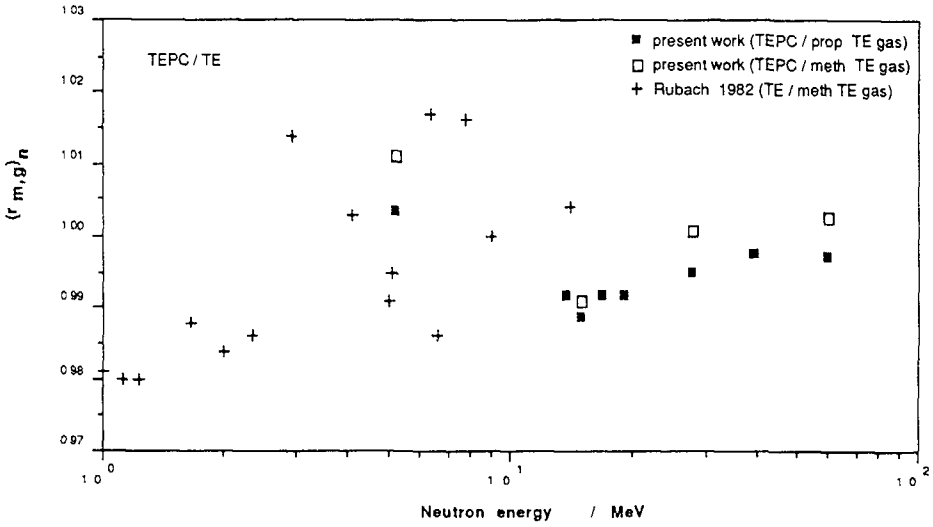

Figure 9 Dose conversion factors for a proportional counter walled with A-150 TE plastic and filled with propane based TE gas (simulated diameter 1 µm) exposed to monoenergetic neutrons from 5 to 60 MeV At some energies, conversion factors were also calculated using stopping power in methane based TE gas and are compared to the values given by Rubach and Bichsel (1982) for a TE chamber in case of an infinitesimal cavity

spectrum (Dietze et al , 1984) The interpretation of the lineal energy spectra is therefore difficult (Figure 8), however at this energy, theoretical calculations are sufficently accurate For neutron therapy beams ranging from e g p(34)+Be to p(65)+Be, the high energy component of the neutron fluence spectrum has a significant influence on the shape of the ionisation yield distributions due to the energy dependence of neutron crosss sections, at these energies, theoretical calculations have large uncertainties The empirical method proposed here to derive the $(r_{m,g})_n$ and W_n values implicitely includes neutrons interactions over the entire spectra Its application to the physically poorly defined neutron therapy beams therefore appears very suitable.

5 2 Neutron dose conversion factors for TEPC's and CPC's from 5 to 60 MeV

Dose conversion factors were derived for monoenergetic neutrons from 5 to 60 MeV for TEPC and CPC filled with propane based TE gas by unfolding the measured dose distributions of lineal energy into their charged particle components (Figure 4 and 5) and by using stopping power tables by Andersen and Ziegler (1977, 1985). $(r_{m,g})_n$ values for TEPC's are found to be close to unity in agreement with the values reported elsewhere at lower neutron energies (Figure 9) (Rubach and Bichsel, 1982;

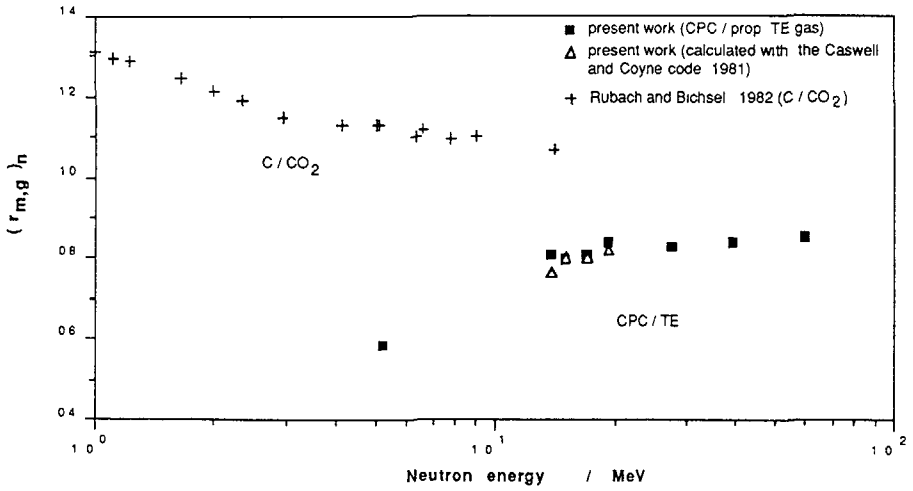

Figure 10 Dose conversion factors for a proportional counter walled with pure graphite and filled with propane based TE gas (simulated diameter 1 µm) exposed to monoenergetic neutrons from 5 to 60 MeV They were derived by using stopping power data by Andersen and Ziegler (1977) and experimental ionization yield spectra (see text) Conversion factors were also derived by comparing ionisation yield and energy loss spectra theoretically calculated using the Caswell and Coyne code for neutron energies between 14 and 19 MeV The values obtained by Rubach and Bichsel for a carbon ionization chamber in case of an infinitesimal cavity are added in order to illustrate the problem encoutered in evaluating dose conversion factors for non hydrogenous gas cavity detectors

Burger and Makarewicz, 1987) A step of about 1 5 - 2 % observed for $(r_{m,g})_n$ between 5 and 14 MeV is attributed to the production of alpha particles above the $^{12}C(n,\alpha)^{9}Be$ reaction treshold of 5 1 MeV, $(r_{m,g})_n$ slightly increases at higher neutron energies up to 1 due to the higher energy of the secondary charged particles At some energies, slightly higher values for $(r_{m\,g})_n$ were obtained using the same method and stopping powers in methane based TE gas, they are in good agreement with the values obtained by Rubach and Bichsel (1982) for TE ionisation chambers assuming an infinitesimal cavity At 14 MeV neutron energy, the uncertainty on $(r_{m,g})_n$ is found to be ±7 % A similar result was obtained by Rubach and Bichsel With the same approach, the uncertainty is reduced to ± 5 % at the level of 60 MeV neutron energy $(r_{m,g})_n$ values for CPC's increase with neutron energy from O 58 at 5 MeV to a plateau value of 0 84 above 20 MeV (Figure 10) The uncertainty on $(r_{m,g})_n$ is found to be ±8 % at 14 MeV and is reduced to ±6 % at 60 MeV At 5 MeV, the uncertainty of $(r_{m,g})_n$ is larger due to large uncertainty in stopping power for carbon ions and to uncertainty of kerma factors in A-150 and in carbon, the presented values do not take into account the influence of phase effect on stopping power of carbon ions Even if the large uncertainties are taken account of, the shape of the curve is different from the curve found for a C/CO_2 chamber by Rubach and Bichsel This is explained by the different composition of the gas mixtures

The more pronounced variation of conversion factors for CPC's with neutron energy is due to the variation of stopping power ratios in carbon and in TE gas for the different types of charged particles produced at energies below 10 MeV For TEPC, the stopping power ratios for protons above 100 keV is almost constant and equal to 1 However stopping power ratio for alpha particle in A-150 and in TE gas critically depends on particle energy between 100 keV and 10 MeV (Figure 11) This variation does not agree with the values obtained by Makarewicz et al. (1986) above 1 MeV The method used was different in that the authors had used the mean excitation energy values for TE gas and TE plastic recommended in ICRU Report 37 (1986) whereas the Bragg additivity rule was used here for the Ziegler's stopping power This points out the uncertainties associated with the approximation of using the Bragg additivity rule for solid compounds due to chemical binding effects Similarly, the stopping power ratios for protons above 400 keV derived from Makarewicz's calculations are about 3 % lower than those calculated from Ziegler's stopping power The application of Makarewicz's data for protons and alpha particles would lead to differences in $(r_{m,g})_n$ of 1 7 % for TEPC and 8 % for CPC for 15 MeV neutrons, for 60 MeV neutrons differences of 0 5 % for TEPC and of 1 4 % for CPC would be obtained

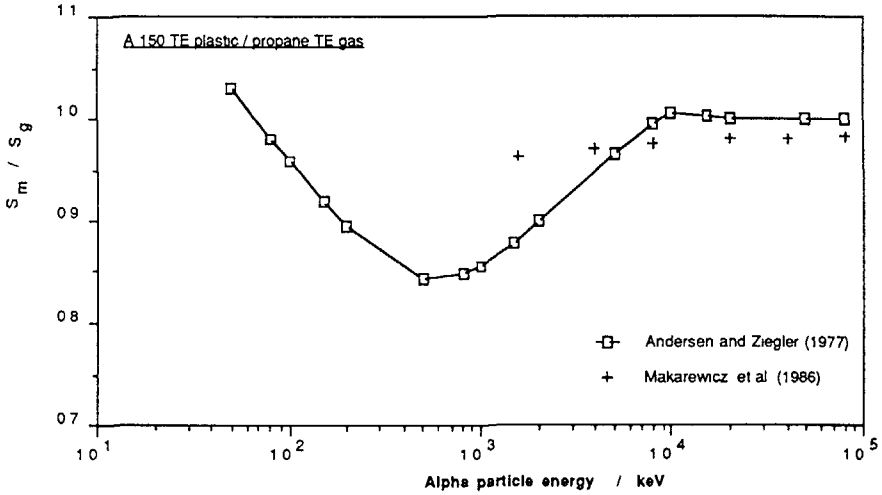

Figure 11 Comparison of stopping power ratio in A-150 TE plastic and in propane based TE gas for alpha particles derived from Andersen and Ziegler fitting formulae (1977) using the Bragg additivity rule, and data obtained by Makarewicz et al (1986) using the mean excitation energy values recommended in ICRU Report 37 (1984)

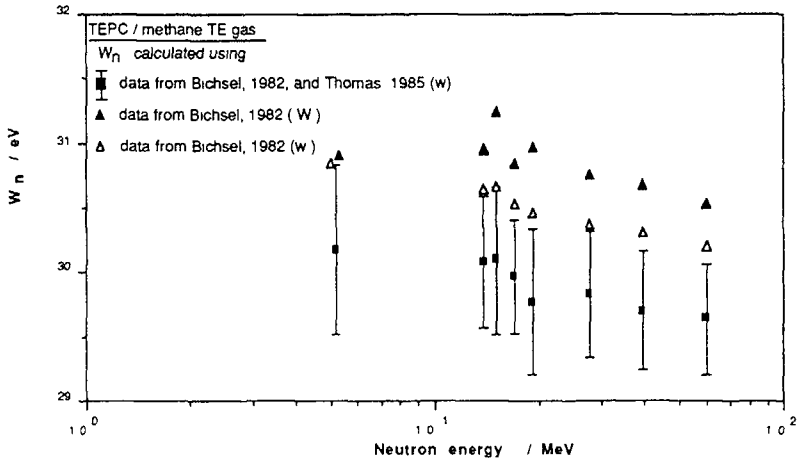

Figure 12. Average W values for monoenergetic neutrons from 5 to 60 MeV derived for a cavity filled with methane based TE gas (diameter = 0 1 mg/cm).2Effective mean energies yield spectra measured with TEPC's and CPC's filled with propane based TE gas Integral and differential W-values were calculated using the W-functions given by Bichsel and Rubach. Final results were obtained using the W values for protons above 1 MeV found by Thomas and Burke Overall uncertainties ΔW (see Table 4) are indicated

5.3. Average W-values for neutrons from 5 to 60 MeV for TEPC's and CPC's filled with propane based TE gas:

Average W-values for neutrons between 5 and 60 MeV were derived from TEPC and CPC measurements and using W-data in methane based TE gas (Figure 12, Table 4). In neutron dosimetry, atomic data are needed for different types of charged particles and over wide energy ranges. W-functions for protons, alpha particles and heavy ions are available for methane based TE gas with an overall uncertainty of ±3 % whereas W-values for propane based TE gas are very scarce (Goodman and Coyne, 1980; Bichsel and Rubach, 1982). W values in methane based TE gas for protons above 1 MeV were recently obtained by Thomas and Burke (1985) with a very low uncertainty (<0.7 %) which reduces the overall uncertainty of present W_n values for TEPC to ±1.5 - 2.5 %. W_n values were calculated using differential w values for crossers. Calculation were also performed using the same method but with integral W functions given by Bichsel (Figure 12); the results are in good agreement with the values obtained by Rubach and Bichsel (1982) at lower neutron energies. Higher W_n values were found for CPC's; they decrease faster with neutron energy.

The presented method has the advantage to correlate the calculation of W_n to the slowing down spectra of the charged particles produced in the counter wall. However, the uncertainty of W_n critically depends on the uncertainty in the average effective energy of the charged particles entering the cavity as determined by unfolding the experimental ionisation yield spectra. Taking these uncertainties into account, overall uncertainties on W_n for CPC in the present calculations were estimated to range at a maximum from ±3 % to ±8 % for neutron energy from 60 to 5 MeV respectively (Table 4). The presented results can only be taken as approximation since they were obtained for methane based TE gas whereas the

Table 4. W_n values for TEPC's and CPC's obtained for monoenergetic neutrons. W-values are calculated for methane based TE gas using the W-values for protons obtained by Thomas and Burke (1985) and the functions given by Bichsel and Rubach (1982) for alpha particles and heavy ions. Values in brackets are the uncertainties on W_n obtained by adding by quadrature the overall uncertainties on W-values for the different ions. Overall uncertainies (ΔW) take into account the uncertainties added by evaluating the mean effective energy of the secondary charged particles entering the cavity from the energy deposition spectra measured with the TEPC and the CPC in the same conditions for each neutron beam (see text).
The same calculation procedure was applied to derive W_n values for three different neutron beams used for therapy.

Neutron	TEPC			CPC		
energy (MeV)	W_n (eV)		ΔW_n (eV)	W_n (eV)		ΔW_n (eV)
5 0	30 17	(0 17)	0 65	38 19	(1 5)	3 0
13 9	30 08	(0 18)	0 51	32 07	(0 68)	2 31
14 95	30 09	(0 21)	0 58	31 66	(0 70)	2 18
17 0	29 97	(0 20)	0 44	31 32	(0 73)	1 87
19 0	29 77	(0 24)	0 56	30 58	(0 73)	1 85
27 8	29 82	(0 21)	0 49	30 33	(0 60)	1 62
39 7	29 70	(0 20)	0 47	30 00	(0 51)	1 38
60 3	29 64	(0 19)	0 43	29 71	(0 44)	1 07
d(14)+Be	29 82	(0 16)	0 40	31 68	(0 78)	2 0
d(0 25)+T	30 09	(0 19)	0 53	31 91	(0 68)	2 31
p(62)+Be	29 76	(0 20)	0 47	30 02	(0 48)	1 24

counters were filled with propane based TE gas As a matter of fact, the experimental results obtained by Nguyen et al (1980) and by Posny et al (1987) show that the assumption of a constant ratio W_n/W_c may not be valid since the ratio of propane based TE gas to methane based TEgas W values is not constant for different charged particles below 500 keV

6 CONCLUSIONS

Dose conversion factors and average W values for neutrons from 5 to 60 MeV were derived for tissue-equivalent and for carbon proportional counters filled with propane based TE gas (simulated diameter 1 μm) The presented method uses the experimental ionisation yield spectra obtained with TEPC's and CPC's in order to indentify the different charged particle components released by neutron interactions in the counter wall and in the gas cavity and to determine their contribution to the total absorbed dose For the proton and the alpha particle components, the frequency distributions of lineal energy in fixed intervals were used to derive the mean effective energy of the charged particles slowing down in the wall before entering the cavity Additional informations on the relative contribution to the absorbed dose of interactions in the wall and in the gas were obtained from theoretical energy deposition and ionisation yield spectra up to 19 MeV Different stopping power tables and W functions used to calculate $(r_{m\,g})_n$ and W_n values were compared

Atomic and molecular data are basic input physical data necessary to use gas cavity detectors in neutron dosimetry The accuracy achievable in neutron absorbed dose measurements with ionisation chambers and with proportional counters critically depends on the uncertainties of stopping powers and W values for different types of charged particles In proportional counters, the $(r_{m\,g})_n$ take account mainly of the stopping power ratios for particles crossing the cavity Uncertainties of stopping power ratios for protons and alpha particle are still relatively large (3 to more than 10 % depending on the energy) mainly due to the approximation made by using the Bragg additivity rule for gas mixtures and for compound materials At high neutron energies, a significant fraction of the absorbed dose is due to heavy ions for which stopping powers in gas and condense phase are documented with large uncertainties W functions in methane based TE gas are known with uncertainties of the order of 3 % More accurate experimental data are available but are still rather scarce and limited to partial energy intervals For proportional counter measurements, W data in propane based TE gas are required Partial experimental data obtained for this TE gas mixture show that the approximation of using W-values inmethane based TE gas presents considerable problems in the evaluation of microdosimetric measurements

The proposed method to derive $(r_{m,g})_n$ and W_n has the advantage to use the informations contained in the experimental ionisation yield spectra over the entire distributions of energy deposition events by the different charged particles released by neutrons The procedure have been improved by the combination of TEPC and CPC measurements In the low neutron energy range, this pragmatic approach may be combined with the more formal theoretical approach using energy deposition calculations At high neutron energies, the method is very suitable since theoretical calculations have large uncertainties The uncertainties of the presented $(r_{m,g})_n$ were assessed to decrease from ±7 % to ± 5 % for TEPC's and from ±8 % to ± 6 % for CPC's from 14 to 60 MeV respectively, at lower neutron energies, larger uncertainties are reached due to the lower energy of the ions and due to the increasing contribution of neutron interactions with the gas Overall uncertainty of W_n were found lower than ±2 5 % for TEPC's and decreases from ± 8 % to ±1 5 % for CPC's between 5 and 60 MeV respectively

Table 5 Ratio of kerma factors of carbon and A-150 TE plastic determined by combination of TE and graphite proportional counter measurements. Values presented earlier (1][2][3) are revised according to the $r_{m,g}$ and W_n values calculated in the present report; the differences (Δ) in kerma ratios between the two analysis are given in the last column The kerma factor ratios are given for monoenergetic neutrons; additional results obtained by using the same procedure for three different neutron therapy beams are given for comparison.

Neutron energy (MeV)	$\frac{(r_{m,g})_C\ (W_n)_C}{(r_{m,g})_{A\text{-}150}\ (W_n)_{A\text{-}150}}$	$K_C / K_{A\text{-}150}$ first analysis	$K_C / K_{A\text{-}150}$ present work	Δ (%)
5 0	0 738		0 159	
13 9	0 872	0 261 (1)(2)	0 265	+ 1 4
15 0	0 847	0 298 (1)(2)	0 296	- 0 5
17 0	0 853	0 347 (1)(2)	0 343	- 1 1
19 0	0 866	0 393 (1)(2)	0 405	+ 2 8
27 8	0 848	0 374(3)	0 372	- 0 6
39 7	0 850	0 437 (3)	0 448	+2 4
60 3	0 855	0 527 (3)	0 537	+ 1 8
d(14)+Be	0 858		0 1495	
d(0 25)+T	0 8382	0 294 (3)	0 284	- 3 6
p(62)+Be	0 8557	0 493 (3)	0 467	- 5 6

(1) Menzel et al, 1984 (2) Dietze, (in preparation) (3) Menzel et al ,(in press)

The same procedure was applied for microdosimetric measurements performed at different European neutron therapy facilities. Accurate values for $(r_{m,g})_n$ and W_n are required for the improvement of neutron dosimetry protocols in order to achieve the accuracy of ± 5 % required for the absorbed dose delivered during treatments At neutron energies above 20 MeV, no $(r_{m,g})_n$ and W_n were available up to now

In neutron dosimetry, kerma factors in different materials, in particular for the elemental constituents of TE substitutes, are needed to enable the determination of the absorbed dose in real tissues The combination of TEPC and CPC measurements were used to determine the kerma ratio of carbon to A-150 TE plastic for neutrons for various neutron fields. The results presented earlier were revised using the $(r_{m,g})_n$ and W_n values reported here Differences between the two analysis up to 3 % were found for well defined monoenergetic neutron fields from 5 to 60 MeV (Table 5) For neutron therapy beams, the present calculations imply larger corrections

ACKNOWLEDGEMENTS

This work was supported by the Commission of the European Communities under contract n° BI-6-010-D, and by the Bundesministerium fur Forschung und Technology (F R G) We would like to thank Drs. JJ Coyne and R S Caswell for providing the analytical code for energy deposition calculations

REFERENCES

1 Andersen, H H and Ziegler, J F Hydrogen stopping powers and ranges in all elements In Vol 3 of *The stopping and ranges of ions in matter*, J F Ziegler ed , Oxford (Pergamon Press) (1977)

2 Armstrong, T W and Chandler, K C Stopping powers and ranges for muons, charged pions protons, and heavy ions Nucl Instrum Methods, **113**, 313 314 (1973)

3 Bichsel, H and Rubach, A Neutron dosimetry with spherical ionisation chambers II Basic physical data Phys Med Biol **27**, 1003-1013 (1982)

4 Bonnett, D E , Blake, S W , Shaw, J E and Bewley D K The Clatterbridge high energy neutron therapy facility specification and performance Brit J Radiol , **61**, 38-46 (1988)

5 Brenner, D J , Zaider M Coyne, J J , Menzel, H G and Prael, R E Evaluation of nonelastic neutron cross sections on carbon above 14 MeV Nuclear Science and Engineering **95** 311-315 (1987)

6 Burger, G and Makarewicz, M Average energy to produce an ion pair in gases (W values) and related quantities of relevance in neutron dosimetry In Nuclear and atomic data for radiotherapy and related radiobiology, IAEA Vienna, **INDC (NDS)-175/L+MO**, 225-238 (1987)

7 Buhler, G Menzel H G and Schuhmacher, H Neutron interaction data in carbon derived from measured and calculated ionisation yield spectra In Proc 9th Symp on Microdosimetry, J A Dennis, J J Booz and B Bauer eds , Radiat Prot Dosimetry, **13**, 13-17 (1985)

8 Buhler, G , Menzel, H G , Schuhmacher, H , Dietze, G and Guldbakke, S Neutron kerma factors for magnesium and aluminium measured with low pressure proportional counters Phys Med Biol , **31**, 601-611 (1986)

9 Caswell, R S and Coyne, J J Kerma factors for neutron energies below 30 MeV Radiat Res , **83**, 217-254 (1980)

10 Caswell, R S *Deposition of energy by neutrons in spherical cavities* Radiat Res , **27**, 92 107 (1966)

11 Caswell, R S , Coyne, J J and Goodman L J Comparison of experimental and theoretical ionisation yield spectra for neutrons In Proc 4th Symp on neutron dosimetry, G Burger and H G Eberts eds , Commission of the European Communities (Luxembourg), **EUR7448**, 201 212 (1981)

12 Combecher, D Measurement of W values of low-energy electrons in several gases Radiat Res , **84**, 189-218 (1980)

13 Deluca, P M , Barschall, H H Haight, R C and McDonald J C Measured neutron carbon kerma factors from 14 1 MeV to 18 MeV, Proc 5th Symp on neutron dosimetry, H Schraube and G Burger eds , Commission of theEuropean Communities (Luxembourg), **EUR 9762**, 193 200 (1985)

14 Dietze, G , Brede, H J and Schlegel-Bickmann D Dosimetry for neutron therapy at the Physikalisch-Technische Bundesanstalt (PTB) In Advances in dosimetry for fast neutrons and heavy charged particles for therapy applications, **IAEA-AG--371/14**, 203-215 (1984)

15 Dietze, G , Buhler, G , Menzel, H G and Schuhmacher, H in preparation

16 Dietze, G , Menzel, H G and Buhler, G , Calibration of tissue-equivalent proportional counters used as radiation protection dosemeters In Proc Workshop on Micordosimetric counters in *radiation protection*, J Booz, A A Edwards and K G Harrison eds , Commission of the European Communities Radiat Prot Dosimetry, **9**, 245-249 (1984)

17 Goodman, L J and Coyne J J W_n and neutron kerma for methane based tissue equivalent gas Radiat Res ,**82**, 13 -26 (1980)

18 Höver, K H , Lorenz, W J and Maier-Borst, W Experience with the fast neutron therapy facility Karin under clinical conditions In Proc 4th Symp on neutron dosimetry, G Burger and H G Eberts eds , Commission of the European Communities (Luxembourg), **EUR7448**, 31 (1981)

19 Huber, R , Combecher, D and Burger , G Measurement of average energy required to produce an ion pair (W value) for low-energy ions in several gases Radiat Res , **101** 237-251 (1985)

20 International Commission on Radiation Units and Measurements, Average energy required to produce an ion pair Report **31**, ICRU Publications, Washington D C (1979)

21 International Commission on Radiation Units and Measurements Microdosimetry Report **33** ICRU Publications, Washington D C (1983)

22 International Commission on Radiation Units and Measurements Stopping powers for electrons and positrons Report **37**, ICRU Publications, Washington D C (1984)

23 Makarewicz, M , Burger, G and Bichsel H On the stopping power for tissue equivalent gaseous ionisation devices used in neutron dosimetry Phys Med Biol **31**, 281-284 (1986)

24 Menzel H G *Fast neutron and pion interaction data from low pressure proportional counter* measurements In Nuclear and atomic data for radiotherapy and related radiobiology, IAEA Vienna **INDC (NDS)-175/L+MO**, 265-284 (1987)

25 Menzel, H G , Bullher, G , Schuhmacher, H , Muth, H , Dietze, G and Guldbakke, S Ionisation distributions and A-150 plastic kerma for neutrons between 13 9 and 19 MeV measured with a low pressure proportional counter Phys Med Biol , **29**, 1537-1554 (1984)

26 Menzel, H G , Pihet, P , Kolkerts, K H , Dahmen, P and Grillmaier, R E Dosimetry research using low pressure proportional counters for neutrons with energies up to 60 MeV In Proc 6th Symp on neutron Dosimetry, Rad Prot Dosimetry, in press

27 Mijnheer, B J , Wootton, P , Williams, J R , Eenmaa, J and Parnell, C J Uniformity in dosimetry protocols for therapeutic applications of fast neutron beams Med Phys , **14**, 1020-1026 (1987)

28 Nguyen , V D , Chemtob, M , Chary, J , Posny, F and Parmentier, N Recent experimental results on W-values for heavy particles Phys Med Bil , **25**, 509-518 (1980)

29 Pihet, P , Menzel, H G , Vynckier, S , Gueulette, J and Wambersie, A Proposal for a microdosimetric intercomparison between European neutron therapy centres In Proc of the EORTC Heavy Particle Therapy Group (Clatterbridge, U K), D K Bewley and R D Errington eds , Brit J Radiol , **60**, 313 (1987)

30 Posny , F , Chary, J and Nguyen, V D W values for heavy particles in propane and in TE gas Phys Med biol , **32**, 509-515 (1987)

31 Rubach, A and Bichsel, H Neutron dosimetry with spherical ionisation chambers I Theory of the dose conversion factors r and W_n Phys Med Biol ,**27**, 893-904 (1982)

32 Schrewe, U J , Brede, H J , Pihet, P and Menzel, H G On the calibration of tissue-equivalent proportioanl counters with built-in alpha sources In Proc 6th Symp on neutron Dosimetry Rad Prot Dosimetry, in press

33 Srdoc D Experimental technique of measurement of microscopic energy distribution in irradiated matter using Rossi counters Radiat Res , **43**, 302-319 (1970)

34 Thomas, D J and Burke, M W value measurements for ^{241}Am alpha particles in various gases Phys Med biol , **30**, 1215-1223 (1985)

35 Thomas, D J and Burke, M W value measurements for protons in tissue-equivalent gas and its constituent gases Phys Med Biol , **30**, 1201-1213 (1985)

36 Waibel, E and Willems, G Stopping power and ranges of low-energy protons in tissue-equivalent gas Phys Med Biol , **32**, 365-370 (1987)

37 Wambersie, A and Gueulette, J Accuracy required in radiotherapy and in neutron therapy In Advances in dosimetry for fast neutrons and heavy charged particles for therapy applications, **IAEA-AG--371/1**, 1-26 (1984)

38 Wuu, C S and Milavickas, L R Determination of the kerma factors in tissue-equivalent plastic, C, Mg, and Fe for 14 7 MeV neutrons Med Phys , **14**, 1007-1014 (1987)

39 Ziegler, J F Helium stopping powers and ranges in all elemental matter In Vol 4 of The stopping and ranges of ions in matter J F Ziegler ed , Oxford (Pergamon Press) (1977)

40 Ziegler, J F , Biersack, J P and Littmark, U The stopping and range of ions in solids In Vol 1 of The stopping and ranges of ions in matter, J F Ziegler ed Oxford (Pergamon Press) (1985)

ENERGY DEPOSITION IN THE NANOMETER SITES BASED ON THE TRACK STRUCTURE CALCULATIONS

P. OLKO*, J. BOOZ
Institut für Medizin,
Kernforschungsanlage Jülich GmbH,
Jülich, Federal Republic of Germany

H.G. PARETZKE
Institut für Strahlenschutz,
Gesellschaft für Strahlen- und
Umweltforschung mbH München,
Neuherberg, Federal Republic of Germany

W.E. WILSON
Pacific Northwest Laboratories,
Richland, Washington,
United States of America

Abstract

In this paper microdosimetric and radial dose distributions, calculated with track structure codes Moca-8 and Moca-14 for different radiation types are presented and compared with existing experimental data. The energy deposition and ionization spectra for low site diameters are shown and the conversion factors between energy deposition and ionization are given. The influence of atomic and molecular data used by the codes on the results is briefly discussed.

I. Introduction

Monte Carlo radiation track structure codes are useful tools for the calculation of various quantities important for radiotherapy and radiobiology. This is especially true for

*) On leave from Institute of Nuclear Physics,
ul. Radzikowskiego 152, Pl-31342 Kraków, Poland.

those quantities which are actually not, or not easily, measurable. In addition, the comparison of second order quantities calculated with such programs (e.g. LET, W-values, microdosimetric or radial dose distributions) with existing experimental data offers a test for the quality of the code and underlying atomic and molecular data.

The aim of this paper is to show several examples of microdosimetric calculations performed with the track structure programs Moca-8 and Moca-14 [1,2] and to compare the results to existing experimental microdosimetric and radial dose distributions. Measurements of microdosimetric spectra with proportional counters or radial dose distributions with ion-chambers deliver information on ionization induced by ions in a sensitive counter volume. Energy deposited is often evaluated by multiplying the number of ionizations in the volume of interest by an average W-value. The derivation of the correct average is, however, difficult for site dimensions and radial distances of less than a few nanometers (at unit density). This paper shows the differences in the ionization and energy deposition spectra and gives approximative conversion factors between the energy and number of ionizations in sites of nanometer diameters.

II. Microdosimetric methods

The yields of ionizations and excitations, produced by ionizing radiation are of basic importance for radiotherapy. Not only the absolute frequency of primary activations but also their spatial distributions are of special interest for understanding the radiation action in biological matter. It is the scope of microdosimetry to investigate statistical and spatial correlation of energy deposition events in small sites. The basic tools for microdosimetry are measurements with proportional counters and calculations based on charged particle track simulations. Up to now, measurements of energy deposition spectra are limited to dimensions of the sensitive volume not much lower than one micrometer. Monte-Carlo track simulations are still the only method to study energy deposition in the sites of nanometer dimension and to provide information on the spatial aspects of an energy deposition event within this site.

The most important simplification introduced in the microdosimetric analysis is the substitution of the whole complicated, spatial pattern of atomic, molecular or nuclear reactions by a single parameter: energy deposited in the site of interest [3]. Energy deposited within the sensitive volume in several interactions is simply added disregarding the type and internal structure of events in the volume. This energy imparted can next be normalized with regard to one of the parameters characterizing the volume of interest (mean-chord length or mass), leading to lineal energy, y, or specific energy, z. Instead of energy imparted, the number of ionizations (ionization yield) in the site is often used, which is more directly connected to actual experimental reality.

The sizes of events in a sensitive volume depend on the shape of the site and the actual spatial pattern of a particle track. These two factors lead to frequency distributions of energy deposition sizes in the sensitive volume. Therefore, the shape of such a microdosimetric distribution contains information on the shape of the site as well as on the geometrical distribution of events in the track.

Monte-Carlo radiation track structure programs are intended to simulate the relevant processes in tracks of charged particles, i.e. the spatial distribution of primary ionizations and excitations, which happened during the passage of a ionizing particle. The spatial distribution of

these energy absorption points represents the frozen picture of energy deposition events at the time of about 10^{-12} s after the particle passage. This structure can be used to evaluate e.g. the primary energy input to sensitive targets of arbitrary structure [4]. Extracting spatial information from computer simulated tracks can be done with simple methods of geometrical probability. In the present calculations effective algorithms to evaluate tracks for microdosimetric distributions were applied [5].

III. Overview of the used track structure programs

All results presented in this paper are based on track structure simulations performed with the electron code Moca-8 and ion code Moca-14. Both programs simulate tracks in the model target water vapor. For easier use of the results in the radiation research for the generation and testing of hypothesis on biological radiation action the spatial coordinates are converted for a mass density of 1 g/cm^3.

Moca-14 is a code for the generation of ion tracks. The program follows the history of an ion and all its secondary electrons. Elastic scattering of the ion is not considered since it is only of the minor importance in the energy range considered for radiation biology. The ion is assumed to travel through the medium with constant energy (so-called track segment regime). All energy deposition events caused directly by the ion are assumed to lie directly on the ion path. For a 0.8 MeV proton, about 50% of the ionizations are created by the ion itself and thus located on the track path. The secondary electron spectrum and all cross-sections are modeled in the program for protons. Lacking adequate cross sections, scaling for other ions is done to a preliminary, first approximation by multiplying the total interaction cross section by the squared effective charge derived from range measurements in nuclear emulsions [6].

This changes the total collision free path and therefore the total frequency of events. The results obtained by this approach should only be considered as qualitatively describing differences in tracks of heavier ions as compared to those for protons and alpha particles. They should not be evaluated in a quantitative way, since many data indicate the failure of such a simple scaling for many track structure quantities. The actual distances between collisions, l, are calculated according to the distribution,

$$f(l) = s\, e^{-s\, l}$$

where s is the macroscopic total interaction cross section. When the interaction point is reached, a decision is taken which process is chosen, ionization or excitation. In the case of an ionization, the energy of the secondary electron and its angle to the the ion axis is calculated and the electron then is followed by the electron transport program Moca-8.

Moca-14 is the modification of the previous code Moca-13 which has been already described in literature [7]. Two major modifications were introduced [2]:

a) The cross section for the ion-induced ejection of electrons from water vapor are calculated from an analytical model that uses photoabsorbtion and ion impact ionization data to evaluate the coefficients in Bethe's asymptotic cross section for inelastic scattering of high velocity ions [8]. The advantage of this formula over the previous one [9] is that it can be extended to higher proton energies for which no experimental cross section data are yet available [8,10].

b) In Moca-13 the energy deposition by excitations due to the incident ion was approximated by assuming an effective

excitation level (12.7 eV from the average excitation energy for fast electrons) and taking into consideration the fraction of the stopping power not used for ionizations. The stopping cross section for water vapour was obtained from Brice's empirical formula [11]. In Moca-14, the simulation of excitation processes is performed by using the cross sections for electrons of the same velocity [7].

The electron transport code, MOCA-8, is physically identical to the corresponding subroutine in the ion code. Moca-8 simulates the electron tracks for energies from 10 eV - 100 keV. The program traces starting electrons and all their secondaries. There are two groups of interactions considered in the program: ionizations and excitations. In the code, 12 types of excitations and 5 types of ionizations as well as the elastic scattering of electrons are considered. When the electron is slowed down below a limiting energy of 10 eV, the rest energy is deposited in one quantum according to an assumed free path distribution. This is done because in this energy range the differences between solids and gases must be expected to be to large for meaningful inferences from these results for radiobiology. The detailed description of the cross section data used in Moca-8 is given in [12].

IV. Monte-Carlo simulation of X-ray spectra

A fairly complete set of microdosimetric distributions for monoenergetic photon radiations, measured with wall-less proportional counter, had already been published 10 years ago [13]. There is, however, no rigorous theoretical model, which explains the shape and the structure of the measured energy deposition spectra. In this paper preliminary results of Monte Carlo calculations of energy deposition spectra in a simulated wall-less counter for monoenergetic X-rays of 12 keV and for 250 kVp X-rays will be reported.

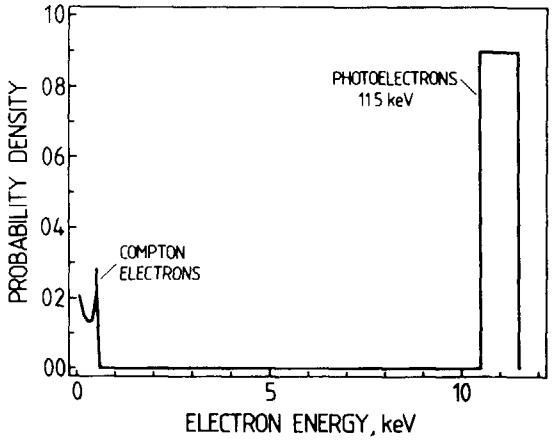

Fig.1
First collision electron spectrum produced in water by monoenergetic 12 keV photons. The 508 eV Auger electrons from K-shell of oxygen are not shown.

The calculations were divided into two parts. In a first step, the electron spectrum, produced in water by photons was calculated with the code PHOEL-2 [14]. This code generates initial energies of photo- and Compton-electrons produced by photons in water. An Auger electron is assumed to be produced following the ejection of a K-shell photoelectron from oxygen. In the present paper monoenergetic 12 keV photons and a typical broad energy spectrum of 250 kVp X-rays, filtered with 1.5 mm Cu HVL [15], were considered.

In a second step the tracks of electrons with energies randomly sampled from the single collision electron spectra, were used to calculate microdosimetric distributions. When a photoelectron was created, the Auger electron of 508 eV energy was started from the same point of origin with a randomly chosen direction, and both electron tracks were scored for the microdosimetric distribution. Fig.1 presents

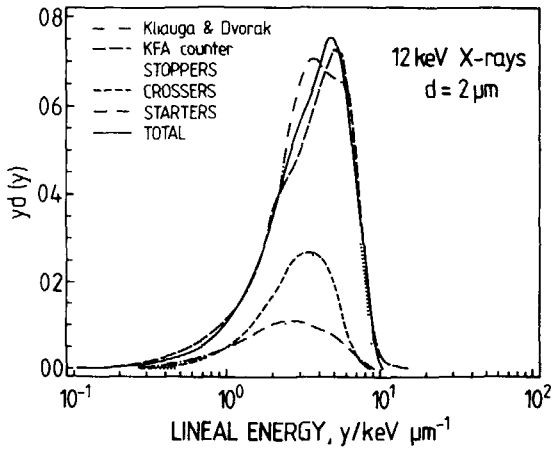

Fig.2
The comparison of calculated (TOTAL) and measured (KFA counter [16] and Kliauga & Dvorak [13]) dose lineal energy distributions for 12 keV photon radiation. The contributions from crossers, stoppers and starters to calculated total spectrum are shown. The fraction of dose due to insiders was negligible but had been included to the total spectrum.

the single collision spectrum for monoenergetic 12 keV photons used in the present calculations without the Auger electrons. 1500 and 500 electron tracks were simulated in this work and scored for 12 keV and 250 kVp X-rays, respectively.

The microdosimetric distributions for photons of energies from 11 to 1250 keV measured with a wall-less, 1 µm diameter counter (See Fig.10 from [13]) show a certain regularity: with increasing photon energy the curves changing their shape and the peak in the distribution is shifted from high to low lineal energy. This was attributed by the authors to a transition from the photoelectric effect to Compton scattering as the predominant mode of the photon interaction with the medium. The analyses of calculated spectra gives more information about this process. The shape (asymmetry) of the dose distributions is not directly connected with only one physical type of interaction and depends on the ratio of electron range to the counter diameter. This relation determines the relative contribution of electrons crossing the sensitive volume and of those, which start or stop in this volume. With increasing photon energy the probability increases, that secondary electrons will not be totally stopped in the site. This leads to lower energy depositions and shifts the peak to lower y-values.

Fig.2 compares the dose distributions (12 keV X-rays, 2 µm simulated diameter) resulting from our simulation in water vapour, with the experimental findings of Kliauga and Dvorak [13] (wall-less, spherical counter) and Schmitz [16] (cylindrical, 5 mm walled KFA counter) for TE-gas. In order to understand the shape and the structure of the spectra, the different types of particles (crossers, starters and

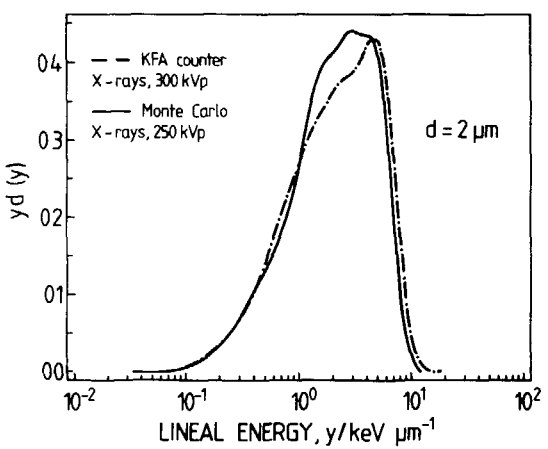

Fig.3
The comparison of calculated dose lineal energy distributions for 250 kVp (1.5 mm Cu) X-rays and measurements carried out with KFA counter for 300 kVp X-rays.

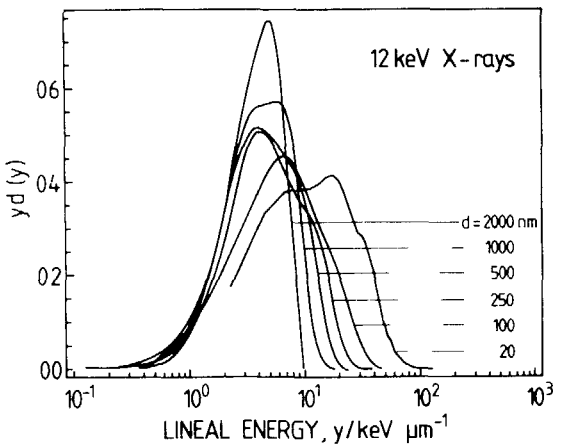

Fig.4
Calculated microdosimetric dose lineal energy distributions for 12 keV photons in sites from 20 nm to 2 μm. Distributions were scored for ionization events and scaled into lineal energy by using a calculated W-value of 30.4 eV.

stoppers) were scored separately. Only ionization events were taken into account in the scoring for microdosimetric distributions to be coherent with the measurements. Lineal energy was evaluated using a W-value of 30.4 eV for water vapour, which was calculated from the set of tracks used to score the microdosimetric distributions. In the present calculations, a monoenergetic 12 keV photon beam was assumed. The photon spectra used in the experiments [13, 16] were not idealy monoenergetic but the general agreement between measurements and calculation is, however, very good.

In Fig.3, the calculated microdosimetric spectrum for a typical X-ray radiation (250 kVp, 1.5 mm Cu filtration) in water vapour is compared with measurement in a similar photon spectrum but with a slightly higher voltage [16] and in TE-gas. The measured distribution is slightly shifted to higher lineal energies and is more asymmetric. This could be caused by material differences and by geometrical factors because, the chord length distribution of a quadratic cylinder (diameter equal to height) is "harder" than for a sphere with identical diameter. Another problem is that Moca-8 can simulate electron tracks only up to 100 keV. In the case of the 250 kVp photon spectrum, 10% of the energy is deposited by electrons of initial energy above this limit. The simulation of microdosimetric distributions for cobalt and ceasium radiation, commonly used in radiotherapy, is actually not possible because more than 90% of the dose is deposited by electrons initially faster than 100 keV. Therefore there is a need to extend the existing cross section library to electron energies of about 1 MeV.

An advantage of track calculations is the possibility of extending calculations to sites of nanometer dimension. Fig.4 shows preliminary dose distributions in terms of y for 12 keV photons and site diameters from 20 nm to 2 μm. Such spectra can be used e.g. to estimate the energy deposition in the DNA.

V. Stopping power and radial dose distribution

As indicated in Sec.III, in Moca-14 the energy loss of an ion is determined by a set of ionization and excitation cross sections. Fig.5 shows the deviation of the resulting stopping power from values recommended by ICRU-36 [2] and ICRU-16 [17]. In the energy range from 0.2 to 1 MeV the results of Moca-14 match very well the values for water compiled in ICRU-16. For energies above 3 MeV, the results of Moca-14 are lower up to about 6% than those of [17].

In Fig.6 results of radial dose distribution calculations performed with code Moca-14 (lines) and experimental results (triangles) [18-22] are presented. Two general tendencies can be seen in this comparison:

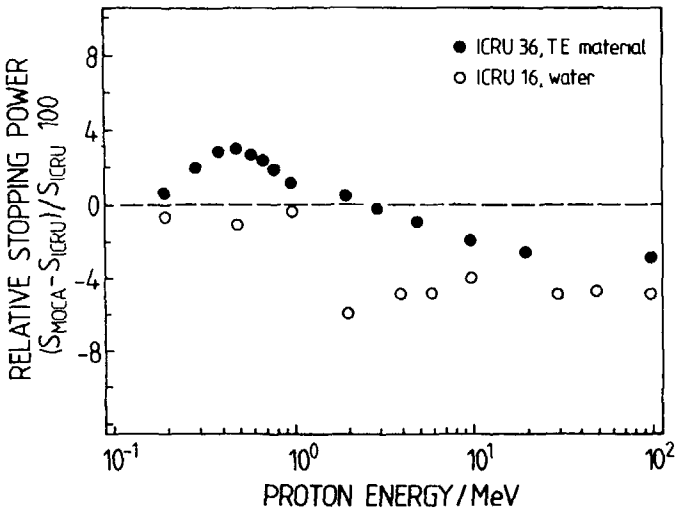

Fig.5
Relative stopping power of protons in water vapor as calculated with MOCA-14 and compared with data for T.E. material (ICRU 36) and water (ICRU 16)

a) For low radial distances (of about 0.1-1 nm) the calculated histograms are higher than experimental points. Possible explanations for this behavior were already suggested in [18, 23]: for calculation of dose, one uses the ionization distribution and multiplies it by a constant, high energy W-value. However, at small radial distances, the energy is deposited mainly by low energy electrons with higher W-values varying e.g. from about 36 eV for 100 eV electrons to about 61 eV for 20 eV electrons [12]. (See also next section and Fig.7). For the experiments with heavy ions (I-127, O-16), lower values were measured at small radial distances than calculated and this difference was attributed to the lack of charge equilibrium (the charge of the accelerated ions was below the equilibrium charge in gas) [20]. The calculated values for the heavier ions ions should be considered as of qualitative nature; the good agreement may be accidental.

b) For the periphery of the track (radial distances greater than 10 nm) the calculations lie sometimes <u>below</u> the measurement points. Part of these deviations was attributed to scattered gas atoms [19] and Auger electron ejection from incident ions [20]. It could also be, however, that the secondary electron spectrum for high energy electrons [7] is

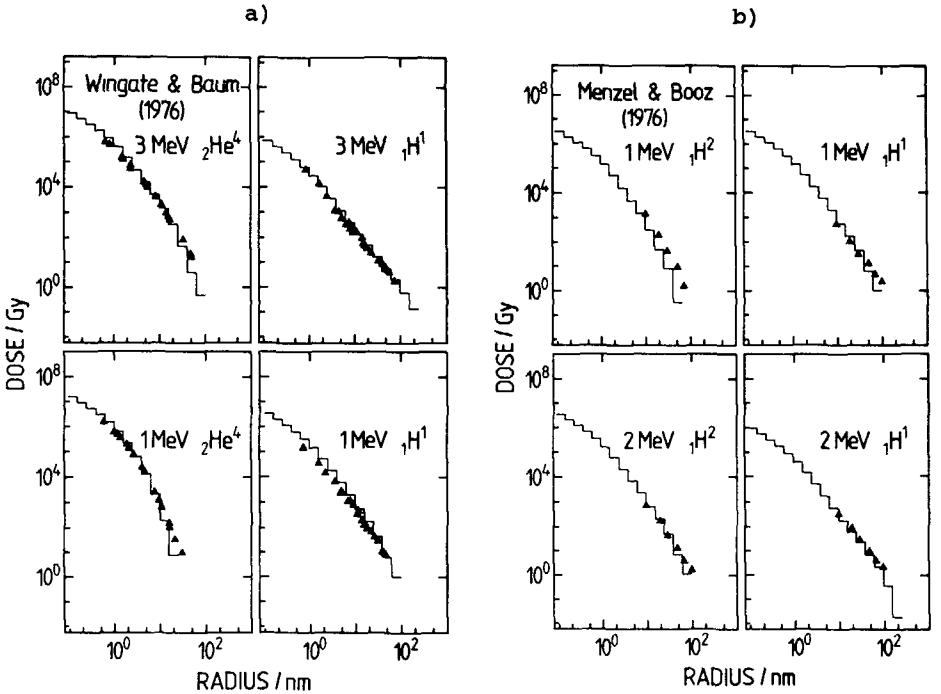

Figs.6 a, b)
Comparison of Monte Carlo calculations (MOCA-14) of radial distribution of dose (line) in water vapour with measurements of a) Wingate and Baum (1976) [18] and b) Menzel and Booz [19] in TE gas. The radii should be interpreted as the result of scaling from distances in dilute gases to unit density material.

Fig.6 c)

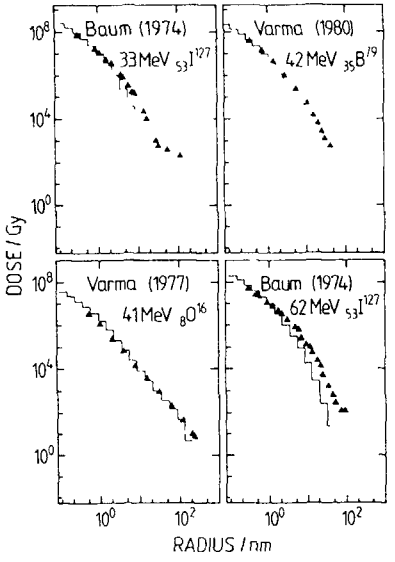

Fig.7

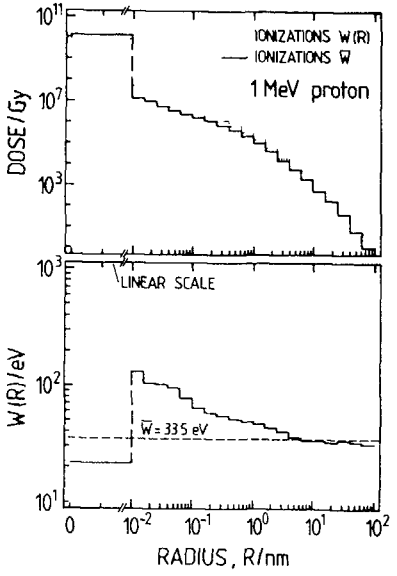

Fig.6 c)
Comparison of qualitative, scaled (according to the effective charge [6]) Monte Carlo calculations (MOCA-14) of radial distribution of dose (line) in water vapour with measurements of Varma and Baum [20-22] in TE gas. The radii should be interpreted as the result of scaling from distances in dilute gases to unit density material.

Fig.7
Comparison of radial dose distributions for 1 MeV proton in water vapour calculated by scaling the ionization distribution by average w value (33.5 eV) and by radial w(r) distribution (depicted on the figure below). The radii should be interpreted as the result of scaling from distances in dilute gases to unit density material.

smaller than that for TE-gas; it could also be attributed to experimental difficulties with low current measurements.

VI. W-value in ion tracks

When charged particles pass through gaseous or liquid matter, they interact with the atoms and molecules and produce ion pairs. The mean energy expended upon complete slowing down in a gas per ion pair formed, W, is a quotient of the particle kinetic energy and the mean number of ion pairs formed. The differential value, w, is calculated for a given differential energy loss of the charged particle after having passed a distance small in comparison with its range.

The W value of ions cannot be assessed by existing ion track structure programs (OREC [24], MOCA-14, PROTON [25]) because these programs lack adequate cross sections in the low energy regime. The set of cross-section data for energies below 0.30 MeV/amu is, till now, rather fragmentary, and ions cannot be traced down below this energy with desired accuracy. Therefore, until now only the differential w value can be calculated. Table 1 gives the values of w for protons of energies from 0.3 to 3.5 MeV in water vapour [26].

For 1 MeV protons, the differential w value obtained is 33.5 eV/ ion pair. Previous calculations of Wilson and Paretzke

TABLE 1

Differential w values for protons in water vapor as calculated with Moca-14

Energy/ MeV	Differential w /eV
0.3	34.1
0.5	33.8
1.0	33.5
2.0	33.2
3.5	33.1

[27] gave 35 eV. The source of the differences lies in program modifications (see sec. III). Zaider et al. reported 30.8 eV from calculation in water vapour. He compared these w-values with experimental results on w for alpha particles of similar initial energy per nucleon: 30.5 ± 0.8 [28] and 37.6 ± 0.2 [29].

In radial dose distribution measurements with ion chambers, absorbed dose is estimated by multiplying the number of ionizations taking place at a given radial distance by a differential w value for the given ion. This procedure leads to an underestimation of the dose for radial distances up to a few nanometers. Fig.7 presents the radial dose distributions for 1 MeV protons calculated as ionization (using an average w value) and energy distributions. Below these distributions, the corresponding radial distribution of w is depicted. For distances up to 10^{-2} nm (scaled from dilute gas targets to unit density materials) w is strongly influenced by the low ionization and excitation cross section ratio for low energy electrons. For mass density of 0.01 and 0.1 nm, w(r) gets values of respectively 130 and 80 eV, but at these distances w(r) has only a physical meaning in dilute gases. The "size" of a hydrogen atom, estimated by the Bohr radius, is equal to about 0.05 nm. At a radial distance of 3 nm, w(r) falls below 40 eV. This shape of w(r) is due to a hardening of the secondary electron spectrum with increasing distance.

The microdosimetric energy and ionization spectra do not differ significantly for large diameters and therefore the w-value is here a good conversion parameter between the ionization and energy frequency distributions. This is not true for sites below several nanometers. Fig.8 presents the dose distributions of lineal energy for 0.3 MeV protons and site dimensions of 1 and 20 nm [26]. For the larger diameter, ionization and energy distributions match fairly

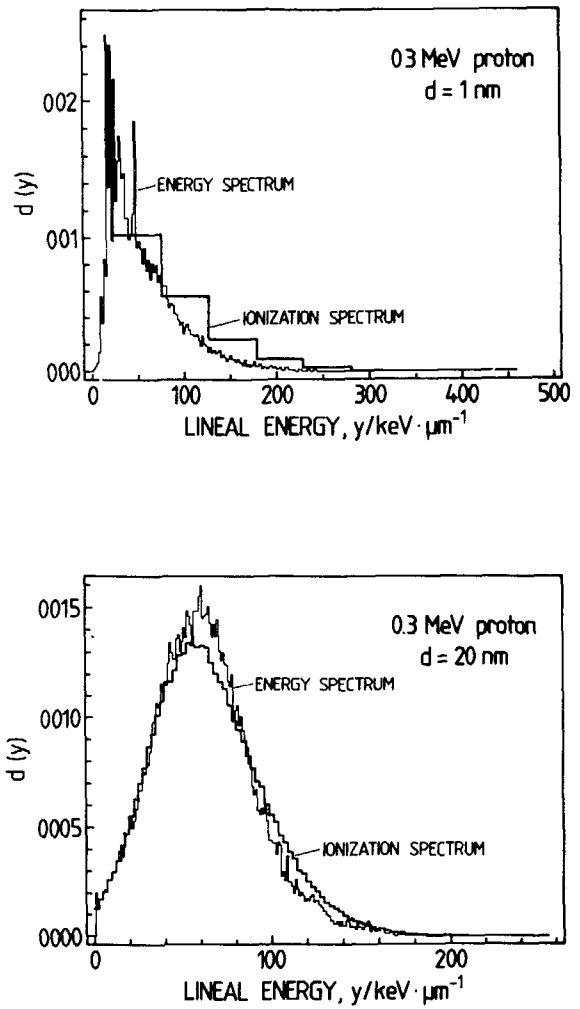

Fig.8
Calculated dose distribution of lineal energy for 0.3 MeV proton and site diameters a) 1 nm and b) 20 nm in water vapour. Thin lines show lineal energy spectra obtained from scoring ionizations and excitations. The thick line was obtained from scoring ionizations only and converting them into lineal energy spectrum with the differential w-value 33.1 eV. The radii should be interpreted as the result of scaling from distances in dilute gases to unit density material.

TABLE 2

Mean Cavity Ionization Yield, $\overline{CIY}$, for protons of 0.3, 1.0 and 3.5 MeV in water vapor as calculated with MOCA-14

d / nm	$\overline{CIY}$ / eV^{-1}		
	0.3 MeV	1 MeV	3.5 MeV
1	.054	.055	.055
2	.045	.046	.047
5	.036	.037	.039
10	.033	.032	.032
20	.031	.030	.029
50	.030	.029	.029
1/w	.0293	.0298	.0302

well. For 1 nm sites and low energy deposition events, however, the distributions differ significantly. It is, therefore, reasonable to consider the Cavity Ionization Yield [30], CIY, i.e. the number of ion pairs produced in the site by a particular value of the energy imparted. For sites which are large in comparison with track length, R (d >> R, insiders), the average Cavity Ionization Yield, CIY, is approximately equal to 1/W. For crossers (d << R) CIY approaches 1/w. When, however, the site size is that small that the mean free path for inelastic collisions is comparable with the site size, then the frequency mean number of ionizations per ionization event in the site approaches 1. Simultaneously, the mean energy deposition becomes equal to the average energy deposit, i.e. the mean energy deposited in the form of a single ionization or excitation. E.g. for 1.0 MeV protons and a site of 2 nm diameters, the frequency mean number of ionizations is $\overline{i}_F$=1.56 which, when using w=33.5 eV, leads to $\overline{y}_F$≈39.2 keV/um. On the other hand, one gets $\overline{y}_F$=25.4 keV/um when scoring both ionization and excitation events. Tab.2 shows the CIY for 0.3,1 and 3.5 MeV protons and site diameters of 1-50 nm. For a given diameter, CIY does not differ significantly in the considered energy range of protons. It should be noted here, however, that energy deposition spectra for the very small sites have a limited physical meaning in dosimetry. For site sizes of a few nanometers or less it is more realistic to analyze the experimental events in terms of number of ionizations rather than in terms of energy deposition.

VII. Summary and Conclusions

The track structure Monte Carlo programs MOCA-8 and MOCA-14 prove to be a powerful tool to investigate energy deposition processes in biological matter. All calculated quantities (LET, w values, microdosimetric and radial dose distributions) match the corresponding experimental findings reasonably well.

For the application of the electron code to photons it would be useful to be able to consider also high energy photon radiations as e.g. from Cs-137 and Co-60. This would imply increasing the upper limit for electron track simulation from 100 keV to 1.2 MeV. For the ion code, the cross sections used for protons should be extended to energies above 4 MeV and below 0.3 MeV. Other fields of development would be to modify the ion code as include the slowing down of ions and to be capable of improve the simulation tracks of ions heavier than alpha particles.

ACKNOWLEGDEMENTS

We are indebted to Dipl. Ing. Th. Schmitz for many valuable remarks on the microdosimetric measurements and Dr. K. Morstin and A. Dydejczyk for calculating electron spectra.

REFERENCES

1) Paretzke, H. G. Radiation Track Structure Theory. In: Nonhomogeneous Kinetics (Ed. G. R. Freeman), Chapt.3, Wiley, N.Y.,1987.

2) Wilson, W. E., Miller, J. H. and Paretzke, H. G. Microdosimetric aspects of 0.3 to 20 MeV proton tracks. I. Crossers. To appear in Radiat. Res.

3) Microdosimetry ICRU Report 36 (International Commission on Radiation Units and Measurements, Betheda, Maryland) (1983)

4) Booz, J. and Feinendegen, L. Applications of Microdosimetry. Proc. of the 8th ICRR, Edinburgh, July 1987 (ed. Fielden E. M. et al.), Vol.2 , pp. 331- 337.

5) Kellerer, A. M. and Chmelevsky, D. Concepts of Microdosimetry. II. Probability Distributions of the Microdosimetric Variables. Rad. Environm. Biophys. 12, pp-321-335 (1975)

6) Barkas, W. H. Nuclear Research Emulsion. Vol. I (London, New York: Academic Press Inc.), page 371 (1963)

7) Wilson, W. E. and Paretzke, H. G. Calculation of Distributions of Energy Imparted and Ionizations by Fast Protons in Nanometer Sites. Radiat. Res. 87, 521-537 (1981)

8) Wilson, W. E. and Miller, J. H. An algorithm for secondary electron emission from water vapor by high velocity ions. PNL-SA-11768 (1984)

9) Wilson, W. E. Analytical expression for cross section data. In Pacific Northwest Laboratory Annual Report for 1977, Part 4, pp. 2.7-2.9 Battelle, Pacific Northwest Laboratories, Richland, VA, 1978.

10) Berger, M. J. Energy Loss Straggling of Protons in Water Vapour. Radiat. Prot. Dosim. 13, No.1-4, pp.87-90 (1985)

11) Brice, D. K. Three-parameter formula for the electronic stopping cross section at non-relativistic velocities. Phys. Rev. A 6, pp. 1791-1805 (1972).

12) Paretzke, H. G. and Berger, M. Stopping Power and Energy Degradation for Electrons in Water Vapor. In 6th Symposium on Microdosimetry (ed. Booz, J. and Ebert, H. G), Harwood, Holland, pp.749-758, 1978

13) Kliauga, P. and Dvorak, R. Microdosimetric Measurements of Ionization by Monoenergetic Photons. Radiat. Res. 73, 1-20 (1978)

14) Turner, J. E., Hamm, R. N., Wright, H. A., Modolo, J. T. and Sardi, G. M. A. A. Monte Carlo calculations of initial energies of Compton electrons and photoelectrons in water irradiated by photons with energies up to 2 MeV. Health Phys. 39, pp.49-55 (1980)

15) F. Wachsmann, F. and Drexler, G. Graphs and Tables for Use in Radiology. ISBN 3-540-07809-6 Springer-Verlag Berlin, Heidelberg, New York (1976).

16) Schmitz, Th. , Private Communication

17) Linear Energy Transfer. ICRU REPORT 16 (1970)

18) Wingate, C. L. and Baum, J. W. Measured radial distributions of dose and LET for alpha and proton beam in hydrogen and tissue-equivalent gas. Radiat. Res. 95, pp. 231-247 (1976)

19) Menzel, H. G. and Booz, J. Measurement of radial energy deposition spectra for protons and deuterons in tissue-equivalent gas. In proc. 5th Symposium on Microdosimetry (Edited by Booz, J., Ebert, F. G. and Smith, B. G. R.) Commission of the European Communities, Luxemburg (1976)

20) Baum, J. W., Varma, M. N., Wingate, C. L. and Kuehner, A. V. Nanometer dosimetry of heavy ions tracks, LET_r^*. In Proc. 4th Symposium on Microdosimetry (edited by Booz, J., Ebert, H. G. and Waker, A.) Commission of the European Communities, Luxemburg.

21) Varma M. N., Baum, J. W. and Kuehner, A. V. Radial dose, LET and W for ^{18}O ions in N_2 and tissue-equivalent gases. Radiat. Res. 70, pp. 511-518 (1977).

22) Varma M. N., Baum, J. W. and Kuehner, A. V. Stopping power and radial dose distribution for 42 MeV bromine ions. Phys. Med. Biol. 25, pp.651-656 (1980).

23) Waligorski, M. P. R., Hamm, R. N. and Katz, R. The radial distribution of dose around the path of a heavy ion in liquid water. Int. J. Radiat. Appl. Instrum., Part D, pp.309-319 (1987)

24) Hamm, R. N.,Turner, J. E., Ritchie, R. H. and Wright, H. A. Calculation of Heavy-Ion Tracks in Liquid Water. Radiat. Res. 104, S-20-S-26 (1985)

25) Zaider, M., Brenner, D. J. and Wilson, W. E. The Applications of Track Calculations to Radiobiology I. Monte-Carlo Simulation of Proton Tracks. Radiat. Res. 95, pp.231-247 (1983)

26) Olko, P. and Booz, J. Energy Deposition by Protons and Alpha Particles in Nanometric Spherical Sites. Submitted to Radiat. Environm. Biophys.

27) Wilson, W. E. and Paretzke, H. G. Calculation of Ionization Frequency Distributions in Small Sites. Radiat. Res. 81, 326- 335 (1980)

28) Appleyard, R. K. Relative yields of ions produced by alpha particles in air and water vapor. Nature 164, pp.838 (1949)

29) Patton, W. F., Hurst, G. S. and Bortner, T. E. Measurement of the Average Energy Lost by a 5 MeV Alpha Particle in Producing an Ion Pair in Water Vapor. Report ORNL-2352, Oak Ridge National Laboratory, Oak Ridge, TN (1957)

30) Booz, J. and Fidorra, J. and Feinendegen, L. E. Quality Factor of Mixed-Radiation Neutron Gamma Rays: Comparison of the Radiation-Component Method and of the y_D Method. In Proc. of the 7th Symp. of Microdosimetry (Ed. by J. Booz, H.G. Ebert and H.D. Hartfiel), Commission of the European Communities, pp.607-621 (1980)

INTERPRETATION OF RADIOBIOLOGICAL EXPERIMENTS PERFORMED WITH HEAVY CHARGED PARTICLES

G. KRAFT
Gesellschaft fur Schwerionenforschung mbH,
Darmstadt, Federal Republic of Germany

Abstract

In heavy ion experiments, a large body of radiobiological data, (cross sections for cell inactivation and mutation, induction of both chromosome aberrations, and of strand breaks of DNA) has been measured for different atomic numbers, from helium ($Z=2$) to uranium ($Z=92$), and at energies between 1 and 1000 MeV/u which covers an LET range from 10 to 16000 keV/μm
These data exhibit a common feature
At LET values below 100 keV/μm all data points of one specific effect form one single curve as a function of LET, independent of the atomic number of the ion In this LET range, the biological effects are independ from the particle energy or track structure and depend only on the energy transfer Therefore, LET is a good parameter in this regime
For LET values greater than 100 keV/μm, the curves for the different ions separate *from the common curve in order of increasing atomic numbers In this regime* LET is no longer a good parameter and the physical parameters of the formation of particle tracks are important
The similarity of the σ-LET curves for different endpoints shows that the 'hook-structure' is produced by physical and chemical effects which occur before the biologically relevant lesions are formed For this part of the reaction chain only a very limited amount of data is available This is especially true for the emission of delta electrons There, the energy and angular distribution of the electrons in a solid target has to be measured Data on the interaction of the electrons and the positive deficiencies are required. The energy dependence of the production of chemical lesions should be known as well as their recombination probabilities

Introduction

In the last 10 years heavy ions have been used in radiobiological experiments more extensively than before This development has basically two reasons An increasing interest in the knowledge of the interaction mechanism of heavy charged particles and the increased availability of suitable heavy ion accelerators like the Bevalac at Berkeley (California), the Unilac at Darmstadt (Germany), the Ganil at Caen (France), and three machines at Riken (Japan) and others

The increasing interest in the mechanism of heavy ion interaction with biological matter is mainly stimulated by the increasing use of particles in radiotherapy According to Table 1, the main activities up to now have been concentrated on the use of proton beams, which combine a good dose distribution with a relatively low level

Table 1: Summary of the particle-therapy
data taken from ref. 1

INSTITUTION	LOCATION	TYPE	DATE FIRST RX	CURRENT PATIENT TOTAL	DATE OF TOTAL
Berkeley 184	CA U.S.A.	p	1955	30	1957
Berkeley 184	CA U.S.A.	He	1957		Dec 1987
Berkeley Bev.	CA. U.S.A.	heavy	1975	2187	May 1988
Uppsala	Sweden	p	1957	73	1976
Harvard	MA U.S.A	p	1961	4139	Dec 1987
Moscow	U.S.S.R.	p	1965	1359	Oct 1987
Dubna	U.S.S.R.	p	1967	80	1977
Gatchina	U.S.S R.	p	1975	457	Oct 1987
S.I.N	Switzerland	π^-	1980	313	Aug 1987
S.I.N	Switzerland	p	1984	262	1987
Chiba	Japan	p	1979	~30	Aug 1986
Tsukuba	Japan	p	1983	67	1987
Los Alamos	NM. U.S.A	π^-	1974	230	1982 closed
TRIUMF	Canada	π^-	1979	~122	1987

Table 2: particle therapy facilities

INSTITUTION	LOCATION	
Loma Linda	CA. U.S.A.	Proton synchrotron under construction.
Clatterbridge	England	Building a 62 MeV proton beam line.
Orsay	France	Tests underway for a proton beam.
N.A.C.	South Africa	Designing a 200 MeV proton beam line.
EULIMA	Not yet decided	Light ion facility; cooperative venture.
Chiba		heavy ion synchrotron: under construction
SIS	Darmstadt	heavy ion syncrotron: under construction
		this machine will be mainly used for physics experiments,
		a proposal for a therapy facility is underway.

of financial investment The pion treatment facilities at Los Alamos are closed and at the SIN the proton activity is growing faster than the pion activity

A trend to heavier particles, however, is also evident when the projected machines or the accelerators under construction are compared

Particles heavier than protons exhibit many physical and radiobiological properties from which therapy could benefit, like reduced lateral scattering, decreased oxygen enhancement ratio, increase in radio sensitivity of normally radioresistant cells and others Many of these properties have been studied in detail by the Berkeley group (see ref 2) but there are still many open questions as, for instance, the LET dependence of the RBE or the action cross sections

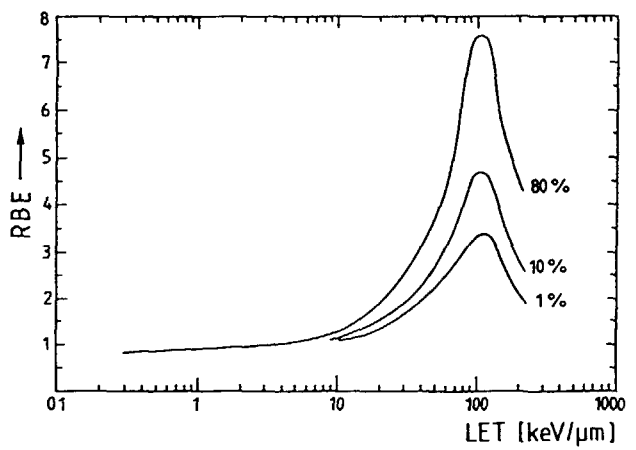

Fig 1 The relative biological effectiveness (RBE) for different survival levels as function of the linear energy transfer (LET), data from ref 3

An increase of the relative biological efficiency (RBE) with increasing linear energy transfer (LET) has been observed in many experiments for different biological endpoints (ref 3,4) The RBE values peak at an LET of approximately 100 keV/µm and decrease rapidly for higher LET values (Fig 1) This functional dependence of the RBE from LET has been explained (see for instance ref 5) by an increasing amount of biological lesions, which should be produced by the passage of the heavier particles through the sensivtive target i e the cell nucleus At 100 keV/µm an optimum number of critical lesions should be produced, just sufficient to inactivate the mitotic activity of a cell For higher LET values more damage than necessary for cell killing should be produced In this overkill region a large amount of the deposited energy should be wasted by an overproduction of critical lesions This interpretation was supported by the fact that the oxygen effect and the repair capacity are drastically diminished in the case of very high LET values If many more lesions are produced than necessary for cell killing, the fixation of a part of the lesions by peroxidation or a repair of some lesions should not influence the survival of the cell An alternative interpretation for the RBE-LET dependence was given by R Katz and coworkers (ref 6/7) on the basis of a track structure model, originally developed for the description of nuclear tracks in photo emulsions According to their model, the decrease at high LET values is a geometrical effect in the thin down' region towards the end of the particle range In this region of the particle track the range of the far out-going δ electrons is diminished and therefore the efficiency is decreased With this assumption the best agreement between model calculation and experiment has been achieved up to now But there are still basic descrepancies between theory and reality (ref 8) In the following, heavy ion experiments covering a large range of particle energies, atomic numbers, and LET values are compiled and the difficulties in their interpretation are explained

Biological Experiments

Exposure Conditions

In the following, experiments are summarized in which the beam is not contaminated by a large fraction of nuclear reaction products and therefore the given LET is assigned to the energy of one species of projectile and not a weighted average over the contribution of different particles having different energies To say it very explicitly, these are not the conditions of the particle therapy where an ion beam penetrates many centimeters of tissue producing a large amount of nuclear reaction products In order to use these data for therapeutical purposes, it is necessary to measure the spectrum of secondary reaction products and to multiply the spectrum of these particles with the biological efficiency of each fraction (ref 9)

It should be also noted that only data of track segment exposures are included in which the variation of the LET inside the target is small compared to its absolute

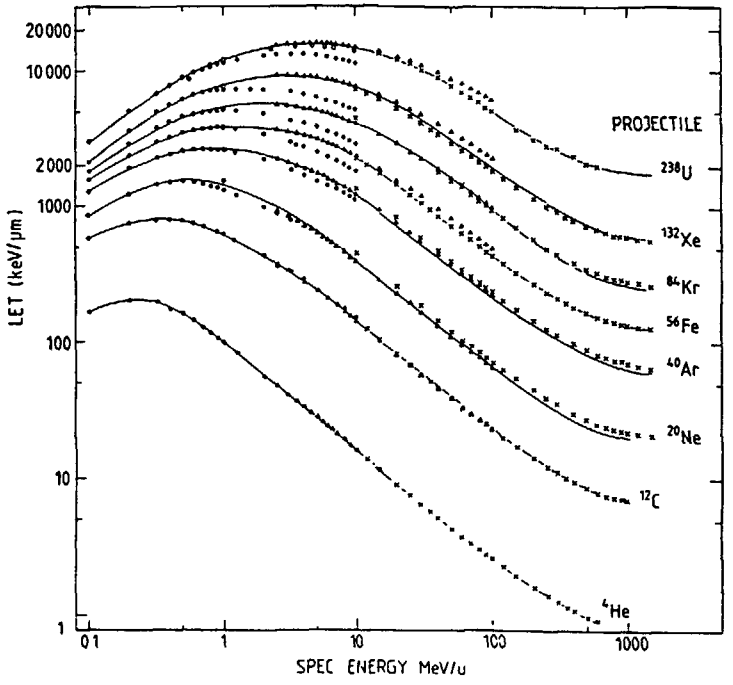

Fig.2 Linear energy transfer of different ions in carbon as a tissue equivalent. Extrapolated values are compared with measurement. Closed circles calculated according to ref. 28, triangles ref. 29, crosses ref. 30, open circles measurements from ref. 25.

value. At very low particle energies (E ≤ 5 MeV/u) this condition is a severe restriction for the biological object used in the experimental set-up.

Because there are some descrepancies between the different tables of energy losses normally used, the LET values used here are shown in Fig. 2 as a function of the specific energy for some representive ions.

Inactivation Measurements

The inactivation process induced by very heavy ions has been studied extensively for various biological objects such as mammalian cells, yeast cells and bacteria spores.

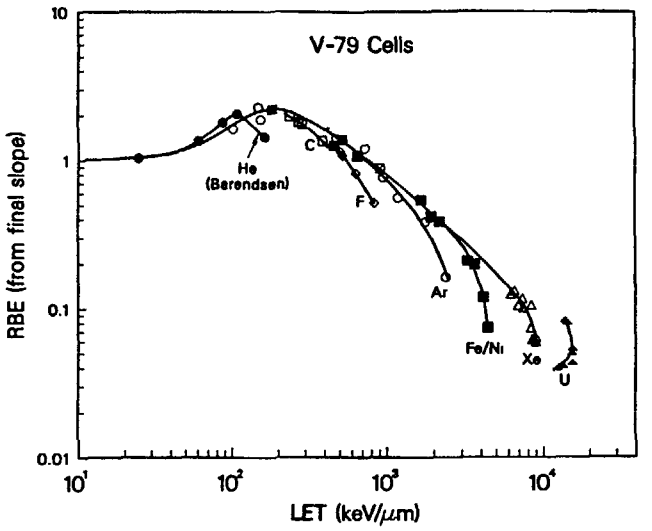

Fig.3 The relative biological effectiveness for inactivation of V79 Chinese hamster cells by heavy ions is compared with α-particle measurements, ref. 3 and 9.

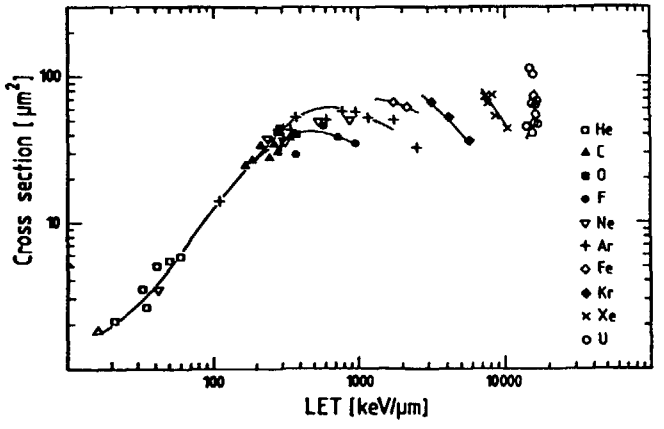

Fig.4 Inactivation cross section of V79 Chinese hamster cells as function of linear energy transfer, ref. 9.

In all these experiments, the inactiviation is measured as the loss of reproductive capacity, i e the loss of colony-forming ability, and the inactivation cross sections are determined from the final slope of the dose effect curves

For mammalian cells, the survival curves are purely exponential curves for LET values much greater than 100keV/µm, and the Relative Biological Efficiency or RBE has been calculated from the D_{37}, where the D_{37} is the particle dose necessary to inactivate 37% of the cells For smaller LET values, a shoulder is present only for highly energetic heavy ions indicating repair processes at low particle fluences In this case the RBE is calculated from D_0 instead of the D_{37} dose

In Fig 3 RBE values from the final slope are plotted for different ions as a function of LET For low LET values all ions exhibit one common RBE-LET curve which might have a common maximum at around 100 keV/µm But for the higher LET values individual graphs are observed The separation for each atomic number becomes even more significant when the inactivation cross sections are plotted as function of LET (fig 4)

The use of cross section is more appropriate for particle radiation than dose Dose is measured normally in a gas filled ionisation chamber and the use of dose implies that there is no difference in the electron production between gas and solid, which is not true In addition, dose can be divided in smaller and smaller portion and the term 'dose does not reflect the grainy' structure of the energy deposition by particles The cross section measures the efficiency per particle to produce a specific biological reaction Cross sections are given as an area and the ratio between the geometrical size of the object (e g the cell nucleus) and the measured inactivation cross section gives the average probability to produce inactivation by the passage of one single heavy ion through the cell nucleus which is the critical structure In a case where one single traversal kills the cell the inactivation cross section reaches the geometrical size of the critical target

In Fig 4 inactivation cross sections of V79 Chinese hamster cells are plotted as a function of the LET The graph clearly shows three main features

1 At LET values smaller than 200 keV/µm all data exhibit a common curve, independent of projectile atomic number In this range, only the amount of energy as

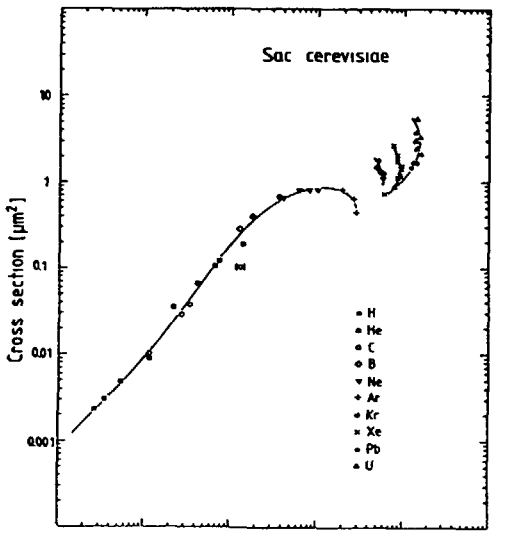

Fig 5 Inactivation cross section of yeast cells as function of LET, ref. 10

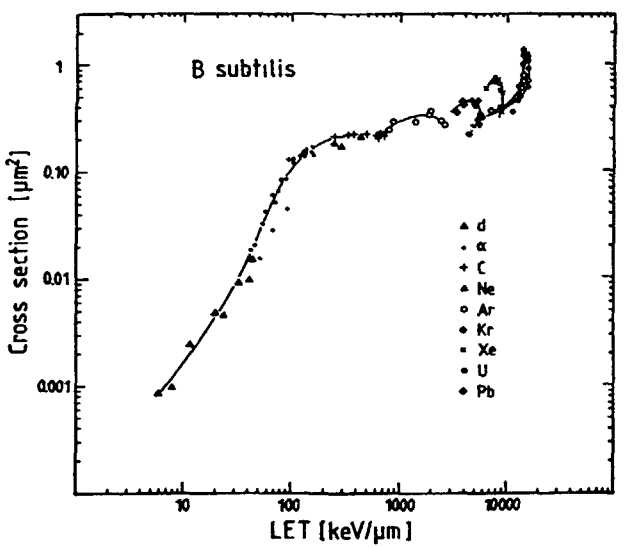

Fig 6 Inactivation cross section of bacteria spores as function of LET, ref. 11.

given by the LET of the particle is important for the inactivation process and the inner structure of the track is of minor importance

2 At LET values greater than 200 keV/µm the common σ-LET curve separates into different branches, and the inactivation cross section reaches different plateau values for each different ion species For greater LET values the inactivation cross section decreases, forming individual σ-LET hooks for each ion

3 Finally, the measured inactivation cross sections are generally smaller than the geometrical cross section of the cell nucleus, indicating that many traversals of heaving particles through the cell nucleus are necessary for cell killing, even though the dose deposited by one traversal is much higher than the dose for cell killing by X-rays, i e the D_{37} dose

A similar structure is observed for the inactivation cross section as a function of the LET for bacteria spores (Fig 5) and yeast cells (Fig 6) However, in the case of the yeast cells and bacteria spores, the "saturation cross section", i e the cross sections where the different ions separate from the common curve, occurs at values close to the geometrical size of the cell nucleus or the area of DNA concentration

From these findings, the assumptions of the overkill model as well as the track structure model have to be examined In the overkill model the inactivation cross section should reach the size of the geometrical cross section of the cell nucleus and should stay constant for higher LET values In the track structure model, the inactivation cross section should exhibit a "hook structure when the measured cross section exceeds the geometrical size of the cell nucleus The experiments with yeast and bacteria are in good agreement with the track structure model but the data for mammalian cells show significant differences

In order to explain the inactivation data in greater detail the production of critical lesions as it is evident in the production of chromosomal aberration and strand breaks of the DNA should be compared with the inactivation data

Chromosome aberration

Chromosome aberrations induced by heavy charged particles exhibit some specific features which are different from their induction by sparsely ionizing radiation

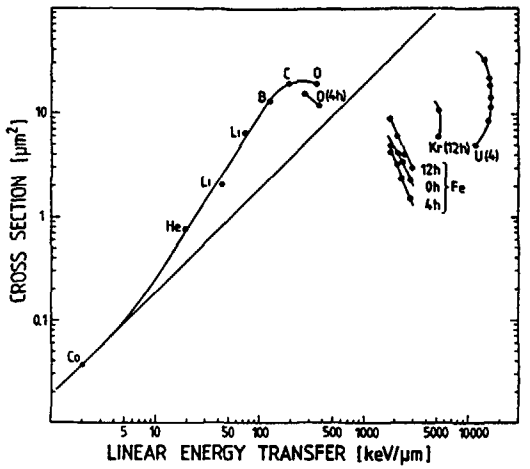

Fig 7 Action cross section of the induction of chromosomal aberrations as function of LET The chromosomal aberrations of lighter ion exposure (ref 13) are scored 8h after irradiation The harvesting time in the other experiments (ref 14) given in brackets

Due to the high ionization density which can be localized in a very restricted part of the cell nucleus, the production of deletions and fragments of chromosomes is much more likely than the production of exchange figures caused by mis-rejoining of two different strands of DNA belonging to different chromosomes Also complete or partial disintegration of chromosomes has been observed when cells are exposed during mitosis where the chromatin is condensed These disintegration events would correspond to the picture of an overkill effect in which more lesions are produced than necessary for mitotic death However, chromosomal disintegrations are very rare events if asynchronous cells are exposed to the particle beam and do not contribute significantly to cell killing

In Fig 7 the action cross section for the induction of chromosomal aberration, i e essentially the induction of break events, is given as a function of LET The data for the light ions up to oxygen are measured with $CH2B_2$ Chinese hamster cells, while the data for the heavier ions are measured with V79 Chinese hamster cells Fortunately, oxygen ion measurements with both cell lines exist and show a difference of only 25% This difference may be due to the different harvesting times As shown in

the case of Fe-ions, the induction probability depends strongly on the harvesting time after irradiation A maximum of chromosomal damage is expressed for times between 8 and 12 h after exposure to heavy particles For light particles such as helium, a maximum of chromosomal damage is observed in the first 4 h after exposure At present, the data base is not sufficient to separate cell cycle effects from the induction process However, the variation in the yield of abnormal metaphases in the first 12 h is small compared to the total range of σ values given in Fig 7, which exhibits the same general structure as the Σ-LET curves for inactivation as given in Figures 5, 6 and 7

For low LET values, the cross section increases more steeply than the RBE = 1 curve, and the different atomic numbers form one common curve For higher LET values the cross section decreases with increasing LET for the individual ions Again, the measured cross sections are much smaller than the size of the cell nucleus, and a low energy uranium ion can traverse the cell nucleus and deposit a high dose without inducing a chromosomal aberration

Induction of Single and Double Strand Breaks of DNA

The induction of single and double strand breaks has been studied extensively for DNA of different organization and origin and in different environmental conditions Mammalian DNA has been exposed inside the cell, and viral DNA like SV40 or ΦX174 in different buffer solutions Because of the great experimental difficulties, only a few measurements of intracellular DNA exist Most of these measurements are concerned with mammalian DNA For lighter ions the induction of single and double strand breaks has been measured by Kampf (ref 18) and for heavier ions by Aufderheide(ref 19) The authors used different cell lines, lens epithelial cells and V79 Chinese hamster cells, and different experimental procedures (sedimentation in a saccharose gradient and alkaline elution) The results may differ because of systematic differences in the cells and methods used In Fig 8 the action cross section for the induction of single strand breaks (SSB) and double strand breaks (DSB) as a function of LET are given For lighter ions, the induction of both DSB and SSB are measured, while for the heavier ions only SSB data exist Measurements for DSB induction are in progress at the UNILAC Darmstadt

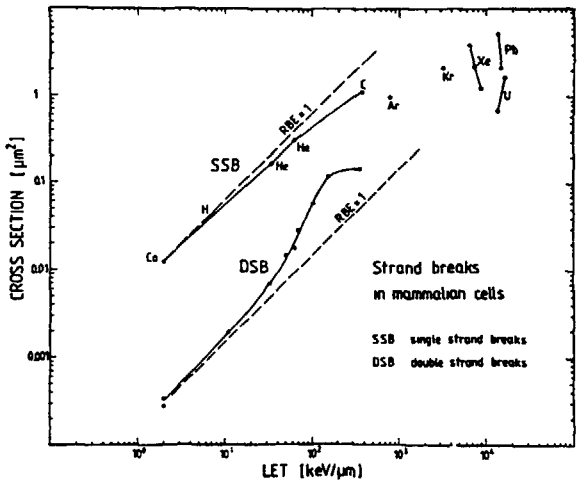

Fig 8 Action cross section for the induction of single and double strand breaks The breaks induced by lighter ions are measured with V79 Chinese hamster cells, for the heavier ions lens epithelial cells are used (see ref 18/19)

An important difference between the induction of SSB and DSB exists for lighter ions For SSB, the increase in efficiency is always less than proportional to the LET, and the σ-LET curve lies below the RBE = 1 curve For the induction of DSB, the increase of the cross section is more than proportional to the increase in LET.

The same general pattern has been observed for extracellular DNA, ΦX 14 DNA, which was exposed to particle radiation in a highly protective buffer solution, where DNA disintegration via water radiolysis is strongly suppressed (Fig 9)

The induction of single and double strand breaks in SV40 DNA in a buffer solution in which the indirect radiation effect is predominant has been examined over a large range of particle energies and LET values (Fig 10) In this case the violation of the DNA strand breaks is mostly caused by OH radicals, which have a long lifetime Therefore, both the induction of single and double strand breaks exhibit the same LET dependence because the initial pattern of high and low ionization density has been averaged by the migration of the long-living radicals

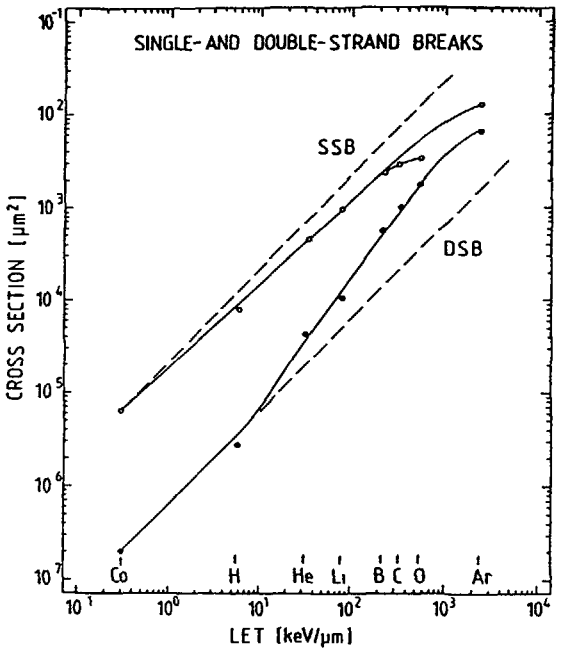

Fig 9 Action cross section of the induction of double and single strand breaks in ØX174 exposed in a highly protective buffer, ref 21

The importance of the indirect radiation effect is also evident from the absolute magnitude of the action cross section in this buffer The SV 40 data exhibit a much higher cross section as the ΦX174 data, even though both DNA molecules are of similar molecular size

Mutation Induction

When double strand breaks of DNA are misrepaired, mutations in the genetic code can occur, which are not lethal These genetic mutations are very rare events and are produced with a probability of 10^{-5} per surviving cell

If the specific mutation of a normal cell to a transformed cell is studied, this probability is even two orders of magnitude lower As a results of these low induction factors, experiments on mutation and transformation induction are very tedious and time consuming and normally have large errors

The induction of genetic mutations by heavy charged particles has been studied in three different systems In spores of bacillus subtilis the resistance to sodium

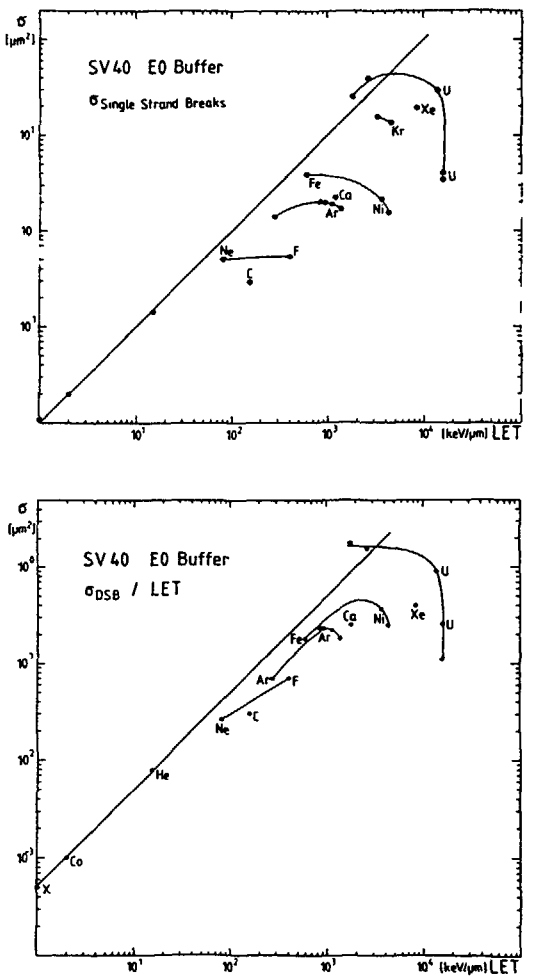

Fig 10 Action cross section of the induction of strand breaks in SV40 DNA in a buffer where the indirect effect is predominant (ref 27)

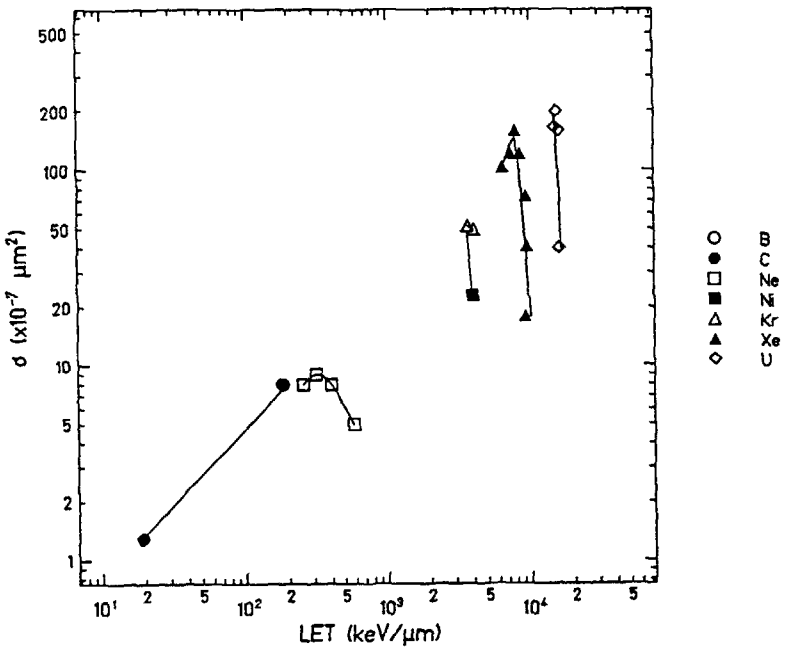

Fig 11 Mutation induction cross section (resistance to sodium azide) of bacillus subtilis spores, ref 15

azide was investigated (ref 15), in yeast cells the canavanine resistance (ref 16) and in mammalian cells the thioguanine resistance were also tested (ref 17) The measured action cross section for this system as a function of particle LET are summarized in Figures 11, 12 and 13

Due to experimental difficulties these data are less complete than the inactivation or strand break data However, the same general trend as for DNA-breaks, chromosome aberrations and inactivation can be observed A steep increase in efficiency for the smaller LET values and a saturation for LET-values greater than 100 keV/µm For the bacteria and yeast cells, the saturation cross section shows the well known hook structure, but for the mammalian cells a steep decrease is observed for higher LET values and the cross section for uranium ions are a factor of 4 smaller than the cross sections at around 100 keV/µm These findings are in good agreement with the action cross section for the induction of transformation in mammalian cells (ref 20)

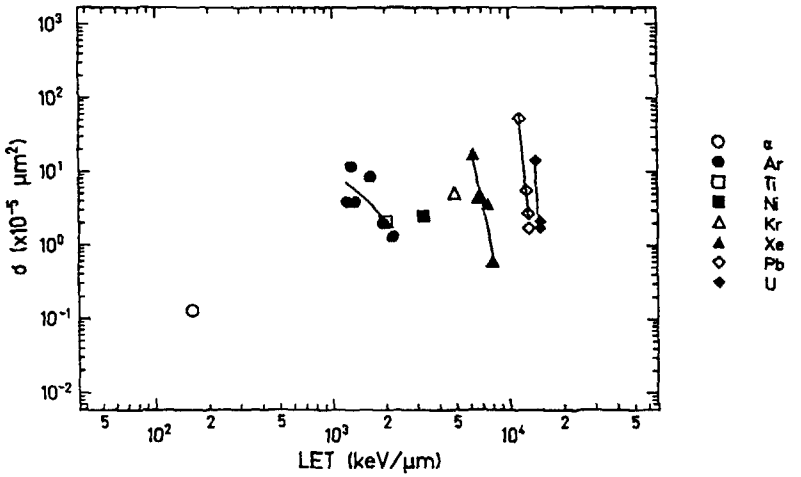

Fig 12 Action cross section for the induction of canavanine resistant yeast mutants, ref 16

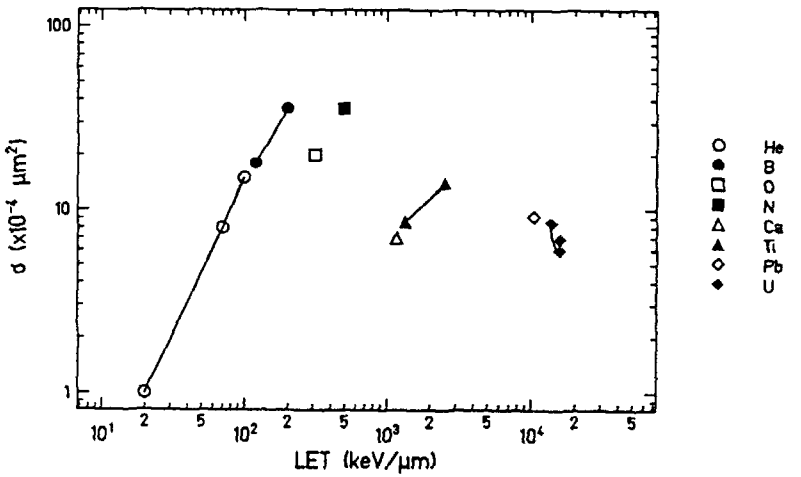

Fig 13 Action cross section for the induction of thioguanin resistance in V79 Chinese hamster cells as function of LET, ref 17

For the very heavy ions both mutation and transformation are significantly suppressed when mammalian cells are hit by heavy ions like uranium But even at these unusually small cross sections, the hook structure as a basic pattern is preserved

Discussion

The compiled data as shown in Fig 5 - 13 contain a large body of information on the action of heavy particles, presently available at heavy ion machines Only the lighter ions are used in radiotherapy and only data of these ions can be directly applied in therapy Data on the heavier particles may be used to elucidate radiation action and to test theories and model calculations over an outermost scale of particle parameters

For very different biological objects and different biological endpoints the LET dependences of the action cross section is very similar (ref 22)

1 For low LET values (LET $\geq$ 200 keV/µm) the cross section exhibits one common curve as a function of LET, independent of the atomic number of the projectile
2 Except for the induction of single strand breaks, for all other endpoints (inactivation, chromosome aberration, double strand breaks and mutation) the σ curve depends nearly quadratically on LET
3 For LET values greater than 200 keV/µm, the curves for the different ions separate from the common curve in order of increasing atomic number and decrease for higher LET values forming σ-LET hooks

The first point, the independence of the action cross sections of the atomic number at low LET values, demonstrates that, for instance, the biological actions of 1 MeV alpha-particles, 15 MeV carbon ions and 300 MeV argon ions are identical From the microdosimetric point of view this is a very surprising result, because distribution of the emitted delta-electrons depends strongly on the particle velocity, and the energy spectrum of the electrons is quite different between 1 MeV alpha-particles and 300 MeV argon ions However, if the radial dose distribution around the particle track is calculated (ref 23) for different initial particle energies having the same LET values, significant differences are found only in the outer region of the particle track, and the radial dose distribution is identical for different particle energies over many decades of doses The dose deposited in the outer part contributes only a small fraction to the total dose and this variation does not influence the result as long as the total energy deposition is translated into biologically relevant effects

Except for the induction of single strand breaks, all other endpoints are sensitive to an increase of the local ionization density With increasing LET values the efficiency for mutation, inactivation, chromosome aberration and double strand breaks increases more steeply than the energy deposition This can be understood with geometrical arguments, with increasing LET the local density of the damage increases too If two sublesions are produced close together, there is a high probability that the interaction of these sublesions will lead to a biologically relevant lesion For example if two single strand breaks are produced close together within a range of a few base pairs, the hydrogen bonds of the remaining bases between the breaks are not strong enough to maintain the integrity of the whole DNA molecule, and it is very likely that a double strand break will result This can be directly observed when the ratio between double and single strand breaks is compared for different ions having different track width but the same LET In the narrower track relatively more DSB are observed than in the wider track

An interpretation of the supralinear increase of the σ-LET curve for all endpoints except SSB implies the importance of the geometrical proximity for sublethal lesions From the data presented here, it cannot be decided whether the formation of double strand breaks is the underlying process that governs the supralinear increase or whether different endpoints may have different interaction processes However, from the commonly adopted interpretation of chromosomal aberrations and inactivation, such as an irrepairable DSB event, and from the interpretation of mutation and transformation, such as a misrepaired double strand break, it is very likely that the nonlinearity in the action cross section is caused by nonlinearities in the induction of strand breaks Very similar arguments are important for the interpretation of the σ-LET hooks and the fact that the saturation cross sections for inactivation are always much smaller than the geometrical size of the critical target

An interpretation of the σ-LET hooks found in the inactivation process in terms of an overkill model is mostly hindered by the fact that for the molecular effects like strand breaks the same dependence has been observed If the diminished efficiency for cell killing of the very heavy particles should be caused by the overproduction of critical lesions, these lesions as, for instance, double strand breaks should be found

in a higher amount in the heavy ions experiments But for the strand breaks as a molecular event this efficiency is diminished too in all measurements

In other models, e g the track strucuture model (ref 7), the decreasing efficiency for the high LET-values is explained by geometrical arguments For these ions the measured inactiviation cross section should exceed the geometrical cross section of the cell nucleus as critical target structure when the passage of an ion through the cell nucleus deposits a lethal dose In addition, the far ranging δ electrons can also transport a lethal dose to cell nuclei, which are not hit directly In this case, the measured cross section is much larger than the geometrical size of the critical target A decrease in the range of the δ-electrons at the end of the particle track in this thinned down region reduces the measured cross section to the size of the cell nucleus and causes a hook structure similar to the one measured, but of σ values greater than the geometrical cross section

The inactivation experiments at least with the mammalian cells show very clearly that the hooks occur below the level of the geometrical cross section In addition, also in the track structure model the production of local damage is proportional to the local energy deposition and the saturation and hook structure is only due to the geometrical thinning down of the track diameter

In the experiments however, the decrease in radiobiological efficiency is present at all levels, even at the molecular level of single and double strand breaks in DNA and it is more likely that the diminished efficiency of the very heavy ions for inactivation, mutation, and chromosome aberrations is due rather to a diminished induction rate of chemical damage like the DNA breaks than by geometrical or other effects In irradiation experiments with constituents of DNA a drastically reduced production of free radicals has been measured for the very heavy ions, which is in good agreement with other data (ref 24)

Therefore, the physical and radiochemical processes, which take place before biochemical effects occur should be re-examined The most critical point in such a review is the emission of the radiobiologically relevant δ electrons Data of the energy loss of the primary projectile has been measured for many projectile and target combinations and found to be consistent within some 20% (ref 25) But for the emission of delta electrons by heavy ion impact, only few data exist in the interesting energy range between 1 and 20 MeV measured in gas targets and no data at all exist for solid state targets like a simple carbon foil (ref 22)

The commonly used theories for the calculation of the emission yield of electrons (ref 26) like BEA, SCA or PWBA treat the heavy ion impact as a small perturbation of the electronic configuration of the target Recent measurements at gas targets have shown that the angular distribution and the energy spectra measured in a heavy ion collision are not in agreement with this approximation (ref. 26). In order to approximate the measured angular and energy distribution it is necessary to consider all electrons of the projectile and target Finally, the emission process and probably more importantly, the direct reactions after the emission are not known at all for a solid state target

In a solid target, subsequent collisions with target atoms are very frequent and many electrons of the projectile stay in excited states Therefore, the electronic configuration of the projectile is different between gas and solid state targets But the electronic configuration of the target is also different between gas and solid In the solid all the electrons, which are emitted in forward direction - these are the majority of electrons - have a chance to create secondary electrons and wholes and to recombine with the holes produced by other electrons In addition, a great fraction of these forward emitted electrons are faster than the projectile and create a plasma like a cone in which the projectile follows Little is known about the electron emissions and the plasma effects in solids and it would be a major contribution not only to the radiobiology of charged particles if one would understand these basic reactions

ACKNOWLEDGEMENTS

Most of the data shown here, are from the different groups working at the UNILAC, GSI I want to thank these collegues for the stimulating and fruitful collaboration Especially I would like to tank W K Weyrather, M Scholz, and S Ritter I want to appreciate the excellent cooperation of U Vogel and K Licht in typing the manuscript This work was supported by the BMFT Bonn and CEC Brussels, contract B16-0197-D

REFERENCES

1 Particles, a Newsletter for those interested in proton light ion and heavy charged particles, Harvard, Feb 1988

2 E A Blakely, F Q H Ngo, S B Curtis, C A Tobias In Adv in Radiat Biol , New York 1983

3 G W Barendsen, H M D Walter, J P Fowler and D D Bewley Radiat Res 18, 106 -199 (1963)
4 P W Todd Rad Res 61, 1965b, p 288
5 E Hall Radiobiology for the radiologist, p 104-110, New York, 1978
6 R Katz, B Ackerson, U Homayoonfar, S C Sharma Radiat Res 47, 402-425 (1971)
7 R Katz, D E Dunn, G L Sinclair Radiat Protect Dos 13 281-284 (1985)
8 W Schimmerling, E L Alpen, P Powers-Risius, M Wong, R Deguzman, M, Rapkin Radiat Res 112, 436-448, (1987)
9 H Wulf, W Kraft-Weyrather, H G Miltenburger, E A Blakely, C A Tobias, G Kraft Radiat Res 104, 122-134 (1985)
10 F Schopfer, J Kiefer, E Schneider, G Kraft In Proceedings of the 6th Symposium on Microdosimetry, edited by J Booz and H G Ebert (London Harwood Publishers) 1051-1060 (1978)
F Schopfer, J Kiefer, E Schneider, G Kraft Radiat Res 82 235-243 (1980)
F Schopfer, E Schneider, E Rase, J Kiefer Radiat Res 92 30-46 (1982)
11 M Schafer, H Bucker, R Facius, G Horneck, G Reitz, G Kraft In Proceedings of the 6th Symposium on Microdosimetry, edited by J Booz and H G Ebert (London Harwood Publishers), 1043-1050 (1978)
M Schafer, R Facius, H Bucker In Solid State Nuclear Track Detectors, edited by H Francois, J P Massue, R Schmitt, N Kurtz, M Monnin and S A Durrani (Oxford Pergamon Press), 1055-1061 (1980)
M Schafer, R Facius, K Baltschukat, H Bucker In Proceedings of the 7th Symposium on Microdosimetry, edited by J Booz and H G Ebert and H D Hartfiel (London Harwood Publishers), 1331-1340 (1981)
12 G Kraft, E A Blakely, L Hieber, W Kraft-Weyrather, H G Miltenburger, W Muller, M Schuber, C A Tobias, H Wulf Ad Space Res 4, 219-226 (1984)
13 L B Skarsgard, B A Kihlmann, L Parker, C M Pujara, S Richardson Rad Res Suppl 7, 208-221 (1967)
14 W Muller
Chromosomenaberrationen der chinesischer Hamster Zell-Linie V79 nach Rontgen- und Schwerionenbestrahlung
Dissertation GSI 85-3 Report, Februar 1985
15 K Baltshukat, G Horneck, H Bucker, R Facius, M Schafer Radiat Environ Biophys , 1986, 25, p 183-187
16 J Kiefer, S Rase, E Schneider, H Straaten, G Kraft, H Liesem Int J of Radiat Biol 42, 591-600 (1982)
17 J Thacker, A Stretch, M A Stephens Int J Radiat Biol 36, 137 (1979)
T Kranert, E Schneider, J Kiefer GSI Scientific report, 88-1, p 228, 1988
18 G Kampf Die Erzeugung von DNS Strangbruchen durch ionisierende Strahlung unterschiedlicher Qualitat und ihre Bedeutung für die Zellinaktivierung, Zfk 504, 1-66 Zentralinstitut fur Kernforschung Rossendorf, Dresden, 1983
19 E Aufderheide, H Rink, L Hieber, G Kraft Int J Radiat Biol 5, p 779-790 (1987)
20 G Ponsel, L Hieber, K Trutschler, S Fenn, E Fromke, A M Kellerer GSI Scientific report 88-1, p 236, 1988
21 R C Christensen, C A Tobias, W D Taylor Int J Radiat Biol 22, 45-477 (1972)
22 G Kraft Nucl Science Applic , 3, p 1-28 (1987)
23 A M Kellerer Proc of the Europ Symp on Life Sciences, Research in Space, Koln, p 221-227 (1977)
24 A Schaefer, J Huttermann, G Kraft GSI Scintific report 87-1, p 207, 1987
25 H Geissel, Y Laichter, W F W Schneider and P Armbruster Nucl Instr and Methods 215 p 329-335 (1983)
26 S Schmid, C Kelbch, H Schmidt-Bocking, G Kraft Proceed of NASI Terrestrial Space Radiation and Biological Effects, Corfu, Oct 11-25, 1987
27 G Kraft, W Kraft-Weyrather, A Lang, R Roots GSI Report 87-11-B5, 1-5, 1987
28 L C Northcliffe, R F Schilling Range and stopping power tables for heavy ions, Nucl Data Tables A7, 233-437 (1970)
29 F Hubert, A Fleury, R Bimbot, and D Gardes Ann Phys 5, (1980)
30 E V Benton, R P Henke USNRDL TR 76, 122 (1967)

BASIC RADIATION PHYSICS QUANTITIES

(Session II)

THE IONIZATION YIELD FOR LOW ENERGY PHOTONS AND ELECTRONS ABSORBED IN TISSUE-EQUIVALENT GAS MIXTURES

D.SRDOČ
Rudjer Bošković Institute,
Zagreb, Yugoslavia

Abstract

The mean energy required to form an ion pair (W) was measured for photons having energy 0.277, 1.49 and 5.89 keV in two tissue-equivalent gas mixtures. Methane- and propane-based tissue-equivalent gases are essential in measurements of radiation energy deposition in small spheres simulating human cells. The dose distribution curves on the cell-size levels (0.1 - 10 μm sphere diameter) are indispensable in human radiotherapy, especially when neutrons and heavy particles are applied. The end effects and products of any kind of absorbed radiation in tissue are broken chemical bonds and free radicals, preceeded by low energy particles, e.g. slowed down electrons. Therefore, the knowledge of the average energy required to form an ion pair at very low particle energy is very important in the so called "bookkeeping" method of studying the particle energy degradation process.

The W value for low-energy electrons was calculated from experimental photon W values. An increase of W values with decreasing energy is observed in accordance with the same trend, as presented in the ICRU Report No. 31. Good agreement between the calculated and the experimental W values is obtained in low-energy region, as well as for high energy W values.

Our results fill the gap between the very low energy region (below 300 eV) and the high energy (above 10 keV) region. In addition to measuring the average W-values, the results obtained by our experimental method threw light on the statistical fluctuations in the ionization yield for low energy photons. It was found that the primary distribution of ion pairs in investigated gas mixtures is asymetrical and more peaked than the Gaussian distribution for low energy incident photons, approaching the Gaussian shape for 6 keV photons.

INTRODUCTION

Tissue-equivalent gas mixtures have been extensively in use in dosimetry and microdosimetry for more than 30 years, yet the most important gas property for radiation physics - the energy required to form an ion pair - has never attracted adequate attention to be measured precisely enough. Several scattered data in literature on the W-value for electrons (Booz, 1967; Waker and Booz, 1975; Smith and Booz, 1978; Leonard and Boring, 1973; Glenn, 1974; Combecher, 1980; Budd et al, 1981) prove the above statement: The published W-values for the same gas mixture are not consistent (Booz et al), or the experimental method has not been described precisely enough to allow critical assessment of the published data (Leonard and Boring, Glenn). The W-values published in earlier papers are shown in Table 1. The ICRU Report No 31 (1979) summarizes and critically reviews published data on W-values in gases, including gas mixtures. The W-values for monoenergetic photons in polyatomic gases were reported by the author (Srdoč, 1973).

The reason for the existing situation could be only guessed. It is very likely that the researchers of Jesse's era were more attracted by monoatomic gases with the prospective for theoretical calculations of W-values. Modern physicists are reluctant to repeat "old fashioned" experiments using DC ionization chambers. The proportional counter technique requires a team consisting of skilled instrument maker, experimental physicists and computer experts. This fortunate combination has been realized under the author's guidance first at Radiological Research Laboratories, Columbia University and lately at Rudjer Bošković Institute, Zagreb, Yugoslavia.

EXPERIMENTAL

Experimental data were obtained following the method developed by Srdoč and Clark (1970).Measurements were performed by a specially designed proportional counter with a steady gas flow to ensure the gas purity. Four spectra were taken under the same conditions: the single electron spectrum, the carbon K_α line spectrum (T = 277 eV), the aluminum K_α line spectrum (T = 1.49 keV) and the X-ray spectrum (T = 5.89 keV) produced

TABLE 1

Authors	Radiation	Energy	W(eV) CH_4 TE gas	W(eV) C_3H_8 TE gas	Comment
		(KeV)			
Booz (1967)	photons	10	31.3 ± 0.7		Proportional
		1.5	31.5 ± 0.5		counter
		0.3	34.4 ± 1.6		technique
		(MeV)			
Leonard and	^{60}Co gamma	1.1	32.2 ± 0.7		Ionization
Boring (1973)	rays	1.3			chamber
	x-rays	250 KV peak	29.2 ± 0.6		technique
		(KeV)			
Waker and	electrons	6	30		Data taken from
Booz (1975)		1.2	32.5		graph ref. Waker
		0.26	36		Booz (1975).
		(MeV)			
Glenn (1974)	^{60}Co gamma	1.1	29.5 ± ?		Ionization
See also	rays	1.3			chamber
Bichsel (1975)					technique
		(KeV)			
Smith and	electrons	2.0	28.3 ± 1.5		Ionization
Booz (1978)		1.5	28.2 ± 1.5		chamber
		0.30	34.0 ± 2.6		technique
		0.25	35.8 ± 2.3		
		0.10	41.8 ± 2.4		
		0.03	61 ± 9		
Srdoč (1979)	photons	5.9	30.7 ± 0.3	27.3 ± 0.3	Proportional
		1.49	31.3 ± 0.3	27.8 ± 0.3	counter
		0.277	32.3 ± 0.3	28.8 ± 0.3	technique
	electrons	5.6	30.7 ± 0.3	27.3 ± 0.3	
		1.2	31.3 ± 0.4	27.9 ± 0.4	
		0.25	34.8 ± 0.5	30.4 ± 0.5	

by the electron capture reaction of ^{55}Fe. Monoenergetic photons were produced by bombarding targets of carbon and aluminum in miniature X-ray tubes. The source of single electrons having essentially zero kinetic energy consisted of a quartz rod covered with a thin semitransparent layer of aluminum on the end facing the active counter volume. The aluminized surface emits photoelectrons when irradiated with UV light. The gas pressure varied from 3.3 to 13.3 kPa and the applied voltage from 1100 V to 1410 V depending on the kind of gas and the gas pressure to ensure the same gas amplification.

The measured spectrum obtained by a proportional counter represents the weighted sum of multiple convolutions of the single electron spectrum, where the weighting factors represent the distribution of ion pairs created by incident particle (the so called primary spectrum). It was found that the single electron spectra in all gases can be well represented by

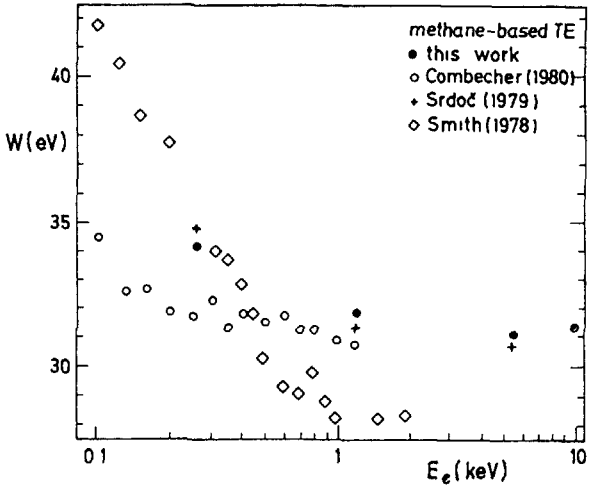

FIG 1 The W value for electrons in methane-based tissue-equivalent gas Comparison with the results of other authors

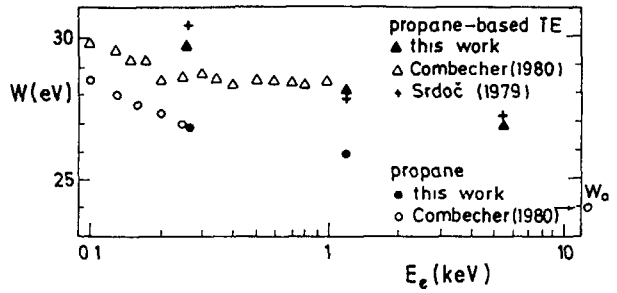

FIG 2 The W value for electrons in propane and propane-based tissue-equivalent gas Comparison with the results of other authors Arrow indicates the high energy W value for propane

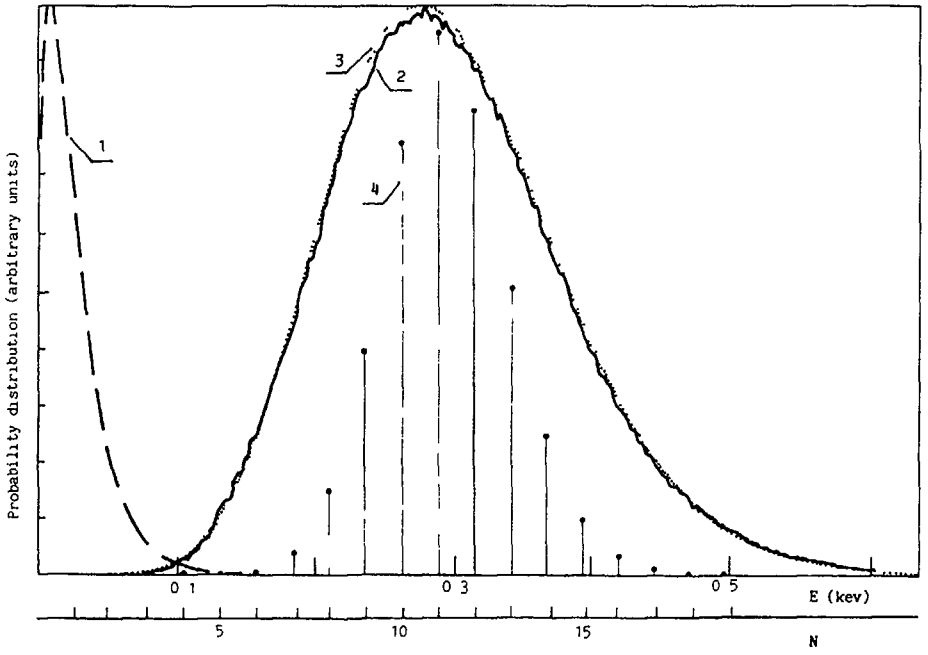

FIG 3 The probability distribution of the number of ion pairs created by 0 277 keV photons in methane based tissue-equivalent gas mixture

the Polya distribution. An iterative deconvolution method was applied to obtain the primary spectrum (Srdoč, Obelić, Krajcar, 1987). The shapes and statistical properties of the distributions of primary ion pairs will be briefly discussed. Distributions of the number of primary created ion pairs P_N for photons of input energy equal to 277 eV, 1489 eV and 5890 eV have been obtained by deconvolution of the experimental pulse height distributions using the convolutions of single electron spectra. The derived primary distributions have been statistically processed and the following characteristic parameters have been calculated: moments and central moments up to the order of 5, coefficients of skewness and kurtosis as well as cumulants and generalized Fano factors. Typical primary ion pair distribution for 0.277 keV photons in methane-based tissue-equivalent gas mixture is shown in Fig. 3.

CALCULATION OF THE W VALUE FOR PHOTONS AND ELECTRONS

The mean ionization yield is often expressed as the mean energy required to form an ion pair W(T):

$$W(T) = T/N_1(T) \qquad (1)$$

At $T \gg I$, where I denotes the ionization energy of the gas, W(T) approaches a constant value characteristic for the gas, showing little variations with the nature of the incident radiation. The data on high energy W values for photons and electrons in various gases are summarized in the ICRU Report 31 (1979).

Inokuti (1975) found an analytical solution of the Fowler equation in the form $N_1(T) = (T-U)/W_a$, giving the following relationship for energy dependence of W value at low incident particle energy:

$$W(T) = W_a/(1 - U/T) \qquad (2)$$

where U is a constant that closely approximates the energy of sub-ionization electron and W_a is the asymptotic value of W for high T.

If the incident particle is a photon instead of an electron, the total number of ion pairs due to absorption of a photon is the sum of ion pairs produced directly by the photon through the photoelectric effect and the Compton effect, plus ion pairs produced by all the electrons due to these effects. The direct contribution due to a high energy photon is usually small in comparison with the bulk of subsequently created ion pairs, so the W values for high energy photons and electrons are virtually the same.

Soft photons (up to a few keV) are absorbed primarily through the photoelectric effect in low Z materials such as the biological tissue. The incident carbon K_α photon (T = 277 eV) can eject a valence electron because the K-shell ionization energy in most organic molecules lies around 290 eV. The released electron has the average energy $E_e = T - E_v$, where T is the photon energy and E_v is the average binding energy of the valence electrons. Methane, the main component of the tissue-equivalent gas mixture has two orbitals for valence electrons at 14.5 eV and 22.9 eV. The E_v value is assumed to be the mean binding energy for the two orbitals equal to 18.7 eV.

Thus, the average electron energy is 258.3 eV. The mean binding energies for valence electrons in propane is 17.9 eV. According to these data we assume that the mean binding energy for polyatomic gases is approx. 17.5 eV, so that the average photoelectron energy E_e is 259.5 eV. This photoelectron produces n_e ion pairs

$$n_e = E_e/W_e \qquad (3)$$

where W_e is the W value for electron having energy E_e, according to Eq. (2). The total number of ion pairs produced by C-K_α photon is then:

$$N_C = 1 + n_e \qquad (4)$$

and this value is calculated from our experimental data. The mean energy required to produce an ion pair for electrons having an approximate energy of 260 eV can now be calculated combining Eq. (3) and Eq. (4):

$$W_e(E_e) = E_e/n_e = (T - E_v)/(N_C - 1) \qquad (5)$$

If the incident photon has an energy higher than the K-shell ionization energy of the gas atoms, then the inner-shell electron can be ejected. The photoelectron released from the carbon K-shell by the Al-K photon has approximately E_{pe}=1.20 keV. The hole in the inner shell which is left after the K-shell excitation is occupied by a valence electron and another valence electron is ejected from the molecule by the Auger process since the fluorescence yield is extremely low for low-Z elements. There are several types of Auger transitions in methane, but the average energy of the Auger electron in methane is assumed to be 255 eV. We suppose that this value can be used as the best approximation for higher alkanes such as propane and polyatomic organic molecules. We also neglect the possibility of direct photoionization of the molecule by Al-K_α photon and ^{55}Fe X-ray. The probability of direct ionization in case of aluminum photon is 0.08, and at higher energies is even lower.

Therefore, in order to calculate the W value for 1.2 keV and 5.6 keV electrons we suppose that the electron is ejected from the K-shell by an incident photon, and that the Auger electron (E_A=255 eV) is formed subsequently. Both the photoelectron and the Auger electron can ionize gas molecules, producing n_{pe} and n_A ion pairs, respectively. Total number of ion pairs produced by the incident aluminum photon or ^{55}Fe X-ray is thus:

$$N = 2 + n_{pe} + n_A \qquad (6)$$

We further suppose that the number of ion pairs produced by the Auger electron, n_A, is equal to the number of ion pairs, n_e in Eq.(4), produced by photoelectron ejected by carbon K_α photon (E_e=260 eV):

$$n_A = n_e = N_C - 1 \qquad (7)$$

TABLE 2

The measured W values for low-energy photons in tissue-equivalent gas mixtures

gas	W(T) (eV)		
	T = 0.277 keV	T = 1.49 keV	T = 5.89 keV
methane-based TE gas	32.4	31.7	31.2
propane-based TE gas	28.6	28.0	27.0

TABLE 3

Calculated W values for low-energy electrons in tissue-equivalent gas mixtures.

gas	W_e (eV)		
	0.26 keV	1.2 keV	5.6 keV
methane-based TE gas	34.2	34.9	31.3
propane-based TE gas	29.8	28.2	27.0

Finally, the W value for electrons having energy E_{pe}=1.2 keV and 5.6 keV can be calculated from

$$W_e(E_{pe}) = \frac{E_{pe}}{n_{pe}} = \frac{T - E_K}{N - 1 - N_C} \qquad (8)$$

where T is incident photon energy, E_K is K-shell ionization energy, and N is the total number of ion pairs produced by incident photon, calculated from experimental data.

RESULTS

The results of our measurements are shown in following tables and figures: Table 2 shows the measured W-values for low-energy photons in tissue-equivalent gases, whereas Table 3 contains the W-values for low energy electrons. The estimated experimental error is $\pm$ 0.15 eV. Figures 1 and 2 show the dependence of W-value for two tissue--equivalent gases on absorbed particle energy. A comparison is given with several other authors.

REFERENCES

Bichsel, H, 1975, Proc 2nd Symp on Neutron Dosimetry in Biology and Medicine, Luxemburg.

Booz, J, 1967, The relation between energy absorption and ionization in tissue-equivalent gas for gamma quants of low energy. In: Proceedings, First Symposium on Microdosimetry, Ispra, (H G Ebert Ed.), Commission of the Europen Communities, Brussels, EUR 3747 d-f-e, p 331-347.

Budd, T, Marchal, M and Kwok, C S, 1981, Advances in cloud-chamber techniques and measurements of W value in a tissue-equivalent gas, Rad Res, **88**, p 228-239.

Combecher, D, 1980, Measurement of W values of low-energyyelectrons in several gases, Rad Res, **84**, p 189-218.

Glenn, D W, 1974, Med Phys, 1, p 103.

ICRU, 1979, Average Energy Required to Produce an Ion Pair, International Commission on Radiation Units and Measurements, Washington, DC, Report no. 31.

Inokuti, M, 1975, Ionization yields in gases under electron irradiation, Rad Res, 64, p 6-22.

Leonard, B E and Boring, J W, 1973, Rad Res, 55, p 1.

Smith, B G R and Booz, J, 1978, KFA Report, Inst fur Medizin, Julich,

Srdoč, D, 1973, Dependence of the energy per ion pair on the photon energy below 6 keV in various gases, Nucl Instr Meth, 108, p 327-332.

Srdoč, D, 1979, The W-value for electrons and photons in tissue-equivalent gases, USDOE Progress Report COO-4733-2, Columbia Univ., New York, p 37-50.

Srdoč, D and Clark, B C, 1970, Generation and spectroscopy of ultrasoft X-rays by non-dispersive methods, Nucl Instr Meth, 78, p 305-313.

Srdoč, D, Obelić, B and Krajcar Bronić, I, 1987, Statistical fluctuations in the ionisation yield for low-energy photons absorbed in polyatomic gases, J Phys, B: Mol Phys, 20, p 4473-4484.

Waker, A J and Booz, J, 1975, Proc 2nd Symp on Neuton Dosimetry in Biology and Medicine, Luxemburg.

EXPERIMENTALLY DETERMINED W VALUES, STOPPING POWERS AND RANGES OF LOW-ENERGY PROTONS AND ELECTRONS IN GASES: METHODS AND PROBLEMS

E. WAIBEL
Physikalisch-Technische Bundesanstalt,
Braunschweig, Federal Republic of Germany

Abstract

W values, stopping powers and ranges are fundamental atomic quantities in dosimetry, depending on the type of radiation, stopping material and energy. The information available on the average energy to produce an ion pair (W value) for protons and electrons in gases of interest is reviewed, particularly for proton energies above 1 keV and electron energies above about 20 eV.

Emphasis is laid on experimentally determined stopping powers and ranges of protons and electrons in gases for that region of low energies where theoretical calculations are quite complex, giving higher uncertainties. Very few experimental data exist for energies below the stopping power maximum. To enable an adequate evaluation of spreading data resulting in recommended values, a careful analysis of uncertainties is needed. In some cases discrepancies far exceed the uncertainties quoted, and it may be supposed that the systematic deviations, depending on the method, are either not well known or not taken into account. The experimental methods are therefore discussed with respect to possible systematic uncertainties.

1. INTRODUCTION

Fast neutrons interact with tissue mainly by collision processes producing various charged recoil particles. Due to the high abundance of hydrogen in this material, the major fraction of energy is transferred to protons covering a wide energy range. Low

energy protons are responsible for strong local radiation effects resulting from high values of stopping power and ionization density. The same is true of low energy electrons which are created during the slowing-down of all types of charged particles.

Radiation doses in therapy should be determined for soft tissue and tissue-equivalent material with an overall uncertainty of no more than 5% [72]. Uncertainties of less than 2% are therefore necessary for W values and stopping powers or stopping power ratios if ionization methods are applied in the determination of absorbed dose.

The average energy W expended to produce an ion pair is needed to convert ionization yields to absorbed dose. W depends on the particle type, the particle energy and the stopping material. In the following, W values and stopping powers of low-energy protons and electrons are reviewed and discussed, restricted to gases of interest for measurements in radiotherapy.

2. W VALUES

2.1 Protons

ICRU report 31 [1] reviewed the experimental and theoretical information on W available up to 1978. Several experimental W values for electrons [2-6] and ions [7-14] in gases have meanwhile been published. Methane, propane, nitrogen, carbon dioxide, tissue-equivalent gas mixtures based on methane and propane, air and argon are among the gases of interest for dosimetry, they may be supplemented by hydrogen and hydrogen-methane mixtures for neutron spectroscopy.

Fig. 1 gives a compilation of W values for protons in methane-based tissue-equivalent gas (64.4% CH_4 + 32.4% CO_2 + 3.2% N_2) as a function of the proton energy. Compared with the status of [1], the data have been substantially extended to energies above 1 MeV by Thomas and Burke (1.2 MeV to 3.5 MeV) [12] and below 50 keV by

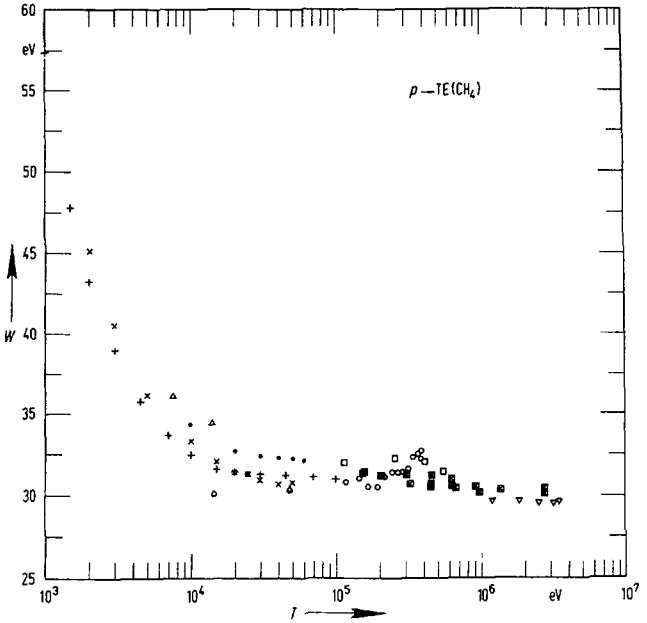

Fig. 1. Experimental values of W for protons in methane-based tissue-equivalent gas. △ Leonard and Boring [16], ● Sidenius [7], ⊠ Rohrig and Colvett [17], □ Kühn and Werba [18], ○ Nguyen et al. [8], × Huber et al. [10], + Waibel and Willems [11], ▽ Thomas and Burke [12].

Sidenius (10 keV to 60 keV) [7], Huber et al (2 keV to 50 keV) [10] and Waibel and Willems (1 keV to 100 keV) [11]. The spread of the data between about 10 keV and 1 MeV is quite large. An apparent maximum around 350 keV suggested by the data from Chemtob et al [15] or Nguyen et al [8] cannot be confirmed from the uncertainties quoted. A monotonous energy dependence seems to be adequate. Further precise measurements are therefore required for this energy region and for energies above 3.5 MeV.

The experimental W values for protons in the constituents of the above mentioned TE gas, CH_4, CO_2 and N_2, have been considerably supplemented since 1978, mainly by the same groups [7-12]. The energy dependence of W for methane is very similar to

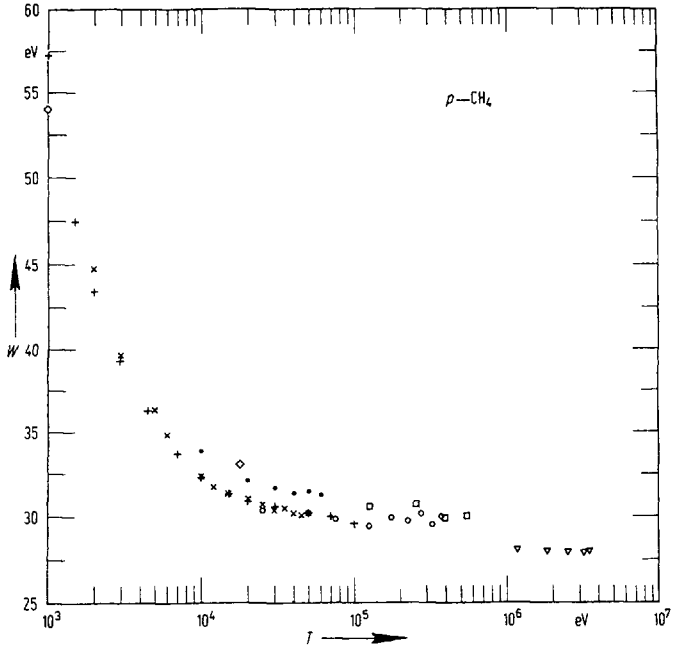

Fig. 2. Experimental values of W for protons in methane. ◇ McClure and Allensworth [20], ● Sidenius [7], □ Kühn and Werba [18], ○ Nguyen et al. [8], + Willems et al. [19], × Huber et al. [10], ▽ Thomas and Burke [12].

that of TE gas (Fig. 2). A step of about 2 eV in W from data at some hundred keV [8,18] to those of Thomas and Burke [12] between 1.2 and 3.5 MeV is evident. Further measurements are required to explain this curve shape. However, the data up to 100 keV [10,19] may be monotonously extended to those above 1 MeV. A similar step can also be observed for carbon dioxide in Fig. 3. Contrary to TE gas and its main component, CH_4, a flat minimum around 20 keV can be confirmed from the data of Sidenius [7] and Waibel and Willems [14], showing the same energy dependence although shifted to higher values. Again, there is need for further investigations for proton energies above 100 keV. At first glance, the W values for protons in nitrogen displayed in Fig. 4 show a disordered field between 20 keV and 1 MeV, but from the data of [28] in accordance with [10,26,8] a minimum with a depth of at least 1.5 eV can be established. At much higher energies, the data from Petti et al [13] at 150 MeV and from Bakker and Segrè [29] at 340 MeV are differential w values which agree satisfactorily with W data near 3 MeV. Improved data are needed between 0.1 and 2 MeV and higher energies, while a satisfactory set of W values for practical work may be derived from 1 keV to 3.5 MeV with overall uncertainties of about 3% disregarding, some strongly deviating data.

Propane-based TE gas is being increasingly applied in neutron dosimetry. Posny et al [14] measured W values for H^+ ions, (and He^+, C^+, N^+, O^+) in this TE gas (54% C_3H_8 + 40.5% CO_2 + 5.5% N_2) and in propane. Their incident energies ranged from 25 keV to 375

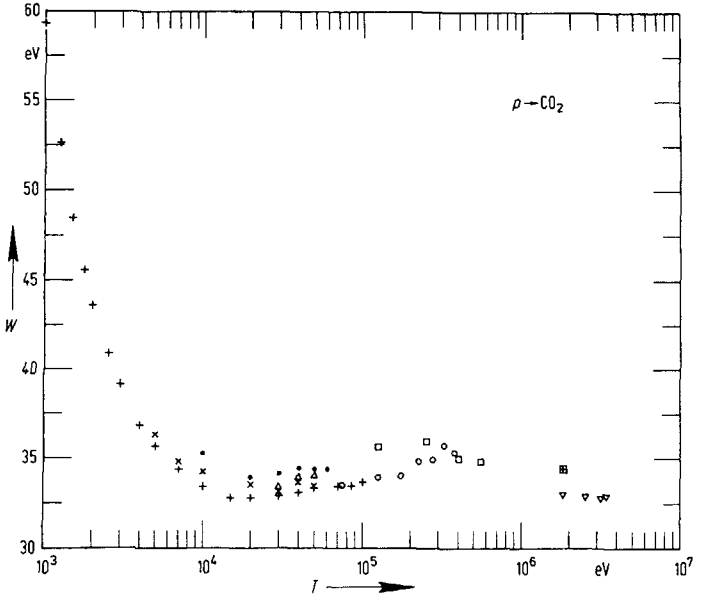

Fig. 3. Experimental values of W for protons in carbon dioxide. ⊠ Larson [21], △ Boring and Woods [22], ● Sidenius [7], □ Kühn and Werba [18], ○ Nguyen et al. [8], × Huber et al. [10], ▽ Thomas and Burke [12], + Willems and Waibel [23].

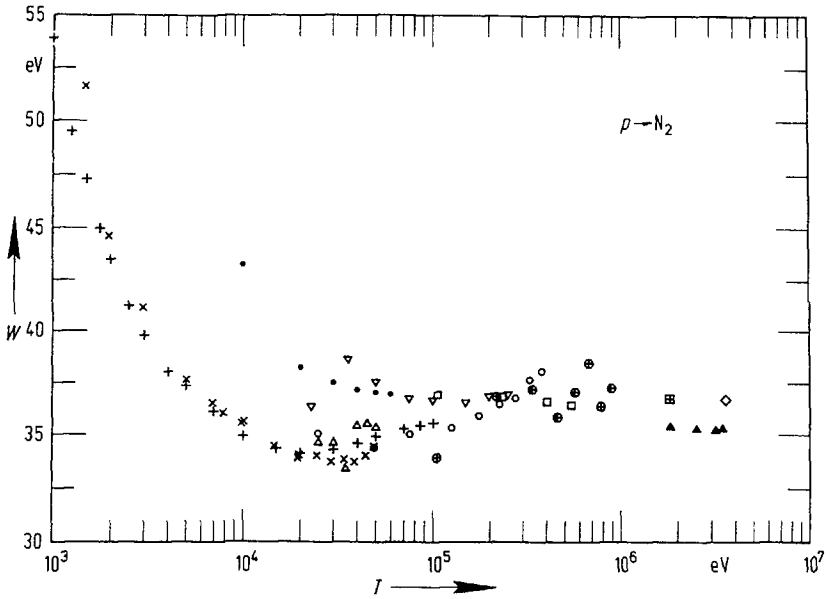

Fig. 4. Experimental values of W for protons in nitrogen.
▽ Lowry and Miller, ⊞ Larson [21], ⊕ Schaller et al. [25],
△ Boring et al. [26], ◇ Parks et al. [27], ● Sidenius [7],
□ Kühn and Werba [18], ○ Nguyen et al. [8], × Huber et al. [10],
▲ Thomas and Burke [12], + Waibel and Willems [28].

keV (Fig. 5). The overall uncertainty of W for protons in propane is quoted at about 3% and for the appertaining TE gas at about 4%. The energy dependence of W shows a slight minimum around 175 keV. More data are required for the whole energy range of interest.

W values for protons stopped in air have been measured by Willems et al [9] at energies from 1 keV to 100 keV and by Huber et al [10] from 5 keV to 50 keV. The uncertainties quoted are about 2%. Single values have been published by Larsen [21] at 1.826 MeV and Bakker and Segrè [29] at 340 MeV. Willems et al have confirmed a flat minimum of W around 20 keV.

The status of W for protons in argon is unchanged since 1979 [1] with the exception of one value for W at 150 MeV by Petti et al [13].

2.2 W values for low-energy electrons

Electrons of energies T between the ionization threshold and about 10 keV are released in great numbers in the tracks of ions and electrons. Data for tissue-equivalent gas mixtures, their constituents and air are therefore of special interest. Since the compilation in ICRU Report 31 [1] Combecher [2] has published W values for electrons in air, N_2, O_2, CO_2, TE gases, H_2, D_2, H_2O, D_2O, Ar, Kr, Xe, methane, ethane, propane, butane, pentane, hexane, nonane, ethylene, acetylene, ethanol, acetone, C_6H_6, and C_6D_6 for up to various energies (200 eV to 1200 eV). He quotes the total experimental error of W to be less than 2%. Smith and Booz [6] have measured W values for electrons in methane-based TE gas, CH_4, CO_2, N_2 and Ar from 30 eV to 2 keV with quoted uncertainties of larger than 5%. Waibel and Großwendt have published W values for air [3], CH_4 [4] and N_2 [5] in the energy region from 20 eV to

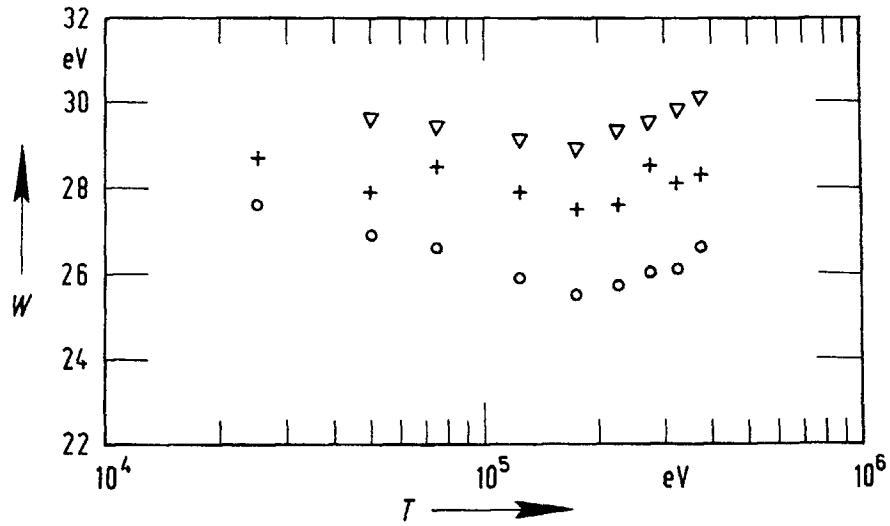

Fig. 5. Experimental values of W for protons in propane and propane-based tissue-equivalent gas from Posny et al. [14],
○ propane, + TE(C_3H_8), ▽ calculated for TE(C_3H_8) from data of the components.

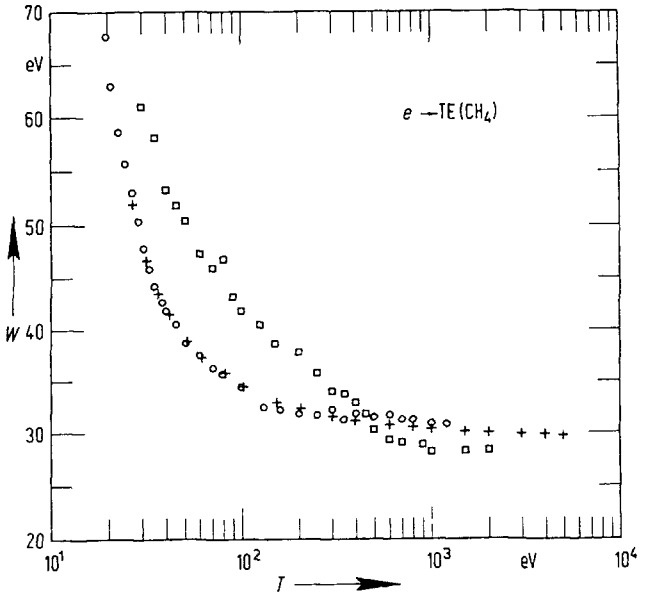

Fig. 6. Experimental values of W for electrons in methane-based tissue-equivalent gas
□ Smith and Booz [6], ○ Combecher [2], + Waibel [30]

5 keV. Preliminary data in the same energy range are provided for methane-based tissue-equivalent gas and CO_2 [30]. The standard deviation of these data [3-5,30] for energies between 50 eV und 5 keV amounts to less than 1% and below 50 eV in most cases to less than 2%.

Figs. 6 to 9 show the experimentally determined W values for $TE(CH_4)$ gas, CH_4, CO_2 and N_2 of the above-mentioned authors. Data for air can be seen in Fig. 5.11 in [1] or Fig. 5 in [3]. Combecher's data agree very well for these gases with those of Waibel and Groβwendt but are markedly higher for energies above 100 eV for electrons in CO_2 (Fig. 7). The less accurate data of Smith and Booz [6] show some stronger deviations for all gases (Fig. 6-8) just as Cole's data [31] for air; he quotes uncertainties of 15% below 100 eV und 5% above 2 keV. The influence of humidity in air on W is discussed in [1]. Further information on W for electrons arising from ^{60}Co radiation in dry air is given by Niatel et al [29].

Above 5 keV, and in some cases even above 500 eV, there is a wide gap in W values for electrons in all gases. This may be bridged for practical purposes by smoothly extending the W values from the region of 1 keV to 5 keV, if available, to the high-energy values recommended by ICRU 31 [1].

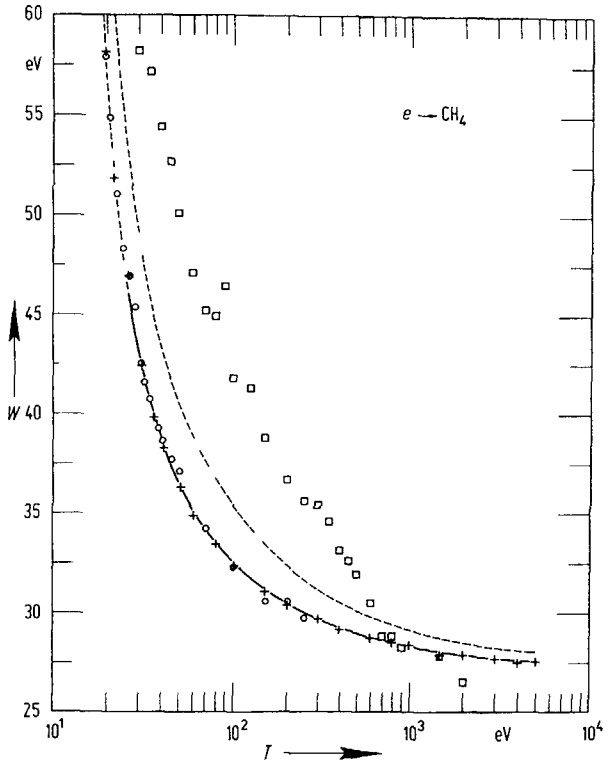

Fig. 7. Experimental values of W for electrons in methane.
□ Smith and Booz [6], ○ Combecher [2], + Waibel and Groβwendt [4], — fitting function [4], --- data without correction for backscattering [4]

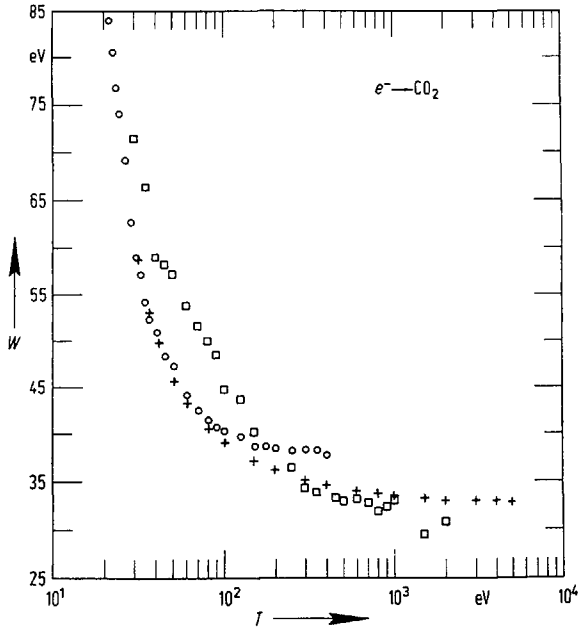

Fig. 8. Experimental values of W for electrons in carbon dioxide. □ Smith and Booz [6], ○ Combecher [2], + Waibel [30].

2.3 Additivity rule for W

Knowledge of deviations from the simple additivity rule of the ionization yield for gas mixtures determined from the W of the components, is of practial and theoretical relevance. This problem is discussed in ICRU 31 [1] for binary mixtures; the strong influence of small amounts of gases, e.g. of noble gases, added to other noble gases on the ionization yield of charged particles is known as the Jesse effect and is presented in [1] from several references. Metastable atomic states leading to ionization via a collision process are responsible for a non-additivity of the ionization yield. For W values, the formula $W_s = (\sum_i x_i W_i^{-1})^{-1}$ should be compared with W_M where W_M is valid for the mixture and W_s for the result from the components i with the portions x_i.

Posny et al [14] have found an agreement between of W_M and W_s for protons in methane-based TE gas and a discrepancy of up to 10% for propane-based TE gas in the energy range from 25 keV to 375 keV. Differences in W due to chemical isomerism and binding has been shown by Combecher [2] for electrons in n and i-butane for energies between 13 eV and 80 eV. He also reports isotope effects in hydrogen, water vapor and benzene. Significantly lower W values were found for deuterated water and benzene at low energies, whereas the difference in W between H_2 and D_2 was not marked.

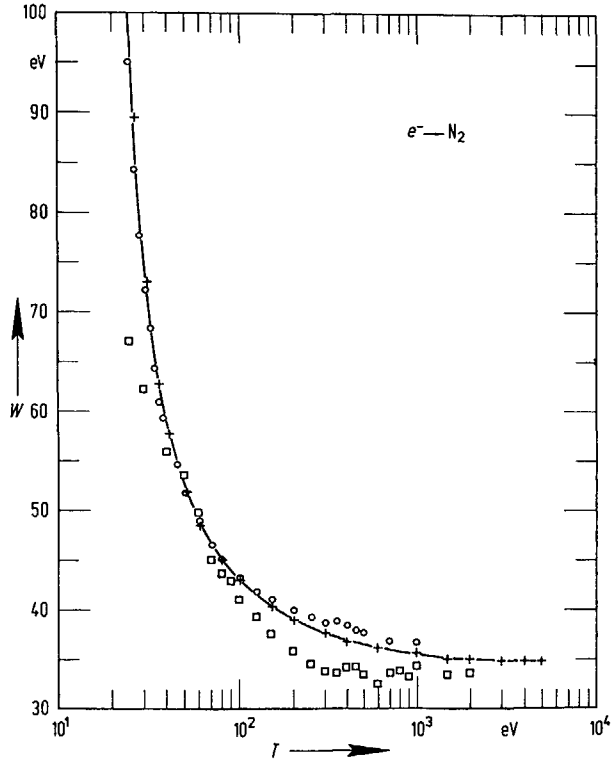

Fig. 9. Experimental values of W for electrons in nitrogen. □ Smith and Booz [6], ○ Combecher [2], + Waibel and Groβwendt [5],— fitting function [5].

2.4 Comments on methods for measuring W

To obtain experimental W values, in principle, the total energy T released to the gas, the number of primary particles n_{prim} and the number of ion pairs n_{sec} created by these particles must be measured. The ratio of these numbers may be replaced by the corresponding ratio of currents i_{prim}/i_{sec}. At very high energies, only a small part of the total particle energy is imparted to the matter to determine the differential quantity w [1]; w equals W only in the case where W is independent of the energy ($dW/dT \approx 0$).

The three basic quantities T, n_{prim} and n_{sec} may be determined by very different methods and are therefore correlated with different systematic uncertainties. The evaluation of W from several authors requires adequate weights which can only be provided if a detailed analysis of uncertainties is possible. In the following some sources of errors are pointed out.

The *particle energy released*: Only for low energies up to (a few) hundred electron volts may there be problems due to work functions of the beamline metals. The energy spread of an electron or ion source must be controlled and taken into account. This spread and an energy shift is possible due to space charge effects in the source [33,34], depending on the actual source parameters. Ripple of the power supplies typically present in ion accelerators should be mentioned. Loss of energy in the entrance window or in the effluent gas if an entrance aperture is used, can lead to marked errors. Another source of energy shift results from the ion collecting voltage during slow-down in the gas chamber, except when the primary particles are pulsed alternately with the collecting voltage.

If w is determined at high particle energy, the energy loss in the ionization cell must be determined with high accuracy, and loss of fast δ-rays from the gas volume must be considered.

The *number of primary particles* must be kept small to avoid space charge effects and strong recombination caused by high ionization densities especially as the ratio of the number of ion pairs and primaries increases almost linearly with energy. As a consequence, only at lower particle energy, are current or charge integrating methods convenient. In many experiments, particle counting methods were applied, in most cases using the ionization pulse in the gas of interest with or without gas amplification. Two essential sources of error should be mentioned: incorrect discrimination against noise, and deadtime losses. Pulse-height analysis and the theory of counting losses must be applied. In the case of current or charge measurements (of the particle beam), the requirements on the precision and stability of the capacitors and resistors of the electronical input loop are most important. Charge exchange of accelerated ions with residual gas molecules in the beam-guiding system leads to imperfectly measured particle currents; the corresponding cross sections are high at low energies. Loss of particles due to the scattering in the effluent gas from the entrance aperture can be taken into account using the pressure dependence of the ionization (see next section).

The *number of ion pairs* may be determined from each ionization pulse, but in most cases it is derived from a mean current i_{sec} or an integrated charge. High collection efficiency must be achieved, and this depends on the chamber geometry, the type of gas, the pressure, the ion density etc.. By extrapolation of the pressure dependent current $i_{sec}(p)$ from the region of complete particle stopping to $p \to 0$, ionization and particles losses in front of the entrance aperture can be taken into account [35]. But optimum collection can be achieved in many cases only if the collecting voltage is varied with a constant ratio E/p of the electrical field strength E and the pressure p. From the dependence $i_{sec}(E/p)$, the energy shift can be easily determined if a parallel-plate ionization chamber is used in the region of high collection efficiency [35]. Attention should also be paid to ionization losses due to the backscattering of primary particles in the gas; this effect is important for electrons [3-5], Fig. 7.

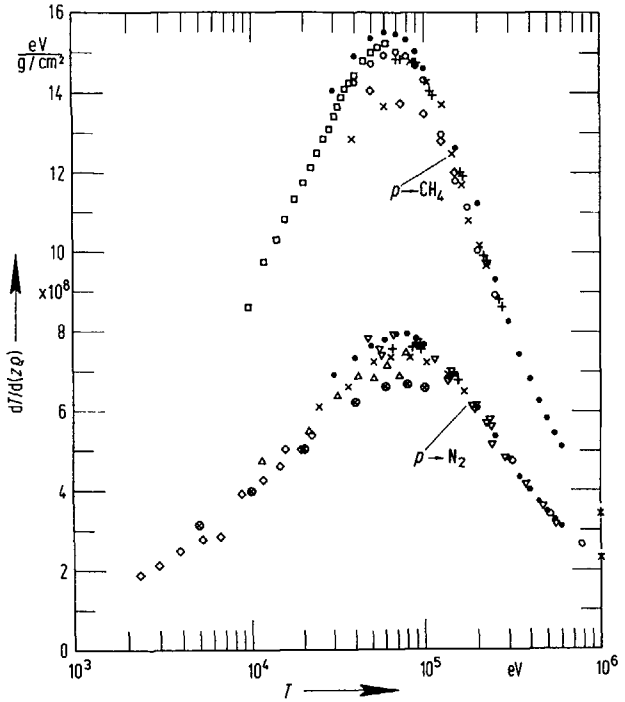

Fig. 10. Experimental values of the mass-stopping power for protons in methane and nitrogen.
CH_4 : □ Sidenius [41], ● Reynolds et al. [45], ✳ Swint et al. [46], + Baumgart et al. [48], ○ Park and Zimmerman[50], ◇ Thorngate [51], × Fukuda [52].

N_2 : △ Phillips [40], ▽ Besenbacher et al. [42], ◇ Dose and Sele [43], ○ Langley [44], ● Reynolds et al. [45], ✳ Swint et al. [46], + Baumgart et al. [47], ⊗ Omrod [49], × Fukuda [52].

3 STOPPING POWER

3.1 Low-energy protons

Since the compilation and evaluation of many experimental stopping power data by Andersen und Ziegler [36,37] in 1977 for all elements and by Janni [38] in 1979 for the elements and many compounds, great efforts have been made to reduce the obvious large discrepancies and uncertainties of experimental and theoretical stopping power data at low energies. Nevertheless, experimental data for protons in gases are very scarce below about 50 keV and show a wide spread for energies of less than 150 keV. Beyond this, in most measuring equipments only very small angle scatterings of the particles were admitted and the so-called electronic stopping power S_e was derived, partly by subtracting calculated contributions from nuclear stopping S_n (e.g. method of Fastrup et al [39]).

In Fig. 10 the proton mass stopping powers of nitrogen and methane and in Fig. 11 of carbon dioxide and methane-based tissue-equivalent gas TE(CH_4) are compiled. The data of Phillips [40], Sidenius [41], Besenbacher et al [42] and Dose and Sele [43] were

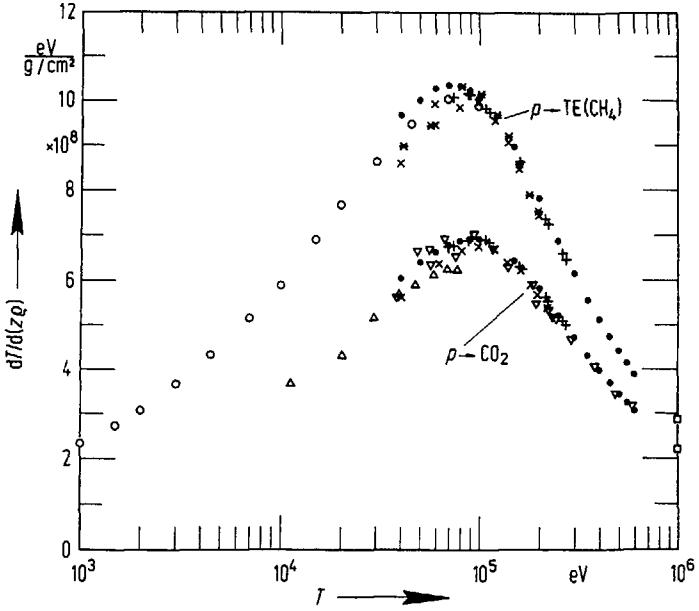

Fig. 11. Experimental values of the mass-stopping power for protons in carbon dioxide and methane-based tissue-equivalent gas.
CO_2 : △ Phillips [40], ▽ Besenbacher [42], ● Reynolds et al. [45], □ Swint et al. [46], + Baumgart et al. [47], × Fukuda [52],
TE gas: ✳ Fukuda [52], ○ Waibel and Willems [53];
calculated from components of : ● Reynolds et al. [45], + Baumgart et al. [47,48], □ Swint et al. [46], × Fukuda [52].

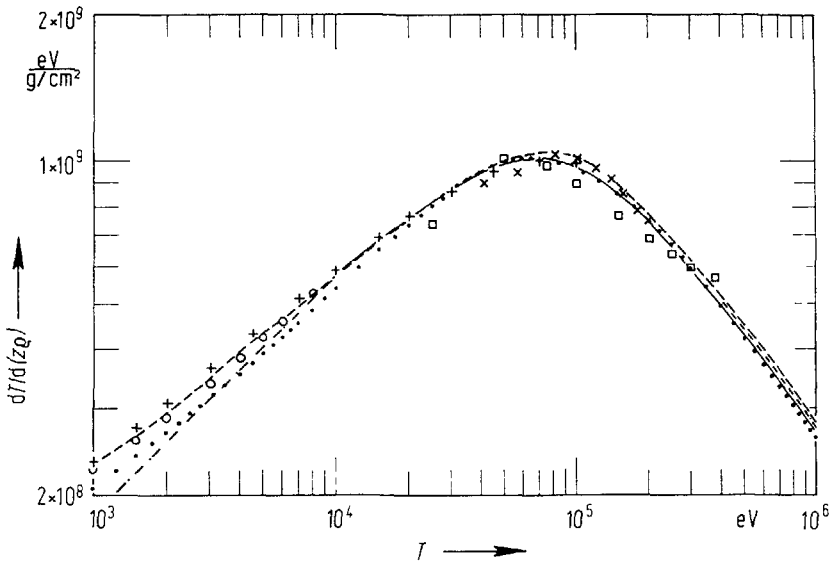

Fig. 12. Comparison of the experimental stopping-power values with other data available for protons in methane-based TE gas. × Fukuda [52], + Waibel and Willems [53]; □ from differentiated extrapolated range data by Fernandez et al. [66]; — ICRU Rep. 36; – – Oldenburg and Booz [70]; • , derived from Janni [38]; –·–·– Andersen and Ziegler [36] (above 10 keV overlapping the full curve); –·–·– Makarewicz et al. [69]; O , Andersen and Ziegler [36] with nuclear stopping power from Berger [56].

taken from curves. The data for TE(CH_4) are extremely scarce, since only those of Fukuda [52] with a slightly different mixture (64.95% CH_4 + 32,2% CO_2 + 2.85% N_2) and of Waibel and Willems [53] result from direct measurements of the gas mixture. The values assigned to Reynolds [45], Swint et al [41], Baumgart et al [47,48] are determined from their sets of experimental stopping powers of the relevant components using the simple additivity rule. For comparison with his direct measurements the corresponding calculation from Fukuda's component data [52] may be of interest and is included in Fig. 11. Only the results of Waibel and Willems [53] from 1 keV to 100 keV for TE(CH_4) include the complete nuclear stopping, because no angular limitation was applied. Fig. 12 shows a comparison of the experiments from [52] and [53] with tabulations and theory.

For propane-based tissue equivalent gas, no stopping power data for protons could be found. Data for propane were given by Park and Zimmerman [50] for 40 keV to 250 keV, Thorngate [51] for 50 keV to 150 keV and Baumgart et al [55] for 60 keV to 750 keV. Most of the proton data on H_2, He, N_2, O_2, Ne, Ar, Kr, Xe are available in graphic representations given by Besenbacher et al [42] and Andersen and Ziegler [36,37]; some additional references for some gases are mentioned in the following.

Data published for protons in oxygen: Phillips [40] 10 keV to 80 keV, Swint et al [46] 0.4 MeV to 3.4 MeV, Dose and Sele [43] 1 keV to 30 keV, Besenbacher et al [42] 40 keV to 1000 keV, Baumgart et al [47] 60 keV to 800 keV, Langley [44] 0.3 MeV to 2.5 MeV, Reynolds et al [45] 30 keV to 600 keV;

in argon :[40] 10 keV to 80 keV, [46] 0.4 MeV to 3.4 MeV, [42] 40 keV to 1000 keV, [49] 5 keV to 80 keV, [54] 40 keV to 400 keV;

in hydrogen:[40] 10 keV to 80 keV, [42] 40 keV to 1000 keV, [47] 60 keV to 800 keV, [44] 0.3 MeV to 2.5 MeV, [45] 30 keV to 600 keV, [54] 30 keV to 400 keV;

in air :Compilation of references by Andersen [37] and Janni [38], [46] 0.4 MeV to 3.4 MeV, [45] 30 keV to 600 keV, [54] 30 keV to 400 keV.

Thorngate [51] and Baumgart et al [55] measured proton stopping powers in several hydrocarbon compounds in the energy region from 50 keV to 150 keV and 60 keV to 750 keV and studied the effect of chemical binding and deviations from the additivity of the atomic stopping powers. Earlier data on hydrocarbons were published by Reynolds et al [45], 30 keV to 600 keV, and by Park and Zimmerman [50], 40 keV to 250 keV.

3.2 Stopping powers for low energy electrons

The last stopping power tables were presented by Pages et al in 1972 [59], Berger and Seltzer in 1982 [60] and ICRU 37 in 1984 [61]. In 1985 Berger [62] reviewed the information available on electron stopping powers in the energy region above 10 keV, which

can well be determined by theoretical calculations, and the region below 10 keV where the calculations are affected by larger uncertainties. The tabulations [60,61] contain collision stopping powers for low-Z material extended to energies from 1 keV to 10 keV.

Experimentally determined electron stopping powers are very scarce for energies below 10 keV especially for gases; the relevant investigations are briefly reported in [60] and [61]. Cole [31] differentiated his 5% particle transmission range in collodion and the 1% ionization transmission range in air for 20 eV to 50 keV to give an approximation of the stopping power. Iskef et al [63] collected data of extrapolated electron ranges between 20 eV and 10 keV from several experiments in gases and solids and after a scaling procedure, derived an "effective" stopping power with an uncertainty of 30%. Waibel and Groβwendt [64] presented approximate stopping power values derived from differential ionization measurements in nitrogen and methane below 5 keV; these data were compared with stopping powers calculated directly from detailed energy-loss cross sections.

This last procedure may be applied as long as there is a lack of accurate experimental and theoretical data for low electron energies, but it should be mentioned that the problem is then shifted to the precise determination of a great variety of cross sections - which may in turn be needed for other radiation transport calculations.

3.3 Stopping power additivity

The validity of Bragg's rule of additivity has been studied in a large number of experiments with anorganic and organic compounds as a function of the chemical binding and the physical state. Twaites [57,58] presents compilations and summaries of the results from about 150 investigations using in most cases protons and helium ions. Chemical binding effects are more significant for materials containing low-Z constituents and at low energies near and below the stopping power maximum. For hydrocarbons, deviations from Bragg's rule of up to 50%, in many other cases only a few percent, were found. Physical state effects are confirmed on the stopping power of low energy heavy-charged particles resulting in deviations of 5 to 10% at the stopping power maximum for H and He ions.

3.4 Remarks on stopping power measurements

The problems of the experimental determination of stopping powers arise from the definition of this quantity: in most cases, a distinction is made between collision stopping power and radiative stopping power. The last type, which leads to bremsstrahlung, is of minor importance for low-energy charged particles. Collision stopping power results in ionization and exitation [60]. The total mean stopping power includes all energy consuming processes, including energy loss due to elastic scattering or to the nuclear stopping power of low-energy ions. For ions, in the following, nuclear and electronic stopping powers are components of collision stopping power. It is a matter of point of view or of application whether only ionization and exitation processes are of interest with respect to radiation damage.

Two types of experiments must be considered: 1) The energy loss ΔT of the particle is measured in a layer of mass per area $\Delta(z\varrho)$ (z coordinate in the beam direction, ϱ density of the stopping medium) as difference of the incoming and the outgoing particle energy using e.g. an electrostatic, magnetic, or time-of-flight method and applying a very small angle geometry, and 2) the energy loss is measured immediately within the layer using either wide-angle geometry with the application of an appropriately thin absorbing detector such as a thin calorimeter foil for solids [71, 65] or an ionization chamber for gases [64,53]. With small-angle geometry, the electronic stopping might be measured but larger angle inelastic scattering at bound atomic electrons are suppressed, and nuclear stopping is incompletely taken into account.

To achieve a precision of 1% in ΔT for energy losses down to 1% of the initial particle energy during an extrapolation procedure, the two energies must be measured with a precision of about 0.01%.

In the second case it is important that the path length of the primary particle within $\Delta(z\varrho)$ is short compared with its range and that the range of secondary electrons is short compared with the layer thickness; this means that secondary radiations should be absorbed within the layer. To reduce the influence of multiple scattering, which leads to inconvenient path prolongation, an extrapolation of $\Delta T/\Delta(z\varrho)$ with $\Delta(z\varrho)\to 0$ is necessary in each case. If an ionization method is applied, the differential ionization must be converted to the corresponding energy loss by the differential w value [49]. These conditions are approximately fulfilled for low-energy protons, as the ranges of secondary electrons are markedly smaller than the absorber thickness $\Delta(z\varrho)$ due to their restricted energy region and to the spectrum which falls steeply with increasing electron energy. For low-energy electrons the measurement of ΔT in the layer can only be used if some corrections are applied taking into account the spectrum of secondary electrons and the ranges; beyond this, for the ionization method a complete set of W values is also needed. In the case of electrons with energies around 1 keV, the extrapolation procedure is quite difficult, a) as multiple scattering is very strong even at low layer thickness, b) due to a widely extended energy spectrum of secondary electrons. It follows that either the first method of measuring ΔT should be applied or that a lot of information on the secondary radiation is needed.

For each type of experiment the layer thickness is needed.For gases, generally the effective path length in the chamber, the pressure and the temperature are to be determined. Problems result from the gas density distributions near an entrance aperture and the pressure gauge calibration. Greater problems arise if a crossed beam technique is used.

It has often been attempted to derived stopping powers by the differentiation of experimentally determined energy-range relations [31,63,66,53] but it could be shown [53] that the results depend strongly on the definition of the ranges. If the type of range under consideration covers most of the collisions in the initial beam direction, the influence of multiple scattering is diminished and there is better coinicidence of the derivative with the real stopping power.

4. RANGES OF LOW-ENERGY PROTONS AND ELECTRONS

While the total path length can be calculated from an integration of the reciprocal stopping power in the so-called continuous

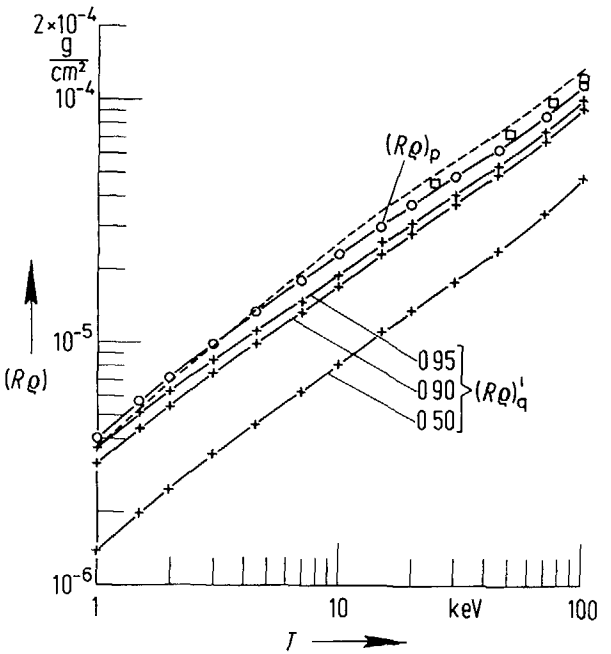

Fig. 13. Energy dependence of the projected mass range for protons in methane-based tissue-equivalent gas.
+——+ mass range $(R\varrho)_q$ for ionization fractions q = 50%, 90%, 95% from [11]. Extrapolated ionization mass range $(R\varrho)_p$ from [11], □ from Fernandez et al [66].- - - mass ranges derived from data of Janni [38].

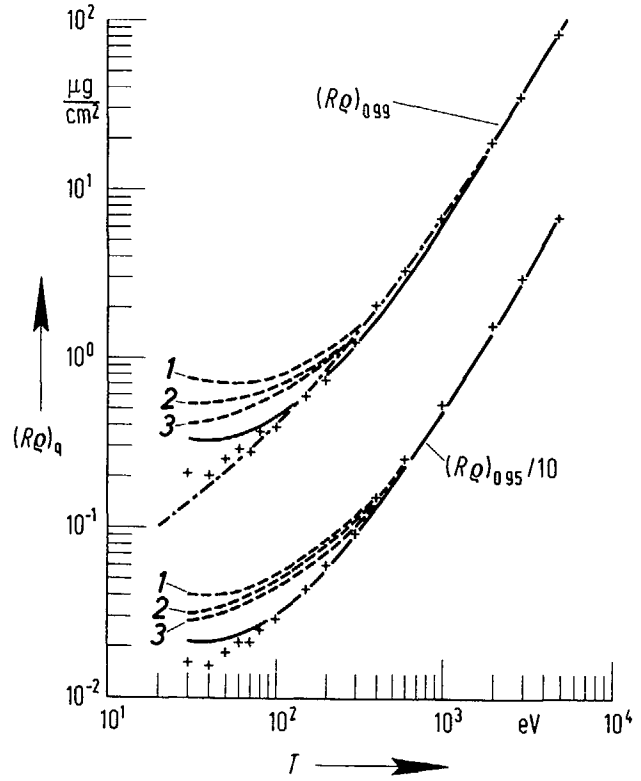

Fig. 14. Energy dependence of the ionization mass ranges $(R\varrho)_{95\%}$ and $(R\varrho)_{99\%}$ for electrons in nitrogen: + experimental results corrected for diffusion; —— Monte-Carlo calculation; - - - uncorrected experimental results for different field-strength to pressure ratios E/p, curve 1: 3.75 V/(cm mbar), curve 2: 7.5 V/(cm mbar), curve 3: 15 V/(cm mbar) from Groβwendt and Waibel [68]; —·— $(R\varrho)_{99\%}$ from Cole's energy-range relation [31] converted from air to nitrogen.

slowing down approximation, measurements generally result in projected ranges in the initial beam direction. As a consequence of different assessments of the range straggling, experimental feasibility or relevance, several definitions are currently in use, ICRU 16 [66]: a) the mean projected range $\bar{R}$ corresponds to an absorber thickness that transmits 50% of the particles, b) the "extrapolated" or "practical" range R_p derived from the extrapolation of the inflexional tangent to the axis of the layer thickness, c) the fractional or "percentile" range R_q which represents a thickness absorbing a fraction q, and d) the maximum range R_m corresponding to an undetectable transmission. In low energy experiments, ranges are determined rather with respect to the ionization than to the number of particles.

Range data for protons are available from Andersen and Ziegler, 1977 [36,37] and Janni, 1982 [38] quoting many references based on experiment as well as on theoretical calculations. Other extrapolated ionization mass ranges have been published by Fernandez et al [66] for CH_4, N_2, CO_2, TE(CH_4),(50% CH_4 + 50% N_2) for proton energies from 25 keV to 375 keV. Waibel and Willems [11] have studied extrapolated and fractional ionizations ranges (q = 95%, 90% and 50%) for proton energies from 1 keV to 100 keV in TE(CH_4) gas (Fig.13).

Calculated electron range data are available from [59-62], for energies above 10 keV; experimental data are cited there. Other references can be found in the review by Berger [62]. Iskef et al [63] have compiled several experimental data for electron energies below 10 keV in gases and solids. Their scaling procedure yields fit expressions with rather poor accuracy. The empirical range-energy expressions of several investigators are more suitable for individual absorbers; these fits are also compiled in [63]. Waibel and Groβwendt [4,5,64,68] have studied electron ranges from 25 eV to 5000 eV in CH_4 and N_2, considering the influence of the diffusion of charge carriers. The ionization measurements were performed at different values of the collecting field-strength-to-pressure ratio E/p and corrected for diffusion using a theoretical model (Fig. 14).

5. CONCLUSIONS

From the review of experimental W values for protons in the gases of interest, it can be seen that even for intermediate energies above 100 keV, further precise measurements are required.

In the high energy region above a few MeV, practically no data are available. For propane-based tissue-equivalent gas, which is becoming increasingly important in neutron applications, new investigations are needed for all energies.

W values for monoenergetic electrons are accurately determined in several gases for energies up to 5 keV, in some cases only up to about 500 eV. At higher energies, information obtained from beta-ray and x-ray measurements is available. Data for the intermediate energy region and above several MeV are very scarce and should be supplemented.

Experimental stopping power data for protons in gases are very scarce below about 50 keV and show a wide spread for energies less than 150 keV. For higher energies above about 0.5 MeV, experimental and theoretical data are in better agreement, but for special gases and gas mixtures used in the field of interest, more data on the stopping powers and stopping power ratios are required for the whole energy region.

Experimental data on the stopping power for electrons with energies below 10 keV are very scarce and affected by large uncertainties. New measurements of the stopping power and of atomic cross sections as well as further theoretical developments are needed.

REFERENCES

1. International Commission on Radiation Units and Measurements. Average Energy Required to Produce an Ion Pair, ICRU Report 31 (1979).

2. Combecher, D.: Measurement of W values of low-energy electrons in several gases, Radiat. Res. 84 (1980) 189-218.

3. Waibel, E. and Großwendt, B.: Determination of W values and backscatter coefficients for slow electrons in air, Radiat. Res. 76 (1978) 241-249.

4. Waibel, E. and Großwendt, B.: Spatial energy dissipation profiles, W values, backscatter coefficients, and ranges for low-energy electrons in methane, Nucl. Instr. Meth. 211 (1983) 487-498.

5. Waibel, E. and Großwendt, B.: Study of W-values, practical ranges, and energy dissipation profiles of low-energy electrons in N2, In Proc. Eighth Symp. on Microdosimetry, eds. J. Booz and H. G. Ebert, Luxembourg 1983 EUR 8395, pp. 301-310.

6. Smith, B. G. R. and Booz, J.: Experimental results on W-values and transmission of low-energy electrons in gases, In Proc. Sixth Symp. on Microdosimetry, eds. J. Booz and H. G. Ebert, Harwood, London 1978, EUR 6064, pp. 759-775.

7. Sidenius, G.: The total ionization of low energy ions in a tissue-equivalent gas and its component gases: absolute measurement, Rad. Eff. 39 (1978) 213-220.

8. Nguyen, V. D., Chemtob, M., Chary, J., Posny, F. and Parmentier, N.: Recent experimental results on W values for heavy particles, Phy. Med. Biol. 25 (1980) 509-518.

9. Willems, G., Waibel, E. and Huber, R.: Energy range relation and W values for low-energy protons in air and methane, In Proc. Eighth Symp. on Microdosimetry, eds. J. Booz and H. G. Ebert, Luxembourg 1983, EUR 8395, pp. 255-263.

10. Huber, R., Combecher, D. and Burger, G.: Measurement of average energy required to produce an ion pair (W value) for low-energy ions in several gases, Radiat. Res. 101 (1985) 237-251.

11. Waibel, E. and Willems, G.: Ionisation ranges and W values for low-energy protons in tissue-equivalent gas, Radiat. Prot. Dosim. 13 (1985) 79-81.

12. Thomas, D. J. and Burke, M.: W value measurements for protons in tissue-equivalent gas and its constituent gases, Phys. Med. Biol. 30 (1985) 1201-1213.

13. Petti, P.L., Verhey, L. and Wilson, R.: A measurement of w for 150 MeV protons in nitrogen ans argon, Phy. Med. Biol. 31 (1986) 1129-1138.

14. Posny, F. Chary, J. and Nguyen, V.D.: W values for heavy particles in propane and in TE gas, Phys. Med. Biol. 32 (1987) 509-515.

15. Chemtob, M., Parmentier, N. and Nguyen, V.D.: Some experimental results on W-values for heavy particles, Phy. Med. Biol. 23 (1978) 1197-1199.

16. Leonard, B.E. and Boring, J. W.: The average enegy per ion pair, W, for hydrogen and oxygen ions in a tissue equivalent gas, Radiat. Res. 55 (1973) 1-9.

17. Rohrig, N. and Colvett, R. D.: Measurement of W for protons, helium-4, ions and carbon-12 ions in tissue-equivalent gas, Radiat. Res. 76 (1978) 225-240.

18. Kühn, H. and Werba, T.: Measurements of the energy expanditure for the production of an ion pair in tissue-equivalent gas for heavy particles, In Proc. Third Symp. on Neutrondosimetry, eds. G. Burger and H. G. Ebert, EUR-5848, Luxembourg 1978.

19. Waibel, E., Willems, G.: Ionisation niederenergetischer Protonen in Methan, Phys.-Techn. Bundesanstalt, Jahresber. 1984, pp. 200-201, Braunschweig 1985, ISSN 0340-4366

20. McClure, G. W. and Allensworth, D.L.: Proportional counter for detection of ions and atoms in keV energy range, Rev. Sci. Instr. 37 (1966) 1511-1515.

21. Larson, H. V.: Energy loss per ion pair for protons in various gases, Phys. Rev. 112 (1958) 1927-1928.

22. Boring, J. W. and Woods, F. R.: The ionization of CO2, C2H4 and C2H2 by low-energy heavy ions, Radiat. Res. 35 (1968) 472-478.

23. Willems, G., Waibel, E.: W-Werte niederenergetischer Protonen in Kohlendioxid, Phys.-Techn. Bundesanstalt, Jahresber. 1987, pp. 181-182, Braunschweig 1988, ISSN 0340-4366.

24. Lowry, R. A. and Miller, G.H.: Ionization yield of protons in nitrogen and argon, Phys. Rev. 109 (1958) 826-831.

25. Schaller, L., Huber, P. and Baumgartner, E.: Messung der Arbeit pro Ionenpaar in Stickstoff für Protonen und He-Ionen im Energiegebiet unterhalb 1 MeV, Helv. Phys. Acta 36 (1963) 113-131.

26. Boring, J. W., Strohl, G. E. and Woods, F. R.: Total ionization in nitrogen by heavy ions of energies 25 to 50 keV, Phys. Rev. 140 (1965) A 1065 - A 1069.

27. Parks, J. E., Hurst, G. S., Stewart, T. E. and Weidner, H.K.: Ionization of the noble gases by protons: Jesse effect as a function of pressure, J. Chem. Phys. 57 (1972) 5467-5474.

28. Waibel, E. and Willems, G.: preliminary results, 1988

29. Bakker, C. J. and Segrè, E.: Stopping power and energy loss for ion pair production for 340-MeV protons, Phys. Rev. 81 (1951) 489-492.

30. Waibel, E.: preliminary results, 1988.

31. Cole, A.: Absorption of 20-eV to 50,000-eV electron beams in air and plastic, Radiat. Res. 38 (1969) 7-33.

32. Niatel, M. T., Perroche-Roux, A. M. and Boutillon, M.: Two determinations of W for electrons in dry air, Phys. Med. Biol. 30 (1985) 67-75.

33. Boersch, H.: Experimentelle Bestimmung der Energieverteilung in thermisch ausgelösten Elektronenstrahlen, Z. Physik 139 (1954) 115-146.

34. Forst, G.: Über die Energieverteilung der Ionen aus einer Hochfrequenz-Ionenquelle, Z. Physik 159 (1960) 7-18.

35. Waibel, E. und Großwendt, B.: Zur Technik der Bestimmung von W-Werten in Gasen, PTB-Mitteilungen 87 (1977) 13-21.

36. Andersen, H. H. and Ziegler, J. F.: Hydrogen: Stopping Powers and Ranges in all Elements (New York, Pergamon Press 1977).

37. Andersen, H. H.: Bibliography and Index of Experimental Range and Stopping Power Data (New York, Pergamon Press 1977).

38. Janni, J. F.: Proton range-energy tables, 1 keV-10 GeV, At. Data Nucl. Data Tables 27 (1982) 147-529.

39. Fastrup, B., Hvelplund, P. and Sautter, C. A.: Stopping cross section in carbon of 0.1-1.0 MeV atoms with $6 \leq Z1 \leq 20$, Kgl. Dan. Vidensk. Selk. Mat.-Fys. Medd. 35, No. 10, (1966).

40. Phillips, J. A.: The energy loss of low energy protons in some gases, Phys. Rev. 90 (1953) 532-537.

41. Sidenius, G.: Systematic stopping cross section measurements with low energy ions in gases, Kgl. Dan. Vidensk. Selk. Mat.-Fys. Medd. 39, No. 4, (1974).

42. Besenbacher, F., Andersen, H.H., Hvelplund, P. and Knudsen, H.: Stopping power of swift hydrogen and helium ions in gases, Kgl. Dan. Vidensk. Selk. Mat.-Fys. Medd. 40, No. 3 (1979).

43. Dose, V. and Sele, G.: Das elektronische Bremsvermögen von Stickstoff und Sauerstoff für niederenergetische Protonen, Z. Phys A 272 (1975) 237-243.

44. Langley, R. A.: Stopping cross sections for helium and hydrogen in H2, N2, O2 and H2S (0.3-2.5 MeV), Phys. Rev. B12 (1975) 3575-3583.

45. Reynolds, H. K., Dunbar, D. N. F., Wenzel, W. A., and Whaling, W.: The stopping cross section of gases for protons, 30-600 keV, Phys. Rev. 92 (1953) 742-748.

46. Swint, J. B., Prior, R. M. and Ramirez, J. J.: Energy loss of protons in gases, Nucl. Instr. Meth. 80 (1970) 134-140.

47. Baumgart, H., Berg, H., Huttel, E., Pfaff, E., Reiter, G. and Clausnitzer, G.: 4He stopping cross sections in H2, He, N2, O2, Ne, Ar, Kr, Xe, Ch4 and CO2, Nucl. Instr. Meth. 215 (1983) 319-328.

48. Baumgart, H., Arnold, W., Berg, H., Huttel, E. and Clausnitzer, G.: Proton stopping powers in various gases, Nucl. Instr. Meth. 204 (1983) 597-604.

49. Omrod, J. H.: Low-energy stopping cross sections in nitrogen and argon, Can. J. Phys. 46 (1968) 497-502.

50. Park, J. T. and Zimmerman, E.: Stopping cross sections of some hydrocarbon gases for 40-250 keV protons and helium ions, Phys. Rev. 131 (1963) 1611-1618.

51. Thorngate, J. H.: Measurements of the additiory of stopping cross-sections for 50-150 keV protons in nine hydrocarbon gases, Heath Phys. 32 (1977) 541-546.

52. Fukuda, A.: Stopping powers of a tissue-equivalent gas for 40-200 keV protons, Phys. Med. Biol. 25 (1980) 877-886.

53. Waibel, E. and Willems, G.: Stopping power and ranges of low-energy protons in tissue-equivalent gas, Phys. Med. Biol. 32 (1987) 365-370.

54. Weyl, P. K.: The energy loss of hydrogen, helium, nitrogen and neon ions in gases, Phys. Rev. 91 (1953) 289-296.

55. Baumgart, H., Arnold, W., Günzl, J., Huttel, E., Hofmann, A., Kniest, N., Pfaff, E., Reiter, G., Tharraketha, S. and Clausnitzer, G.: Proton and helium stopping cross sections in gaseous hydrocarbon compounds, Nucl. Instr. Meth. Phys. Res. B 5 (1984) 1-9.

56. Berger, M. J.: private communication (1986).

57. Thwaites, D. I.: Bragg's rule of stopping power additivity : A compilation and summary of results, Radiat. Res. 95 (1983) 495-518.

58. Thwaites, D. I.: Current status of physical state effects on stopping power, Nucl. Instr. Meth. Phys. Res. B 12 (1985) 84-89.

59. Pages, L., Bertel, E., Joffre, H. and Sklavenitis, L.: Energy loss, range, and bremsstrahlung yield for 10-keV to 100-MeV electrons in various elements and chemical compounds, Atomic Data 4 (1972) 1-127.

60. Berger, M. J. and Seltzer, S. M.: Stopping powers and Ranges of Electrons and Positrons, NBSIR 82-2550, U.S. Department of Commerce, Washington D. C. (1982).

61. International Commission on Radiation Units and Measurements: Stopping Powers for Electrons and Positrons, ICRU Report 37, (1984).

62. Berger, M. J.: Energy loss and range of electrons, In Nuclear and Atomic Data for Radiotherapy and Related Radiobiology, IAEA, Vienna (1987), STI/PUB/741, pp. 323-345.

63. Iskef, H., Cunningham, J. W. and Watt, D. E.: Projected ranges and effective stopping powers of electrons with energy between 20 eV and 10 keV, Phys. Med. Biol. 28 (1983) 535-545.

64. Waibel, E. and Großwendt, B.: Stopping power and energy range relation for low energy electrons in nitrogen and methane, In Proc. Seventh Symp. on Microdosimetry, eds. J. Booz, H.G.Ebert and H. D. Hartfield, Brussels 1981, EUR 7147, pp. 267-276.

65. Iskef, H. and Watt, D. E.: A calorimetry technique for measurement of the stopping power of low energy electrons (< 10 keV), In Proc. Eighth Symp. on Microdosimetry, eds. J. Booz and H. G. Ebert, Luxembourg 1983, EUR 8395, pp. 275-284.

66. Fernandez, F., Chemtob, M., Posny, F., Chary, J., Perrier, J.C., and Nguyen, V. D.: Parcours d'ionisation projetes: déduction du pouvoir d'arret des protons de 50 keV à 400 keV dans different gaz, In Proc. Seventh Symp. on Microdosimetry, Brussels 1981, EUR 7147, pp. 167-178.

67. International Commission on Radiation Units and Measurements, Linear Energy Transfer, ICRU Report 16, (1970).

68. Großwendt, B. and Waibel, E.: The influence of charge carrier diffusion on the ionometric determination of electron ranges in the low energy region, Nucl. Instr. Meth. 197 (1982) 401-409.

69. Makarewicz, M., Burger, G. and Bichsel, H.: On the stopping power for tissue-equivalent gaseous ionisation devices used in neutron dosimetry, Phys. Med. Biol. 31 (1986) 281-284.

70. Oldenburg, U. and Booz, J.: Mass stopping power and pathlenght of neutron produced recoils in tissue and tissue equivalent materials, I. Neutron energy ≤ 6 MeV, Commission of the European Communities, EUR 4786 e, Luxembourg 1972.

71. Hubbell, H. H.Jr. and Birkhoff, R. D.: Calorimetric measurement of electron stopping power of aluminium and copper between 11 and 127 keV, Phys. Rev. A26 (1982) 2460-2467.

72. International Commission on Radiation Units and Measurements. Determination of Absorbed Dose in a Patient Irradiated by Beams of X or Gamma Rays in Radiotherapy Procedures, ICRU Report 24 (1976).

PROTON STOPPING IN SOME OXYGEN COMPOUNDS AT INTERMEDIATE ENERGIES: INFLUENCES OF CHEMICAL AND PHYSICAL STATE

P. BAUER*, P. MERTENS**,
C. MITTERSCHIFFTHALER*, H. PAUL*

* Institut für Experimentalphysik,
Johannes-Kepler-Universität Linz,
Linz, Austria

** Hahn-Meitner-Institut für Kernforschung Berlin GmbH,
Berlin (West)

Abstract

For the therapeutical use of fast proton beams, a precise knowledge of the stopping power of pure elements and chemical compounds for protons is necessary, especially at the stopping power maximum. This maximum is found at a projectile velocity $v_1=(1.5\text{-}2.5)v_0$, depending on the velocity distribution of the slowest target electrons (Here, v_0 is Bohr's velocity).

Unfortunately, the scatter of published stopping power data increases drastically with decreasing projectile energy: at and below the maximum, experimental errors are typically ~20 %.

In the course of the experimental cooperation between Berlin and Linz, we obtained precise stopping power data (accuracy ± 3 %) for C,Al,Si,Ni,Cu,Ge,Ag and Au, for proton energies between 30 and 500 keV $(1.1\text{-}4.5)v_0$. The data may be understood in terms of a binary encounter model, which gives the stopping cross section as a sum of contributions from electronic subshells of the target, each of them being characterized by the mean velocity $\bar{v}$ and the velocity distribution f(v).

For proton stopping cross sections in chemical compounds, deviations from simple additivity (i.e. from Bragg's rule) are expected where the valence electrons dominate the stopping process, i.e. at and below the stopping power maximum. Indeed, our measurements on Al_2O_3 and SiO_2 show deviations from Bragg's rule of 35 % and 20 %, resp., at $v=0.9\ v_0$, the stopping cross sections of the molecules being smaller than the added stopping cross sections of the constituents. This is in qualitative agreement with the fact that the valence electrons are bound more strongly in the molecule than in the atoms or gas molecules. The ratio of the stopping cross sections $\varepsilon_{Al2O3}/\varepsilon_{SiO2}$ equals the ratio of the number of valence electrons (1.5) within ~2 % in the proton energy range from 20 keV to 300 keV ($0.9\ v_0$ to $3.5\ v_0$), where contributions from core electrons are small. This leads to the interpretation that the valence electrons dominate the stopping process in the same way in both molecules.

For H_2O vapor, the stopping cross section at low energy is again dominated by the valence electrons, but here our measurements show that these valence electrons stop more effectively than in SiO_2. This can be qualitatively understood from the velocity distributions of the valence electrons, which can be deduced from Compton profile measurements. One finds that the mean valence electron velocity in liquid water is slightly smaller than in SiO_2, which qualitatively explains our findings. It remains an open question whether the 15 % physical state effect (difference between gaseous and solid H_2O) implied by the old Wenzel-Whaling data is real or not.

---

1) Introduction

Both in the direct use of fast protons[1] for therapy, and for the recoil protons occurring in neutron therapy[1], one needs the stopping power $S = \lim_{\Delta x \to 0} \overline{\Delta E}/\Delta x$ for various chemical compounds. (Here, $\overline{\Delta E}$ is the mean energy loss in a path length Δx). The energy region near the stopping power maximum will be of special interest, since this is where the radiation effect will be largest. This maximum arises at proton energies of 50 keV to 170 keV, i.e. where the proton velocity is comparable to the mean

velocity of the most weakly bound target electrons. In the following, it will be convenient to use the stopping cross section

$$\varepsilon = \lim_{\Delta x \to 0} \frac{\overline{\Delta E}}{n \Delta x} = \int T d\sigma$$

where n is the number of molecules per unit volume, T is the energy transferred and σ the corresponding cross section. Clearly, ε can be obtained from the mass stopping power S/ρ (ρ being the mass density) by use of atomic constants.

If a chemical compound $A_k B_l$ can be treated like a simple mixture, the stopping cross section of a molecule will be given by[2]

$$\varepsilon(A_k B_l) = k\, \varepsilon(A) + l\, \varepsilon(B) \quad \text{(Bragg's additivity rule)}$$

But in the region of the stopping cross section maximum, we have to expect many uncertainties concerning the applicability of this rule[3].

2) Elemental Substances

Before considering compounds, it is useful to start with the stopping cross sections for the elements. Here the monumental data collection by Andersen and Ziegler[4] has brought to light the existence of surprisingly large discrepancies between different data sets, often larger than the stated precision. This is true even for "easily measurable" substances, e.g. for copper.

In this situation, it is useful to consider also the theoretical descriptions. As an example, Fig.1 shows the fit curve to experimental data from ref.4 together with Bethe's high energy description and with the statistical Lindhard-Scharff model which is valid at low energies. The model of Lindhard and Scharff will be only qualitatively correct, i.e. it will not describe the Z_2 oscillations of the stopping cross section, while the Bethe theory can be expected to be quite accurate. By including shell

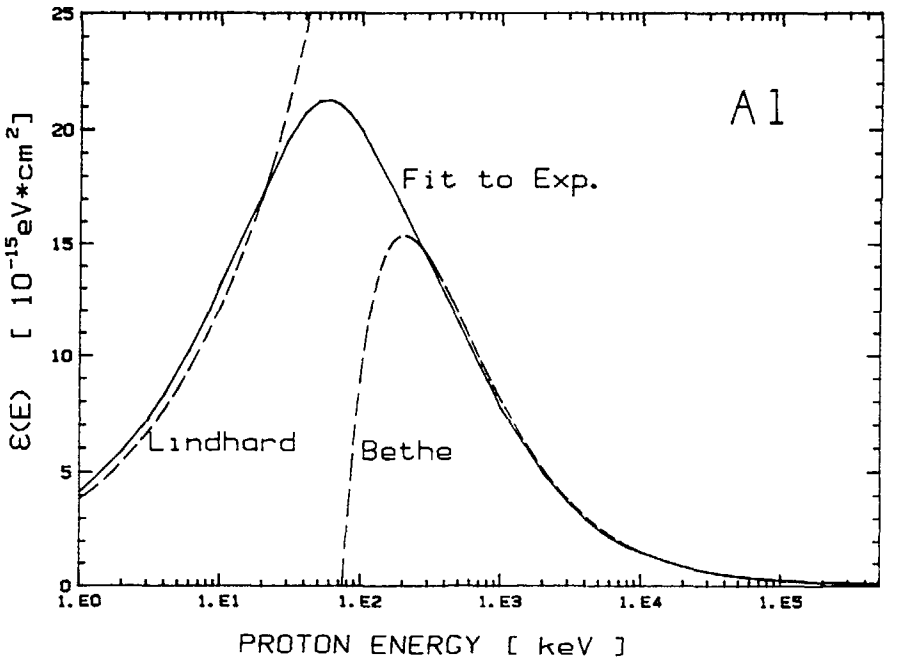

Fig.1: Stopping cross section of Al for protons. The fit curve to experimental data by Andersen and Ziegler (full curve) is shown together with the velocity-proportional stopping curve (Lindhard-Scharff-model) and the results of the Bethe theory (broken curves).

correction terms, the Bethe theory can be made valid down to lower proton energies. For the region of the stopping cross section maximum, there is unfortunately no satisfactory a priori theory. Thus, at least at the moment, the only possible approach is to perform precise measurements in this energy region.

Over a period of ten years, we have performed careful measurements[5,6,7] of ε for protons (and deuterons) on various conductors and semiconductors: C,Al,Si,Ni,Cu,Ge,Ag and Au. Fig.2 shows some of the results obtained by the Berlin-Linz

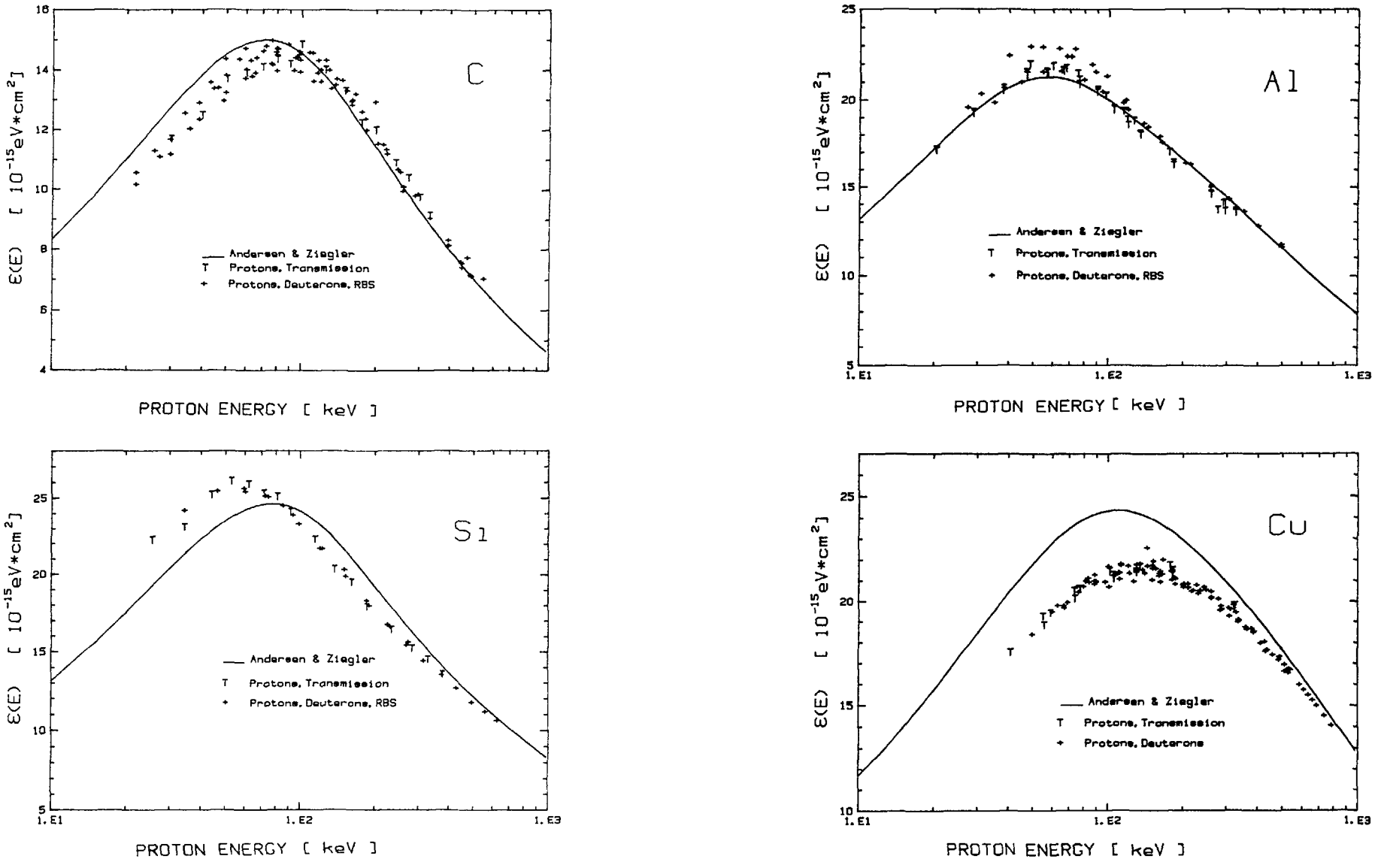

Fig.2: Some typical results of the cooperation Berlin-Linz: stopping cross sections of C,Al,Si and Cu for hydrogen ions, measured independently in Berlin (T) and in Linz (+). For comparison, the fits by Andersen and Ziegler are shown as full curves.

Table 1: *Measuring Methods used.*
(RBS...Rutherford backscattering, T...transmission)

University of Linz	RBS, evaluation of spectrum widths RBS, change of spectrum widths by target tilting *) RBS, evaluation of spectrum heights *) T, change of X-ray yield by film *) T, shift of nuclear resonances *) *) for Cu only (ref.11)
Hahn-Meitner-Institut Berlin	T, foil set, electrostatic spectrometer

cooperation[5,6,7]. Most of the Linz measurements were done using Rutherford backscattering and evaluating the width of the spectrum obtained[8]. All of the Berlin measurements were done by the transmission method, using an electrostatic spectrometer for precise measurement of the particle energy, and evaluating the stopping cross section from the slope of a straight line fitted to the measured energy loss versus target thickness data for a set of foils covering a wide thickness range. Recently, we have critically reviewed these two methods[9,10]. To check the accuracy obtainable in our energy range, we measured Cu in Linz by four additional methods[11] (two backscattering and two transmission methods), which are listed together with the standard methods in Table 1. We estimate the accuracy of single data points as 3 % which agrees well with our long-time measuring experience. Fig.2 shows, that for higher energies, the agreement of our results to Andersen and Ziegler is quite good, the deviations being less than ~5 %, while at low energies the discrepancies sometimes exceed the 20 % level. If we compare, instead to the tabulation of Janni[12], the deviations are in general less due the generally smaller values of the stopping cross section maximum in Janni's tabulation.

For the purpose of understanding, it is instructive to compare our data to our semi-empirical binary encounter model[13]. In this model, we treat separately the contributions to ε from electrons in different subshells and, for the solids, from plasma electrons (close collisions and distant collisions). Here the electrons in a subshell are characterized by their (isotropic) velocity distribution $f(v_2)$; for the differential number of $4\pi v_2^2 f(v_2)dv_2$ electrons, $\int_{T_{min}}^{T_{max}} T d\sigma$ is calculated using the transfer cross section by Gerjuoy[14] and $T_{min} = U_i = m(\bar{v}_i)^2/4$ (m being the electron mass and $\bar{v}_i$ the mean velocity of the i-th subshell). For close collisions with plasma electrons, U_i is given[15] by $\frac{3}{4}(\hbar\omega_p)^2/E_F$, where ω_p denotes the plasmon frequency and E_F the Fermi energy. The contribution of distant collisions with plasma electrons is described according to Pines[16] with a slight modification[13] (onset at $v_1=\sqrt{1.75}\,v_F$ instead of $v_1=\sqrt{2}\,v_F$, v_F denoting the Fermi velocity). The results of these BEA calculations (see refs.5 and 13) are found to describe the shapes of the measured stopping cross section maxima well, the absolute values being accurate to typically 10 %, even for elements as different as Ar,Al,Si and Cu: In Ar, all electrons are found in atomic subshells, whereas for Al (ref.5) and Si (ref.13) the stopping power maximum is almost only due to the contribution of the plasma electrons; in Cu, both shell electrons and plasma electrons contribute to the stopping cross section maximum[5].

3) Non-elemental substances

For a large variety of chemical compounds and various ions the influence of the chemical bond upon the stopping cross section (i.e. the validity of Bragg's rule) has been investigated over many years; the results were summarized by Thwaites in 1983[17] and in 1985[18].

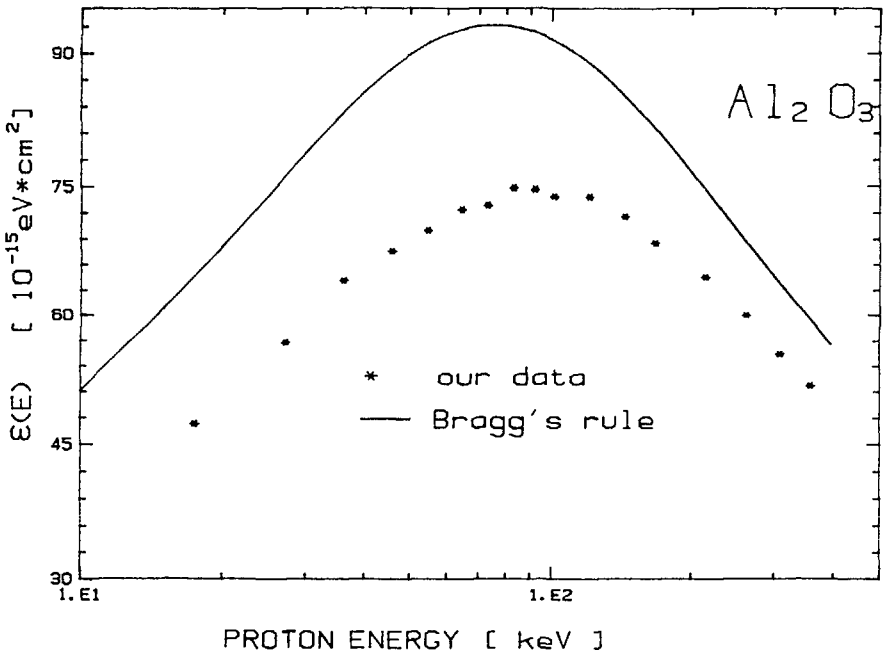

Fig.3: Stopping cross section of Al_2O_3 for protons, measured by the transmission method in Berlin. The full curve is obtained using our data for the pure metal and Reiter's gas data for oxygen.

A large deviation from the simple Bragg's rule is to be expected where ε is governed by valence electrons, and where the chemical bonds are strong ("chemical effect"). The deviations, if found, should therefore be large at ion energies up to the maximum of ε, and become smaller toward higher energy, where core electrons stop more efficiently. As an example, we test two very stable compounds: Al_2O_3 and SiO_2. The results of our measurements, obtained by transmission, are shown in figs. 3 and 4. The Bragg's rule curves in these figures are obtained as follows:

$$\varepsilon_{Br}(Al_2O_3) = 2\varepsilon(Al) + \tfrac{3}{2}\,\varepsilon(O_2)$$

$$\varepsilon_{Br}(SiO_2) = \varepsilon(Si) + \varepsilon(O_2).$$

For ε(Al) and ε(Si) we used here the data measured for thin solid films (see refs. 5 and 6) and for $\varepsilon(O_2)$ the gas data of Reiter et al[19]. One can see that Bragg's rule is too high by about 25 % and 20 %, resp., and that this deviation decreases toward higher energy, as it should. The sign of the deviation may be qualitatively explained by the fact that we have to add energy to decompose a compound into its constituents; this energy raises the valence electrons to more weakly bound states. This corresponds - at least in hydrogenlike atoms - to smaller mean velocities and therefore to larger stopping cross sections for the constituents at low ion energies. A similar argument would lead us to expect an

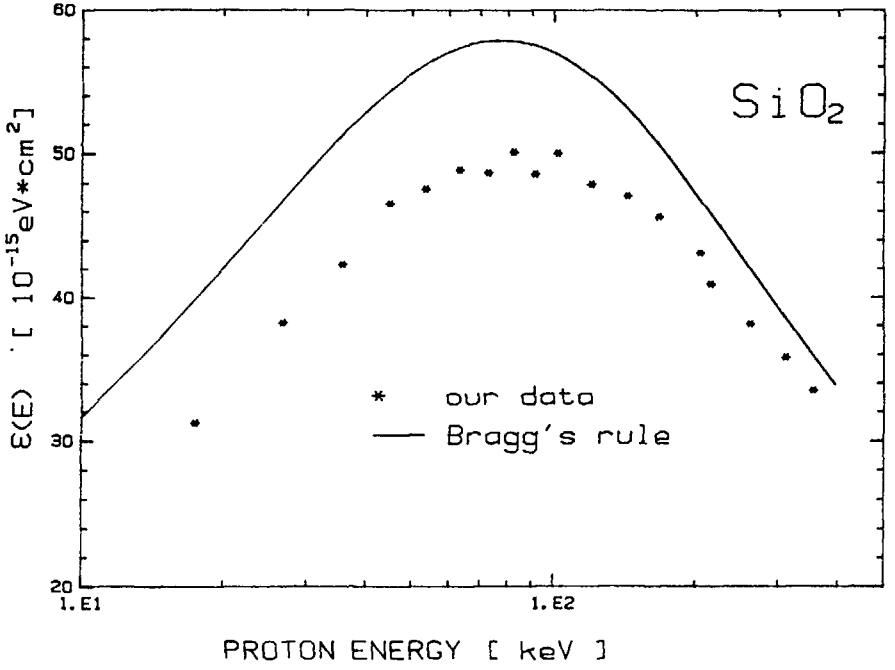

Fig.4: Stopping cross section of SiO_2 for protons, measured by the transmission method in Berlin. The full curve is obtained using our data for the pure semiconductor and Reiter's gas data for oxygen.

increase in ε if an elemental substance in the condensed state is vaporized ("physical effect"). Thus, e.g., the stopping cross section for electrons in H_2O as calculated by Paretzke[20] is smaller in the liquid phase than in the gas phase for electron energies below 60 eV. As indicated by Thwaites[18], in the more recent experiments with light ions, smaller stopping cross sections are found in the condensed phase *in the entire energy range*. Note, that Kaplan's argument[21] would lead to the opposite sign of the effect.

To describe the chemical effect in a practically useful way, Ziegler in his 1978 table[22] has introduced separate data for ε(solid) and ε(gas), which in this case would mean ε(O in oxide) and ε(O in gas). This approach would appear reasonable for elemental substances (as mentioned above). Following Ziegler's idea, Santry and Werner have tried[23] to deduce ε(O in oxide) from their data obtained for Al_2O_3 and SiO_2 and He-ions by using eqs. (1') and (2'):

$$\varepsilon(\text{O in oxide}) = \frac{\varepsilon(Al_2O_3)-2\varepsilon(Al)}{3} \qquad (1')$$

$$\varepsilon(\text{O in oxide}) = \frac{\varepsilon(SiO_2)-\varepsilon(Si)}{2} \qquad (2')$$

Indeed they found better agreement with Ziegler's ε(O in solids), which is smaller than his ε(O in gas). But they obtained two different curves for ε(O in oxide).

In order to arrive at a better description of our experimental results, we try to use more appropriate constituents[24] in applying Bragg's rule, and we write:

$$\varepsilon(Al_2O_3) = 2\varepsilon(Al^{+++}) + 3\varepsilon(O^{++++}) + \varepsilon(18\ \text{val.el.}) \qquad (3)$$

$$\varepsilon(SiO_2) = \varepsilon(Si^{++++}) + 2\varepsilon(O^{++++}) + \varepsilon(12\ \text{val.el.}) \qquad (4)$$

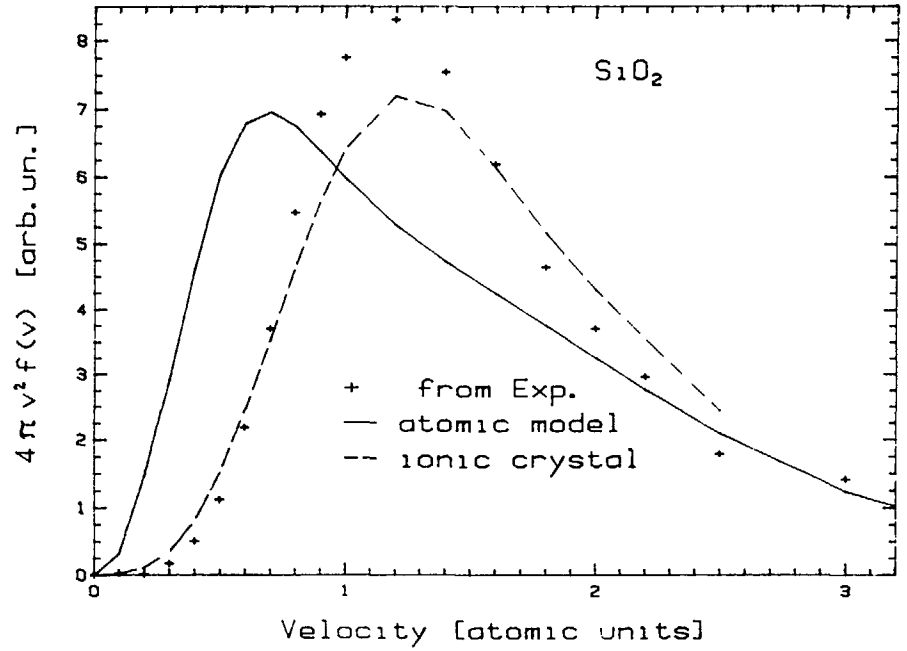

Fig.5: Velocity distribution of valence electrons in SiO_2. Results deduced from Compton profile measurements are shown as +, those deduced from Compton profiles calculated in the atomic model and the ionic crystal model, are shown as full line and broken line, resp.

The advantage of this approach is that by considering the stopping of valence electrons separately from the core electrons, we need not know to which ion core the valence electrons should be assigned. This is of advantage even for these oxides, where the measured Compton profiles (CPs) have been interpreted in terms of electron states in an ionic crystal[25]. We have calculated the velocity distribution for the valence electrons starting with the experimental CP-data[25] and with CP-data obtained by calculations assuming an atomic model or an ionic crystal[25] (Fig.5). In all cases, the contribution of the core electrons was calculated using the Hartree-Fock-model[26] and subtracted. The "experimental"

velocity distribution differs qualitatively from the one obtained in the atomic model. This is as expected, since the physical state effect for Si and the chemical state effect both tend to change the distributions. The agreement between the "experimental" and "ionic crystal" velocity distribution is better , but still not complete, presumably because the chemical bond has partially covalent character.

It has been mentioned above, that the contributions of the Al^{+++} and the Si^{++++} cores to the stopping cross section are small for proton energies around the maximum of ε. The same is true for the O^{++++} core. Thus, these contributions may, to a first approximation, be neglected in eqs. (3) and (4). Consequently the stopping cross sections of the oxides are essentially given by ε (val.el.). Assuming the chemical states of the valence electrons in Al_2O_3 and SiO_2 to be very similar, we predict:

$$\frac{\varepsilon(Al_2O_3)}{\varepsilon(SiO_2)} \triangleq \frac{\varepsilon(18\ \text{val.el.})}{\varepsilon(12\ \text{val.el.})} \triangleq \frac{18}{12} = \frac{3}{2} \qquad (5)$$

Inspection of Figs. 3 and 4 shows that eq.(5) is indeed fulfilled below ≙ 200 keV. Above this energy, the influence of inner shell electrons becomes important, so the ratio becomes larger than 1.5. We should like to mention that our recent data for He-projectiles[27] (which agree with the Santry-Werner data within the errors) give the same ratio 1.5 in the low energy range.

4) Application to H_2O

For H_2O, an eq. similar to eqs.(3) and (4) holds:

$$\varepsilon(H_2O) = 2\varepsilon(H^+) + \varepsilon(O^{++++}) + \varepsilon(6\ \text{val.el.}) \qquad (6)$$

The electronic stopping cross section of H^+ is zero, and hence, $\varepsilon(H_2O) \triangleq \varepsilon(6\ \text{val.el.})$.

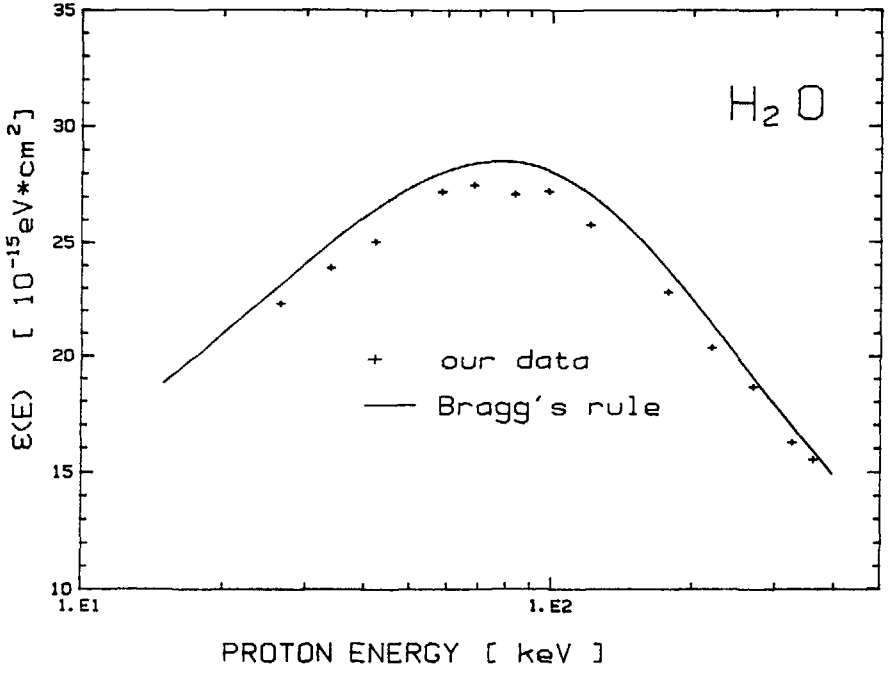

Fig.6: Stopping cross section of H_2O-vapor for hydrogen ions, measured by transmission in Linz. The curve is derived from the gas data for H_2 and O_2 by Baumgart.

Fig.6 shows the results of our measurements on water vapor[28], which differ by only ~4 % from the simple Bragg rule value

$$\varepsilon(H_2O) = \varepsilon(H_2) + \tfrac{1}{2}\,\varepsilon(O_2)$$

where the H_2 and O_2 gas data have been taken from Baumgart et al[29]. It appears worthwhile to compare the stopping of one valence electron in H_2O, deduced from ε(6 val.el.) ≙ $\varepsilon(H_2O)$, to the stopping of one valence electron in SiO_2, deduced from ε(12 val.el.) ≙ $\varepsilon(SiO_2)$. From Figs.4 and 6 we see that below 200 keV the valence electrons in H_2O stop more efficiently than in SiO_2.

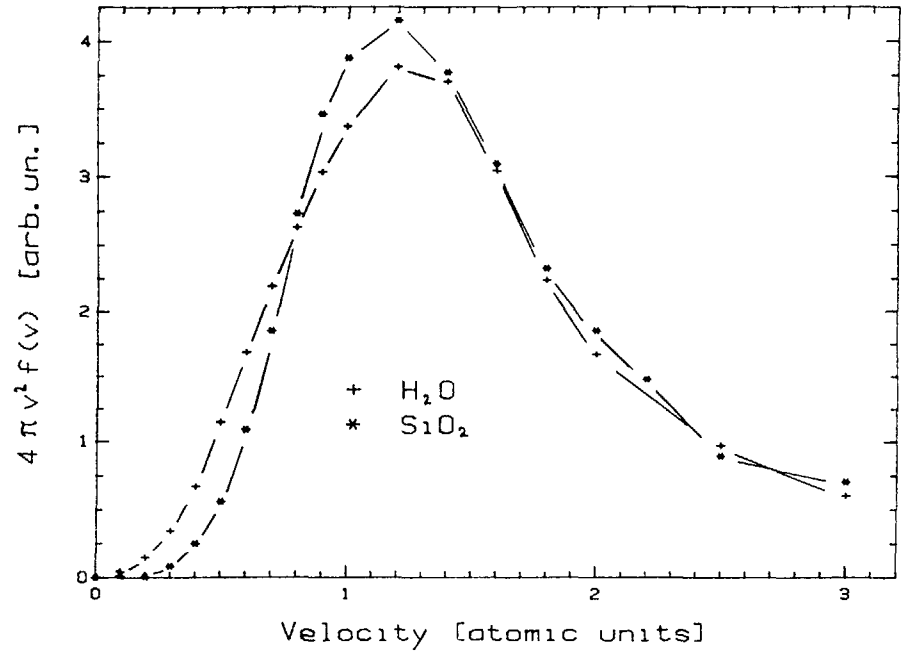

Fig.7 Velocity distribution of valence electrons in liquid H_2O and in SiO_2 obtained from measured Compton profiles.

This indicates that the chemical state of the valence electrons in H_2O is different from that in SiO_2, as one would expect. Indeed, the comparison of the corresponding velocity distributions of the valence electrons, obtained from CP-measurements on SiO_2[25] and on liquid water[30], show (see Fig.7) that $\overline{v_2}$ is slightly smaller in water than in SiO_2

In H_2O vapor, a further reduction of $\overline{v_2}$ may be expected On the other hand, a theoretical estimate of the influence of the physical state on the Compton profile of H_2O shows[31] that this influence should be small, leading to practically identical velocity distributions for the valence electrons in liquid water and in H_2O vapor. This point needs further investigation (see below), but fact remains that $\overline{v_2}$ (val.el. in H_2O) is smaller than $\overline{v_2}$ (val.el. in SiO_2) which qualitatively explains our experimental stopping values.

Fig.8 shows our measurements on water vapor together with the old data of Phillips[32] and Reynolds et al[33] on H_2O vapor and of Wenzel and Whaling[34] on D_2O ice. One can see that our data confirm the results of ref.33 in the overlapping energy region and extend the measurements toward lower energy. Compared to the ice-data, a physical state effect of up to 15 % seems to appear which is rather large and might be quite important for biological

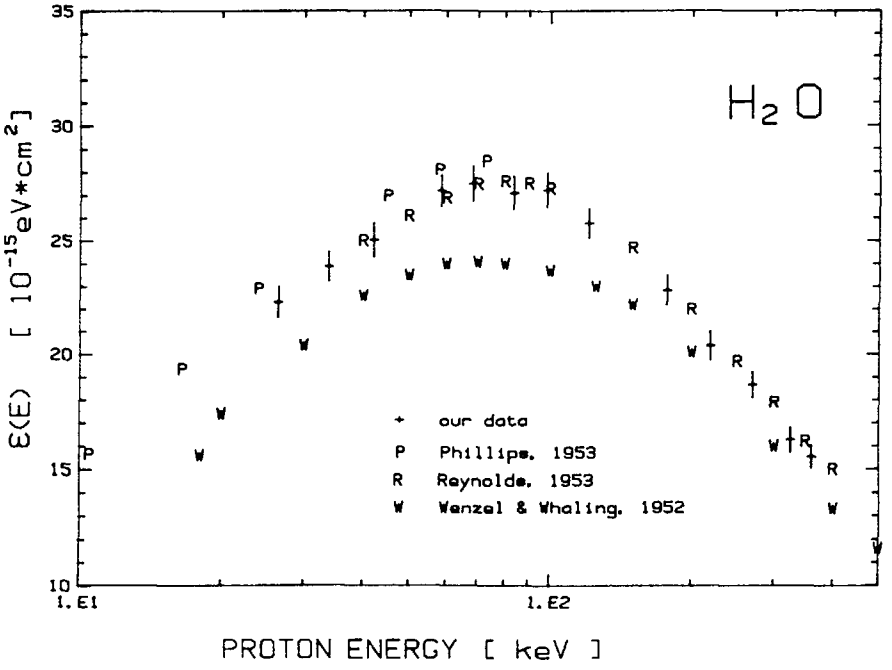

Fig 8 Comparison of energy loss data for protons in water. Measurements for H_2O vapor (symbols +, P and R) are shown together with data obtained for D_2O-ice (symbol W).

applications. It should be noted, that the results of ref.34 are supported by more recent data by Andrews and Newton[35] for low energy deuterons. Some measurements of this physical state effect in H_2O are available for He projectiles[36,37,38]. All of these experiments find a physical state effect of the same sign at ion energies from 0.3 MeV up to 4.7 MeV, at low energies exceeding the 10 % level.

Definite conclusions cannot yet be drawn concerning the physical state effect for hydrogen ions because of uncertainties concerning the charge state of the ions in the solid and in the vapor phase even for the hydrogen ion it is not clear, if the difference in the ε data (if present) is due to a nonequivalent state of the valence electrons or due to different charge states in the different physical states. Thus we conclude that new stopping measurements of protons in the condensed phase are urgently needed both from the standpoint of fundamental understanding and of biological applications.

ACKNOWLEDGEMENTS

This work was partly supported by the 'Jubilaumsfonds der Osterreichischen Nationalbank' (Proj. 2457) and by the Linzer Hochschulfonds .

REFERENCES

1) These proceedings, Report of Working Group C
2) W.H.Bragg and R.Kleeman, Philos.Mag.10 (1905) 318 and W.Whaling, Handbuch der Physik 34 (1958) 193
3) M.Inokuti and M.J.Berger, Nucl.Instr.Meth. B27 (1987) 249
4) H.H.Andersen and J.F.Ziegler, Stopping Powers and Ranges in all Elements: Hydrogen (Pergamon, New York, 1977)
5) D.Semrad, P.Mertens and P.Bauer, Nucl.Instr.Meth. B15 (1986) 86
6) P.Mertens and P.Bauer, Nucl.Instr.Meth. B, in press
7) P.Bauer and P.Mertens, to be published
8) P.Bauer, F.Aumayr, D.Semrad and B.M.U.Scherzer, Nucl.Instr. Meth. B1 (1984) 1
9) P.Bauer, Nucl.Instr.Meth. B27 (1987) 301
10) P.Mertens, Nucl.Instr.Meth. B27 (1987) 315
11) D.Semrad, P.Bauer, F.Aumayr, P.Huber and W.Obermann, Nucl.Instr.Meth. 218 (1983) 811
12) J.F.Janni, Atomic Data and Nucl.Data Tab. 27 (1982), Part 2-5
13) E.Kuhrt, R.Wedell, D.Semrad and P.Bauer, Phys.stat.sol. (b) 127 (1985) 633
14) E.Gerjuoy, Phys.Rev. 148 (1966) 54
15) E.Kuhrt and R.Wedell, Phys.stat.sol. (b) 116 (1983) 585
16) D.Pines, Elementary Excitations in solids, W.A.Benjamin Inc., New York, 1964
17) D.I.Thwaites, Rad.Research 95 (1983) 495
18) D.I.Thwaites, Nucl.Instr.Meth. B12 (1985) 84
19) G.Reiter, H.Baumgart, N.Kniest, E.Pfaff and G.Clausnitzer, Nucl.Instr.Meth. B27 (1987) 287
20) H.G.Paretzke, in: Kinetics of nonhomogeneous processes, ed. G.R.Freeman, John Wiley & Sons, 1987
21) I.G.Kaplan, these proceedings
22) J.F.Ziegler, Stopping Powers and Ranges in all Elements: Helium (Pergamon, New York, 1978)
23) D.C.Santry and R.D.Werner, Nucl.Instr.Meth. B14 (1986) 169
24) e.g., D.Powers, A.S.Lodhi, W.K.Lin and H.L.Cox, Thin Sol. Films, 19 (1973) 205
25) M.Rosenberg, F.Martino, W.A.Reed and P.Eisenberger, Phys.Rev. B18 (1978) 844
26) E.Clementi and C.Roetti, At.Data and Nucl.Data Tables 14 (1974) 177
27) P.Bauer, Ch.Mitterschiffthaler, P.Mertens, Poster contr., 11th Int.Conf.At.Phys., Paris, 1988
28) Ch.Mitterschiffthaler, Diploma thesis, in preparation, Univ. of Linz
29) H.Baumgart, W.Arnold, H.Berg, E.Huttel and G.Clausnitzer, Nucl.Instr.Meth. 204 (1983) 597

30) B.G.Williams (ed), Acta Cryst. A32 (1976) 513
31) A.Seth and E.J.Baerends, Chem.Phys.Lett. 52 (1977) 248
32) J.A.Phillips, Phys.Rev. 90 (1953) 532
33) H.K.Reynolds, D.N.Dunbar, W.A.Wenzel and W.Whaling, Phys.Rev. 92 (1953) 742
34) W.A.Wenzel and W.Whaling, Phys.Rev. 87 (1952) 499
35) D.A.Andrews and G.Newton, J.Phys. D10 (1977) 845
36) S.Matteson, D.Powers and E.K.L.Chan, Phys.Rev. A15 (1977) 856
37) R.B.J.Palmer and A.Akhavan-Rezayat, J.Phys. D11 (1978) 605
38) D.I.Thwaites, Phys.Med.Biol. 26 (1981) 71

ATOMIC AND MOLECULAR PROCESSES OF ENERGY LOSS BY ENERGETIC CHARGED PARTICLES*

L.H. TOBUREN
Battelle Pacific Northwest Laboratories,
Richland, Washington,
United States of America

Abstract

Understanding the biological consequences of energy loss by charged particles, whether they are high energy therapeutic ion beams or ion recoils produced by neutron interactions in tissue, requires access to a wide range of atomic and molecular data. The relative biological effectiveness of different high LET radiations, as well as a detailed understanding of the chemical and biological damage initiated, depends on the spatial pattern and form of the energy deposited within the stopping media. For fast charged particles the primary means of energy deposition is ionization of the media with the spatial pattern determined by subsequent energy transport by secondary electrons. To provide detailed descriptions of the spatial pattern of energy deposition and energy transport along charged particle tracks requires a comprehensive knowledge of the cross sections for 1) the production of electrons, as a function of ejected electron energy and emission angle; 2) electron capture and loss by the moving ion; 3) the relative probability of multiple ionization processes, i.e., simultaneous production of two or more secondary electrons; 4) the interactions of secondary electrons with the constituents of the media; 5) for dissociative ionization/excitation of the molecular constituents of the media; and 6) the subsequent ion-molecule and excited state molecular energy transfer reactions within the stopping medium.

A good deal of information presently exists for ionization by bare charged ions[1], particularly protons and alpha particles. Likewise data on charge transfer is available for a broad range of ion-atom/molecule collisions.[2] Data are becoming available on multiple ionization processes from a wide range of sources, however there is presently no compilation or review of these data available. For application to radiation therapy, and radiation research involving high LET radiation, there are still large gaps in our knowledge of atomic and molecular data. For example, there is very little known regarding the cross sections for ionization by ions carrying bound electrons. Likewise charge transfer cross sections for structured ions are fragmentary and widely

*Work supported by the Office of Health and Environmental Research (OHER) U.S. Department of Energy under Contract DE-AC06-76RLO 1830.

[1]L.H. Toburen, "Continuum Electron Emission in Heavy Ion-Atom Collisions: in High-Energy Ion-Atom Collisions ed by D. Berényi and G. Hock (Elsevier Scientific Publishing Co. NY, 1982) pp.53-82.

[2]C.F. Barnett, J.A. Ray, E. Ricci, M.I. Wilker, E.W. McDaniel, E.W. Thomas and H.B. Gilbody "Atomic Data for Fusion" ORNL-5206 Vol. 1 (1977).

scattered in the literature. Effects of the phase of the stopping media (solid, liquid, gas) on interaction cross sections, data of particular interest to Radiological Physics, have only begun to be addressed. This presentation will briefly review the status of our knowledge of differential and total ionization cross sections, discuss the availability of charged particle cross sections of interest in Radiological Physics, and describe some of the areas where data is urgently needed.

INTRODUCTION

The use of charged particle beams in radiation therapy and in studies of high linear-energy-transfer (LET) radiobiology has focused increased attention on understanding the detailed processes of energy deposition in complex biological systems. Of particular interest is understanding the relative biological effectiveness of charged particles and neutrons; the latter is especially important in radiation protection. Wide ranges of biological effectiveness for different biological end points have been observed for different types of radiation and for various irradiation conditions, e.g., different doses, dose rates, and dose fractions. Understanding the basis for this wide range of observed biological responses requires investigation of the complex sequence of physical, chemical, and biological events initiated by the absorption of energy from the radiation field and determination of how these processes may be affected by the differences in the spatial and temporal distributions of energy deposition. For high-LET radiation, each interaction leading to energy loss may result in the release of one or more secondary electrons that have sufficient energy to produce further ionization and/or excitation. The secondary electrons transport energy from the track path following which atomic and molecular constituents of the media may be left in various stages of excitation and/or ionization, chemical bonds may be ruptured, radical chemical species created, etc. An understanding of biological effectiveness of different radiation types relies therefore, on understanding the relative yields of these physical and chemical process and their influence on the subsequent evolution of the chemical and biological stages of radiation damage. For high-LET radiation, it is particularly important to determine the consequences of correlation between the spatial and temporal distributions of energy deposition and the molecular and subcellular structure of the biological target. Because direct measurement of spatial patterns of energy deposition in biological media are technically infeasible, such information is usually obtained from appropriate theoretical models of the energy transport processes. These models are based on our knowledge of the atomic and molecular properties of the fundamental interactions.

Energy deposition by charged particles can be described at several levels of complexity. Traditionally, stopping power, or LET, has been used to describe the differences in energy deposition by charged particles of different energies and species. These quantities address the fate of the radiation (a Class 1 problem as described by Inokuti[1]), but provide no information on the fate of the media (a Class 2 problem as discussed by Inokuti[1]). The concept of LET becomes inadequate for studies of the mechanisms of radiation damage where the detailed structure of the charged particle track influences the biological effectiveness of the radiation. This is particularly evident in studies with very high-LET ions, where the same biological response may be induced by ions with widely varying LET. Conversely, ions with nearly equivalent LET but different velocities may produce large differences in observed biological response.[2] In order to overcome the shortcomings of LET-based descriptions of radiation effects it is necessary to address the Class 2 problem. One must be able to describe the interaction process from the point of view of the absorbing medium. For high-LET radiation, this requires knowing the spatial pattern of ionization and excitation produced by the primary ion, and its secondary electrons.

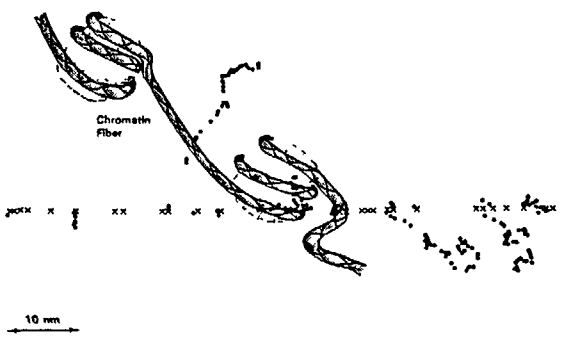

Figure 1. Simulated 1-MeV proton track in water compared to the dimensions of a segment of chromatin fiber.

Furthermore, we need to know the type of interactions which occur, i.e., single/multiple ionization, molecular dissociation, charge transfer, etc.

Figure 1 illustrates the scale relevant to understanding the effects of charged particle track structure on damage to crucial substructures of the cell. The dimensions of this simulated proton track, i.e., separation between primary and secondary ionizations and range of secondary electrons, are comparable to the size of chromatin structures. As the ion energy increases more-energetic secondary electrons will be produced, reducing the local density of ionization; a denser pattern of ionization would occur for lower energy ions. An increase in the ion charge will also increase the local density of ionization. It is these variations, along with more subtle changes, such as the relative probability of producing inner-shell ionization, that are expected to influence the relative biological effectiveness of the different high-LET particles.

Various models have been, or are being developed, to describe charged-particle track structure.[3-6] Homogeneous track models, such as those of Katz and coworkers[3] and of Chatterjee,[4] are a great improvement over the concept of LET for describing the energy deposition characteristics of fast charged particles. These models consider variations in the radial distribution of dose along the charged-particle track, but still provide average rather than point-by-point distributions. A shortcoming of such models is that they predict the average dose delivered at a given distance from the track, whereas energy deposition in small volumes is a stochastic process. Small volumes of sizes comparable to sensitive cellular components that lie at substantial distances from the particle path may either be hit or missed by secondary electrons. This is illustrated in Fig. 2, where recent data we have obtained in measurements at the Darmstadt UNILAC accelerator are shown. Here, the amount of energy (Dose D(b), or Z_b in microdosimetric terms) deposited in a simulated 0.5 μm diameter tissue volume is compared to the amount predicted by homogeneous track models as a function of the radial distance from the track axis. Note that at the larger distances from the particle path, the amount of energy actually deposited in a small volume may be orders of magnitude greater than the predicted average. The quantity R_b referred to in Fig. 2 is the ratio of the number of recorded energy deposition events per ion which, for large radial distance b, essentially reflects the geometric probability of an event occurring in the small detector volume. Note that the products of R_b and the measured energy

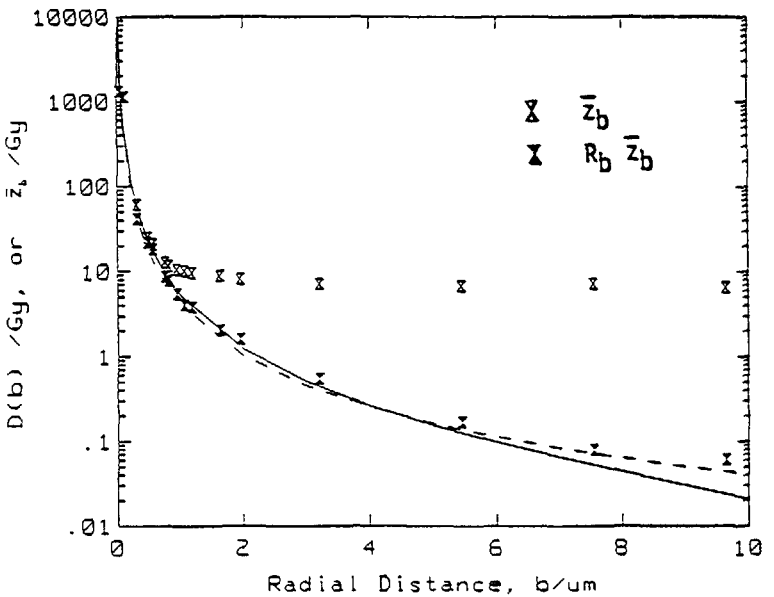

Figure 2. The absorbed dose delivered to a 0.5-μm-diameter volume as a function of the radial distance from the path of a 13.8-MeV/amu Ge ion. The homogeneous charged-particle track calculations are from Waligorski and Katz[3] (—) and Chatterjee and Schäfer[4] (--).

deposition are in excellent agreement with the average values given by homogeneous track models. Using full Monte Carlo calculations,[5,6] one should be able to reproduce the stochastic nature of the experimental data of Fig. 2. Such calculations have not yet been carried out for heavy ions, however, owing to a lack of cross-section data needed as input to these codes.

The subsequent sections of this paper will discuss the atomic and molecular data that are needed as input to conduct stochastic Monte Carlo calculations of charged-particle track structure. A brief review will be given of the data currently available, where these data may be found, and where additional data are needed. This review is not intended to be comprehensive but will, we hope, provide a starting point for discussions of data needed to obtain detailed understanding of the interactions of high-LET radiation with biologically relevant material.

STOPPING POWER

Although our goal is to discuss data needed for detailed models of track structure, any such detailed model must also be able to accurately predict average quantities of energy loss. Thus, accurate stopping-power data are needed to test these models and to provide information and guidance as to the effects of the target phase (solid, liquid, gas) on the energy deposition process. A good deal of information is available for the stopping of electrons,[7] protons,[7-10] and alpha particles,[7-10]. Data are available for numerous target materials and particle energies and some of the work includes effects of target phase.[8,10] For light ions the data seem adequate for radiological application. Results for heavy ions are, unfortunately, less complete. A comprehensive compilation of stopping power, based primarily on theory, and illustrated with data where available, has been presented by Ziegler et al.[11] Although this compilation is very useful, it seems appropriate to obtain additional experimental data for testing the computed values. This is especially true for the very heavy ions of interest to radiation biology. An example of such data is provided by the recent work of Baek et al.[12] on the effect of target structure on the stopping power of carbon ions. In some cases, stopping-power measurements have been conducted as a part of accelerator operations at major laboratories, such as those at GSI-Darmstadt and LBL-Berkeley. These data, however, are often available only in technical reports that are in some instances difficult to obtain. Reviews of these data, in a readily available form, would be very useful to the scientific community.

CHARGE TRANSFER CROSS SECTIONS

Charge transfer becomes increasingly important as fast charged particles slow down and begin to pick up and/or lose electrons in interactions with the atomic and molecular constituents of the stopping medium. These processes contribute to the energy loss of the ion as well as change the charge of the ion, thus affecting subsequent interaction probabilities. A substantial literature of charge transfer cross sections has been developed for light particles such as protons, alpha particles, neutral hydrogen atoms, etc. A comprehensive and critical review of these data relevant to fusion energy development has been provided in the "Red Book" published by Oak Ridge National Laboratory.[13] A second volume, describing collisions of carbon and oxygen ions with electrons, H, H_2, and He, has recently been published.[14] A review of charge-changing collisions for He, Li, Be, and B and their ions, in a wide range of atomic and molecular targets, has been published by Okuno[15] and more recently data for hydrogen and helium atoms and ions have been compiled by Nakai et al.[16] These compilations provide an excellent review of data relevant to fusion and are also useful for radiation research. However, for radiation research reviews of this type need to be extended to other ions and targets. For example, in neutron dosimetry data are needed for charged-particle recoils (H^+, C^{n+}, O^{n+}, N^{n+}, He^{n+}) and their neutral species in targets relevant to dosimetry and biology (H_2O, hydrocarbons, etc.). Likewise, similar data on charge transfer are needed for faster and heavier charged particles used in radiation biology and therapy (i.e., uranium ions, iron ions,...). Although some data are becoming available for high-energy heavy ions,[17,18] they are widely scattered in the literature. It is time-consuming to track these data down and, in some cases, they are available only from the laboratory involved in the research. An organized effort to compile charge transfer data relative to radiation research and therapy would benefit a broad segment of the research community.

IONIZATION

The primary mechanism for energy loss by fast charged particles is ionization of the atomic and molecular constituents of the stopping medium. In addition, the subsequent energy transport by secondary electrons produced in these ionizing collisions is the origin of the spatial characteristics of charged-particle track structure. Therefore, detailed and comprehensive data on ionization cross sections are mandatory if comprehensive track-structure models are to be developed. In this section a brief discussion will be given of the total, differential, and multiple ionization cross sections relevant to radiation research.

Total Ionization Cross Sections

Total yields of electrons and ions are important ingredients in developing track-structure models. In Monte Carlo calculations the mean free path between interactions of the ion with constituents of the stopping medium is based on total ionization cross sections. Likewise, boundary conditions for testing more detailed differential cross sections incorporated in Monte

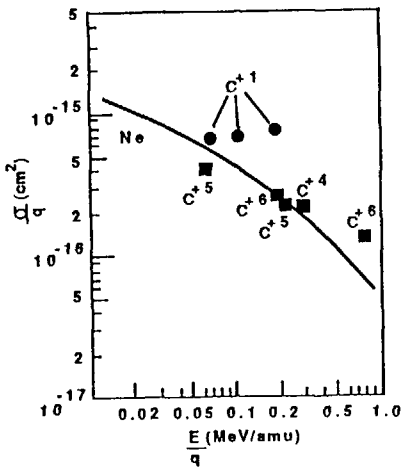

Figure 3. Reduced cross sections for ionization of neon by carbon ions. Square symbols are data of Schlachter, et al.,[23] closed circles are from our measurements. The solid line is a classical trajectory calculation presented by Schlachter et al.[23]

Carlo codes are provided by accurate total cross sections. Ionization cross sections for both electron and proton impact have been the subject of extensive study. Reviews by Rudd et al.,[19] DeHeer et al.,[20] Tawara and Kato,[21], and Schram et al.[22] provide a broad range of data for proton and electron impact. Data for heavier ions, or for light ions carrying bound electrons, are much more difficult to find. In addition, scaling laws developed for highly charged ions may be inappropriate for ions of low charge states. This is illustrated in Fig. 3 where some of our recent data for ionization of neon by C^+ are compared with data published by Schlachter et al.[23] Values are scaled according to a scheme applicable to highly charged ions. The solid line represents results of a classical-trajectory Monte Carlo calculation for highly charged states that was also performed by those authors. A great deal more work is needed if we are to understand fully the nature of ionization by fast (or slow) charged particles which carry bound electrons. This is true even in this simplest case of total yields of target ions and electrons.

Differential Cross Sections for Ionization by Charged Particles

Ionization cross sections, differential in ejected electron energy and emission angle, are the basic data needed to investigate the spatial pattern of energy deposition by charged particles. These cross sections for ion interactions with media constituents provide the source term for energy transport by secondary electrons. The corresponding cross sections for the interaction of these secondary electrons with the medium determine the spatial location of subsequent interactions. There has been a great deal of attention given to doubly differential cross sections (DDCS) for electron and proton interactions with atoms and simple molecules. The most comprehensive data for electron impact ionization are given by Opal et al.[24] Data for electron impact ionization have also been presented by Rudd and coworkers[25-27] and Oda et al.[28]. No attempt is made here to be comprehensive; data are also available from several other sources. This is another instance of where a comprehensive review of data would be highly beneficial to those involved in track-structure physics. Such a review could bring together all available data, point out discrepancies and limitations, and make available a complete set of the published cross sections.

Perhaps the most comprehensive data regarding DDCS are those for proton impact. Three laboratories have been instrumental in these studies: our laboratory, the University of Nebraska, and Hahn-Meitner Institute in Berlin. Several reviews have also been published.[29-31] The review by Toburen[31] provides a comprehensive list of references to DDCS for ion impact measurements published up to 1981. In general, our understanding of DDCS for electrons, protons, and alpha particles (all bare ions) is quite good. Systematics with regard to ion energy and target structure are well understood. Our understanding of the interaction process for ions which carry bound electrons is, however, much less advanced. For the simplest cases, He^+ and H° impact, there are considerable data[31-36] with some degree of understanding of the effects of projectile electrons on the ionization mechanisms. For heavier ions that carry greater numbers of bound electrons there are fewer data and our state of understanding is more limited. The data shown in Fig. 4 illustrate some of our recent results for intermediate velocity oxygen ions. The singly differential cross sections shown here for three charge states of the incident ion are all similar for ejection of electrons with energies greater than about 100 eV. This reflects the inefficient screening of the projectile nuclear charge by bound electrons for close collisions associated with large energy transfer. For lower ejected electron energies that are representative of more distant collisions, the higher charged ions are more efficient in ejecting electrons, as one might

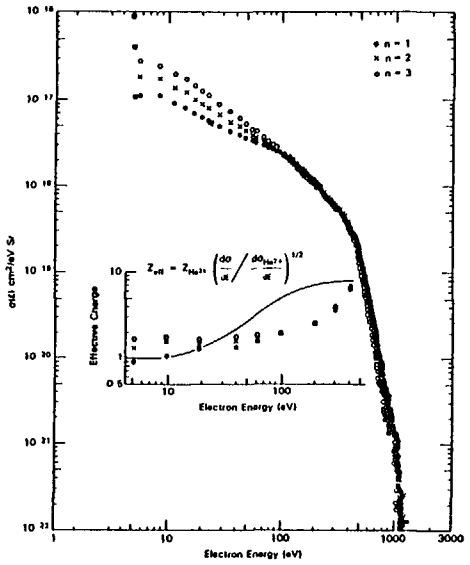

Figure 4. Singly differential cross sections for ionization of water vapor by oxygen ions at 3.28 MeV/amu. The insert illustrates the effective change of the oxygen ion as a function of ejected electron energy. The solid line shown in the insert is based on a model of effective charge derived from He^+ data.[35]

expect. If the collision were sufficiently distant for the projectile to look like a point charge, i.e., if screening of the projectile nuclear charge by its bound electrons were complete, the collision strength would be reflected by the net ionic charge. However, note that even at the lowest ejected electron energy shown, 5 eV, the ratio of cross sections for the different charge states is far from the 1:4:9 one might expect for charge states 1, 2, and 3, respectively.

Also shown, as an insert in Fig. 4, is the effective charge of the different incident oxygen ions, as a function of the energy of the ejected electrons. This effective charge is determined by comparing cross sections for oxygen ion impact with similar data for alpha particles. Note that the dependence of the effective charge of the incident ion on ejected electron energy found for He^+ ions,[35] shown as the solid line, is quite different from that derived from the oxygen ion data. To date there is insufficient experimental data available to derive systematics for the effects of screening of the projectile charge by bound electrons. In addition, the theory of such collisions has not yet advanced to the point where it can be used to provide reliable guidance. A good deal of new data are needed in this area, not only for slow collisions, where electron capture processes lead to a large number of electrons being bound to the projectile, but also at high energies, where a relatively small number of electrons may remain bound to the projectile. For example, uncertainty in the effects of screening by a few bound electrons on the ionization cross section for Ge ions reduces the reliability by which one can use Monte Carlo calculations to describe the details of track structure which contribute to the radial distributions of ionization shown in Fig. 2.

Data are emerging on the secondary electron spectra produced by low-energy ions carrying bound electrons, but we still have little quantitative understanding of the mechanisms involved in the ionization process. In Fig. 5 our data for ionization of Ne by C^+ are compared with lower-energy Ne^{2+} data of Woerlee et al.[37] The systematic variations in these data lend themselves to the use of relatively simple scaling laws to interpolate DDCS between measurements at different ion energies and for different ion species. For example, Woerlee et al. deduce from their data that the quasi-molecule formed during the collision is the origin of the secondary electrons and that the ionization mechanism is direct radial or rotational coupling between

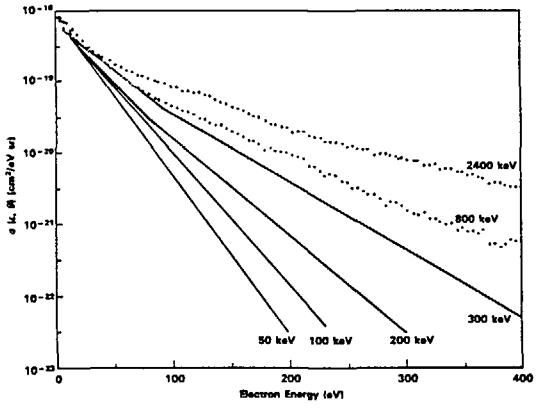

Figure 5. Doubly differential cross sections for electron emission from neon by C^+ from our laboratory ions (••••) compared to lower energy Ne^{2+} results from the work of Woerlee et al.[37] (——). These data are for electron emission at 90° with respect to the ion beam.

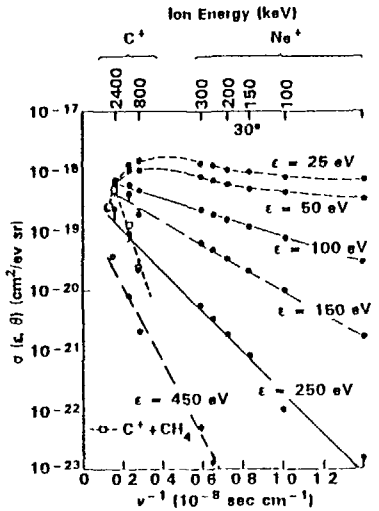

Figure 6. Double differential cross sections for ionizations of neon by C^+ and Ne^{2+} ions. The Ne^{2+} data is from Woerlee et al.[37] Also shown is data for ejection of 250 eV electrons from CH_4 by C^+ ions.

highly promoted outer molecular orbitals and the continuum. A simple empirical relationship derived from their work is used to plot their data for electron emission at 30° in Fig. 6 along with our higher velocity C^+ - Ne results. Note an apparent systematic agreement between the Ne^{2+} - Ne and C^+ - Ne results at relatively widely varying ion energies. Similar results are obtained at other emission angles. It appears from this comparison that details of the atomic structure of the target and projectile are not very important. However, this simple logic breaks down when C^+ - CH_4 data are plotted on the same graph (see open symbols in Fig. 6). For methane data, the slope of the line extrapolating the high-energy data toward lower ion velocities is considerably different from the apparent consistency observed with the C^+ - Ne results. It may be, therefore, that the apparent agreement between the results for C^+ - Ne and Ne^{2+} - Ne is purely coincidental. Further data are badly needed to resolve these questions.

Another potentially important aspect of high-energy heavy ion collisions is the emission of very high-energy secondary electrons. Electron with energies up to hundreds of keV have been detected in ion collisions where ion energies are only a few MeV/amu.[38] These electrons are emitted in the high fields of super-heavy quasi-molecules formed during collisions. Although the cross sections for emission of these high-energy electrons are relatively small, it is possible that their long range may have biological significance. As additional data become available, they should be included in track structure descriptions of heavy ion collisions if a complete correlation is to be made between radiobiological effects and track structure parameters.

Multiple Ionization

Considerable work has recently been performed regarding the production of multiply charged atomic targets by ion impact. These processes may have important consequences in radiation biology as they may lead to decidedly different chemical species than simple single ionization. In addition, the production of two or more secondary electrons in a single collision may lead to correlated excitation/ionization events in the path of a charged particle. We have recently reviewed data for single and double ionization of He by bare and clothed charged particles[39] and find that data for ions from about 0.04 to 1 MeV/amu are well described by an independent electron model. The actual ion energy range of applicability depends on the number of bound projectile electrons.

For low-energy ions, our studies of target charge states produced in ion-atom collisions indicate that the heavier ions and higher Z targets lead to higher yields of multiply ionized targets. Systems as much as 50% of the ionization yield result in multiply charged states.[40] Although there has been much interest in simple atomic targets, the influence of target atomic and molecular structure has not been extensively studied. Additional data are also needed to determine the effects of molecular structure and target phase on the production of multiply charged target atoms.

Data Sources

In addition to the reviews of data referenced above in discussing particular interaction processes of interest, the U.S. Army Missile Command[41] has published an excellent review of data encompassing a wide range of ion-atom/molecule collision processes. Although this review was compiled for relevance to gas lasers it presents data that are also of interest to radiobiology. The Institute for Plasma Physics, Nagoya University, Japan, has also published excellent reviews.[42] In addition to data reviews there are several agencies that publish periodic literature reviews and provide listings, by reaction, of references. These include reviews sponsored by the International Atomic Energy Agency,[43] U.S. Department of Energy,[13,14,44] and the Japanese Atomic Energy Agency.[16] A Bibliography of chemical kinetics and collision processes has also been published by Plenum.[45]

It can be noted that most of the data compilation and evaluation has been performed by and for the fusion research community. Where their interests overlap with our needs, these reviews provide a source of data for radiation research and therapy. This overlap is, unfortunately, quite small, and we need a similar effort to review, evaluate, and compile data of special application to radiation biology. Not only would such an effort provide a useful source of data to users, but it would uncover areas where data needs are most obvious thereby encouraging further investigation.

REFERENCES

1) M. Inokuti, "Atomic Processes Pertinent to Radiation Physics." in Electronic and Atomic Collisions, ed. by N. Oda and K. Takayanagi (North Holland Publishing Co., Amsterdam, 1980) pp. 31-45.

2) G. Kraft and W. Kraft-Weyrather, "Chromosome Aberrations Induced by Heavy Ions." Scientific Report (GSI-Darmstadt, FGR, 1986) ISSN 0174-0814, p. 220.

3) M.P.R. Waligorski, R.N. Hamm, and R. Katz, "The Radial Distribution of Dose Around the Path of a Heavy Ion in Liquid Water." Nucl. Tracks Radiat. Meas. 11, 309-319 (1986).

4) A. Chatterjee and H.J. Schäefer "Microscopic Structure of Heavy Ion Tracks in Tissue." Radiat. Environ. Biophys. 13, 215-227 (1976).

5) M. Zaider, D.J. Brenner, and W.E. Wilson, "The Application of Track Calculations to Radiobiology, I. Monte Carlo Simulation of Proton Tracks." Radiat. Res. 95, 231-247 (1983).

6) W.E. Wilson and H.G. Paretzke, "Calculation of Ionization Frequency Distributions in Small Sites." Radiat. Res 81, 326-335 (1980).

7) ICRU Report 16, "Linear Energy Transfer." (ICRU Publications, P.O. Box 4869, Washington, DC 20008); and references therein.

8) D.I. Thwaites, "Bragg's Rule of Stopping Power Activity: A Compilation and Summary of Results." Radiat. Res. 95, 495-518 (1983).

9) H. Bichsel and L.E. Porter, "Stopping Power of Protons and Alpha Particles in H_2, He, N_2, O_2, CH_4, and Air." Phys. Rev. A 25, 2499-2510 (1982).

10) L.E. Porter and D.I. Thwaites, "Physical State Effects of the Mean Excitation Energy of Water as Determined from Alpha Particle Stopping-Power Measurements." Phys. Rev. A 25, 3407-3410 (1982).

11) J.F. Ziegler, The Stopping and Range of Ions in Matter (Pergamon, New York, 1978).

12) W.Y. Baek, G.H. Both, D. Giessen, W. Neuwirth, and M. Zielinski, "Energy Loss of ^{12}C Projectiles in Different Carbon Modifications." Phys. Rev. A 35, 51-59 (1987).

13) C.F. Barnett, J.A. Ray, E. Picci, M.I. Wilker, E. W. McDaniel, E.W. Thomas, and H.G. Gilbody, "Atomic Data for Controlled Fusion Research." ORNL-5206, Vol. I (Oak Ridge National Laboratory, Oak Ridge, TN, 1977).

14) R.A. Phaneuf, R.K. Phaneuf, and M.S. Pindzola, "Atomic Data for Fusion." ORNL-609, Vol. V (Oak Ridge National Laboratory, Oak Ridge, TN, 1987).

15) K. Okuno, "Charge Changing Collisions for Heavy Particle Collisions in the Energy Range form 0.1 to 10 MeV." IPPJ-AM-9 (Nagoya University, Nagoya 1978).

16) Y. Nakai, A. Kikuchi, T. Sirai, and M. Sataka, "Data on Collisions of Helium Atoms and Ions with Atoms and Molecules (II)." JAERI-M, 84-069 (1984); and "Data on Collisions of Hydrogen Atoms and Ions with Atoms and Molecules (II)." JAERI-M, 83-143 (Japan Atomic Energy Energy Research Institute, Tokai-mura, 1983).

17) B. Franzke, "Charge State Distributions and Charge-Changing Cross Sections of Heavy Ions in the Energy Range up to 10 MeV/amu." Ann Israeli Phys. Soc. 4, 111-120 (1981).

18) W.G. Graham, K.H. Berkner, R.V. Pyle, A.S. Schlachter, D.W. Sterns, and J.A. Tanis, "Charge Transfer Cross Sections for Multiply Charged Ions Colliding with Gaseous Targets at Energies from 310 keV/amu to 8.5/amu." Phys. Rev. A 30, 722-728 (1984).

19) M.E. Rudd, Y-K. Kim, D.H. Madison, and J.W. Gallagher, "Electron Production in Proton Collisions: Total Cross Sections." Rev. Mod. Phys. 57, 965-994 (1985).

20) F.J. de Heer, J. Schutten, and H. Moustafa, "Ionization and Electron Capture Cross Sections for Protons Incident on Noble and Diatomic Gases between 10 and 140 keV." Physics 32, 1766-1792 (1966).

21) H. Tawara and T. Kato, "Total and Partial Cross Sections of Atoms and Ions by Electron Impact." At. Data Nucl. Data Tables 36, 167-353 (1987).

22) B.L. Schram, F.J. de Heer, N.J. Van Der Wiel, and J. Kistemaker, "Ionization Cross Sections for electrons (0.6 - 30 keV) in Noble and Diatomic Gases." Physica 31, 94-112 (1965).

23) A.S. Schlachter, K.H. Berkner, W.G. Graham, R.V. Pyle, P.J. Schneider, K.R. Staldter, J.W. Stearns, and J.A. Tanis, "Ionization of Rare-Gas Targets by Collisions of Fast Highly Charged Projectiles." Phys. Rev. A 23, 2331-2339 (1981).

24) C.B. Opal, E.C. Beaty, and W.K. Peterson, "Tables of Energy and Angular Distributions of Electron Ejected from Simple Gases by Electron Impact." JILA Report No. 108 (University of Colorado, Boulder, CO., 1971).

25) R.D. DuBois and M.E. Rudd, "Absolute Doubly Differential Cross Sections for Ejection of Secondary Electrons from Gases by Electron Impact. II. 100-500 eV Electrons on Neon, Argon, Molecular Hydrogen, and Molecular Nitrogen." Phys. Rev. A 17, 843-848 (1978).

26) M.E. Rudd and R.D. DuBois, "Absolute Doubly Differential Cross Sections for Ejection of Electrons from Gases by Electron Impact. I. 100- and 200-eV Electrons on Helium." Phys. Rev. A 16, 26-32 (1977).

27) M.A. Bolorizadeh and M.E. Rudd, "Angular and Energy Dependence of Cross Sections for Ejection of Electrons from Water Vapor. I. 50-2000-eV Electron Impact." Phys. Rev. A 33, 882-887 (1986).

28) N. Oda, F. Nishimura, and S. Tahira, "Energy and Angular Distributions of Secondary Electrons Resulting from Ionizing Collisions of Electrons with Helium and Krypton." J. Phys. Soc. Jpn. 33, 462-467 (1972).

29) M.E. Rudd, "Mechanisms of Electron Production in Ion-Atom Collisions." Radiat. Res. 64, 153-180 (1975).

30) N. Stolterfoht, "Excitation in Energetic Ion-Atom Collisions Accompanied by Electron Emission." in Topics in Current Physics, Structure and Collisions of Ions and Atoms, ed by I.A. Sellin (Springer-Verlag, New York, 1978) pp. 155-200.

31) L.H. Toburen, "Continuum Electron Emission in Heavy Ion-Atom Collisions in High-Energy Ion-Atom Collisions ed by D. Berényi and G. Hock (Elsevier Scientific Publishing Co., New York, 1982) pp. 53-82.

32) L.H. Toburen, W.E. Wilson, and R.J. Popowich, "Secondary Electron Emission from Ionization of Water Vapor by 0.3- to 2.0-MeV He^+ and He^{2+} Ions." Radiat. Res. 82, 27-44 (1980).

33) L.H. Toburen and W.E. Wilson, "Differential Cross Sections for Ionization of Argon by 0.3-2.0 MeV He^{2+} and He^+ Ions." Phys. Rev. A 19, 2214-2224 (1979).

34) M.A. Bolorizadeh and M.E. Rudd, "Angular and Energy Dependence of Cross Sections for Ejection of Electrons from Water Vapor. III. 20-150 keV Neutral Hydrogen Impact." Phys. Rev. A 33, 893-896 (1986).

35) L.H. Toburen, N. Stolterfoht, P. Ziem, and D. Schneider, "Electronic Screening in Heavy Ion-Atom Collisions." Phys. Rev. A 24, 1741-1745 (1981).

36) S.T. Manson and L.H. Toburen, "Energy and Angular Distributions of Electrons from Fast He^+ + He Collisions." Phys. Rev. Lett. 23, 529-531 (1981).

37) P.H. Woerlee, Yu. S. Gordeev, H. de Waard, and F.W. Saris, "The Production of Continuous Electron Spectra in Collisions of Heavy Ions and Atoms. B: Direct Coupling with the Continuum." J. Phys. B 14, 527-539 (1981).

38) G. Mahler, T. de Reus, J. Reinhardt, G. Soff, and U. Müller, "Delta Electron Emission in Super Heavy Quasi-atoms with $Z \geq 137$." Z. Phys. A 320, 355-358 (1985).

39) R.D. DuBois and L.H. Toburen, "Single and Double Ionization of Helium by Neutral to Fully Stripped Ion Impact." Phys. Rev. A, (in press).

40) R.D. DuBois, "Ionization and Charge Transfer in He^{2+} - Rare Gas Collisions. II." Phys. Rev. A 36, 2585-2592 (1987).

41) E.W. McDanial, M.R. Flannery, E.W. Thomas, H.W. Ellis, K.J. McCann, F.L. Eisele, W. Pope, S.T. Manson, J.W. Gallagher, J.R. Rumble, E.C. Beaty, and T.G. Roberts." Compilation of Data Relevant to Gas Lasers, Vol. I-VI, Technical Report H-78-1 (U.S. Army Missile Command, DRSMI-RPT, Redstone Arsenal, Alabama, 1979).

42) Reports IPPJ-AM-1 through IPPJ-AM-16. (Institute of Plasma Physics, Nagoya University, Nagoya, Japan.)

43) International Bulletin on Atomic and Molecular Data for Fusion, ed by J.J. Smith (IAEA, Vienna, 1988); see also CIAMDATA87, an Index to the Literature on Atomic and Molecular Collision Data Relevant to Fusion Research (IAEA, Vienna, 1987).

44) R.H. Schuler, A.B., Ross and W.P. Helmen, "Bibliographies of Radiation Chemistry: Introduction to the Series." Radiat. Phys. Chem. 17, 3-4, 1981; and J.A. LaVerne, R.H. Schuler, A.B. Ross and W.P. Helman "Bibliographies of Radiation Chemistry: Studies of the Heavy Particle Radiolysis of Liquids and Aqueous Solutions." Radiat. Phys. Chem. 17, 5-20 (1981).

45) M. Berman, R.D. Gilardi, N.S. Goel, V. Povard and G. R. Riegler Bibliography of Chemical Kinetics and Collision Processes, ed by A.R. Hochsteim (Plenum Data Corporation, New York, 1969).

ELECTRON COLLISION CROSS-SECTION MEASUREMENTS AND DATA FOR GAS PHASE MOLECULES (ATOMS) OF INTEREST TO RADIOTHERAPY*

S. TRAJMAR
Jet Propulsion Laboratory,
California Institute of Technology,
Pasadena, California,
United States of America

Abstract

Detailed analysis and understanding of the early stages of radiation interaction with matter require the knowledge of pertinent electron-molecule collision cross sections. In spite of half a century of activities in this field and a recent increase in demands and efforts to generate cross section data, our knowledge still can be characterized only as fragmentary. In this paper the status of electron-molecule (atom) collision cross section data of interest to radiotherapy is briefly summarized in the low and intermediate-energy regions (about threshold to hundred eV impact energies). The emphasis is on data obtained from measurements carried out under single-collision conditions and associated with elastic scattering, momentum transfer, excitation (rotational, vibrational, electronic), and dissociation into neutral and charged fragments. Differential, integral and total electron collision cross section measurements and theoretical results are discussed and a projection of trends and expectations for the near future is attempted. The recent developments both in experimental and theoretical methods are very encouraging. The optimum approach to the generation of the very large body of data required is a joint experimental-theoretical effort. (Theoretical methods are not yet completely reliable and need experimental verifications. On the other hand, experimental determination of a detailed and complete set of cross sections is a difficult and tedious job; it is overwhelming in general and practically impossible in some cases.)

I INTRODUCTION

Analysis and understanding of the early stages of radiation interaction with matter require the knowledge of pertinent electron-molecule (atom) collision cross sections. These collision processes represent the energy deposition into the matter and are precursors to a large variety of chemical reactions. A general discussion on the role of electron collision cross section data in radiation physics and chemistry was given e.g. by Inokuti[1,2] and Kaplan and Miterev[3]. Although the interaction of radiation with matter in the condensed phase is the major concern in radiotherapy, much can be learned from gas phase studies and the knowledge of gas phase electron collision cross section data is very important. In spite of half a century of activities in this field and recent increase of cross section measurement efforts, our knowledge can be characterized as only fragmentary.

In this article we will concern ourselves with electron impact excitation in gas phase at low and intermediate impact energies (from threshold to about 100eV). These electrons in radiation physics and chemistry are traditionally called slow electrons. Excitation here is meant in a broader sense and includes rotational, vibrational and electronic state excitations, elastic scattering as well as excitation to repulsive states resulting in disassociation both to neutral and charged fragments. Electrons at these energies are very effective in elastic scattering and in causing excitation of the nuclear motion and the valence shell electrons. Inner and intermediate shell excitations are negligible except for heavy elements. The present status of differential, integral, momentum transfer and total electron scattering cross section data of interest to radiotherapy, the techniques utilized to generate such data, and significant recent developments in this field will be summarized. The question of ionization and dissociative attachment has been treated here and elsewhere adequately by others[4,5,6].

At high impact energies electron collision cross sections can be obtained with good accuracy from perturbation theories and the consistency of data can be checked by the Bethe theory as discussed by Inokuti[2,7] and Kaplan and Miterev[3]. This is not the case, however, at low and intermediate impact energies where theoretical treatment of the scattering problem is difficult and the calculations at the present are in general unreliable. One must depend, therefore, to a great extent on experimental measurements.

II DEFINITION OF PERTINENT CROSS SECTIONS

The parameter which quantitatively characterizes a collision process is the cross section. Most of the cross section measurements carried out in recent years utilized a molecular beam/electron beam arrangement and yielded differential cross sections (DCS) defined as:

$$DCS(E_o,\theta,E) \equiv \overline{\sum_i \sum_f N_i \frac{d^2\sigma_{if}(E_o,\theta,E)}{d\Omega dE}} \qquad (1)$$

* Work supported in part by the National Aeronautics and Space Administration and in part by the National Science Foundation

Here E_o is the impact energy, θ is the scattering polar angle, E is the energy-loss, i and f refer to the initial and final state of the molecule, N_i is the population fraction in state i and Ω is the solid angle. The azimuthal angle dependence disappears since we are dealing with randomly oriented target molecules. The summation over final and averaging over initial, experimentally undistinguishable states is carried out and the bar above the right hand side of eq. (1) refers to the averaging made by the finite energy and angular resolution of the measuring apparatus.

We can integrate eqn. (1) over the energy-loss range associated with a given scattering process n and obtain:

$$DCS_n(E_o,\theta) = \overline{\sum_i \sum_f N_i \frac{d\sigma_{if}(E_o,\theta)}{d\Omega}} \tag{2}$$

Integration over all solid angles yields the integral cross section:

$$\sigma_n(E_o) = 2\pi \int_o^\pi DCS_n(E_o,\theta) sin\theta d\theta \tag{3}$$

For elastic scattering we also define the momentum transfer cross section:

$$\sigma^m(E_o) = \sigma_o(E_o) = 2\pi \int_o^\pi (1 - cos\theta) DCS_o(E_o,\theta) sin\theta d\theta \tag{4}$$

The total electron collision cross section is given as:

$$\sigma_{TOT}(E_o) = \sum_n \sigma_n(E_o) \tag{5}$$

The summation includes elastic and all inelastic processes.

Theoretical calculations yield the scattering amplitude which is related to the differential cross section as:

$$\frac{d\sigma_{if}(E_o,\theta)}{d\Omega} = \frac{k_f}{k_i} |f_{if}(E_o,\theta)|^2 \tag{6}$$

where k_i and k_f are the initial and final momenta of the scattered electron.

For experiments in which the scattered electron is detected in coincidence with other secondary particles (electrons, ions, photons), cross sections differential with respect to the energy and angle of these secondary species have to be correspondingly defined.

These cross sections are needed to calculate the linear energy transfer, stopping power or collision strength (all equivalent quantities).

III EXPERIMENTAL METHODS

Differential cross section measurements are carried out by crossing the target molecular beam (or static gas cell) with a nearly monoenergetic electron beam, usually at 90° as shown schematically in Fig. 1. The energy and angular distribution of the scattered electrons contain the information concerning the nature of the electron collision processes, the energy level scheme of the target, and the corresponding cross sections. Sometimes secondary particles are detected to extract information on a particular process or the scattered electrons are detected in coincidence with secondary particles to obtain more detailed information. One customary way to represent the scattering data is by the energy-loss spectrum as shown, as an example for He, in Fig. 2. The location of features characterizes the energy level scheme of the target and the scattering intensities are related to the corresponding DCS. An energy-loss spectrum is similar to a photo-absorption spectrum and indeed, it can be shown that at the limit of zero momentum transfer (high impact energy, small scattering angle) they become equivalent. In general, however, dipole selection rules do not apply to electron impact excitation. Spin and symmetry forbidden transitions readily occur in electron collisions at low impact energies and high scattering angles. The energy-loss spectra of molecules are complex because of vibrational-rotational structure and transitions associated with dissociating electronic states. The major difficulties in extracting DCS from energy-loss spectra are: 1) the decomposition of the heavily overlapping structure of molecular energy-loss spectra into contributions from individual processes, 2) the determination of precise scattering geometry and target

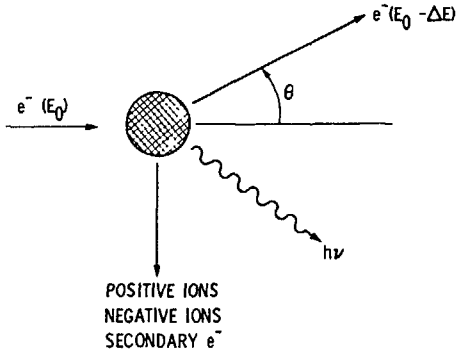

Figure 1. Schematic representation of electron scattering experiments.

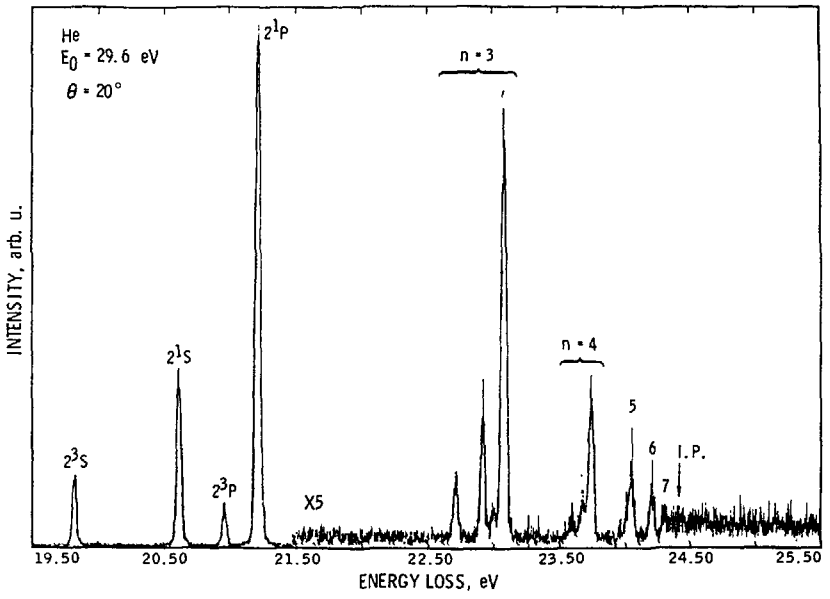

Figure 2. Energy-loss spectrum of He at 29.6eV impact energy and 20° scattering angle.

and electron beam fluxes or, equivalently, devising a calibration procedure for converting the measured scattering intensities to absolute DCS. This is not a simple task especially at low impact energies. The most practical method is to carry out relative scattering measurements for the test gas and for a standard gas under identical conditions and utilize the known DCS for the standard gas to normalize the relative DCS of the test gas. The standard gas is usually He for which the elastic DCS are well established. (For more details see Refs. 8 and 9.)

From the DCS one can obtain the integral cross sections or the momentum transfer cross sections. Integral cross section for excitation processes can also be obtained from measuring the photon emission subsequent to the electron impact excitation. The optical excitation functions obtained this way include cascade contributions and they represent emission rather than excitation cross sections. They can be converted, however, to excitation cross sections if cascade can be properly accounted for. In ionization measurements (including dissociative ionization and attachment) it is convenient to monitor the total ion yield and extract cross sections from these signals. Although dissociation processes leading to excited or ionic products have been extensively studied by monitoring photon emission or ion yields not much information is available on dissociation into neutral ground state fragments. This is mainly due to experimental difficulties of detecting low-energy neutral fragment species. There are very encouraging developments in this area, however. Dissociation in fast neutral beams results in fast neutral fragments which can be conveniently detected by charged particle detectors.

Total electron collisions cross sections have been measured with a few percent accuracy by different types of transmission-attenuation experiments. They are important in modeling energy deposition processes. In addition, because of their high accuracy, they can serve as checks on other cross sections through eqn. 5.

At very low electron impact energies beam techniques are difficult. Cross section information at these energies have been obtained by swarm techniques which can yield total electron scattering, and momentum transfer cross sections with high accuracy ($\sim 3\%$). Integral inelastic cross sections can also be deduced from swarm measurements but this procedure becomes ambiguous when more than a very few channels are open. Unfortunately, this is the situation with molecules at very low impact energies. The energy ranges of beam and swarm techniques now overlap and the two types of measurements not only yield complementary information but also serve to cross check each other. The relationship between the single collision beam studies and the multiple collision swarm measurements is discussed in Ref. 10.

IV CROSS SECTION DATA

A Elastic Scattering

With present electron scattering techniques molecular rotational excitation structure, in general, cannot be resolved. Therefore, published "elastic" cross sections usually represent elastic plus rotational excitation cross sections and should be more properly called vibrationally elastic cross sections. Some scattering measurements were carried out on H_2 with rotational resolution and attempts were made to unfold rotational structure from experimentally unresolved energy-loss spectra for a few simple molecules. (See below.) Both differential and integral elastic scattering cross sections have been obtained mainly from beam-beam type experiments.

Recent reviews on elastic cross section data have been published by Brandsen and McDowell[11], Trajmar et al.[12], Csanak et al.[13] and very recently on H and H_2 by King et al.[14] and McConkey et al.[15], respectively. Extensive coverage exist for He, Ne, Ar, Kr, Xe, H_2, N_2, O_2, CO, H_2O and CO_2. Fragmentary data are available for alkali and alkali earth metals, F, Cu, Zn,

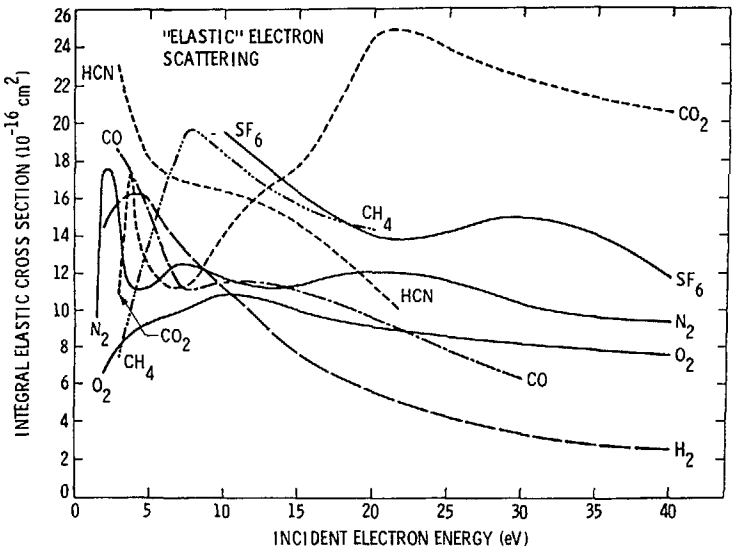

Figure 3. Integral elastic electron scattering cross sections for several molecules.

Cd, Hg, Tl, Pb, and Bi atoms and for NO, HF, HCl, HBr, F_2, LiF, KI, CsF, CsCl, H_2S, HCN, N_2O, SO_2, NH_3, As_4, SF_6, SiH_4, Si_2H_6 and for some hydrocarbon and halogenated hydro-carbon molecules. Very recently Weyherter et al.[16] reported differential elastic scattering cross sections for Ar, Kr and Xe in the 0.05 to 2.0eV impact energy range. (This work represents an extension of beam techniques to the until now inaccessible energy region.) Only theoretical data are available for the important *H, C, N* and *O atoms. Work is* presently in progress to determine elastics scattering cross sections for H[17] and O[17] . Integral elastic scattering cross sections are equivalent to total electron scattering cross sections at impact energies which are lower than the inelastic scattering threshold (or up to energies where inelastic processes can be neglected) and data obtained from various transmission and swarm measurements can be used as elastic data. Fig. 3 shows samples of integral vibrationally elastic cross sections and demonstrates the substantial variation both in magnitude and energy.

Integration of elastic DCS with the (1-cosθ) weighting factor (eqn. 4) or swarm measurements yield the momentum transfer cross sections. This quantity appears in the Boltzman equation describing the diffusion of electrons through an atomic and molecular gas. Compilation and summary of momentum transfer data have been published by Itakawa[18], Spencer and Phelps[19] and Hayashi[20]. In Fig. 4, examples for several atomic and molecular species are shown.

Effort to generate and recommend a set of consistent elastic and momentum transfer cross sections for various atomic and molecular species and recent results are reported by M. Hayashi in this volume.

B Rotational Excitation

Direct measurement of pure rotational excitation cross sections have been reported only for H_2. Unfolding of experimentally unresolved rotational structure were carried out for N_2, CO, HCl, H_2O, CO_2 and CH_4. At very low impact energies rotational excitation cross sections were obtained from swarm measurements.

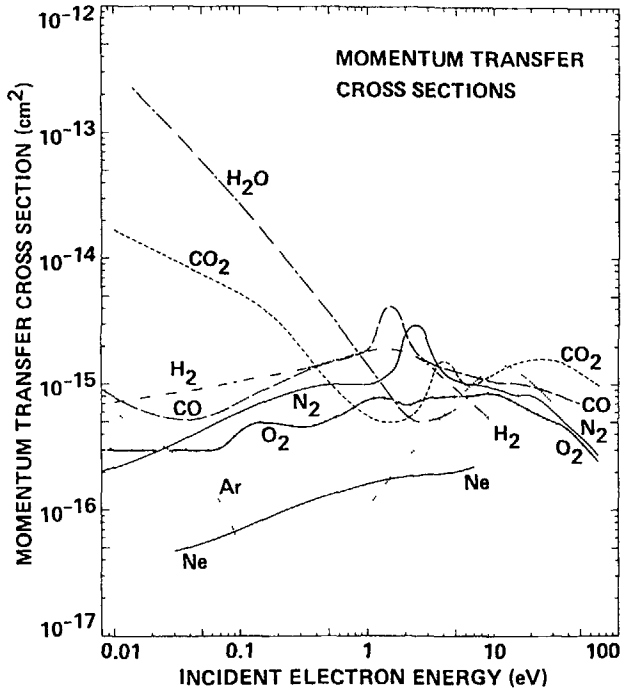

Figure 4. Momentum transfer cross sections for several atomic and molecular species.

For homonuclear diatomic molecules in a direct excitation process the excitation is due to the polarizibility or the electric quadrupole moment of the molecule and the $\Delta J = \pm 2$ (± 4) selection rule applies. Cross sections are of the order of $10^{-18}cm^2$ at impact energies greater than a few tenths of 1eV. Resonance excitation (temporary electron capture) mechanisms can greatly increase the cross section over limited impact energy ranges and values of about $10^{-16}cm^2$ are typical. At very low impact energies (below 0.1eV) the rotational excitation cross sections are about $10^{-16}cm^2$ and for large molecules at near threshold energies may be significantly larger. For molecules with strong dipole moment the $\Delta J = \pm 1$ excitation dominates over all other processes and cross sections can be as large as $10^{-13}cm^2$.

The available rotational excitation cross section data are summarized in Refs. 9, 12 and 13.

C Vibrational Excitation

Low-energy electron collisions are effective in exciting both optically allowed and forbidden molecular vibrations. Direct excitation processes are usually associated with cross sections of the order of $10^{-18}cm^2$ for fundamental modes and about a factor of ten smaller for overtone and combination bands. Again, resonance mechanisms can greatly increase the value of cross sections and influence the Δv selection rules. Rotational structure accompanying vibrational excitation, with the exception of H_2, cannot be resolved with present electron scattering techniques.

Vibrational excitation cross sections are available for H_2, N_2, O_2, CO, HF, HCl, HBr, H_2O, H_2S, CO_2, SO_2, COS, CH_4, C_2H_2, C_2H_4, C_2D_2, CCl_3F and CCl_2F_2. For a summary of these cross sections see Refs. 9, 12 and 21.

D Electronic State Excitation

Electron impact excitation of electronic states of the rare gases have been extensively studied. For the important atomic species H, C, N and O the situation is far from satisfactory. Some data are available for H[14] and O[22,23] but no measurements have been reported and only theoretical calculations are available for C and N. Fragmentary data exist for a number of metal atomic species.

Cross sections for excitation of stable electronic states of molecules are in general scarce. (Excitation of repulsive, dissociating electronic states will be discussed below and excitation into electronic states which are continuous in the electron coordinate, that is ionization, is not treated here.) Only N_2 and H_2 have been extensively studied and some data are available for CO, NO, O_2, SO_2 and CH_4. Especially little is known about the cross sections at low, near-threshold energies. The main reasons for this situation are: (a) difficulties to experimentally resolve or distinguish individual electronic excitations (due to overlapping vibrational-rotational structure); (b) resonances and the possibility of the breakdown of the Franck-Condon principle; (c) experimental difficulties associated with the handling and detection of low-energy electrons; (d) requirement of substantial time and resource investments for measurements on a large variety of processes over wide energy and angular ranges.

The above remarks refer to electron scattering measurements. A large body of data on excitation of electronic states is available in the form of optical excitation functions. In these measurements the photo emission induced by electron impact is measured and the emission cross section is deduced. To transform the electron impact induced emission cross sections into electron impact excitation cross sections, one has to take into account cascading effects. In some cases this has been done and the optical measurements can be very useful and complimentary to direct electron scattering measurements. For a recent discussion of this subject see Ref. 24. A critical review of this field is overdue.

Excitation of electronic states by resonance mechanism does not appear to play a significant role except at impact energies very close to threshold. The largest cross sections ($\sim 10^{-16}cm^2$) are associated with optically allowed processes at intermediate impact energies. The value of these cross sections increases gradually with impact energy from threshold to about ten times threshold energy and then slowly decreases at higher energies. The angular distributions are forward peaked and this character is more enhanced as the impact energy increases. At low impact energies optically (spin and/or symmetry) forbidden transitions dominate the electron-impact energy-loss spectra. These states can have long radiative lifetimes and be very effective in loosing their energy through various chemical reactions. Cross sections for spin forbidden transitions (which occur readily by electron impact via exchange process) peak near threshold and the DCS are nearly isotropic in angle. No simple general characteristics can be defined for symmetry forbidden transitions. These cross sections are usually small ($\sim 10^{-18}cm^2$) and show a large variety of angular behaviors. There is, however, one very unique character associated with $\Sigma^+ \longleftrightarrow \Sigma^-$ type of excitations. For these processes the DCS goes to zero at 0° and 180° scattering angles.

For a summary of cross section data see Refs. 12 and 21.

E Dissociation

Most of the investigations of molecular dissociation by electron impact in the past were concerned with dissociation into excited or positively charged

ion fragments which could be conveniently monitored by observing the decay radiation or utilizing charged particle detectors, respectively

Cross section studies for producing excited species concern mostly H, D and OH from various hydrogen containing molecules and in a few cases N, O and S from N_2, O_2, CS_2 and SO_2 These processes are not of major importance in radiotherapy A recent summary of the available data has been given by McConkey[24]

The information available on cross sections for electron impact dissociation of molecules to ions (both positive and negative) is mostly qualitative Measurements aimed to obtain these partial ionization cross sections can utilize the well developed charged particle detection techniques but require mass selection and the main source of problem and errors are associated with the extraction and quantitative detection of ionic species produced with a wide range of kinetic energies The positive ion fragments observed in these studies originate predominantly from dissociative ionization (e g $XY + e^- \longrightarrow X^+ + Y + 2e^-$) However, at higher impact energies (E_o greater than about 10eV) polar dissociation may also take place (e g $XY + e^- \longrightarrow X^+ + Y^- + e^-$) which results in both positive and negative fragments The production of negative ions by this mechanism differs distinctively from dissociative attachment (which is not treated here) The latter one is a resonance process and occurs only at low, well-defined electron energies while the former one is operational at higher energies but over a wider range Some absolute cross section data are available for positive and negative ion fragment production but most of the measurements carried out so far yielded only relative partial ionization data in the threshold to 200eV region A summary is given by Mark[25] Recently Srivastava and coworkers[26] developed a technique for detection of both positive and negative ion fragments generated by the interaction of a pulsed, magnetically collimated electron beam and a thermal molecular beam A pulsed extraction method allows them to detect all fragments irrespective of their kinetic energies The conversion of the measured ion signals to absolute partial ionization cross sections is achieved by applying the relative flow method and utilizing known ionization cross sections of a standard gas They have extended the electron impact energy range to 1000eV and measured total and partial ionization cross sections for Ne, Ar, Kr, Xe, H_2, D_2, N_2, O_2, CO, CO_2, SO_2, CH_4, NH_3, H_2O, CH_3OH, SiH_4 and Si_2H_6 so far[27] It was found that their results differ significantly in some cases from previously published data They attribute these discrepancies to inadequate extraction of energetic ions in previous works Only a very limited information and cross section data are available for polar dissociation processes The peak cross sections for these processes are about the same as those for dissociative attachment on ground state molecules ($\sim 10^{-19} cm^1$) but the values of these cross sections are significant from threshold to high impact energies similarly to the excitation of other electronic states of molecules A discussion on polar dissociation is given by Srivastava and Orient[28]

Measurements concerning electron impact dissociation of molecules into neutral fragments are very scarce because of the difficulty of detecting low-energy neutral species A method developed by Winters and coworkers[29] for the determination of total dissociation cross sections (which are dominated by dissociation into neutral fragments) relies on the 100% trapping of all dissociation products by appropriate getters and on the measurement of the pressure change This method was applied to N_2, CH_4, C_2H_6, CF_4, C_2F_6, CF_3H and C_3F_8 The peak cross section values were of the order of $10^{-16} cm^2$

An important new development in the area of dissociation to neutral fragments is represented by the application of fast beam techniques Such techniques were introduced in the 1960's and have been recently applied to molecular dissociation by electron impact by Cosby and Helm In this technique a position sensitive detector is used for the detection of the two correlated neutral fragments which are produced in the dissociation and have sufficient energy to allow the use of charged particle detectors[30] Preliminary results have been reported for O_2[31] and CO[31]

F Total Scattering Cross Sections

Total electron scattering cross sections obtained by various transmission/attenuation methods or from swarm experiments at very low energies are the most reliable cross sections They are available for a large number of molecules (and atoms), over a wide energy range and measurements carried out by various investigators by various methods usually agree within a few percent At low impact energies elastic scattering is the major contributor to the total cross section Rotational and vibrational excitations contribute significantly only in resonance regions At intermediate and high impact energies excitation of electronic states and ionization become dominant For summary of available data see Refs 12 and 21 which represent adequate coverage up to 1984 This field is still very active and several papers reported additional data in recent years

G Cross Section Data for Excited Species

Electron collision processes discussed here so far concern atomic and molecular targets in their ground state Under certain conditions electron collisions with excited (especially long lived metastable) states may be important Very few measurements have been reported in this area due mainly to experimental difficulties related to the production of these species in sufficient concentration (or flux) to make collision studies feasible Various discharge or electron beam excitation schemes have been utilized to generate metastable N_2, O_2 and rare gas species and some extremely fragmentary data exists for these metastables Lasers, in principle, could excite specific optically allowed states but, due to

the unavailability of lasers required for pumping vibrational and electronic states of most molecules, practically no important measurements have been reported as yet. Application of fast ion beam and charge exchange techniques show promise for progress in this area.

H H_2O

H_2O is a major constituent of biological systems and its interactions with electrons play a pivotal role in radiotherapy. We, therefore, specifically summarize the low- and intermediate-energy electron impact excitation (including elastic scattering, dissociation and total electron scattering) cross section data for H_2O.

In Table I the pertinent measurements and corresponding references are listed.

The numerical values can be found in the reviews of Trajmar et al.[12], Csanak et al.[13] and Trajmar and Cartwright[21]. Table I brings these reviews up to date and supplies references for recent works. For further discussion of swarm and electron beam data and for reports on H_2O cross section data in Radiation Physics and Chemistry, see also Ref 1b, p. 12, 136, and 152 and Ref. 10b, p. 178. Recent summaries of theoretical calculations and comparisons with experiments are given by Gianturco and Jain[51], Jain[52] and Brescansin et al.[53].

Cross sections for H_2O have been collected and expressed in the form of semi-analytical functions suitable for electron deposition calculations by Olvero[54].

V IMPORTANT RECENT DEVELOPMENTS

Due to a great deal of demand for electron collision cross section data in a large variety of fields (including ionospheric physics, discharge and electron-beam excited lasers, fusion plasmas, discharge processing of microelectronic components etc.) activities aimed specifically at the generation of reliable and extensive sets of collision data have been considerably increased in recent years. These activities lead to improved and novel techniques and to new approaches.

In general most cross section data have been available at intermediate and high impact energies and at very low energies from swarm experiments. Experimental difficulties associated with low-energy measurements (space charge effects, sensitivity of electron beam to small electric and magnetic fields and surface changes, large variation of detector response function to electron resid-

Table I. Summary of cross section data for H_2O.

	Type	Energy Range (eV)	Angular Range (deg)	Reference
Elastic	DCS	500 - 516	4 - 77.5	32
	DCS	500	4 - 30	33
	DCS (rot.res)[a]	2.14 - 6.0	30 - 105	34
	DCS, σ, σ^m	4 - 200	10 - 120	35
	DCS, σ, σ^m	100 - 1000	10 - 130	36
	DCS, σ, σ^m	2.2 - 20.0	15 - 150	37
Rotational				
	DCS	2.14 - 6.0	15 - 105	34
Vibrational	DCS (relative)[b]	15 - 53	20 - 110	39
	DCS, σ	Threshold - 10	20 - 110	40
	DCS	Threshold - 3.0	120	41
	DCS, σ	2.2 - 20	30 - 150	42
Electronic	GOS[c]	300, 400, 500	-	43
	GOS[c]	300, 400, 500, 600	-	44
Total	σ_T	2.2 - 38	-	45
	σ_T	0 - 10	-	46
	σ_T	1 - 400	-	47
	σ_T	0.5 - 80	-	48a and c
	σ_T	0.5 - 3000	-	48b
	σ_T	81 - 3000	-	49
	σ_T(also D_2O)	15.3 500	-	50

[a] Rotational structure resolved

[b] Relative to elastic

[c] Generalized Oscillator Strength

ual energy, breakdown of the Franck-Condon Principle, resonance effects, etc.) have been overcome only in recent years. Important progress was made in extending beam scattering techniques to very low impact energies[16] and near threshold energies for electronic state excitations[55].

Very significant is the revival and application of fast beam techniques to electron impact dissociation of molecules to neutral fragments[30,32] and to the study of collisions involving free radicals and metastable species[56]. In the area of dissociative ionization, the introduction of pulsed electron beam and extraction and the application of time of flight analysis[26] represent important progress.

Significant progress was also made in the theoretical arena and joint experimental/theoretical approach to produce reliable sets of cross sections proved especially effective This matter will be elaborated further in Chapter VI

Attempts to generate sets of consistent cross section data from swarm and beam measurements and from theoretical calculations, by subjecting them to consistency checks or by using the Boltzman equation and measured transport coefficients, are very important and should be pursued Such efforts have been carried out by A V Phelps and coworkers[57] in the USA and by M Hayashi in Japan[20,58]

Modern, beam scattering techniques developed for the gas phase studies have been recently applied to condensed state targets by the University of Sherbrooke group in Canada[59] Energy loss spectra obtained from condensed state deviates substantially from those of the gas phase Besides scattering by individual sites new sacttering channels associated with intermolecular and collective modes, coherent and incoherent multiple scattering and transitions forbidden in gas phase may appear In addition the scattering by individual sites is modified with respect to gas phase due to the influence of the environment The degree of change depends on the nature of the process, e g valence shell election excitation processes are severely modified while inner shell election excitations are not significantly influenced In spite of these complications cross sections for individual channels can be extracted The Canadian group obtained such cross sections for solid H_2O in the 1 to 18 eV impact energy range They also observed resonances in solid N_2, CO, O_2 and H_2O and dissociative attachment in solid O_2

VI COMPARISON OF EXPERIMENTAL AND THEORETICAL RESULTS

Scattering calculations cannot be carried out without certain approximations and simplifications The practical modus operandi is, therefore, to introduce approximations which contain the essence of the physics of the collision process but simplify the mathematics as much as possible The results of the calculations are checked against experiments and if good agreement is found for certain types of processes under certain conditions, then cross sections over a range of impact energies and scattering angles can be obtained conveniently from these calculations

As mentioned above at high impact energies perturbation approaches yield good results At very low impact energies, where only a limited number of scattering channels are open, close coupling methods are reliable From the theoretical point of view the intermediate energy range is the most difficult (while from experimental points of view it is the easiest)

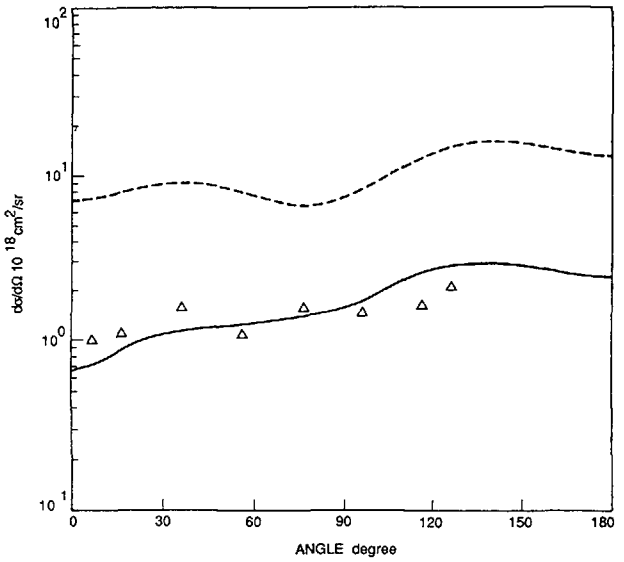

Figure 5 Differential cross sections for the $X^1\Sigma_g^+ \rightarrow W^3\Delta_u$ excitation of N_2 at 15eV impact energy Dashed line two channel calculation, solid line five channel calculation (both from Huo and McKoy, Ref 61), triangles experimental data (from Zetner and Trajmar, Ref 62)

Theoretical treatment of the elastic scattering, rotational and vibrational excitation at low impact energies can be done with satisfactory accuracy for most modeling purposes For detailed discussion on these matters see Refs 13 and 21 There are, however, unresolved discrepancies between experiment and theory even for simple molecules like H_2[15,60]

Methods to treat electronic state excitation of molecules have appeared in large numbers in recent years and substantial progress has been achieved The situation up to 1984 is summarized in ref 21 A more recent review is given by Collins and Schneider[61]

The earliest calculations on electronic state excitations involved the Born or Born Ochkur Rudge approximations Comparison of these results with experiments indicated large discrepancies (see e g Fig 14 in Ref 21) The introduction of the distorted wave approach yielded distinct improvements but serious disagreements in some cases with experiments still existed especially for forbidden transitions In recent years the situation dramatically improved by the application of close coupling methods As an example the differential cross section for the excitation of the $W^3\Delta_u$ state of N_2 at 15eV impact energy is shown in Fig 5 Calculation with two channels[62] (dashed curve) yields

DCS which are about an order of magnitude larger than experimental data[63] (rectangles) Inclusion of five channels in the scattering calculation[62] (solid line) yields excellent agreement with the experimental data This figure also demonstrates the need and usefulness of coordinated experimental/theoretical approach

VII CONCLUSIONS AND SUMMARY

A very large body of cross section data is needed to properly model and understand the interaction of radiation with matter Experimental determinations of these cross sections is a difficult and tedious job and in certain cases impossible with presently available techniques The alternative approach of a priori calculation of these cross sections has not proved very successful in general It is easy to understand then why our knowledge concerning these cross sections has been rather meager Recent developments in both experimental and theoretical areas, and especially coordinated, joint experimental/theoretical approaches give us much optimism, however Iterative checks between calculations and experiments, utilization of measurements as checks and large scale computations to supply the bulk of the data seems to be a very promising and efficient way to supply the needed data

REFERENCES

[1] (a) M Inokuti, "Radiation Physics as a Basis of Radiation Chemistry and Biology", *Applied Atomic Collision Physics*, Vol 4 Condensed Phases, ed S Datz, Academic Press, New York, 1983 pp 179 236, (b) Proceedings of the Workshop on Electronic and Ionic Collision Cross Sections Needed in Modeling of Radiation Interaction with Matter, Argonne National Laboratory, Dec 6-8, 1983, ed M Inokuti, Argonne National Laboratory Report ANL 84-28

[2] M Inokuti, "Cross Sections for Inelastic Collisions of Fast Charged Particles with Atoms and Molecules" in *Nuclear and Atomic Data for Radiotherapy and Related Radiobiology*, International Atomic Energy Agency, Vienna, 1987 pp 357 65

[3] I G Kaplan and A M Miterev, "Interaction of Charged Particles with Molecular Medium and Track Effects in Radiation Chemistry" in *Advances in Chemical Physics*, eds I Prigogine and S A Rice, Vol LXVIII, John Wiley and Sons, New York, 1987 pp 255 386

[4] *Electron Impact Ionization*, eds T D Mark and G H Dunn, Springer-Verlag, Wien, 1985 and chapter in this volume by Mark

[5] *Electron-Molecule Interactions and Their Applications*, ed L G Christophorou, Academic Press, Inc , Orlando, 1984 Vol I and II

[6] S K Srivastava, "Present Status of the Measured Dissociative Attachment Cross Section", in *Production and Neutralization of Negative Ions and Beams*, (Fourth Int Symposium, Brookhaven, 1986), ed J Alessi, Am Inst of Physics, 1987 pp 69-79

[7] M Inokuti, *Rev Mod Phys 43*, 297 (1971)

[8] S Trajmar and D F Register, "Experimental Techniques for Cross Section Measurements" in *Electron Molecule Collisions*, eds K Takayanagi and I Shimamura, Plenum Press, New York, 1984 Chapter VI

[9] H Ehrhardt, K Jung, G Knoth and M Radle, "Rotational and Vibrational Excitation of Molecules by Low Energy Electrons Through Direct and Resonance Interactions" in *Atomic and Molecular Physics*, eds D K Rai and D N Tripathi, World Scientific, Singapore, 1987

[10] (a) A Chutjian, B V McKoy, L C Pitchford and S Trajmar, *Comments At Mol Phys 21*, 43 69 (1987), (b) *Swarm Studies and Electron-Molecule Collisions*, eds L C Pitchford, B V McKoy, A Chutjian and S Trajmar, Springer Verlag, New York, 1987

[11] B H Brandsen and M R C McDowell, "Electron Scattering by Atoms at Intermediate Energies II Theoretical and Experimental Data for Light Atoms", *Physics Reports 46*, 249 394 (1978)

[12] S Trajmar, D F Register and A Chutjian, "Electron Scattering by Molecules II Experimental Methods and Data", *Physics Reports 97*, 219-356 (1983)

[13] G Csanak, D C Cartwright, S K Srivastava and S Trajmar, "Elastic Scattering of Electrons by Molecules", Chapter I in *Electron- Molecule Interactions and Their Applications*, Vol I, ed L G Christophorou, Academic Press, 1984

[14] G C King, S Trajmar and J W McConkey, "Electron Impact on Atomic Hydrogen–Recent Results and New Directions" (submitted to Comments on Atomic and Molecular Physics, 1988)

[15] J W McConkey, S Trajmar and G C King, "Electron Impact Excitation of Molecular Hydrogen–What We Do and Do Not Know" (submitted to Comments on Atomic and Molecular Physics, 1988)

[16] M Weyhreter, B Barzik, A Mann and F Linder, *Z Phys D 1*, 333 (1988)

[17] (a) T W Shyn, University of Michigan (private communication, 1988) (b) J F Williams, University of Western Australia (private communication, 1988)

[18] Y Itikawa "Momentum Transfer Cross Sections for Electron Collisions on Atoms and Molecules and Their Application to Effective Collision Frequencies", Argonne National Laboratory Report, ANL-7939, April, 1972

[19] F E Spencer, Jr and A V Phelps, Proc 15th Symp of Engineering Aspects of Magnetohydrodynamics, University of Pennsylvania, Philadelphia, May, 1976 and private communication

[20] M Hayashi, "Recommended Values of Transport Cross Sections for Elastic Collision and Total Collision Cross Section for Electrons in Atomic and Molecular Gases", Report IPPJ-AM 19, Institute of Plasma Physics, Nagoya University, Japan, Nov 1981

[21] S Trajmar and D C Cartwright, "Excitation of Molecules by Electron Impact", Chapter 2 in *Electron Molecule Interactions and Their Applications Vol I*, ed L G Christophorou, Academic Press, 1984

[22] J P Doering and coworkers, *J Geophys Res 90*, 5279 (1985), ibid *91*, 775 and 3279 (1986), ibid *92*, 3445 and 7749 (1987), ibid to appear (1988)

[23] T W Shyn and coworkers, Geophys Res Lett 12, 171 (1985), *J Geophys Res 91*, 1691 (1986), ibid to appear (1988)

[24] J W McConkey, "Optical Excitation Cross Sections for Electron Collisions with Atoms and Molecules", in Ref 1b, pp 129-41

[25] T D Mark, "Partial Ionization Cross Sections", Chapter 5 in Ref 4

[26] E Krishnakumar and S K Srivastava, *J Phy B 21*, 1055 (1988)

[27] S K Srivastava (private communication, to be published, 1988)

[28] S K Srivastava and O J Orient, "Polar Dissociation as a Source of Negative Ions" in 3rd International Symposium–Production and Neutralization of Negative Ion Beams ed Krsto Prelec, Am Inst of Phys 1983, pp 56 66

[29] H F Winters, "Total Dissociation Cross Sections of Fluoroalkanes for Electron Impact Their Usefulness for Understanding Plasma Assisted Etching Environments" in Ref 10b, pp 347-50

[30] H Helm and P C Cosby, *J Chem Phys 86*, 6813 (1987)

[31] (a) P C Cosby and H Helm, a, 40th Gaseous Electronics Conference, Oct 13 16, 1987, Atlanta, Abstract CA-5 (b) *Bull Am Phys Soc 33*, 940 (1988), Abstract BX61

[32] E N Lassettre and E R White, *J Chem Phys 60*, 2460 (1974)

[33] J P Bromberg, unpublished, from Ref 32

[34] K Jung, T Antoni, R Mueller, K H Kochem and H Ehrhardt, *J Phys B 15*, 3535 (1982)

[35] A Danjo and H Nishimura, *J Phys Soc Japan 54*, 1224 (1985)

[36] A Katase, K Ishibashi, Y Matsumoto, T Sakae, S Maezono, E Murakami, K Watanabe and M Hideaki, *J Phys B 19*, 2715 (1986)

[37] T W Shyn and S Y Cho, *Phys Rev A36*, 5138 (1987)

[38] (Has been deleted)

[39] S Trajmar, W Williams and A Kuppermann, *J Chem Phys 58*, 2521 (1973)

[40] G Seng and F Linder, *J Phys B 9*, 2539 (1976)

[41] K Rohr, *J Phys B 10*, L735 (1977)

[42] T W Shyn, S Y Cho and T E Cravens, *Phys Rev A* (to appear, 1988)

[43] E N Lassettre and A Skerbele, *J Chem Phys 60*, 2464 (1974)

[44] K N Klump and E N Lassettre, *Can J Phys 53*, 1825 (1975)

[45] E Bruche, *Ann Phys* (Leipzig) *1*, 93 (1929)

[46] V F Sokolov and Yu A Sokolova, *Sov Tech Phys Lett , 1*, 268 (1981)

[47] O Sueoka, S Mori and Y Katayama, *J Phys B 19*, L373 (1986)

[48] (a) C Szmytkowski, Abstracts of Contributed Papers, XVth Int Conf on the Physics of Electronic and Atomic Collisions, eds J Geddes, H B Gilbody, A E Kingston, C J Latimer and H J R Walters, ICPEAC, Brighton, England, 1987 p 269, (b) C Szmitkowski, A Zecca, G Karwasz, S Oss, K Maciag, B Mariukovic, R Brusa and R Grisenti, ibid p 270, (c) C Szmitkowski, *Chem Phys Lett 136*, 363 (1987)

[49] A Zecca, G Karwasz, S Oss, R Grisenti and R S Brusa, *J Phys B 20*, L133 (1987)

[50] H Nishimura and K Yano, *J Phys Soc Japan* (to appear, 1988) and private communication

[51] F A Gianturco and A Jain, *Phys Rep 143*, 347 (1986)

[52] A Jain, *J Phys B 21*, 905 (1988)

[53] L M Brescansin, M A P Lima, T L Gibson, V McKoy and W M Huo, *J Chem Phys 85*, 1854 (1986)

[54] J J Olvero, *J Geophys Res 77*, 4797 (1972)

[55] P W Zetner and S Trajmar, XVth Int Conf on the Physics of Electronic and Atomic Collisions, July 22-28, 1987, Brighton, England, Book of Abstracts, eds J Geddes, H B Gilbody, A E Kingston, C J Latimer and H J R Walters, p 307, and J C Nickel, P W Zetner, G Shen and S Trajmar (to be published, 1988)

[56] R C Wetzel, F A Baiocchi, T R Hayes and R S Freund, *Phys Rev A 35*, 559 (1987), T R Hayes, R C Wetzel and R S Freund, ibid A 35, 578 (1987), and H R Hayes, R C Wetzel, F A Baiocchi and R S Freund, *J Chem Phys 88*, 823 (1988)

[57] (a) A V Phelps, "Relations Between Electron-Molecule Scattering and Swarm Experiments and Analysis", in Ref 10b, pp 127 41, (b) A V Phelps and L C Pitchford, *Phys Rev A31*, 2932 (1985), (c) JILA Information Center Reports, No 26 (May 1, 1985), No 27 (May 1, 1985) and No 28 (September 1, 1985)

[58] M Hayashi, "Electron Collision Cross Sections for Molecules Determined from Beam and Swarm Data" in Ref 10b, pp 167-87 and in present volume

[59] See e g , R Azria, L Parenteau and L Sanche, *Phys Rev Lett 59*, 638, (1987), M Michand and L Sanche, ibid *59*, 645 (1987), M Michand and L Sanche, *Phys Rev A, 36*, 4672 and 4684 (1987) and references therein

[60] M A Morrison, R W Crompton, B C Saha and Z L Petrovic, *Australian J Phys 40*, 239 (1987)

[61] L A Collins and B I Schneider, "Recent Advances in the Theory of Electron Impact Excitation of Molecules", in *Electronic and Atomic Collisions*, eds H B Gilbody, W R Newell, F H Read, and A C H Smith, Elsevier Science Publishers B V , 1988, pp 57 72

[62] W M Huo and V McKoy (private communication, 1988)

[63] P Zetner and S Trajmar (to be published)

TOTAL AND PARTIAL ELECTRON IMPACT IONIZATION AND ATTACHMENT CROSS-SECTIONS OF ATOMS, MOLECULES AND CLUSTERS (QUASI-LIQUIDS): A REVIEW OF EXPERIMENTAL AND THEORETICAL METHODS AND DATA FOR RADIOTHERAPY

T.D MARK
Institut fur Ionenphysik,
Universitat Innsbruck,
Innsbruck, Austria

Abstract

Today's knowledge of accurate absolute ionization cross sections pertaining to radiotherapy originate mostly from rather recent studies. This review first summarizes recent developments of the principal experimental, semiclassical and semiempirical methods used for the absolute ionization cross section determinations. Moreover, a critical review will be given of the available experimental data for radiotherapy (partial and total electron impact ionization cross section functions). Finally, this review is particularly dedicated to the discussion of recent studies of the inelastic interaction of slow and fast electrons in quasiliquids and/or in quasisolids (i.e. electron attachment to and electron ionization in van der Waals clusters consisting of rare gases, N_2, O_2, H_2O, etc.).

1 INTRODUCTION

Many areas of science require accurate values of electron impact ionization and/or attachment cross sections as a function of energy, $\sigma(E)$. These areas include for instance electrical discharges, gas lasers, quantitative mass spectrometry and radiotherapy /1/.

Despite numerous studies in the last 75 years about these basic atomic processes, quantitative knowledge in terms of absolute cross sections has been far from satisfying /2/. In particular, the measurements and/or calculations of partial ionization cross sections for the production of a specific ion or ion species are not yet as detailed, accurate and manifold as could be wished. Nevertheless, there has been recently considerable progress in this field, experimentally as well as theoretically, e.g., (i) development of the penetrating extraction field method in conjunction with an integrated deflection mass spectrometry for both atomic and molecular gas targets /3/, (ii) the fast neutral beam method which has proven to be most useful for measurements of highly reactive and metastable species /4/, or (iii) development of new semiclassical and/or semiempirical formulae for the accurate prediction of atomic /5/ and molecular /6/ ionization cross sections.

This paper begins by describing the principal experimental (Chapter 2), semiclassical and semiempirical (Chapter 3) methods used for the absolute ionization cross section determinations. It continues with a critical review of the available experimental data /2-4, 7-13/ (Chapter 4).

Finally, in the field of atomic data for radiotherapy and related radiobiology not only gas phase atomic or molecular data are of interest. On the contrary, since e.g. water is a major component of cells, there is strong need on condensed phase data. With the recent advent of electron-cluster interaction studies a new powerful method has been introduced to study qualitatively and quantitatively the inelastic interaction of slow and fast electrons in quasi-liquids and/or quasi-solids /14/. Particularly promising and exciting new results on this topic are, e.g., zero electron energy resonances in attachment cross sections /15/, sequential single electron ionization leading to large cross sections for multiple ionization /16/, Coulomb explosion of multiply charged condensed van der Waals molecules /17/, sequential decay series of metastable cluster ions /18/ and Raman induced dissociation of neutral van der Waals clusters in the visible /19/. Some of these results pertaining to the field of radiobiology will be presented in this review (Chapter 5).

2 EXPERIMENTAL METHODS

2 1 Definitions

Because of ambiguities in the nomenclature some definitions are in order to introduce the present subject: Consider a parallel, homogeneous and monoenergetic beam of electrons crossing a semi-infinite medium with N_t (cm^{-3}) target particles at rest. If $n_e(0)$ represents the initial electron beam flux ($cm^{-2}s^{-1}$), the beam flux $n_e(x)$ at the penetration depth x is given by the exponential absorption law (Beer's law)

$$n_e(x) = n_e(0) \exp(-N_t \cdot \sigma \cdot x) \qquad (1)$$

with σ a constant with a dimension of cm^2, termed cross section. Assuming single collision conditions (i.e., $N_t \cdot \sigma \cdot x << 1$), the number of ions produced per second along a collision interaction path x = L (i.e. over which the ions are collected and analyzed) is

$$n_i(L) = n_e(0) \cdot N_t \cdot \sigma_c \cdot L \qquad (2)$$

with σ_c the counting ionization cross section (usually not directly accessible by experiment /20/). The total positive ion current i_t produced along this interaction volume is

$$i_t = n_e(0) \cdot e \cdot N_t \cdot \sigma_t \cdot L \qquad (3)$$

with e elementary charge and σ_t total ionization cross section. If the produced ions are analyzed with respect to their mass m and charge z.e, the respective individual ion current is

$$i_{zi} = n_e(0) \cdot z \cdot e \cdot N_t \cdot \sigma_{zi} \cdot L \qquad (4)$$

with σ_{zi} partial ionization cross section for the production of a specific ion or ion species i with charge ze. In order to treat the production of individual ions by electron impact, this partial cross section must be known quantitatively as a function of electron energy (termed cross section function). It is useful to note that the total and the counting cross sections are directly related to the partial cross sections via the weighted and simple sum, respectively

$$\sigma_t = \sum_i (\sigma_{zi} \cdot z), \text{ and } \sigma_c = \sum_i \sigma_{zi} \qquad (5)$$

2.2. Total ionization sections

One of the earliest and widliest used experimental methods to determine total ionization cross sections is the condenser plate method of Tate and Smith /21/. This is the method which has been later used very successfully by Rapp and Englander-Golden /22/ to produce their benchmark total ionization cross section functions for the rare gases and several small molecules. In short, in this method a magnetically collimated electron beam is directed through a target gas of known density. All ions which are produced in a well defined region are completely removed and collected. The main limitation of this method is the absolute measurement of the gas density, a difficult matter for many gases. De Heer and Inokuti /23/, in their definitive 1985 review of total electron impact ionization cross sections, discussed and summarized experiments and results up to this year (see also Ref /9/). Moreover, Djuric et al. /24,25/ have recently overcome some of the difficulties by using a capacitance manometer to determine the gas pressure of H_2O, CH_3OH and C_2H_5OH in their parallel plate ionization chamber /26/.

2.3. Partial ionization cross sections

The first mass spectrometric determination of partial cross section functions have been made in the 30's. Some of these studies we repeated later on, however, up to recently /2-4,7-11,27/ large differences existed in both, magnitude and shape, of partial ionization cross section functions. As pointed out by many workers this was due to large discrimination effects occurring at the ion source exit and mass spectrometer slits (discussed in more detail below). Moreover, a common problem (never solved satisfactorily) is the absolute calibration. Closely related to this is the fact that discrimination may occur at the ion detector. There exist, however, some recent experimental studies using new and sophisticated approaches in order to overcome those difficulties. Some of these new studies come very close to meet the main condition for measuring accurate functions, i.e. a constant and/or complete ion source-mass spectrometer collection efficiency (i) independent of the mass to charge ratio of the ion under study, (ii) independent of the incident electron energy and (iii) independent of the initial kinetic ion energy.

These studies are:

(1) Improved crossed beam investigations /28-33/
(2) Crossed fast (after charge transfer neutralization) atom beam techniques /34-44/
(3) Improved metastable ion detection /45-48/
(4) Trapped ion mass spectrometry /49/
(5) Improved extraction and transmission techniques, including the use of cycloidal mass spectrometry /50-56/, large acceptance sector field spectrometer /57/, field free diffusive extraction /58,59/, and penetrating-field extraction and deflection method /8,60-71/.

The last of these methods, recently developed in our laboratory to be used with Nier type ion sources and sector field spectrometer systems (e.g. see Fig. 1), will be discussed as one example in detail in the following paragraph, because of the widespread use of this instrumentation in mass spectrometry laboratories:

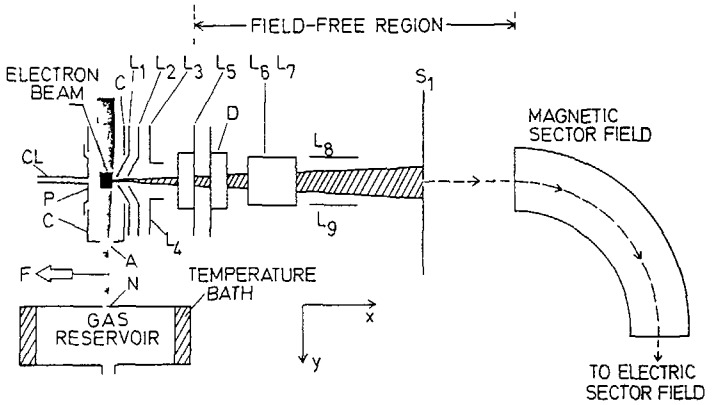

Fig. 1. Schematic view of electron impact-mass spectrometer apparatus after Mark /7-11/. P, pusher; C, collision chamber; CL, capillary-leak gas inlet; A, aperture; N, nozzle for molecular-beam gas inlet; L_1, collision-chamber exit-slit electrodes (L_1, P, and C are at a common source potential of typically +3 kV); L_2, penetrating-field extraction electrodes; L_3 and L_4, beam-focussing electrodes; L_5, earth slit (end of accelerating region); D, defining slit; L_6, L_7, L_8, and L_9, beam-centering and deflection electrodes; S_1 mass-spectrometer entrance slit.

The extraction of ions from the ionization region in a Nier /72/ type ion source depends under usual experimental conditions on various parameters, i.e. the initial energy of the ions, the mass to charge ratio, the guiding magnetic field, the electron beam space charge and the applied extraction field. Usually, ions are extracted from the ionization region (in which there is a crossed electric and magnetic field) by a weak electric field applied between the collision chamber exit slit and an electrode opposite to the exit slit (i.e., pusher). This extraction, however, is not complete and results in discrimination for ions with different m/z (e.g. see discussions in Ref. /2,3,7,8,27/. In an alternative approach a penetrating field from external electrodes may be used, i.e. all electrodes confining the collision chamber are kept at the same potential (e.g. ion acceleration voltage of 3 kV), and ions (produced by crossing an effusive neutral beam /73/) are drawn out of the collision chamber through the ion source exit slit under the action of an electric field applied to the external electrodes (Fig.1). It has been shown that this penetrating field extraction assures saturation of the ion current, i.e. complete ion collection is achieved for parent ions /60/. Ions extracted in this manner are then centered by various elements, pass a defining aperture and reach the end of the acceleration region at the so called earth slit (Fig. 1). Stephan et al. /60/ additionally introduced in front of the mass spectrometer entrance slit 2 pairs of deflection plates (Fig.1), which serve to sweep the ion beam across the mass spectrometer entrance slit S_1 in the y direction (perpendicular to S_1) and z direction (parallel to S_1). This allows the recording and/or integration of the ion beam profile, and hence discrimination at S_1 can be avoided. It is of special interest to note that this technique has been recently improved to allow the quantitative detection of fragment ions and thus the determination of all partial ionization cross section functions of a molecule under study. Accurate cross sections are now available for CF_4, CCl_4 and CF_2Cl_2 /67,68,71/.

Excellent data on partial ionization cross sections have been recently obtained by Freund and coworkers /4,38,41-44/ using a method where an electron beam is crossed with a fast neutral beam prepared by charge transfer neutralization of a mass selected ion beam. This approach was first used for atomic ionization cross-section measurements by Peterson et al. /34/; it has since been used by Ziegler et al. /39/ and has been refined by Harrison and coworkers /35,36,40/. Extensions by Freund and coworkers have made it a powerful method for studying molecular and dissociative ionization /4/. The biggest advantage of this method is that it permits preparation of a pure beam, even of such elusive species as metal atoms, metastables, and free radicals. The high velocity (typically 1 to 5 keV) permits accurate neutral flux measurements. The high collimation of the focused ion beam is

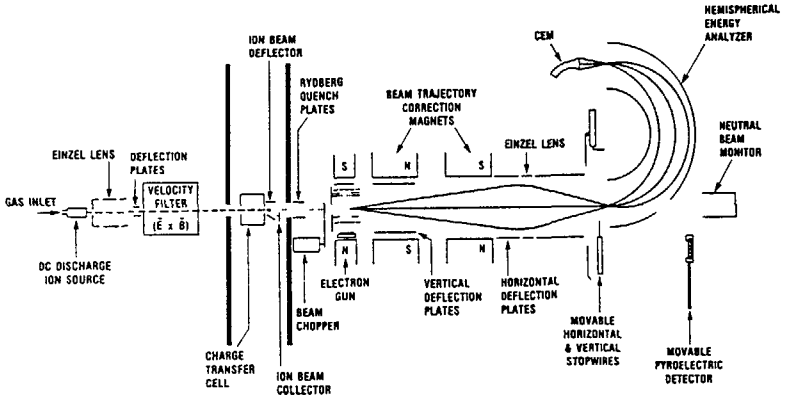

Fig. 2. The fast beam apparatus at AT&T Bell Labs after Freund /4/.

preserved in the charge transfer process, permitting complete collection of ions, even fragment ions from molecular dissociations. A difficulty with the method is that charge transfer can produce neutral atoms or molecules in various excited states.

In the fast neutral beam apparatus of Freund et al. (Fig. 2), atomic or molecular ions are (i) extracted from a dc discharge, (ii) accelerated to 3 kV, and (iii) mass separated with a Wien filter. The ion beam is then neutralized by charge transfer with a gas selected to have an ionization potential energy resonant with that of the ions. The pressure is adjusted to neutralize several percent of the ions, with the remainder being deflected to a collector.

According to Freund /4/ the resulting neutral beam in general has a flux of 10^{10} s. Its relative intensity is measured by kinetic secondary electron ejection from a metal surface. For accurate flux measurements, a pyroelectric crystal is used to calibrate the secondary electron ejection coefficient. Ionization is produced by crossing the fast neutral beam with a well-characterized electron beam. The resulting ions are steered and focussed with magnetic and electrostatic fields to a hemispherical energy analyzer. This analyzer separates ions of different charge or mass, since all ions retain essentially the same velocity as the 3 keV parent neutral beam. For molecular species, 100% collection of fragments is possible. Ions are finally detected by a channel electron multiplier.

In order to complete this survey on recent experimental studies a number of other investigations - mostly using quadrupole mass filters - should be mentioned, e.g. see reference /74-84/.

3. SEMICLASSICAL AND SEMIEMPIRICAL METHODS

The theoretical treatment of the basic electron impact ionization process (i.e. in the exit channel a full three body problem) has received a great deal of attention. Quantum mechanical (approximation) calculations are difficult, few and some of them not as accurate as necessary. Therefore, other methods have been developed, with the goal to obtain reasonably accurate cross sections. Three different approaches have been used, i.e., (i) empirical and semiempirical formulae, (ii) classical collision theories, and (iii) semiclassical collision theories. Theoretical methods have been reviewed several times /2,7-11, 20,85-91/, in particular the accuracy and reliability of the most widely used formulae /8,9,20/.

Here, recent theoretical developments will be presented which allow the easy calculation of electron impact ionization cross sections as a function of electron energy for atoms and molecules /5,6,92-94/.

3.1. Calculation of absolute ionization cross sections for single ionization of atoms with atomic numbers $1 \leq Z \leq 92$

The use of classical mechanics to describe electron impact ionization has been pioneered by Thomson /95/. The

original approach has been modified by several authors by adopting different initial conditions in the classical description of the problem. According to Rudge /85/, none of these formulae represent a substantial improvement over the early Thomson theory because these approximations suffer from the same defects at high and low energies as does the Thomson theory. In order to obtain a logarithmic decrease in the ionization functions (as predicted correctly by the Born-Bethe approximation /96/), Gryzinski reconsidered the problem in 1965 /97/ by assuming that the atomic electron has a continuous velocity distribution. He then found that the electron impact ionization cross-section, σ, for single ionization is

$$\sigma = \sum_{n=1}^{N} 4\pi a_o^2 \xi_n \left(\frac{E_i^H}{E_{in}}\right)^2 \frac{1}{u} \left(\frac{u-1}{u+1}\right)^{3/2} \left\{1+\frac{2}{3}\left(1-\frac{1}{2u}\right)\ln\left[2.7+(u-1)^{1/2}\right]\right\} \quad (6)$$

where a_o is the Bohr radius, ξ_n is the number of equivalent electrons in the nth sub-shell, E_i^H is the ionization energy of H, E_{in} is the ionization energy of an electron in the nth sub-shell, $u = E/E_{in}$, and E ist the energy of an incident electron. Burgess and Vriens /98/ have suggested means of improving the Thomson theory further by incorporating certain features of the quantal treatment into the approximation, e.g. exchange effects. Although their formulae are a significant improvement, they do not give the correct magnitude and behavior of the ionization functions for certain, rather simple, atoms such as neon, nitrogen, and fluorine.

A comparison of these classical and semi-classical formulae with the Born-Bethe formulae (which should be accurate at high electron energies) reveals that the Born-Bethe formula contains, in addition to the u-dependent term, a dependence on $(\langle r \rangle)^2_{nl}$ /99/ (where r is the radius of the nl shell). The importance of the relation between ionization cross-sections and values of the weighted sum of contributions of the mean squared radius of the outer electron shells has already been demonstrated by several authors calculating maximum ionization cross-sections of atoms /99,100/ or using the additivity rule for molecular ionization cross-sections /101/. In order to improve the classical theory, Deutsch and Mark /6/ proposed to incorporate this fundamental feature of the quantal treatment into the classical formulation. They hoped that this would yield not only the correct shapes, but also the correct magnitude of the ionization curves, even in cases of Ne, N and F. After a thorough study of these relations, Deutsch and Mark /6/ found that a good approximation is to replace $4a_o^2 (E_i^H/E_{in})^2$ by $g_{nl} r_{nl}^2$ in Equ. (6), where r_{nl} is the radius of maximum charge density and g_{nl} is a weighting factor /102/, i.e.

$$\sigma = \sum_{nl} g_{nl} \xi_{nl} r_{nl} \cdot \frac{1}{u} \left(\frac{u-1}{u+1}\right)^{3/2} \left\{1 + \frac{2}{3}\left(1 - \frac{1}{2u}\right) \ln\left[2.7+(u-1)^{1/2}\right]\right\} \quad (7)$$

Using the rare gases as test cases, the weighting factor, g_{nl}, was determined via a fitting procedure using reliable experimental data /60,66,43/ to be 3 for s electrons and 0.5 for electrons other than s electrons. It was found that it is sufficient to include in the summation over shells only the outermost sub-shells because the contribution of inner shells is negligible. Moreover, this procedure was recently refined by Margreiter et al. /93,94/ thereby removing also existing discrepancies between experimental and theoretical cross section values for heavy atoms, e.g. uranium /103/. This was achieved by following Bethe's original approach, i.e. determining the weighting factor in more detail for each n and l number used, respectively.

Using equ. (7) Margreiter et al. /93,94/ have calculated the electron ionization cross section functions for single ionization of all elements from H up to U. Moreover, a similar approach has been applied successfully to the calculation of the ionization cross sections of excited (metastable) atomic species /104/. Fig. 3 shows as an example partial ionization cross sections as a function of electron

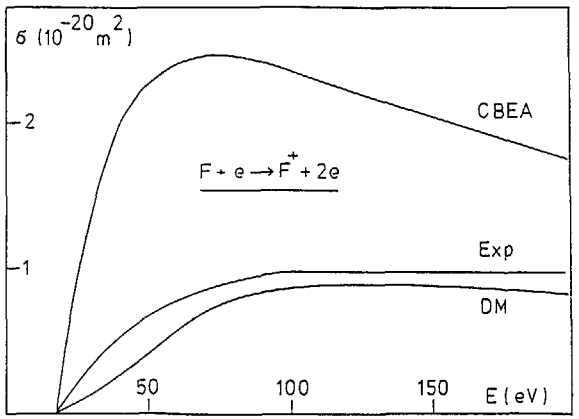

Fig. 3 Cross section as a function of electron energy for single ionization of Ne and F after Deutsch and Mark /6/. CBEA, classical binary encounter approximation /97/, DM, improved semiclassical approximation /6/, Exp, experimental results in Ne /60/ and in F /42/.

energy for Ne and F. It can be seen that the formula proposed by Deutsch and Mark /6/ gives much better agreement with the experimental data than the classical binary encounter approximation (equ. (6)). Moreover, equ. (7) appears also to be superior to other classical or semiclassical treatments.

3 2 Calculation of absolute total ionization cross sections of molecules

It has been shown in recent years (see, for example /105/) that some of these classical, semiclassical, and semi-empirical formulae derived for atomic targets can be used to estimate total ionization cross-sections as a function of electron energy of a wide variety of molecules (e.g. hydrocarbons, chlorine compounds, etc.). These formulae fail, however, in predicting data for molecules containing fluorine /105/. An especially characteristic example is CF_4, reported recently by Stephan et al. /68/. Conversely, Fitch and Sauter /106/, have recently presented an empirical scheme based on the additivity rule of Otvos and Stevenson /101/, which allows the calculation of the total ionization cross-section at ~ 70 eV for organic molecules containing H, C, N, O, F, Cl, Br, and I. The atomic coefficients for the calculation are determined by these authors by a linear regression using 179 total ionization cross-section measurements from the literature. Deutsch and Schmidt /105/ have extended these calculations to compounds including P, As, B, and Si and to electron energies of 20 and 35 eV. From this, it follows that the modified additivity rule may be used to estimate as yet unmeasured total ionization cross-sections of fluorine compounds at one electron energy (usually giving an estimate of the maximum of the cross-section), whereas the above-mentioned formulae cannot be used, although it would be desirable to calculate the energy dependence of the respective cross-sections. As it turns out /5/, fluorine (and to a lesser degree, oxygen and nitrogen) contributes less to a total ionization cross-section of a compound than expected from classical (and semi-classical) collision theory (or summation of the mean square orbital radii from Hartree-Fock calculations as performed by Mann /100/). In an attempt to not only estimate the total cross-section of a fluorine compound (and other molecules) at one electron energy but to predict the complete total ionization cross-section function, Deutsch et al. /5/ have modified the existing classical and semi-classical collision theories, taking into account the anomalous behavior of fluorine (and other elements) with help of an empirical correction factor K_n (see Fig. 4) derived within the framework of the additivity rule (this procedure takes -in a similar fashion as discussed above for the atoms - into account that classical and semiclassical theories do no include quantum size effects). For instance, the corrected Lotz /107/ formula is therefore

$$\sigma = \sum_{n=1}^{N} \xi_n K_n \frac{b \ln u}{E E_n} \qquad (8)$$

where E is the energy of the incident electron, E_n is the binding energy of electron in the nth sub-shell, $u = E/E_n$, $b = 4.5 \times 10^{-14}$ cm^2(eV)^2, and N is the number of sub-shells

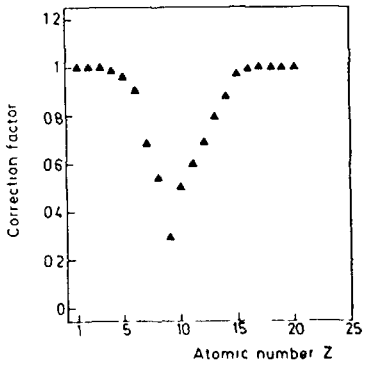

Fig. 4 Correction factor K_n as a function of atomic number Z after Deutsch, Scheier and Mark /5/.

(orbitals) considered. It is therefore necessary to know the orbital structure of the molecules considered, in particular the correlation between orbital and molecular constituent.

This approach has been applied successfully by Deutsch et al. /5/ to several test cases including F_2, CCl_2F_2, CF_4, SF_6, UF_6, and N_2 considering the most widely used theoretical formulae. Fig. 5 shows as an characteristic example total ionization cross sections of CF_4 calculated with the uncorrected formulae (upper part) and with the corrected formulae (lower part). It can be seen that the agreement between the experimental data and the calculated values is much better for the corrected theories. This is especially true for the low-energy regime, a region which is of particular interest for many applications.

4 CRITICAL REVIEW OF AVAILABLE DATA

It would be outside the scope of the present review to give a full account of available cross sections. Moreover, there exist several definitive reviews on this subject, most notably the 1966 review by Kieffer and Dunn /27/ and several recent ones /2-4,7-13,109,110/. Therefore in this chapter a few representative examples of up to date data will be given and discussed.

Despite numerous studies in the last 75 years /111/ reliable experimental data for most classes of species is sparse. For instance, absolute cross section measurements are available only

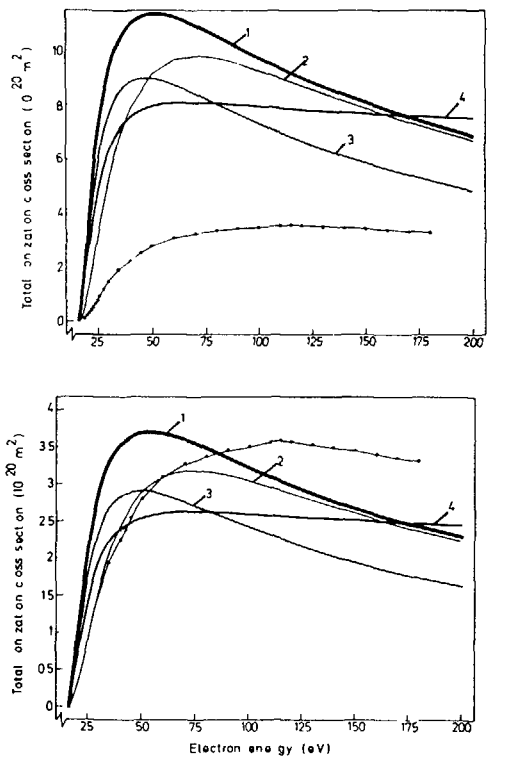

Fig. 5. Total ionization cross section of CF_4 as a function of electron energy after Deutsch, Scheier and Märk /5/. Points experimental results of Stephan, Deutsch and Mark /66/. Curves given in the upper part are calculated with the uncorrected formulae, in the lower part with the corrected formulae.
1: Lotz /107, 2: Gryzinski /97/, 3: Burgess-Vriens /98/, and 4: Elwert /108/.

for five metastables (H^* /31,112/, He^* /35/, Ne^* /113/, Ar^* /113/ and N_2^* /38/), and (besides for atoms as H, N, O, C, S, I, Br, Cl and F /3,4/) for five free molecular radicals (CD_2, CD_3, SiF, SiF_2 and Si_3 /4, 41,42/).

According to a review by Freund /4/ and by Märk /3/ cross sections for single ionization from threshold up to several hundred eV exist for only 22 atoms, and of those, only the rare gases and some alkalis have been measured by different laboratories with sufficient agreement (i.e., ionization crosss sections of all five rare gases by Freund and co-workers /4, 43/, Rapp and Englander-Golden /22/ and Märk and co-workers /60,66/ agree to better than 10% over the entire energy range). For another 10 atoms, only total ionization cross sections have been measured; for the rest there exist no published values.

In case of molecular targets the situation is even worse: there exist only a few reliable data sets (i) on total ionization cross sections (for more details see Ref. /9,23/ and (ii) on partial ionization cross sections for the production of the parent ion (for more details see Ref. /3/). For the production of fragment ions via electron impact ionization of molecular targets the only reliable determinations appear to be the measurements by Adamczyk et al. /50-56/ in H_2, N_2, H_2O, CO_2, NH_3, CH_4 and SF_6 using a cycloidal mass spectrometer, by Freund et al. /41,42,44/ in CD_2, CD_3, SiF, SiF_2 and SiF_3 using the fast neutral beam method, and by Märk et al. /67,68,71/ in CF_4, CCl_4 and CF_2Cl_2 using the deflection mass spectrometry method.

Fig. 6 gives as an example quantitative information available for Ar, Fig. 7 for N_2, Fig. 8 for SiF, Fig. 9 for CF_4 and Fig. 10 for SF_6.

5. ELECTRON ATTACHMENT AND ELECTRON IONIZATION IN QUASI-LIQUIDS AND/OR QUASI-SOLIDS (CLUSTERS)

In the field of radiotherapy and radiobiology not only gas phase ionization cross section data are of interest, but in parti-

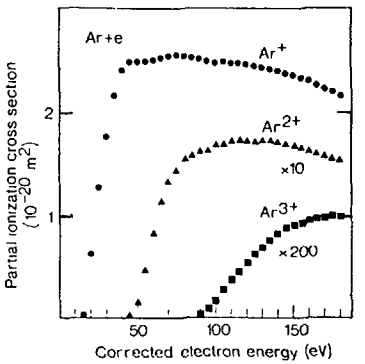

Fig. 6 Absolute partial ionization sections for Ar /60,47/ after Märk /3,11/

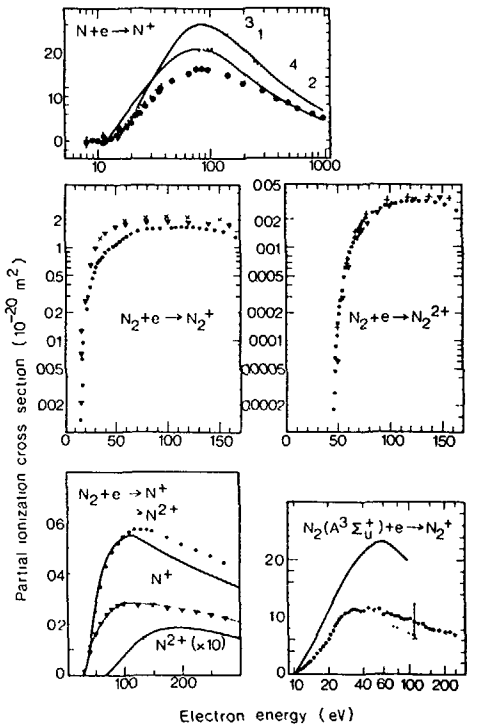

Fig. 7 Absolute partial ionization cross sections for N_2 /22,36, 38/,54,114-117/ after Märk /3,11/.

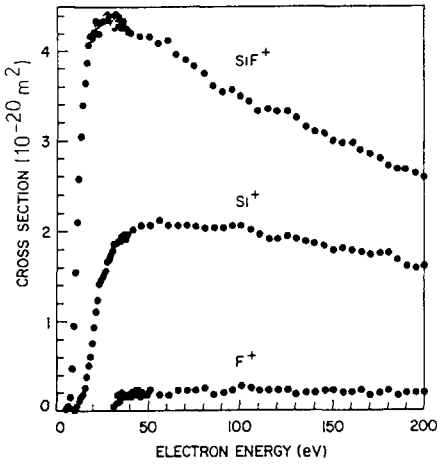

Fig. 8 Absolute partial ionization cross sections for SiF after Hayes et al. /44/.

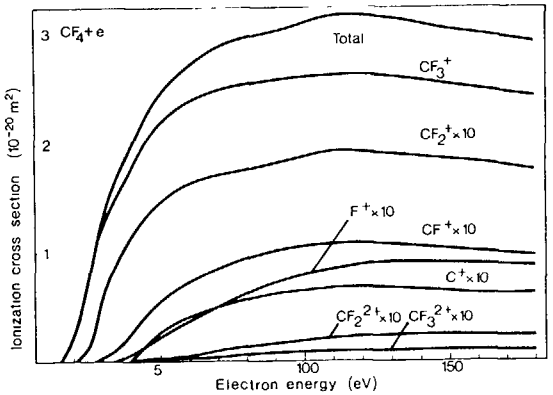

Fig. 9 Absolute partial and total ionization cross sections for CF_4 after Märk /3/.

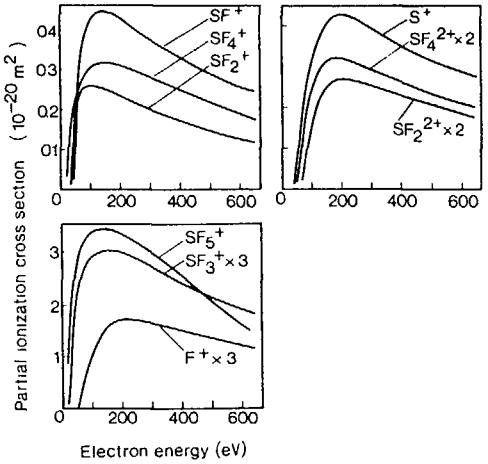

Fig. 10 Absolute partial ionization cross sections for SF_6 /56/ after Märk /3/.

cular there is urgent need on qualitative and quantitative information about electron interaction with condensed phase targets of the respective atoms or molecules. With the recent possibility to study in detail the inelastic interaction of electrons with clusters /14/, a powerful new tool has become available to investigate electron attachment and electron impact ionization in quasi-liquids and/or quasi-solids. Here, only two examples pertaining directly to the present subject will be discussed in some detail in the following.

5.1. Giant resonances in the thermal electron attachment cross sections of van der Waals clusters

Low energy-electron attachment (< 15 eV) to the oxygen molecule in the gas phase has been the subject of intensive study in the past twenty years. Reactions involving molecular oxygen and its anions are of importance in understanding air and radiation

chemistry. Dissociative attachment to O_2 is produced in the energy range 4.4 to 10 eV via

$$O_2(X^3\Sigma_g^-) + e \rightarrow O_2^{-*}\ (^2\Pi_u) \rightarrow O^-(^2P) + O(^3P) \qquad (9)$$

The cross section for this process shows a single structureless peak at ~ 7 eV, suggesting that only a single repulsive state is responsible for the occurrence of this reaction. Nondissociative attachment to O_2 (which has a positive /118/ electron affinity of 0.440 ± 0.008 eV) occurs by a resonance process,

$$O_2(X^3\Sigma_g^-;\ v = 0) + e \rightarrow O_2^{-*}(X^2\Pi g;\ v' \geq 4). \qquad (10)$$

The molecular anion so formed is unstable with respect to autodetachment and has a predicted lifetime of ~ 10^{-10} s /119/ unless it can be stabilized collisionally in a high-pressure environment. A two-step mechanism was suggested including reaction (10) and (11),

$$O_2^{-*}(X^2\Pi_g;\ v' \geq 4) + M \rightarrow O_2^-(X^2\Pi_g; v' < 4) + M + \text{energy} \qquad (11)$$

According to Spence and Schulz /120/ and Mc Corkle, Christophorou and Anderson /121/ the "effective" cross section for this "three-body attachment" shows pronounced structure with energy. Recent studies, however, which investigated the pressure and temperature dependence of attachment rates have demonstrated that attachment in pure O_2 and some O_2-M (where M denotes some other molecule) systems cannot be explained solely by the Bloch-Bradbury mechanism involving reaction (10) and (11) but that also attachment to van der Waals molecules has to be involved /122/. Although the density of van der Waals molecules in those experiments is much smaller than that of O_2 molecules, attachment to van der Waals molecules was thought to be much larger because of an assumed reduction in the effective resonance energy (0.076 eV for $O_2^-(v'=4)$ with respect to $O_2(v=0)$ /123/).

In order to resolve this question, Märk et al. /15,124/ recently studied electron attachment to O_2 clusters as a function of electron energy and cluster size. The clusters were produced by nozzle expansion and the attachment was investigated in a crossed molecular beam/electron impact ionization/mass spectrometer system under single collision conditions /125/. Electron attachment to O_2 clusters gives two homologous series, $(O_2)_n^-$ and $(O_2)_nO^-$. Reported attachment cross section functions showed significant differences, e.g. $(O_2)_nO^-$ ions show a similar behavior as O^- produced via reaction (9) (i.e. a single peak at ~ 7 eV), whereas $(O_2)_n^-$ ions show an additional peak at ~ 0 eV (see Fig. 11). This thermal energy resonance changes dramatically with cluster size, i.e. increasing in magnitude (giant resonance) and decreasing in FWHM with increasing n. Similar results have been recently observed for CO_2 /126,127,128/, H_2O /128/, N_2O /127, 128/, SO_2 /129,130/ and SF_6 /128,131/ clusters. This clearly demonstrates that thermal electron attachment is of prime importance in case of quasiliquid molecular targets, irrespective of the situation in case of the respective monomer-electron interaction (e.g. in terms of electron affinity and cross section behavior).

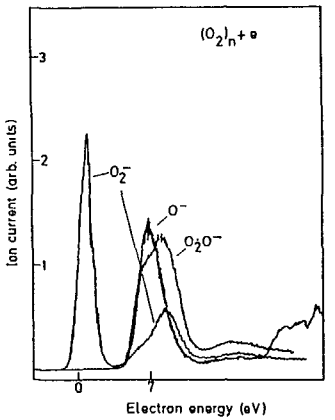

Fig. 11 $(O_2)^-$ and $(O_2)O^-$ signals produced by electron attachment to O_2 clusters as a function of electron energy after Märk et al. /15,124/. Also shown is the energy dependence of O^- produced via dissociative attachment to the O_2 monomer.

The production and stability of multiply charged van der Waals cluster cations has been the subject of considerable recent interest /14,132/. Of particular interest to radiobiology are studies on the electron energy dependence of the production of multiply charged atomic and molecular cluster ions close to threshold, because these studies give new insight into the formation mechanism for these ions, i.e. multiple ionization of van der Waals clusters (quasiliquids) proceeding via sequential single ionization collisions of one incoming electron within the cluster.

Using high resolution, high mass range and high sensitivity mass spectrometry /133/ we were recently able to obtain well resolved cluster ion mass spectra including doubly and triply charged cluster ions of Ar /16/, O_2 /134/, N_2 /135/, NH_3 /136/ and SO_2 /137/. This allows the study of the threshold ionization cross section behavior yielding the respective appearance energies. Fig. 12 shows as an example relative ionization cross section

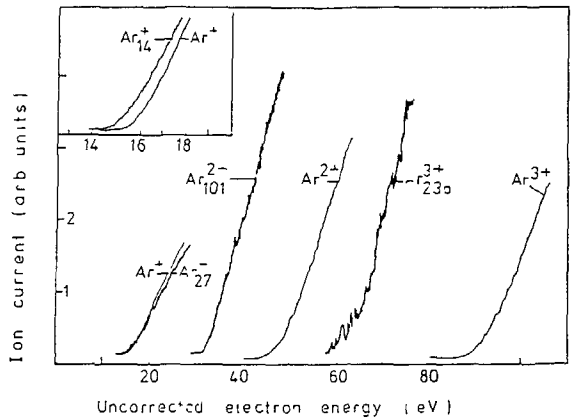

Fig. 12 Ionization cross section functions near threshold for Ar^+, Ar^{2+}, Ar^{3+}, Ar_{14}^+, Ar_{27}^+, Ar_{101}^{2+} and Ar_{226}^{3+} after Scheier and Mark /16/.

functions near threshold for the production of singly, doubly and triply charged Ar cluster ions. Also shown for comparison and calibration purposes are cross section functions of the respective monomer ions. The onset of the singly charged cluster ions (see inset in Fig. 12) are shifted by appr. 0.5 to 1 eV to lower energies due to solvation effects /138/. The onsets of the doubly and triply charged cluster ions are shifted way below the onsets of Ar^{2+} and Ar^{3+}, respectively. These large red shifts, also observed in case of O_2, N_2, NH_3 and SO_2 clusters /134-137/, cannot be attributed to solvation effects.

Instead, Märk and coworkers /16, 134-137/ interpreted these results,

i.e. that IE $(X_n^{z+}) \approx z \cdot IE(X^+)$,

as evidence for the occurrence of sequential multiple ionization process. That is, e.g. X_n^{2+} is produced by two sequential single ionization events of one incoming electron at two different Ar monomers within the cluster Ar_n.

Such a multiple step sequential ionization mechanism also explains the large ionization cross sections observed for multiply charged cluster ions,

i.e. $\sigma(X_n^+/X_m) \sim \sigma(X_n^{2+}/X_m)$ /139/.

This is in contrast to observations for the respective monomers, where $\sigma(X^+/X) >> \sigma(X^{2+}/X)$ /2,3/, and has to be taken into account when inelastic electron scattering in condensed media is considered

It is hoped that further research on electron cluster interaction will shed more light on electron energy degradation in liquid and solid targets and that this new and potential experimental approach will prove to be a valuable tool in radiotherapy and radiobiology.

ACKNOWLEDGEMENTS

Work partially supported by the Österreichischer Fonds zur Förderung der wissenschaftlichen Forschung.

REFERENCES

1. M. Inokuti et al., Nucl. Atomic Data for Radiotherapy, Related Radiobiology, IAEA (1987) 445-447
2. T.D. Märk and G.H. Dunn, Electron Impact Ionization, Springer, Wien (1985)
3. T.D. Märk, Chapter 5 in Ref. 2
4. R.S. Freund, In: Swarm Studies and Inelastic Electron-Molecule Collisions (L.C. Pitchford et al., Eds.) Springer, New York (1987) 329-346
5. H. Deutsch, P. Scheier and T.D. Märk, Int. J. Mass Spectrom. Ion Proc., 74 (1986) 81
6. H. Deutsch and T.D. Märk, Int. J. Mass Spectrom. Ion Proc., Rapid Commun., 79 (1987) R1
7. T.D. Märk, Int. J. Mass Spectrom. Ion Proc., 45 (1982) 125
8. T.D. Märk, Beitr. Plasmaphysik, 22 (1982) 257
9. T.D. Märk, In: Electron-Molecule Interactions and their Applications, Vol. 1 (L.G. Christophorou, Ed.) Academic Press, Orlando (1984) 251-334
10. T.D. Märk, In: Gaseous Ion Chemistry and Mass Spectrometry (J.H. Futrell, Ed.) Wiley, New York (1986) 61-93
11. T.D. Märk, In: The Physics of Ionized Gases (J. Puric, D. Belic, Eds.) World Scientific, Singapure (1987) 145-160
12. K.L. Bell, H.B. Gilbody, J.G. Hughes, A.E. Kingston and F.J. Smith, J. Phys. Chem. Ref. Data, 12 (1983) 891
13. H. Tawara and T. Kato, Nucl. Data Tabl., 36 (1987) 167
14. T.D. Märk, Int. J. Mass Spectrom. Ion Proc., 79 (1987) 1-59
15. T.D. Märk, K. Leiter, W. Ritter and A. Stamatovic, Phys. Rev. Letters, 55 (1985) 2559
16. P. Scheier and T.D. Märk, Chem. Phys. Letters, 136 (1987) 423
17. D. Kreisle, O. Echt, M. Knapp, E. Recknagel, K. Leiter, T.D. Märk, J.J. Saenz, J.M. Soler, Phys. Rev. Letters, 56 (1986) 1551
18. P. Scheier and T.D. Märk, Phys. Rev. Letters, 59 (1987) 1813
19. A. Stamatovic, F. Howorka and T.D. Märk, Chem. Phys. Letters, in print (1988); A. Stamatovic, F. Howorka, P. Scheier and T.D. Märk, Chem. Phys. Letters, 145 (1988) 95; A. Stamatovic, P. Scheier, F. Howorka and T.D. Märk, Int. J. Mass Spectrom. Ion Proc., 83 (1988) R1
20. S.M. Younger and T.D. Märk, Chapter 2 in Ref. 2.
21. J.T. Tate and P.T. Smith, Phys. Rev., 39 (1932) 270
22. D. Rapp and P. Englander-Golden, J. Chem. Phys., 43 (1965) 1464
23. F.J. de Heer and M. Inokuto, Chapter 7 in Ref. 2
24. N.L. Djuric, I.M. Cadez and M.V. Kurepa, Int. J. Mass Spectrom. Ion Proc., in print (1988)
25. N.L. Djuric, private communication, 1988; see SPIG (1988)
26. M.V. Kurepa, I.M. Cadez and V.M. Pejcev, Fizika, 6 (1974) 185
27. L.J. Kieffer and G.H. Dunn, Revs. Mod. Phys., 38 (1966) 1
28. F. Karstensen and H. Köster, Astron. Astrophys., 13 (1971) 116
29. M. Schneider, J. Phys. D7 (1974) L 83
30. F. Karstensen and M. Schneider, Z. Physik, A 273 (1975) 321; J. Phys., B 11 (1978) 167
31. P. Defrance, W. Claeys, A. Cornet and G. Poulaert, J. Phys. B14 (1981) 111
32. J.M. Dettmann and F. Karstensen, J. Phys., B15 (1982) 287; H.H. Wendt and F. Karstensen, Phys. Rev., A 29 (1984) 562
33. J.A. Syage, Chem. Phys. Lett., 143 (1988) 19
34. C.J. Cook and J.R. Peterson, Phys. Rev. Letters, 9 (1976) 164
35. A.J. Dixon, M.F.A. Harrison and A.C.H. Smith, J. Phys., B9 (1976) 2617 and references therein
36. E. Brook, M.F.A. Harrison and A.C.H. Smith, J. Phys., B11 (1978) 3155)
37. T.D. Märk and F.J. de Heer, J. Phys. B12 (1979) L 429
38. P.B. Armentrout, S.M. Torr, A. Dosi and R.S. Freund, J. Chem. Phys., 75 (1981) 2786
39. D.L. Ziegler, J.H. Newman, K.A. Smith and R.F. Stebbings, Planet. Space Sci., 30 (1982) 451
40. R.G. Montague, M.F.A. Harrison and A.C.H. Smith, J. Phys. B 17 (1984) 3295
41. F.A. Baiocchi, R.C. Wetzel and R.S. Freund, Phys. Rev. Letters, 55 (1984) 771
42. T.R. Hayes, R.C. Wetzel and R.S. Freund, Phys. Rev. A 35 (1987) 578
43. R.C. Wetzel, F.A. Baiocchi, T.R. Hayes and R.S. Freund, Phys. Rev., A 35 (1987) 559
44. T.R. Hayes, R.C. Wetzel, F.A. Baiocchi and R.S. Freund, J. Chem. Phys., 88 (1988) 823
45. N.G. Adams, D. Smith and D. Grief, J. Phys., B12 (1979) 791
46. P. Varga, W. Hofer and H. Winter, J. Phys., B14 (1981) 1341
47. K. Wiesemann, J. Puerta and B.A. Huber, J. Phys., B20 (1987)587 and 2nd ECAMP, Amsterdam (1985) p. 415
48. H.R. Koslowski, J. Binder, B.A. Huber and K. Wiesemann, J. Phys., B 20 (1987) 5903
49. S. Gefen anc C. Lifshitz, Int. J. Mass Spectrom. Ion Proc. 58 (1984) 251 and references therein
50. B. Adamczyk, A.J.H. Boerboom, B.L. Schram and J. Kistemaker, J. Chem. Phys., 44 (1966) 1
51. B.L. Schram, B. Adamczyk and A.J.H. Boerboom, Rev. Sci. Instrum., 43 (1966) 638
52. J. Schutten, F.J. de Heer, H.R. Moustafa, A.J.H. Boerboom and J. Kistemaker, J. Chem. Phys., 44 (1966) 3924
53. B. Adamczyk, A.J.H. Boerboom and M. Lukasiewicz, Int. J. Mass Spectrom. Ion Phys., 9 (1982) 407
54. S. Halas and B. Adamczyk, Int. J. Mass Spectrom. Ion Phys., 10 (1972/73) 157
55. K. Bederski, L. Wojcik and B. Adamczyk, Int. J. Mass Spectrom. Ion Phys., 35 (1980) 171
56. T. Stanski and B. Adamczyk, Int. J. Mass Spectrom. Ion Phys., 46 (1983) 31
57. N. Nagy, P. Skutlartz and V. Schmidt, J. Phys. B 13 (1980) 1249
58. A. Crowe, J.A. Preston and J.W. Mc Conkey, J. Chem. Phys. 57 (1972) 1620

59. A. Crowe and J.W. Mc Conkey, Int. J. Mass Spectrom. Ion Phys., 24 (1977) 181 and references therein
60. K. Stephan, H. Helm and T.D. Mark, J. Chem. Phys., 73 (1980) 3663; Adv. Mass Spectrom., 8A (1980) 122
61. T.D. Mark and A.W. Castleman, J. Phys., E13 (1980) 1121
62. K. Stephan, H. Helm, Y.B. Kim, G. Sejkora, J. Ramler, M. Grossl, E. Mark and T.D. Mark, J. Chem. Phys., 73 (1980) 303
63. T.D. Mark, E. Mark and K. Stephan, J. Chem. Phys., 74 (1981) 3633
64. Y.B. Kim, K. Stephan, E. Mark and T.D. Mark, J. Chem. Phys., 74 (1981) 6771
65. E. Mark, T.D. Mark, Y.B. Kim and K. Stephan, J. Chem. Phys., 75 (1981) 4446
66. K. Stephan and T.D. Mark, J. Chem. Phys., 81 (1984) 3116
67. K. Leiter, K. Stephan, E. Mark and T.D. Mark, Plasma Chem. Plasma Proc., 4 (1984) 235
68. K. Stephan, H. Deutsch and T.D. Mark, J. Chem. Phys. 83 (1985) 5712
69. R. Seefeldt, W. Moller and M. Schmidt, Z. Phys. Chemie, Leipzig, 226 (1985) 4
70. L.N. Gorokhov and N.E. Khandamirova, Proc. 10th Int. Mass Spectrom. Conf., Swansea (1985)
71. K. Leiter and T.D. Mark, Proc. 7th Int. Symp. Plasma Chemistry, Eindhoven (1985) and K. Leiter, P. Scheier, G. Walder and T.D. Mark, Int. J. Mass Spectrom. Ion Proc., in print (1988)
72. See for instance C. Brunnee and H. Voshage, Massenspektrometrie, Verlag Thiemig, Munchen (1964) p. 53
73. B. Adamczyk and L. Michalak, Int. J. Mass Spectrom. Ion Proc., 71 (1986) 211
74. O.I. Smith and J.S. Stevenson, J. Chem. Phys., 74 (1981) 6777
75. O.I. Smith, Int. J. Mass Spectrom. Ion Proc. 54 (1983) 55
76. M.W. Siegel, Int. J. Mass Spectrom. Ion Phys., 44 (1982) 19
77. M.J. Wiegand and L.R. Boedeker, Appl. Phys. Lett., 40 (1982) 225
78. O.J. Orient and S.K. Srivastava, J. Chem. Phys., 78 (1983) 2949; J. Chem. Phys., 80 (1984) 140
79. H. Chatham, D. Hils, R. Robertson and A. Gallagher, J. Chem. Phys., 81 (1984) 1770
80. G. Monnom, P. Gaucherel and C. Paparoditis, J. Physique 45 (1984) 77
81. D. Mathur and D. Badrinathan, Int. J. Mass Spectrom. Ion Proc., 57 (1984) 167 and 68 (1986) 9; Phys. Rev., A 35 (1987) 1033; ICPEAC (1987) 252
82. O.J. Orient and S.K. Srivastava, J. Phys. B20 (1987) 3923; E. Krishnakumar and S.K. Srivastava, ICPEAC (1987) 248
83. H.U. Poll and J. Meichsner, Contrib. Plasma Phys., 27 (1987) 359
84. M.B. Shah, D.S. Elliott and H.B. Gilbody, ICPEAC (1987) 244
85. M.R.H. Rudge, Revs. Mod. Phys., 40 (1968) 564
86. L. Vriens, Case Studies in Atomic Collision Physics (E.W. Mc Daniel, M.R.C. Mc Dowell, Eds.) North Holland Amsterdam 1 (1969) 337
87. M. Inokuti, Revs. Mod. Phys., 43 (1971) 297
88. L.A. Vainstein, I.I. Sobelman and E.A. Yukov, Electron excitation cross sections of atoms and ions, NAUKA, Moscow (1973)
89. K.L. Bell and A.E. Kingston, Adv. Atom. Molec. Phys., 10 (1974) 53
90. R.K. Peterkop, Theory of ionization of atoms by electron impact (D.G. Hummel, Transl.) Colorado Ass. Univ. Press, Boulder (1977)
91. Y. Itikawa and T. Kato, IPPJ-AM-17, Institute of Plasma Physics Report, Nagoja University (1981)
92. H. Deutsch and T.D. Mark, ICPEAC (1987) 246
93. D. Margreiter, H. Deutsch and T.D. Mark, Proc. 11th Int. Mass Spectrometry Conference, Bordeaux (1988)
94. D. Margreiter, Diplomarbeit, Universitat Innsbruck, 1988
95. J.J. Thomson, Philos. Mag. 23 (1912) 449
96. H. Bethe, Ann. Phys., 5 (1930) 325
97. M. Gryzinski, Phys. Rev. A 138 (1965) 305
98. A. Burgess, in Atomic Collision Processes (M.R.C. Mc Dowell, Ed.) North Holland, Amsterdam (1963) p. 237; L. Vriens, Phys. Rev., 141 (1966) 88
99. P. Tiwari, D.K. Kai and M.L. Rustgi, J. Chem. Phys., 50 (1969) 3040
100. J.B. Mann, J. Chem. Phys., 46 (1967) 1646
101. J.W. Otvos and D.P. Stevenson, J. Am. Chem. Soc., 78 (1956) 546
102. A similar weighting factor has already been introduced by Mann /100/ in order to derive meaningful maximum cross-sections from the Born-Bethe formula.
103. J.C. Halle, H.H. Lo, and W.L. Fite, Phys. Rev. A, 23 (1981) 1708
104. H. Deutsch, pers. communication, 1988
105. H. Deutsch and M. Schmidt, Beitr. Plasmaphys. 24 (1984) 475; 25 (1985) 475
106. W.L. Fitch and A.D. Sauter, Anal. Chem., 55 (1982) 832
107. W. Lotz, Z. Phys., 206 (1967) 205; Astrophys. J. Suppl. 14 (1967) 207
108. G. Elwert, Z. Naturforschg., A7 (1952) 432
109. P. Laborie, J.M. Rocard and J.A. Rees, Electronic Cross Sections and Macroscopic Coefficients, Dunod, Paris (1971)
110. H. Tawara, T. Kato and M. Ohnishi, IPPJ-AM-37, Report, Inst. Plasma Phys., Nagoya Univ. (1985)
111. P. Lenard, Ann. Physik, 8 (1902) 149
112. A.J. Dixon, A. von Engel, and M.F.A. Harrison, Proc. Roy. Soc. Lond., A 343 (1975) 333
113. A.J. Dixon, M.F.A. Harrison and A.C.H. Smith, 8th ICPEAC, Belgrade (1973) p. 405
114. D. Rapp, P. Englander-Golden and D.L. Briglia, J. Chem. Phys., 42 (1965) 4081
115. T.D. Mark, J. Chem. Phys., 63 (1975) 3731
116. R.N. Daly and R.E. Powell, Proc. Phys. Soc., 89 (1966) 273
117. A. Crowe and J.W. Mc Conkey, J. Phys. B6 (1973) 2108
118. R.J. Celotta, R.A. Bennett, J.L. Hall, M.W. Siegel and J. Levine, Phys. Rev. A6 (1972) 631
119. L.G. Christoporou, D.L. Mc Corkle, and A.A. Christodoulides, in Electron Molecule Interactions and Their Applications (L.G. Christophorou, Ed.) Academic Press, New York (1984) 477
120. D. Spence and G.J. Schulz, Phys. Rev. A5 (1972) 724
121. D.L. Mc Corkle, L.G. Christophorou and V.E. Anderson, J. Phys., B5 (1972) 1211

122. Y. Hatano and H. Shimamori, in Electron and Ion Swarms (L.G. Christophorou, Ed.) Pergamon, New York (1981) 103
123. H. Shimamori and R.W. Fessenden, J. Chem. Phys., 74 (1981) 453
124. T.D. Mark, K. Leiter, W. Ritter and A. Stamatovic, Int. J. Mass Spectrom. Ion Proc., 74 (1986) 265
125. T.D. Mark, P. Scheier, K. Leiter, W. Ritter, K. Stephan and A. Stamatovic, Int. J. Mass Spectrom. Ion Proc., 74 (1986) 281
126. A. Stamatovic, K. Leiter, W. Ritter, K. Stephan and T.D. Mark, J. Chem. Phys., 83 (1985) 2942
127. M. Knapp, O. Echt, D. Kreisle, T.D. Mark and E. Recknagel, Chem. Phys. Lett., 126 (1986) 225
128. M. Knapp, O. Echt, D. Kreisle, T.D. Mark and E. Recknagel, in: In Physics and Chemistry of Small Clusters (P. Jena, B.K. Rao and S.N. Khanna, Eds.) Plenum, New York, (1987) 693
129. T.D. Mark, P. Scheier and A. Stamatovic, Chem. Phys. Lett., 136 (1987) 177
130. A. Stamatovic, P. Scheier and T.D. Mark, Z. Phys. D 6 (1987) 351
131. A. Stamatovic, P. Scheier and T.D. Mark, J. Chem. Phys., in print (1988) May/June issue
132. T.D. Mark and A.W. Castleman, Jr., Adv. At. Mol. Phys., 20 (1985) 65
133. P. Scheier and T.D. Mark, Int. J. Mass Spectrom. Ion Proc., 76 (1987) R11
134. P. Scheier, A. Stamatovic and T.D. Mark, Chem. Phys. Letters, 144 (1988) 119
135. P. Scheier, A. Stamatovic and T.D. Mark, J. Chem. Phys., 88 (1988) 4289
136. P. Scheier, G. Walder, A. Stamatovic and T.D. Mark, Chem. Phys. Lett., submitted (1988)
137. P. Scheier, G. Walder, A. Stamatovic and T.D. Mark, J. Chem. Phys., submitted (1988)
138. H. Helm, K. Stephan, and T.D. Mark, Phys. Rev. A 19 (1979) 2154; D.R. Worsnop, S.J. Buelow and D.R. Herschbach, J. Phys. Chem., 88 (1984) 4506
139. Moreover, it can be seen that the ionization cross section of Ar^{2+}_{101} in Fig. 12 increases linearly with the excess electron energy, whereas Ar^{2+} increases quadratically. This is further evidence in favor of the multiple step sequential ionization mechanism suggested by Mark and coworkers /14,16,134-137/.

ELECTRON COLLISION CROSS-SECTIONS FOR ATOMS AND MOLECULES DETERMINED FROM BEAM AND SWARM DATA

M HAYASHI
Nagoya Institute of Technology,
Nagoya, Japan

Abstract

This paper deals with the electron collision cross-sections for H_2O molecule needed as input for electron transport calculations and for the modeling of radiation effects in biological materials. Recently, some new beam data have been published for H_2O. With these data we have improved the cross-section values. We have discussed the values of total ionization cross-sections, and it is concluded that the recent measured values of Orient et al are too large.

---

1. Introduction

Elastic and inelastic electron collision cross-sections for atoms and molecules of interest in radiation physics and chemistry, plasma processing, gas lasers, gaseous dielectrics and space sciences have been determined from available electron beam and electron swarm data utilizing the Boltzmann equation method. The discussion will cover a number of atomic and molecular species. My first review on this subject was reported in 1985 at the Meeting of Lake Tahoe (Hayashi 1987).

Table 1. The gases for which the author has determined sets of cross-sections (1987)

He	Ne	Ar	Kr	Xe		
H	O	F	Cd	Hg		
H_2	N_2	O_2	F_2		(Cl_2)	
CO	NO	HCl				
H_2O	SO_2	N_2O	CO_2		(COS)	
C_2H_2	NH_3				(NF_3)	(BF_3)
CH_4	SiH_4	CF_4	CCl_2F_2	CCl_4	(GeH_4)	(SiF_4)
C_2H_4						
SF_6						
C_2H_6	Si_2H_6	C_2F_6				
C_3H_8					(C_3F_6)	(C_4F_8)

The goal of electron collision studies is to provide absolute values of cross-sections for all processes involved: elastic scattering, rotational excitation, vibrational excitation, electronic excitation, dissociation, attachment and ionization, as a function of incident electron energy and scattering angle.

We have determined the cross-section sets for 34 atoms and molecules in the 0 to 1000 eV energy range over the last ten years. These atoms and molecules are listed in table 1. The molecules in parentheses will be studied in the near future.

The simple molecules of interest in the field of radiobiology and radiotherapy are H_2O, H_2, O_2 and N_2. Inspite of several studies, a set of electron collision cross-sections for H_2 (Buckman et al 1985, Morrison et al 1987, Tawara et al 1987), O_2 (Phelps 1985, Itikawa et al 1987) and N_2 (Phelps et al 1985, Itikawa et al 1986) are still not well known. For H_2O, most important small molecule in the field of radiation research, the values of electron collision cross-sections are also not well known (for example, Zaider et al 1983, Inokuti 1984). Our old cross-section set for H_2O have been given in a previous report (Hayashi 1987). Lately some new, beam-experimental data and theoretical works have been published for H_2O. With these data we have improved the cross-section values for electron energies from 10 to 1000 eV and we will discuss these values here.

2. Electron collision cross-section set for H_2O

2.1 Total cross-section

A review for total electron scattering cross-section, which is the sum of elastic and all inelastic cross-sections, have already been given by Trajmar et al (1983). To avoid repetition we will summarize here only recent works not included in this comprehensive review. There have been some new measurements of the total cross-sections after 1985 by Sueoka et al (1986), Szmytkowski (1987) and Nishimura (1988). The total cross-sections is relatively easy to measure, therefore, the old data and these new data almost coincide with each others, except for Sueoka's values. From these values, we have determined the recommended values of total cross-sections in the range of 0.35 - 1000 eV and these values are shown later. Very recently, theoretical study have also been reported by Jain (1988).

2.2 Elastic scattering

Lately, elastic differential cross-sections (DCS) for H_2O have been measured by Danjo et al (1985), Katase et al (1986) and Shyn

et al (1987). Theoretical works have also been published by Gianturco et al (1986), Brescansin et al (1986), Katase et al (1986), Jain et al (1988) and Sato et al (1988). Using these values together with old experimental data, we have been determined the recommended values of DCS for the electron energies from 0.35 to 1000 eV and then calculated the integral elastic cross-sections q_t and momentum transfer cross-sections q_m.

The H_2O molecules have large rotational excitation cross-sections below about 10 eV.

2.3 Ionization cross-section

Recently, total ionization cross-sections for H_2O have been measured by Bolorizadeh et al (1986) and Orient et al (1987). The values of Orient et al are very large compared with Schutten et al's values (1966).

2.4 Electron swarm data

One of the electron transport coefficients, characteristic energy D_T/μ at low E/N have been measured by Elford (1988). Related new Boltzmann equation analysis have been carried out by Ness et al (1988). These works discussed the values of elastic q_m and rotational excitation cross-sections q_r mainly, and their calculated D_T/μ values coincide perfectly with experimental values of Elford.

3. New results and conclusion

We have determined the new tentative electron collision cross-section set for H_2O. These values are shown in figure 1 and also tables 2 and 3.

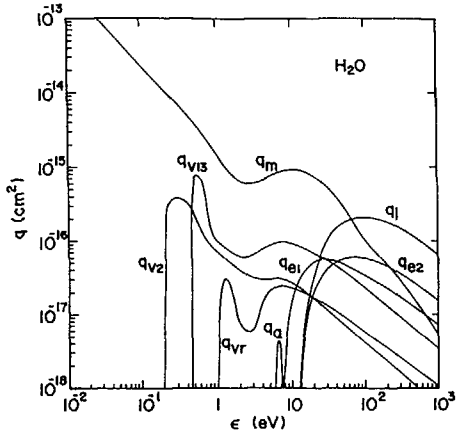

Figure 1. Electron collision cross-sections for H_2O. Rotational excitation and super elastic collision cross-sections are not shown.

Integral elastic collision cross-section q_t and momentum transfer cross-section q_m have been determined from all DCS values as discussed already. The error is about 10 - 15 %. We do not discuss the rotational excitation and also super elastic collision cross-sections here. We believe that the values of q_r given by Ness et al (1988) are exact.

The vibrational excitation cross-sections q_v have been separated into three parts. The values q_{v13} are the sum of q_{v1} and q_{v3}, because the threshold energy is almost the same. The values of q_{vr} are the sum of q_v values other than q_{v2} and q_{v13}. The absolute values of q_{vr} are not well known experimentally and have small effect on the electron swarm parameters. We assume the threshold energy of 1 eV for q_{vr}. We have to say that the values of q_{v2} and q_{v13} measured by Seng et al (1976) have been multiplied by factor 2 for trial,

Table 2. Electron collision cross-sections q and sum of these q values Q_S and recommended values of total cross section Q_T for H_2O.

ε (eV)	q_t	q_{v2} (0.198)	q_{v13} (0.453)	q_{vr} (1.0)	q_{el} (7.5)	q_{e2} (13.32)	q_i (12.62)	Q_S	Q_T
2	16.8	0.40	0.61	0.078				17.9	19.0
3	13.5	0.32	0.64	0.062				14.5	15.2
4	12.8	0.30	0.76	0.148				14.0	14.2
5	13.0	0.30	0.88	0.21				14.4	14.7
6	13.9	0.312	0.94	0.232				15.4	15.3
8	15.2	0.30	0.97	0.239	0.024			16.7	17.0
10	15.8	0.264	0.93	0.23	0.125			17.4	17.5
12	15.8	0.234	0.88	0.216	0.27			17.4	17.1
15	14.9	0.198	0.80	0.196	0.39	0.048	0.070	16.6	16.4
20	12.7	0.160	0.69	0.17	0.516	0.203	0.33	14.8	14.3
25	10.8	0.134	0.608	0.15	0.564	0.320	0.64	13.2	13.1
30	9.5	0.116	0.544	0.134	0.576	0.408	0.98	12.3	12.0
40	7.53	0.092	0.452	0.112	0.54	0.528	1.48	10.7	10.6
50	6.22	0.076	0.388	0.096	0.492	0.585	1.76	9.62	9.6
60	5.30	0.065	0.34	0.084	0.444	0.603	1.90	8.74	8.7
80	4.21	0.051	0.276	0.068	0.384	0.594	2.04	7.62	7.6
100	3.55	0.042	0.234	0.058	0.336	0.576	2.05	6.84	6.8
120	3.10	0.036	0.198	0.050	0.300	0.546	2.02	6.25	6.3
150	2.62	0.030	0.164	0.043	0.269	0.504	1.92	5.55	5.6
200	2.11	0.023	0.130	0.035	0.227	0.450	1.73	4.71	4.7
300	1.55	0.016	0.092	0.026	0.174	0.36	1.46	3.68	3.60
400	1.21	0.012	0.074	0.021	0.142	0.305	1.26	3.03	2.90
500	0.97	0.010	0.061	0.018	0.12	0.255	1.10	2.53	2.40
700	0.75	0.008	0.047	0.015	0.114	0.20	0.85	1.98	1.85
1000	0.55	0.006	0.034	0.011	0.106	0.155	0.63	1.49	1.41

The cross sections are expressed in units of 10^{-16} cm^2.

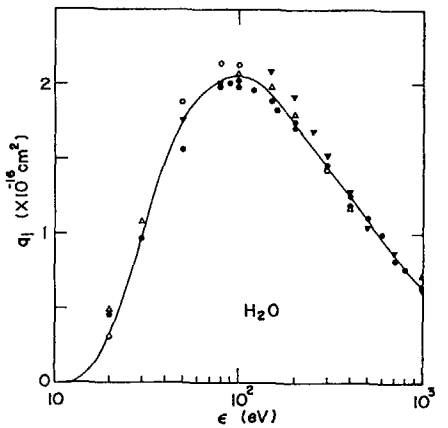

Figure 2. Total ionization cross sections for H_2O as a function of electron energy. Full curve is present tentative values. ● Schutten et al (1966), △ Olivero et al (1972) X 0.9, ▼ Bolorizadeh et al (1986) X 0.8, O Khare et al (1987) Theory.

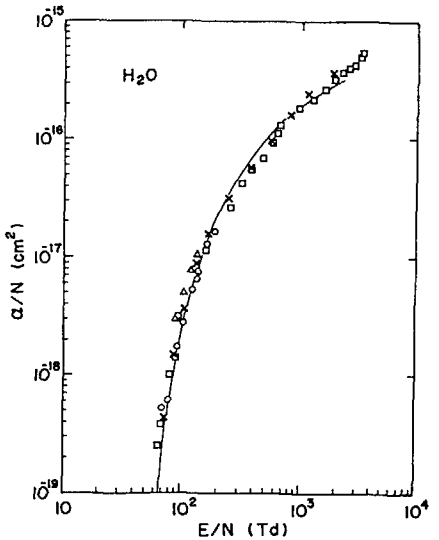

Figure 3. Townsend ionization coefficient for H_2O as a function of E/N, the ratio of electric field to gas number density. Full curve is present calculated values from the cross-sections shown in figure 1. Points are measured by Prasad (1960), Ryzko (1966), Risbud (1979) and Kodali (1982).

Table 3a. Momentum transfer cross-sections q_m for H_2O.

ε (eV)	q_m (X $10^{-16}cm^2$)	ε (eV)	q_m (X $10^{-16}cm^2$)	ε (eV)	q_m (X $10^{-16}cm^2$)
0	5000	0.9	17.2	12	9.2
0.01	2900	1.0	14.6	15	8.7
0.02	1380	1.2	11.2	20	7.6
0.03	880	1.5	8.65	25	6.47
0.04	645	1.7	7.7	30	5.5
0.05	500	2.0	6.8	40	3.99
0.06	410	2.2	6.35	50	2.94
0.07	345	2.5	6.07	60	2.24
0.08	298	2.7	6.0	70	1.78
0.1	233	3	6.03	80	1.45
0.12	190	3.5	6.25	100	1.05
0.15	150	4	6.55	120	0.84
0.2	110	5	7.25	150	0.64
0.3	70	6	8.0	200	0.464
0.4	51	7	8.6	300	0.296
0.5	39.3	8	8.95	400	0.204
0.6	31.2	9	9.2	500	0.152
0.7	25.0	10	9.3	700	0.091
0.8	20.7	11	9.3	1000	0.053

therefore, the values of Q_S almost coincide with Q_T values, as shown in table 2. Here Q_S is the sum of elastic and all inelastic q values, and Q_T is the recommended values of total collision cross-section measured by experiment directly. And also, swarm parameters calculated by these increased values of q_v are better than those calculated with the original ones.

Electronic excitation cross-sections q_e have to be measured experimentally in the near future. We have almost no experimental values of q_e for H_2O. If we have exact ionization cross-sections q_i,

Table 3b. Total attachment cross-sections q_a for H_2O.

ε (eV)	q_a (X $10^{-18}cm^2$)	ε (eV)	q_a (X $10^{-18}cm^2$)	ε (eV)	q_a (X $10^{-18}cm^2$)
4.3	0.00	6.9	4.7	8.7	1.02
5	0.02	7	3.6	9	0.70
5.5	0.07	7.1	3.1	9.5	0.37
5.8	0.22	7.2	2.4	10	0.20
5.9	0.80	7.3	1.6	10.2	0.19
6	2.5	7.5	1.1	10.5	0.24
6.1	4.3	7.6	0.90	11	0.40
6.2	5.5	7.7	0.80	11.2	0.50
6.3	5.9	7.8	0.80	11.3	0.50
6.4	6.2	8	1.00	11.5	0.40
6.5	6.3	8.2	1.25	12	0.18
6.6	6.2	8.3	1.30	12.5	0.05
6.7	5.9	8.4	1.30	13	0.00
6.8	5.3	8.5	1.25		

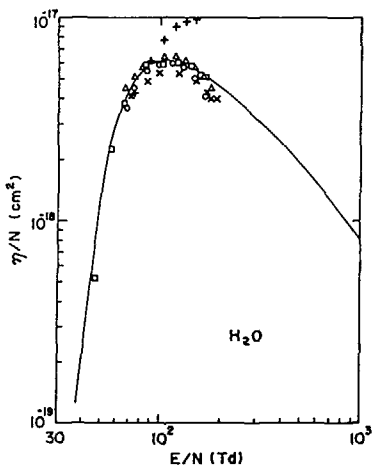

Figure 4. Electron attachment coefficient for H_2O as a function of E/N. Full curve is present calculated values. Points are measured by Prasad (1960), Crompton (1965), Ryzko (1966), Risbud (1979) and Kodali (1982).

together with q_m and q_v, we can determine the total q_e values from Townsend ionization coefficient α. The threshold region of q_e is very sensitive to the values of α at low E/N, around 100 Td for H_2O. The values of q_e have been separated into two parts, q_{e1} and q_{e2}. The values of q_{e1} are sum of q_e with threshold energies from 7.5 to 13.3 eV and q_{e2} are sum of q_e with threshold energies from 13.3 eV up to the ionization continuum limit, 16.6 eV. The transition of 9.7 eV threshold energy may have large q_e values, then for a more exact approximation q_e have to be separated into three values. To fit the values of α, we have determined the values of q_{e1} and q_{e2} tentatively, as shown in table 2.

Very interesting subject is the determination of total ionization cross-sections q_i for H_2O. There are very large discrepancies, about factor of 2, between experimental data. After some discussions and calculations, we have determined the values of q_i as shown in figure 2 and table 2. These values are much smaller than the values of Orient et al (1987). If we use the values of Orient et al, we have to increase the values of q_e too, and then the values of Q_S become much larger than Q_T for the 40 - 200 eV region. It is pointed out that the error of Q_T is about 5 %. Experimental data for q_i at lower than 60 eV are very scarce, so more studies are needed. Partial ionization cross-sections for H_2O^+ production have been measured by Mark et al (1976), but we could not convert these to total ionization cross-sections q_i.

Calculated values of Townsend ionization coefficients α and attachment coefficients η by using the new cross-section set are shown in figures 3 and 4, respectively, as compared with experimental data.

In table 2, each cross-section values q, sum of these cross-sections Q_S and recommended values of Q_T measured by a lot of experiments are shown. Momentum transfer cross-sections q_m and total attachment cross-sections q_a are given in table 3. This is our cross-section set for H_2O(1988).

ACKNOWLEDGEMENTS

The author wish to thank A. V. Phelps, R. W. Crompton, S. Trajmar, K. Takayanagi, Y. Itikawa, M. Inokuti, Y. Hatano and H. Nishimura for useful discussions and encouragement. I would like to say many thanks to my students, A. Niwa and M. Teranishi for their assistance.

P. S.

Very recently, new total ionization cross-section data for H_2O have been reported by Djurić et al (1988). These values are shown in

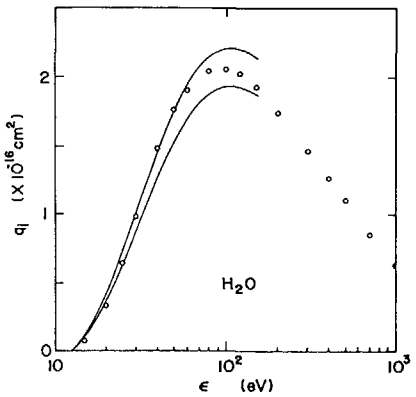

Figure 5. Total ionization cross-sections for H_2O as a function of electron energy. O Present values given in table 2, full curves are upper and lower limit values of q_i given by Djurić et al (1988).

figure 5 with our q_1 values of table 2. New data are almost same as our values, but we think that our values of q_1 have to improve a little.

Djurić N Lj, Čadež I M and Kurepa M V 1988 Int. J. Mass Spectrom. Ion Phys. 83, R7-R10

REFERENCES

Bolorizadeh M A and Rudd M E 1986 Phys. Rev. A33 882-887
Brescansin L M, Lima M A P, Gibson T L, McKoy V and Huo W M 1986 J. Chem. Phys. 85 1854-1858
Buckman S J and Phelps A V 1985 JILA Information Center Report No. 27, 1-14
Danjo A and Nishimura H 1985 J. Phys. Soc. Jpn. 54 1224-1227
Elford M T 1988 Abstracts of Japan-Australia Workshop on Gaseous Electronics and Its Applications 68-71
Gianturco F A and Jain A 1986 Phys. Rep. 143 347-425
Hayashi M 1987 Swarm Studies and Inelastic Electron-Molecule Collisions, Edited by Pitchford L C et al, Springer-Verlag 167-187
Inokuti M ed. 1984 Argonne National Laboratory Proceeding, ANL-84-28
Itikawa Y et al 1986 J. Phys. Chem. Ref. Data 15 985-1010
Itikawa Y et al 1987 ISAS Research Note 374 1-98
Jain A 1988 J. Phys. B21 905-924
Jain A K, Tripathi A N and Jain A 1988 Phys. Rev. A37 2893-2899
Katase A et al 1986 J. Phys. B19 2715-2734
Märk T D and Egger F 1976 Int. J. Mass Spectrom. Ion Phys. 20 89-99
Morrison M A, Crompton R W, Saha B C and Petrović Z Lj 1987 Aust. J. Phys. 40 239-281
Ness K F and Robson R E 1988 Australian Bicentenary Congress of Physics, Gaseous Electronics WM3
Nishimura H and Yano K 1988 J. Phys. Soc. Japan 57 1951-1956
Orient O J and Srivastava S K 1987 J. Phys. B20 3923-3936
Phelps A V 1985 JILA Information Center Report No. 28 1-11
Phelps A V and Pitchford L C 1985 JILA Inform. Center Rep. No. 26 1-21
Sato H, Kimura M and Fujima K 1988 Chem. Phys. Lett. 145 21-25
Schutten J, de Heer F J et al 1966 J. Chem. Phys. 44 3924-3928
Shyn T W and Cho S Y 1987 Phys. Rev. A 36 5138-5142
Sueoka O, Mori S and Katayama Y 1986 J. Phys. B19 L373-L378
Szmytkowski C 1987 Chem. Phys. Lett. 136 363-367
Tawara H et al 1987 IPPJ-AM-55, Inst. Plasma Phys., Nagoya Univ. 1-32
Trajmar S, Register D F and Chutjian A 1983 Phys. Rep. 97 219-356
Zaider M, Brenner D J and Wilson W E 1983 Radiat. Res. 95 231-247

200

FUNDAMENTAL PROCESSES IN RADIOLYSIS — COLLISION DYNAMICS DATA ON SOME ELEMENTARY PROCESSES

Y. HATANO
Department of Chemistry,
Tokyo Institute of Technology,
Tokyo, Japan

Abstract

A brief survey is given of recent progress in understanding fundamental processes in radiolysis with special emphasis on the present status of the knowledge of their cross section data and its implications to that of the condensed phase. Topics are chosen from our recent investigations of some elementary processes: (1) "Energy deposit" on molecular compounds: absolute VUV-photoabsorption and photoionization cross sections, (2) Dissociation of superexcited molecules, (3) Penning ionization and its related processes, and (4) Electron attachment processes.

1. Introduction

Radiation chemistry is of great importance in radiation research and may have an important role in understanding radiation therapy.

A brief survey is given in this paper of recent progress in understanding fundamental processes in radiolysis with special emphasis on the present status of the knowledge of their cross section data and its implications to that of the condensed phase.[1] Radiation chemistry needs collision cross section data, which must be correct, absolute, and comprehensive.[2] Radiation chemistry, however, has another important role in the relation between radiation research and atomic collision research. This is a fact that radiation chemistry is a source of new ideas and information in atomic collision research.[1] In this paper, therefore, topics are also chosen from our recent investigations of some elementary processes.

2. Fundamental processes in radiolysis

The succession of events that follow absorption in matter of high energy radiation is divided into three characteristic temporal stages: physical, physicochemical and chemical stages.[3] The physical stage of radiation effects is the primary activation of molecules due to the collision of high energy incident particles, i.e., photons, electrons, heavy charged particles, neutrons, etc., with molecules to form electronically excited or ionized states of molecules and ejected electrons. Electrons thus formed have energies enough to ionize again surrounding molecules. At the steady state of radiolysis, electrons are formed in a wide energy range via cascading electon-molecule collision processes as follows.[1]

Formation of electrons in a wide energy range
↓
Electron energy loss processes, i.e., electron molecule collision processes, and ionization and excitation of molecules.
↓
Formation of the lower energy electrons, and ionization and excitation of molecules.
↓
Electron disappearance, i.e., recombination, attachment and diffusion, and molecular dissociation, luminescence, internal conversion, intersystem crossing, and ion-molecule reactions, etc.
↓
Stable end-products

Consequently, electron-molecule collisions such as ionization and excitation of molecules, recombination or attachment of

TABLE 1. Fundamental Processes in the Radiolysis of a Liquid Organic Compound AB.[1)]

AB	$AB^+ + e^-$	; Direct ionization
	AB'	; Superexcitation
	AB*	; Excitation (Direct excitation)
AB'	$AB^+ + e^-$	; Autoionization
	A + B	; Dissociation
	AB''	; Internal conversion, etc.
AB^+	$A^+ + B$	; Ion dissociation
$AB^+ + AB$ or S	Products	; Ion-molecule reaction
$[AB^+ + e^-]$	AB*	; Geminate recombination
$AB^+ + e^-$	AB*	; Electron-ion recombination
$AB^+ + S^-$	Products	; Ion-ion recombination
$e^- + S$	S^-	; Electron attachment
$e^- + nAB$	e^-_S	; Solvation
AB*	A + B	; Dissociation
	AB*'	; Internal conversion and Intersystem crossing
	BA	; Isomerization
	AB + hν	; Fluorescence
AB* + S	AB + S*	; Energy transfer
AB* + AB	$(AB)_2$*	; Excimer formation
2A	A_2	; Radical recombination
	C + D	; Disproportionation
A + AB	A_2B	; Addition
	A_2 + B	; Abstraction

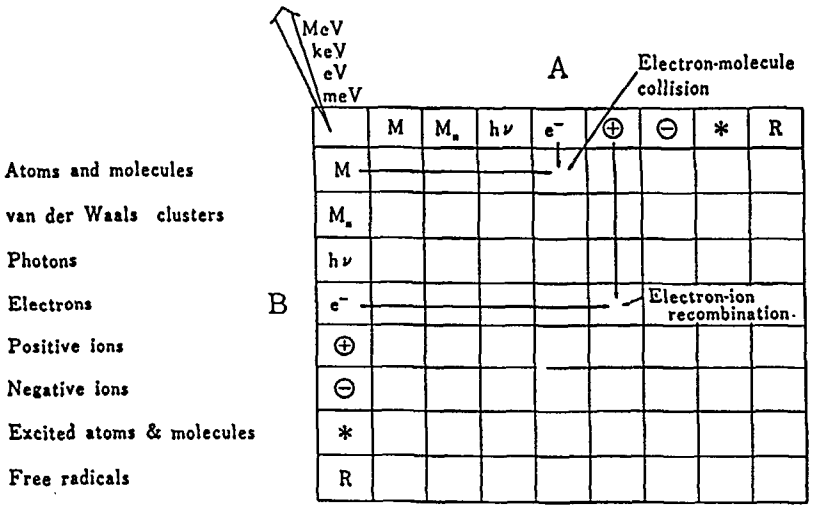

Fig. 1. The matrix representation of various collision processes between A and B at collision energies expressed by the vertical scale. Electron-molecule collisions, for example, are shown on the matrix. 1)

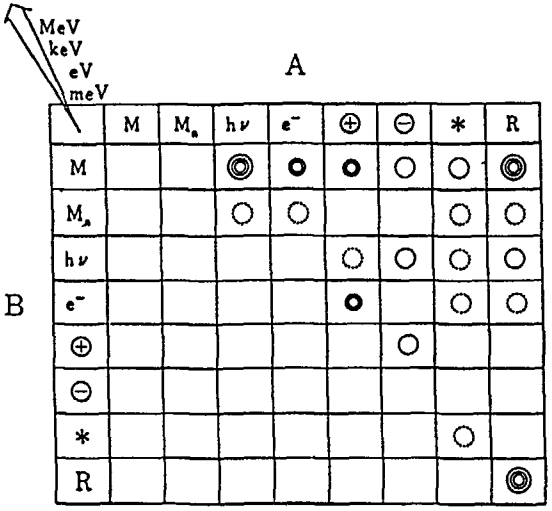

Fig. 2. A brief matrix-representation of the present status of the knowledge of each collision process. The data on a particular collision process at various collision energies are projected on the matrix. The degree of the data accumulation is expressed in the frame by the symbols; fom rich(◎) to poor (blank). 1)

electrons, etc , have an important role in radiolysis The physicochemical stage is the reaction of transient species such as excited and ionized states of molecules, free radicals, and electrons themselves The reaction of thermalized species like thermal free radicals, which are not unique to radiation chemistry, is sometimes called the chemical stage of the radiation effects

Let us consider and summarize briefly in Table 1 what happens when, for example, one MeV γ-rays are irradiated upon a liquid organic compound AB

A solvation process in Table 1 is not usually included in the fundamental processes in the gas-phase radiolysis, whereas this process is quite important in the condensed-phase radiolysis, particularly of polar compounds Recently, however, this process is considered to be important also in the gas phase A geminate recombination, characterizes condensed-phase radiolysis in addition to a free-charge recombination Transient species in radiolysis are thus classified as two types, firstly, charged species, i e , electrons and ions, and secondly, neutral species, i e , excited molecules and free radicals These species constitute the above mentioned fundamental processes in radiation chemistry In analyzing these processes radiation chemists must understand the present status of the knowledge of atomic collision research and elementary reaction dynamics The use of the matrix representation[1] is quite helpful to understand or to survey diverse information on these various processes For example, some electron collision processes are shown in Fig 1 The present status of the knowledge of each collision process is shown qualitatively in Fig 2 The results of a particular collision process at various collision energies are projected on the matrix The matrix representation is helpful not only for analyzing a complex mechanism of radiolysis but also for finding new ideas of collision dynamics research

3 Fundamental molecular parameters

Radiation chemistry needs the data on various fundamental gas phase molecular parameters, which must be correct, absolute and comprehensive [2] Since radiation chemists are interested in various molecules not only in the gas phase but also in the condensed phase, and in a variety of materials ranging from rare-gas atoms and diatomic molecules to complex molecules such as hydrocarbons, alcohols, etc , and to polymers, then fundamental gas-phase molecular parameters are of great importance in understanding radiation chemistry not only in the gas phase but also in the condensed phase These are divided into static and dynamic parameters The former includes ionization potentials, appearance potentials, electron affinities, and potential energy curves Thermochemical parameters such as basicities, acidities, proton affinities, and hydride-ion affinities of molecules and the parameters for cluster ions are also important The latter includes rate constants or cross sections for elementary reaction or collision processes which are listed in Table 1

4 Collision dynamics data on some elementary processes

A survey is given in the following of collision dynamics data on some elementary processes which are chosen from our recent research programs in progress These processes, as shown in Table 1, are of great importance in radiolysis

4 1 VUV-photoabsorption and photoionization cross sections and dissociation dynamics of superexcited molecules

A molecule which receives energy exceeding its ionization threshold (I_p) does not always ionize because the molecule

except monoatomic molecules have dissociation channels into neutral fragments. The ionization process competes with the neutral fragmentation. These processes are schematically represented in the following for a molecule AB.

$$AB + \text{Energy} \longrightarrow AB^+ + e^- \quad ; \text{Direct ionization} \quad (1)$$

$$(>I_p) \longrightarrow AB' \quad ; \text{Superexcitation} \quad (2)$$

$$AB' \longrightarrow AB^+ + e^- \quad ; \text{Autoionization} \quad (3)$$

$$AB' \longrightarrow A + B \quad ; \text{Dissociation} \quad (4)$$

$$AB' \longrightarrow \text{Others} \quad (5)$$

In this mechanism AB' is a superexcited molecule which decays through autoionization and dissociation (or neutral fragmentation). An ionization efficiency η is defined as σ_i/σ_t where σ_i is the cross section for both direct- and auto-ionization processes and σ_t is the cross section for the total energy absorption, i.e., the sum of the cross sections for direct ionization and superexcitation. The value of η in the energy region below the ionization threshold should be zero in general, while that above the threshold increases with increasing the energy and approaches unity in the energy region enough above the threshold. In the energy region above, but close to, the threshold the dissociation process plays a very important role in the decay of a superexcited molecule.

It has been pointed out both theoretically[3-5] and experimentally[6-9] that superexcited states, in particular neutral fragments formed from their dissociation, play an important role in radiolysis. The neutral fragments are translationally or vibrationally sometimes electronically excited because of a large internal energy of superexcited states. Such excited fragments are called hot atoms or free radicals, and expected to have anomalous reactivities.

For better substantiation of superexcited states and their dissociation processes, it is indispensable to measure the kinetic energy of dissociaion fragments and their angular distribution[10] as well as to measure the threshold energy of dissociation.[11] The former is translational spectroscopy, and the latter is excitation spectrum measurements. Electron impact experiments as combined with these measurements in the past two decades have made clear comprehensively at least an outline of the electronic structures of superexcited states and their dissociation processes for some simple molecules.[10] The superexcited states of molecules are molecular high Rydberg states converging individually to each ionic state and classified into the following three types.

1) Vibrationally (or rotationally) excited states.
2) Doubly excited states.
3) Innner-core excited states.

Recently synchrotron radiation as a new photon source has been used to substantiate further the electronic structures of superexcited states and their dissociation processes as well as to understand the formation mechanism of superexcited states.[12] An important role of synchrotron radiation in the chemistry of excitation and ionization of molecules is demonstrated in Fig. 3.

In the case of photon impact experimants at the photon energy E, $\sigma_t(E)$ corresponds to the optical oscillator strength distribution df/dE and the ionization efficiency $\eta(E)=\sigma_i(E)/\sigma_t(E)$ should be called the ionization quantum yield. Since these data have been very few particularly for chemically important molecules such as hydrocarbons and other organic molecules, the absolute $\sigma_t(E)$ and $\sigma_i(E)$ values of these molecules in some isomeric series such as C_3H_6, C_4H_8, C_6H_{12}, C_2H_6O and C_3H_8O isomers have been measured in the wavelength region from 30nm to the ionization threshold of each molecule (120-140nm).[13-16] Figure 4 shows, for example, the

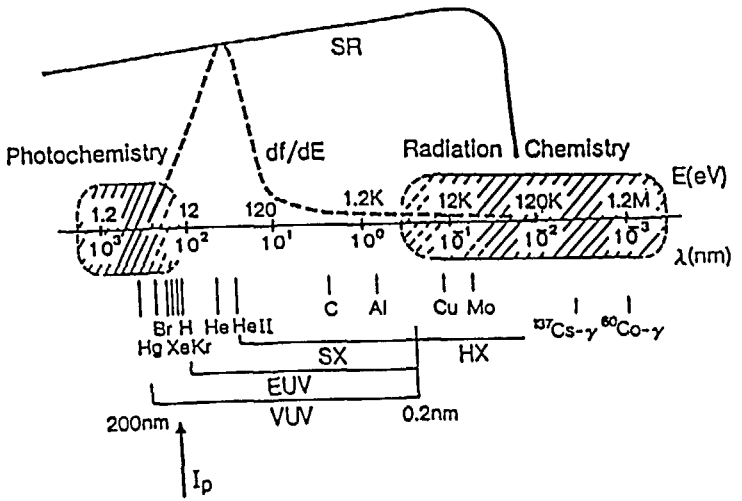

Fig. 3. The synchrotron radiation chemistry as a bridge between radiation chemistry and photochemistry.[12]

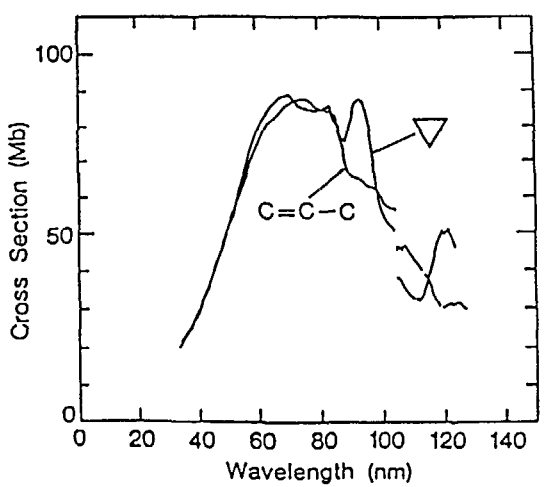

Fig. 4. Photoabsorption cross sections of the C_3H_6 isomer molecules, propylene and cyclopropane.[13]

$\sigma_t(E)$ values of the C_3H_6 isomers, i.e., propylene and cyclopropane.[13] The following are almost the common new features of the obtained $\sigma_t(E)$ and $\sigma_i(E)$ data for these isomeric series.

1) The $\sigma_t(E)$ values show the maximum at about 70-80 nm for each molecule, which means that the probability of the energy deposition on the molecule is the maximum at about 16-18eV.
2) In the wavelength region shorter than that at the maximum the $\sigma_t(E)$ values are almost the same among the isomers and equal to the sum of the cross sections for the constituent atoms.
3) In the longer wavelength region, however, the cross sections have different peaks and shoulders depending on an isomer, i.e. on its molecular structure.
4) The $\eta(E)$ value quickly increases from the ionization threshold with increasing the E value, shows a peak or a shoulder, and increases again at about the second ionization potential with increasing the E value. Comparing such $\eta(E)$ curves between different molecules, the following new interesting correlation has been obtained. With increasing the energy difference between the first and the second ionization potentials, the peak near the first threshold appears more clearly. With decreasing the energy difference it is more difficult to find a peak or a shoulder.
5) For some molecules, the $\eta(E)$ values are still clearly deviated from the unity even at the energy region of about 20 eV which is far above the threshold.

The obtained results will make an important contribution to fundamental physical chemistry particularly as a trigger to develop new quantum chemistry,[17] and will also make a helpful contribution to radiation research in estimating the energy deposition spectra of molecules.[12]

More detailed information has been obtained of the dissociation dynamics of superexcited molecular hydrogen using synchrotron radiation as an excitation source.[18,19] Similar experiments have been in progress also of more complex molecules.

A Lyman-α excitation spectrum has been observed using synchrotron radiation in the energy region corresponding to the double electron excitation of H_2.[18] This is the first observation of the neutral fragmentation process of the doubly excited states of H_2. There exist in the spectrum three thresholds which are compared with theoretically predicted Franck-Condon energy thresholds of doubly excited states. Lyman-α, Lyman-α coincidence[19] and Lyman-α angular disribution have been also measured. The cross section of Lyman-α fluorescence in the photodissociation of the doubly excited states is very small, e.g., in the order of 10^{-20} cm^2 at 30 eV, in comparison with that from the single electron excitation.[18,19] In the case of low energy electron impact dissociation of H_2, however, the dissociation cross section of the doubly excited states is not so different from that of the singly excited state.[10]

4.2 Electron attachment processes

Electron attachment is a process in which electrons are captured by atoms or molecules to form negative ions. Electron attachment or negative-ion formation processes are of great importance not only in atomic collision research but also in radiation research. Electron attachment processes have been extensively studied theoretically and experimentally, and these are comprehensively summarized in some review papers.[20-30] Electron atttachment processes are classified into two types; dissociative and non-dissociative processes as shown in the following reaction scheme,

$$e^- + AX \underset{1/\tau}{\overset{\sigma \text{ or } k}{\rightleftharpoons}} AX^{-*} \begin{cases} \nearrow A + X^- & (6) \\ \searrow AX^- + \text{energy}. & (7) \end{cases}$$

Interaction of low-energy electrons with molecules, AX, produces unstable negative ions, AX^{-*}, with a cross section σ or a rate constant k. The autodetachment of electrons from AX^{-*} with a lifetime τ may compete with the dissociation of AX^{-*} or with the formation of stable molecular negative ion, AX^-, which requires the release of excess energies from AX^{-*}. The lifetime τ is related to the electron-energy width of the attachment resonance. The value of $1/\tau$ is a rate constant for the autodetachment process. In the presence of third-body molecules, AX^{-*} is collisionally stabilized to form stable AX^-. The branching ratios among the unimolecular processes of decaying AX^{-*} depend on the interrelationship of the potential energy curves between AX and AX^-, and also on electron energies. The relative importance of the collisional stabilization process in the overall decaying processes of electrons depends largely on these unimolecular processes particularly the lifetime τ and of course on the number density and character of third-body molecules, in which one may expect some environmental effects on the overall scheme of electron attachment processes. In addition to the determination of cross sections or rate constants for electron attachment or negative-ion formation and their electron energy dependences, it has been of prime importance to clarify the attachment mechanism, not only the overall mechanism but how environmental conditions affect the mechanism.

Recent studies of thermal electron attachment to O_2, N_2O and other molecules have revealed that the electron attachment to pre-existing van der Waals (vdW) molecules or neutral clusters plays a significant role in the overall mechanism.[20,23] The experimental results have been compared with theories and discussed in terms of the effect of van der Waals interaction on the electron attachment resonance. The obtained conclusions have been related with investigations of electron attachment, solvation and localization in the condensed phase. A significant development in such studies has been started in electron attachment studies using experimental techniques which

were originated from radiation chemistry; one is the microwave technique combined with pulse radiolysis, the other is the competition kinetics of steady state γ-radiolysis. Such studies have given a important contribution to advances in electron attachment studies themselves and have triggered a very recent development in beam experiments of electron-van der Waals molecule collisions [31-33].

Since oxygen is probably the most extensively studied molecule in both experimental and theoretical investigation of low-energy electron attachment, the experimental results and discussion are briefly described in the following particularly for O_2 [20,23].

The well, and only, accepted mechanism has been the overall two-step three-body mechanism which was originally suggested by Bloch and Bradbury and was later modified by Herzenberg to be consistent with modern experimental data, the mechanism for O_2-M mixture, where M is a molecule other than O_2, is expressed as follows,

$$e^- + O_2 \xrightarrow{k_1} O_2^{-*} \qquad (8)$$

$$O_2^{-*} \xrightarrow{k_2} O_2 + e^- \qquad (9)$$

$$O_2^{-*} + O_2 \xrightarrow{k_3} O_2^- + O_2 \qquad (10)$$

$$O_2^{-*} + M \xrightarrow{k_4} O_2^- + M \qquad (11)$$

The vibrational characteristics of the negative ion O_2^{-*} are established from electron impact and scattering experiments and the electron affinity of O_2 is 0.44 eV. For convenience, the potential energy diagrams for $O_2(X^3\Sigma_g^-)$ and $O_2^-(X^2\Pi_g)$ are shown in Fig. 5. It can be seen that the lowest resonance involves the vibrational levels, O_2 (v=0) and O_2^- (v'=4), at low electron energies and the resonance energy is about 0.08 eV.

Since all electron-decays in O_2-M mixtures show pseudofirst order behavior, each decay curve gives an electron lifetime τ_0 which is related to the densities (O_2) and (M) as

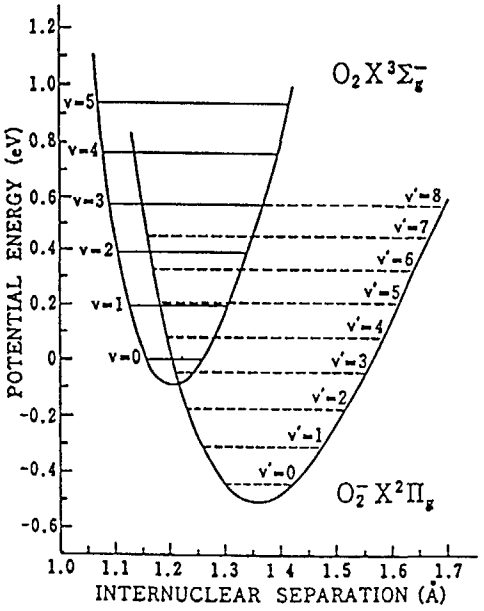

Fig. 5. Potential-energy curves for O_2 and O_2^- [20,23]

$$\tau_0[O_2] = \frac{1}{k_1} + \frac{1}{k_M[M]} \qquad (12)$$

when $(O_2) \ll (M)$, where $k_M (=k_1k_4/k_2)$ is the overall three body rate constant. Based on Eq.(12), Shimamori and Hatano[34] determined the value of $k_1 = 4.8\times10^{-11}$ cm^3/sec and the values of k_M for various stabilization partners. The autoionization lifetime of $O2^{-*}$ i.e., the value of $1/k_2$, was also estimated to be about 100 psec which was comparable to the predictions of theoretical treatments. There existed, however, some remarkable inconsistencies between these results and other data obtained by Christophorou and coworkers[35-37] from electron attachment experiments at very high gas pressures (<30 atm). They reported the value of k_1 much larger than that obtained by Shimamori and Hatano and correspondingly a considerably shorter lifetime of $O2^{-*}$ in

the order of 1 psec. Such inconsistencies have been demonstrated more clearly and analyzed by recent studies of Kokaku and coworkers.[38,39]. They have found that the BB mechanism can account for the data in the low pressure range but fails to explain the result at higher pressures. The result at higher pressures has been explained well by the following van der Waals molecule mechanism.

$$O_2 + M \underset{}{\overset{K_{eq}}{\rightleftharpoons}} (O_2 \cdot M) \qquad (13)$$

$$e^- + (O_2 \cdot M) \xrightarrow{k_5} (O_2 \cdot M)^{-*} \qquad (14)$$

$$(O_2 \cdot M)^{-*} \xrightarrow{k_6} O_2 + M + e^- \qquad (15)$$

$$(O_2 \cdot M)^{-*} + M \xrightarrow{k_7} O_2^- + 2M \qquad (16)$$

where K_{eq} is the equilibrium constant for vdW molecule formation. The density of vdW molecules is determined by $K_{eq}(O_2)(M)$, and the value of K_{eq} can be estimated by Stogryn and Hirschfelder's theoretical treatment.[40] Several experiments have provided evidnece for the existence of vdW molecules in the gas phase.[41,42] In the kinetic treatment made by Kokaku and coworkers,[38,39] the estimated values of k_5 are $(2\text{-}20)\times10^{-9}$ cm^3/sec depending on M, where it is highly attractive that all the values for k_5 are much larger than the value of k_1 $(=4.8\times10^{-11} cm^3/sec)$. This result shows that in the case of vdW molecules the initial electron capture mechanism differs Substantially from the case of isolated molecules. A recent study by Shimamori and Fessenden[43] has also verified clearly the presence of the vdW mechanism. They have measured the temperature dependence of three-body rate constants in pure O_2, O_2-N_2, and O_2-CO mixtures. The result for O_2 is shown in Fig. 6. According to Herzenberg's theory,[44] the three-body rate constant, as denoted

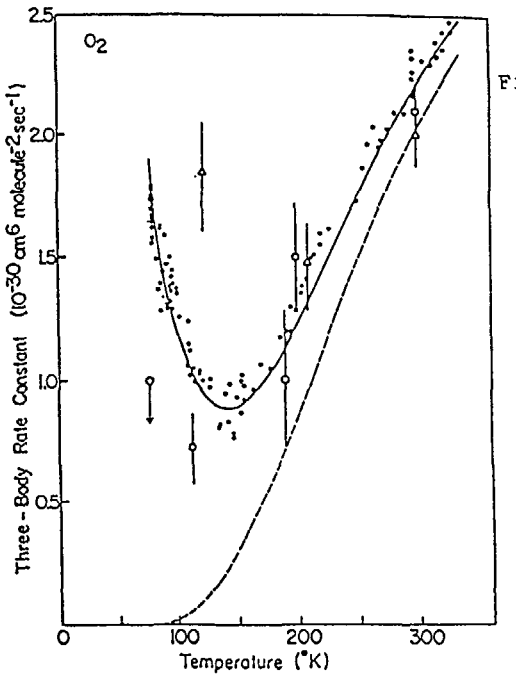

Fig. 6.

The temperature dependence of the three-body rate constant of O_2.[43] The broken line shows the temperature dependence of the rate constant calculated from Herzenberg's theory. The solid line shows a calculated curve which involves both the contributions from the broken line and the rate constant due to electron attachment to van der Waals molecule $(O_2)_2$.

here by k^{BB} which corresponds to the experimentally obtained k_M, can be expressed as

$$k^{BB} = \frac{2}{3}\left(\frac{h^2}{2\pi mk}\right)^{3/2} \xi \cdot k_L \cdot \left(\frac{1}{T}\right)^{3/2} \exp(-E_0/kT) \qquad (17)$$

where h, m, and k have their usual meanings, k_L the Langevin's rate constant, ξ the stabilization efficiency, T the absolute temperature, and E_0 the resonance energy. Equation (17) predicts a simple decrease in the rate constant with reduced temperature. The expected curve for O_2 calculated from Eq.(17) assuming ξ to be unity is drawn in Fig. 6. An extra contribution which increases with lowered temperature is evident, and explained well again by the electron attachment to the vdW molecule $(O_2)_2$. Since it has been verified, therefore,

TABLE 2. Rate Constant k_5, Resonance Energy E_r, Resonance Width Γ_5, Electron Density $v_r f_r$ and Cross Section σ_h.[20]

$(O_2 \cdot M)$	E_r(meV)	Γ_5(μeV)	$v_r f_r$	σ_h($\AA^2$)	k_5($10^{-11}cm^3/sec$)
$(O_2 \cdot N_2)$	20	800	0.71	2500	3000
$(O_2 \cdot C_2H_6)$	30	450	0.89	1700	1100
$(O_2 \cdot C_2H_4)$	45	270	0.92	1100	380
O_2	88(E_0)	10(Γ_1)	0.47	570	3(k_1)

that experimental evidence for the electron attachment to van der Waals molecules has been obtained from either pressure or temperature dependent experiment, Toriumi and Hatano[45-47] have changed systematically both pressure and temperature in the wide ranges and determined the important rate parameters for the BB mechanism such as the rate constant for the initial electron attachment to O_2 (k_1), the lifetime τ of O_2^{-*} i.e., the resonance width, and the overall three body attachment rate constants from the experiments on O_2-C_2H_6, O_2-C_2H_4 and O_2-N_2 mixtures. The values of τ are again in good agreement with those obtained by theories. Each three body rate constant is, respectively, smaller than that obtained previously without taking into consideration of the vdW mechanism. The value of k_1 obtained from O_2-N_2 system, which is selected as a convenient system to determine the value of k_1, is about $3\times10^{-11}cm^3/sec$. This value agrees within experimental errors with those obtained from O_2-C_2H_6 and O_2-C_2H_4 systems, and with the value, $4.8\times10^{-11}cm^3/sec$, which was obtained previously by Shimamori and Hatano. It should be noted here that the value, $3\times10^{-11}cm^3/sec$, is in good agreement with the theoretical values.[48-51]

The important rate parameters for the vdW mechanism such as the rate constant for the initial electron attachment to $(O_2 \cdot M)$ where M=C_2H_6, C_2H_4 and N_2, and the lifetime τ of $(O_2 \cdot M)^{-*}$, i.e., the resonance width, have been also obtained from this experiment and summarized in Table 2.[20] The values of k_5 in Table 2 are again much larger than the above-mentioned k_1 values. The resonance energy and width are also summarized in Table 2. The resonance energy for $e^- + (O_2 \cdot M) \rightarrow (O_2 \cdot M)^{-*}$ is much smaller than that for $e^- + O_2 \rightarrow O_2$, while its width for the former process is much larger than that for the latter process. The large enhancement in the attachment rate constant from k_1 to k_5 has been discussed qualitatively as related to the decrease in the resonance energy and the increase in the resonance width. The reason for the decrease in the resonance energy has been ascribed to the fact that the resonance state is much stabilized by the polarization interaction between O_2^- and M. Such situation is depicted in Fig. 7 where schematic potential energy curves are shown for O_2-M and O_2^--M systems.[20] Figure 7 shows that near to the equilibrium intermolecular distance the effective resonance energy of O_2^--M

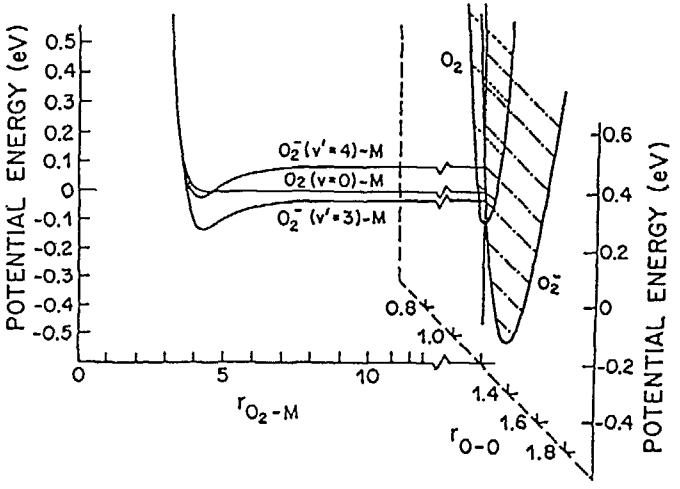

Fig. 7. A model of variation of potential energies for O_2(v=0)-M and O_2^-(v'=4)-M systems as a function of intermolecular distance.[20,23]

system is much reduced and even superimposed on the O_2-M curve. The existence of a number of vibrational states in both ion complex and neutral systems may be another major factor of the large transition probabilities.

At extremely low energy electron collision such as electron attachment to vdW molecules, a "small" vdW molecule is supposed to collide with "large" electron clouds, of which cross section is determined by a size of the de Broglie wave length of incident electrons. With decreasing the resonance energy, therefore, the attachment cross section should increase. It should be noted that the maximum value of emprically obtained cross section values for dissociative attachment processes at low energy are reasonably explained by the de Broglie wavelength of incident electron.[52,53]

The resonance width Γ_5 is expressed by the Wigner's threshould rule. In the case of isolated O_2 the resonance state $O_2^{-*}(X^2\Pi_g, v'=4)$ can couple with only one electronic partial wave with an angular momentum $\ell=2$. In the case of vdW molecules intermolecular interaction may couple with additional partial waves such as p wave and s wave with low energy. If the orbital of $O_2^-(\Pi g)$ is distorted by a third-body molecule, new attachment channels can open with lower angular momentum of electrons and the resonance width may increase.

It has been necessary to make a quantitative calculation of these effects using precise wave functions of O_2-M system. Very recently, Huo et al.[54] have made such calculations on O_2-N_2 system and compared their result with experiments. They have been successful in explaining the large enhancement in the attachment rate constant for vdW molecules using SCF wave functions.

The high pressure electron swarm data[35-37] which were simply elucidated only by the BB mechanism are well explained up to about 4×10^{20} molecules/cm^3 by the combination of the BB mechanism and the vdW mechanism.. It is obvious that the contribution from the vdW molecule is dominant in these density ranges. Electron attachment to O_2 has been investigated in supercritical hydrocarbon fluids at densities up to about 10^{22} molecules/cm^3 using the pulsed electric conductivity technique,[55] and the results have been explained in terms of the effect of the change in the electron potential energy and the polarization energy of O_2^- in the medium fluids. In general electron attachment to O_2 is considered to be a convenient probe to explore electron dynamics in the condensed phase.

A similar conclusion has been obtained also in the case of N_2O,[20,23] from which some general conditions have been extracted under which one can predict the existence of electron attachment to vdW molecules. The common feature to both O_2 and N_2O is that the rate constants of electron attachment to those isolated molecules are relatively small (10^{-11}-10^{-13}cm^3/sec) on an absolute scale. This is due to the presence of activation energy, i.e., the resonance energy, for electron attachment. In contrast there is virtually no activation energy in the electron attachment to vdW molecules containing O_2 or N_2O, thus yielding much larger rate constants for this process. The formation of vdW complexes appears to act just like it has an effect of lowering the activation energy or the resonance energy. Consequently one may expect to observe the contribution of vdW molecules only for compounds which have activation energies for electron attachment, or for the molecules of which attachment cross section for electron energies near thermal increases with increasing electron energy. One may expect generally that even in the case of molecules with negative electron affinities or with high threshold electron energies for attachment some environmental effects or the effect of the vdW molecule formation bring about the large enhancement in the cross sections or the rate constants for the lower energy electron attachment to these molecules.

Based on the discussions presented in the preceding sections, the reasons for such expectation are summarized as follows:[20,23]

1) The lowering of the resonance energy due to a deeper ion-neutral potential in comparison with neutral-neutral potential of the vdW molecule.
2) The additional vibrational structures of the vdW molecule.
3) The symmetry breaking due to the vdW interaction which allows the molecule to attach electron with additional partial waves.
4) The deformation of the molecular structure or the change of the vibrational modes due to the surrounding molecules.
5) The effective vibrational relaxation of the formed negative ion with excess energies due to the presence of a built-in third body molecule in the vdW molecule.

The distinct features of the electron attachment to vdW molecules as summarized above may become a substantial clue to understand the fundamental nature of electron attachment not only in dense gases but also in the condensed phase. It is also apparent that most of the electron attachment in bulk system is no longer a simple process as consisted of the interaction of electron with isolated molecules. A definitely important role of pre-existing vdW molecules formed by weak intermolecular force must be admitted.

4.3 Penning ionization and its related processes

Deexcitation processes of excited rare gas atoms play an important role in various phenomena in ionized gases. Penning ionization by long-lived metastable atoms has been studied experimentally using W-value methods, static aftergrow methods, flowing afterglow methods, beam methods, and pulse radioysis methods.[56,57] Comparative discussions on the methods have concluded a superior advantage of the pulse radiolysis method,[56] which was first demonstrated by Ueno and Hatano[58], over the other methods in determining absolute rate constant or cross section values for this process. The deexcitation rate constants of $He(2^3S)$ and $Ne(^3P0,1,2)$ by various atoms and molecules were obtained at room temperature using a pulse radiolysis method.[58-61] An attempt has been made to correlate the obtained rate constant values with various molecular parameters such as ionization potentials and polarizabibities. A relatively good correlation has been obtained for $He(2^3S)$ between the deexcitation probability P ($P=k_{ex}/k_{th}$) and the excess energy ΔE ($\Delta E=E_{He}-Ip(M)$), where k_{ex}, k_{th}, $E(He^*)$, and $Ip(M)$ are the experimentally obtained thermal rate constant, the calculated gas kinetic rate constant, the excitation energy of $He(2^3S)$, and the ionization potential of the target atom or molecule M, respectively. However, the reason for the correlation is not well understood. A similar experiment has been made also for the de-excitation of $Ne(^3P_2$, $^3P_1$, and $^3P_0)$ by atoms and molecules. A pulse radiolysis is very advantageous also to obtain the collisional energy dependence of cross sections. A velocity averaged absolute cross section, $_M$, is obtained as a function of mean collisional energy, E, from the temperature dependence of an absolute rate constant. Recently the temperature dependence of the rate constants has been measured for the deexcitation of $He(2^3S)$ by atoms and molecules.[62] According to the theory of Penning ionization, the collisional energy dependence of its cross section is given, if the interaction potential $V^*(R)$ for He^*-M and the autoionization rate $\Gamma(R)$ ħ from He^*-M to $He-(M^+-e^-)$ are obtained, by the following simple equation:

$$\sigma_T \propto E^{\alpha/\beta-1/2} \text{ or } k(T) \propto T^{\alpha/\beta} \qquad (18)$$

where σ_T and E are the total Penning ionization cross section and the collisional energy, respectively, and $\Gamma(R)$ and $V^*(R)$ are empirically represented as

$$\Gamma(R) = A \exp(-\alpha R), \qquad (19)$$
$$V^*(R) = B \exp(-\beta R), \qquad (20)$$

TABLE 3. The Values of α/β and P [62]

	α/β	P
N_2	1.4	0.05
CO	1.1	0.07
Ar	1.0	0.07
Kr	1.0	0.07
NO	0.6	0.16
O_2	0.6	0.18
C_2H_4	0.3	0.31
CO_2	0.1	0.39

where A, B, α, and β are constants and R is an intermolecular distance. The slope of log-log plots of k(T) vs T gives the values of α/β. The obtained α/β value for each molecule M listed in Table 3 increases with decreasing the value of P, where P is a de-excitation probability per collision or 1/P is an effective collision number for energy transfer. Since β is not so relatively different for each M, Table 3 shows clearly that the bigger α, i.e., the shorter range interaction between He(2^3S) and M, gives the smaller P, i.e., the less efficient energy transfer from He(2^3S) to M. This conclusion satisfies the exterior electron density model by Ohno et al.[66]

Deexcitation of the resonance state of rare gas atoms has been studied less extensively than that of the metastable state because of experimental difficulties owing to the short lifetime of the resonance state. There have been reported, however, several theoretical formulations[67,68] based on a long-range dipole-dipole interaction for the deexcitation cross section of radiative atoms. It has been, therefore, necessary to compare the theory with the results of the resonance or the lowest radiative state atoms. It has been reported[69,71] recently that the collisional energy dependence of the deexcitation cross sections of He(2^1P), Ar($^1P_1$), and Ar($^3P_1$) by atoms and molecules by using a pulse radiolysis method which is very advantageous to obtain the absolute values of the deexcitation cross sections of the resonance atoms as well as the metastable states.

A comparison, as shown in Fig. 8, between the experimental results of the collisional energy dependence of the de-excitation cross section of He(2^1P) by Ar and the theoretical ones calculated from the W-K theory[67] and the K-W[68] theory makes clearly possible for the first time to compare in detail the experimental results with theoretical ones.[69] The present experimental result can discriminate different theories and supports evidently the modified new theory, the K-W theory, which means that a theory should take the bent trajectory into consideration.

It is also the fact that very few studies have been reported on simple excitation transfer, in which Penning ionization is energetically impossible, from resonant rare gas atoms to atoms and molecules. The temparature dependence of the deexcitation

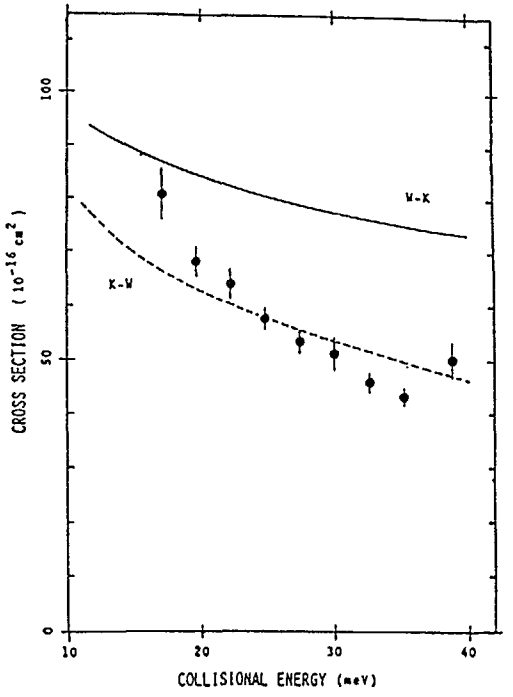

Fig. 8.

Collisional energy dependence of the deexcitation cross section of He(2^1P) by Ar; ●: Expriment; ——: WK theory; --- ; KW theory.[69]

rate constants of the resonance states of Ar, $^1P_1$ and $^3P_1$, by SF_6 and N_2 has been measured,[70] thus obtaining the collisional energy dependence of the deexcitation cross sections. The results of the cross sections for SF_6 are compared with the W-K theory and a good agreement is obtained. The results for N_2 agree with predictions of the cross sections for a nonresonant case. Even in the case of the de-excitation of the resonance state, such as $Ar(^1P_1)$ or $Ar(^3P_1)$, the cross section value and its collisional energy dependence are very similar to those for the metastable state, i.e., $Ar(^3P_0)$ or $Ar(^3P_2)$. This result satisfies again the W-K theory because of the fact that N_2 has almost no optical absorption in the energy of $Ar(^1P_1)$ and $Ar(^3P_1)$. It is concluded, therefore, that a long-range dipole-dipole interaction is important in the deexcitation processes of $Ar(^1P_1)$ and $Ar(^3P_1)$ by SF_6, but that a short-range interaction with curve crossing dominates in the deexcitation of $Ar(^1P_1)$ and $Ar(^3P_1)$ by N_2.

REFERENCES

1) Y. Hatano, Proceedings of the Workshop on Electronic and Ionic Collision Cross Sections Needed in the Medeling of Radiation Interactions with Matter, Argonne National Laboratory, Dec. 6-8, 1983, ed. M. Inokuti, ANL Report 84-28 (1984), P.27.

2) M. Inokuti, ibid., P. iii.

3) R. L. Platzman, Vortex, 23, 327 (1962).

4) R. L. Platzman, Radiat. Res., 17, 419 (1962).

5) R. L. Platzman, "Radiation Research", ed. G. Silini, North-Holland (1967), p.20.

6) Y. Hatano, S. Shida and M. Inokuti, J. Chem. Phys., 48, 940 (1968).

7) S. Shida and Y. Hatano, Int. J. Radiat, Phys. Chem., 8, 171 (1976).

8) Y. Hatano, "Hot Atom Chemistry: Recent Trends and Applications in the Physical and Life Sciences and Technology", ed. T.Matsuura, Kodansha (1984), p.98.

9)Y. Hatano, Radiochim. Acta, 43, 119 (1988).

10)Y. Hatano, Comments At. Mol. Phys., 13, 259 (1983).

11)F. J. de Heer, H. A. van Sprang and G. R. Möhlman, J. Chim. Phys., 77, 773 (1980).

12)Y. Hatano, "Radiation Research", ed. E. M. Fielden et al., Taylor and Francis (1987), p.35.

13)H. Koizumi, T. Yoshimi, K. Shinsaka, M. Ukai, M. Morita, Y. Hatano, A. Yagishita and K. Ito, J. Chem. Phys., 82, 4856 (1985).

14)H. Koizumi, K. Hironaka, K. Shinsaka, S. Arai, H. Nakazawa, A. Kimura, Y. Hatano, Y. Ito, Y. W. Zhang, A. Yagishita, K. Ito and K. Tanaka, ibid., 85, 4276 (1986).

15)H. Koizumi, K. Shinsaka, T. Yoshimi, K. Hironaka, S. Arai, M. Ukai, M. Morita, H. Nakazawa, A. Kimura, Y. Hatano, Y. Ito, Y. Zhang, A. Yagishita, K. Ito and K. Tanaka, Radiat. Phys. Chem., 32, 111 (1988).

16)H. Koizumi, K. Shinsaka and Y. Hatano, ibid., (1988), in press.

17)Y. Hatano, "Dissociation dynamics of superexcited molecules", in 5th Conf. At. Mol. Phys. Quant. Chem., Sydney, Jan. 25-29, 1988 (unpublished).

18)S. Arai, T. Yoshimi, M. Morita, K. Hironaka, T. Yoshida, H. Koizumi, K. Shinsaka, Y. Hatano, A. Yagishita and K. Ito, Z. Phys. D4, 65 (1986).

19)S. Arai, M. Kamosaki, M. Ukai, K. Shinsaka, Y. Hatano, Y. Ito, H. Koizumi, A. Yagishita, K. Ito and K. Tanaka, J. Chem. Phys., 88, 3016 (1988).

20)Y. Hatano, "Electronic and Atomic Collisions", ed. D. C. Lorents, W. E. Meyerhof and J. R. Peterson, Elsevier (1986), p. 153.

21)R. N. Compton, "Photophysics and Photochemistry in the Vacuum Ultraviolet", ed. S. P. McGlynn, G. L. Findley and R. H. Huebner. D. Reidel Publ. Co. (1985), p.261.

22)L. G. Christophorou, D. L. McCorkle and A. A. Christodoulides, "Electron-Molecule Interactions and Their Applications", Vol.1, ed. L. G. Christophorou, Academic Press (1984), p.477.
23)Y. Hatano and H. Shimamori, "Electron and Ion Swarms", ed. L. G. Christophorou, Pergamon (1981), p.103.
24)R. N. Compton, "Electronic and Atomic Collisions", ed. N. Oda and K. Takayanagi, North-Holland (1980), p.251.
25)H. S. W. Massey, "Negative Ions", Cambridge Univ. Press (1976).
26)G. E. Caledonia, Chem. Rev., 75, 333 (1975).
27)G. J. Schulz, Rev. Mod. Phys., 45, 423 (1973).
28)L. G. Christophorou, "Atomic and Molecular Radiation Physics", Wiley Interscience (1971).
29)R. N. Compton and R. H. Huebner, Adv. Radiat. Chem., 2, 281 (1970).
30)J. N. Bardsley and F. Mandl, Rept. Prog. Phys., 31, 471 (1968).
31)A. Stamatović, "Electronic and Atomic Collisions", ed. H. B. Gilbody, W. R. Newell, F. H. Read and A. C. H. Smith, North-Holland (1988), p.729.
32)T. D. Märk, ibid., p.705.
33)T. D. Märk, K. Leiter, W. Ritter and A. Stamatović, Phys. Rev. Lett., 55, 2559 (1985).
34)H. Shimamori and Y. Hatano, Chem. Phys., 21, 187 (1977).
35)L. G. Christophorou, Chem. Rev., 76, 409 (1976).
36)R. E. Goans and L. G. Christophorou, J. Chem. Phys., 60, 10 (1974).
37)D. L. McCorkle, L. G. Christophorou and V. E. Anderson, J. Phys. B5, 1211 (1972).
38)Y. Kokaku, Y. Hatano, H. Shimamori and R. W. Fessenden. J. Chem. Phys. 71, 4883 (1979).
39)Y. Kokaku, M. Toriumi and Y. Hatano, ibid., 73, 6167 (1980).
40)D. E. Stogryn and J. O. Hirschfelder, ibid., 31, 1531 (1959).
41)B. L. Blaney and G. E. Ewing, Ann. Rev. Phys. Chem., 27, 553 (1976).
42)B. M. Smirnov, Sov. Phys. Usp., 27, 1 (1984).
43)H.Shimamori and R. W. Fessenden, J. Chem. Phys., 74, 453 (1981).
44)A. Herzenberg, ibid., 51, 4942 (1969).
45)M. Toriumi and Y. Hatano, ibid., 79, 3749 (1983).
46)M. Toriumi and Y. Hatano, ibid., 81, 3748 (1984).
47)M. Toriumi and Y. Hatano, ibid., 82, 254 (1985).
48)F. Koike, J. Phys. Soc. Jpn., 35, 1166 (1973).
49)F. Koike, ibid., 39, 1590 (1975).
50)F. Koike and T. Watanabe, ibid., 34, 1022 (1973).
51)G. Parlant and F. Fiquet-Fayard, J. Phys., B9, 1617 (1976).
52)L. G. Christophorou and J. A. Stockdale, J. Chem. Phys., 48, 1956 (1968).
53)L. G. Christophorou, Environmental Health Perspectives, 36, 3 (1980).
54)W. M. Huo, R. W. Fessenden and C. W. Bauschlicher, Jr., J. Chem. Phys., 81, 5811 (1984).
55)M. Nishikawa and R. A. Holroyd, ibid., 79, 3754 (1983).
56)Y. Hatano, "Current status of destruction rate constant measurements involving electronically excited species", in 3rd Int. Symp. on Dynamics of Molecular Collisions, Kaiserslautern, 1983 (unpublished).
57)A. J. Yencha, "Electron Spectroscopy: Theory, Techniques and Applications", Vol.5, ed. C. R. Brundle and A. D. Baker, Academic Press (1984), p.197.
58)T. Ueno and Y. Hatano, Chem. Phys. Lett., 40, 283 (1976).
59)T. Ueno, A. Yokoyama, S. Takao and Y. Hatano, Chem. Phys., 45, 261 (1980).
60)A. Yokoyama, S. Takao, T. Ueno and Y. Hatano, ibid., 45, 439 (1980).
61)A. Yokayama and Y. Hatano, ibid., 63, 59 (1981).
62)H. Koizumi, M. Ukai, Y. Tanaka, K. Shinsaka and Y. Hatano, J. Chem. Phys., 85, 1931 (1986).
63)A. Niehaus, Adv. Chem. Phys., 45, 399 (1981).
64)A. Niehaus, "Eletronic and Atomic Collisions", ed. S. Datz, North-Holland (1982), p. 237.

65)A.Niehaus, "Radiation Research", ed. O F. Nyggard, H. I . Adler and W. K. Sinclair, Academic Press (1975), p.227.

66)K. Ohno, S Matsumoto and Y. Harada, J Chem. Phys., 81, 4447 (1984)

67)T. Watanabe and K. Katsuura, ibid., 47, 800 (1967).

68)M. Kohmoto and T Watanabe, J. Phys.,B10, 1875 (1977).

69)M. Ukai, Y Tanaka, H. Koizumi, K Shinsaka and Y. Hatano, J Chem Phys , 84, 5575 (1986)

70)M Ukai, H. Koizumi, K Shinsaka and Y. Hatano, ibid., 84, 3199 (1986)

71)M Ukai, H. Nakazawa, K Shinsaka and Y. Hatano, ibid., 88, 3623 (1988)

CHARGE TRANSFER INVOLVING DOUBLY CHARGED IONS: LOW ENERGY SCATTERING EXPERIMENTS AS A SOURCE OF STATE-TO-STATE RELATIVE CROSS-SECTION DATA

Z. HERMAN, J. VANČURA
J. Heyrovský Institute of Physical Chemistry
and Electrochemistry,
Czechoslovak Academy of Sciences,
Prague, Czechoslovakia

Abstract

Single-charge transfer processes of doubly charged atomic and molecular ions are important elementary processes in ionized media. Their state-selective cross sections are in agreement with the "reaction window" concept. The possibility of obtaining state-to-state relative cross sections of these processes in the eV and sub-eV collision energy region from scattering experiments is discussed.

1. INTRODUCTION

Elementary processes of charge transfer (charge exchange, electron capture) play an important role in systems with high energy content. Considerable attention has been paid so far to obtaining information on processes involving singly-charged ions and large amount of data exists on systems involving both atoms and molecules. Much less attention has been paid to charge transfer processes involving multiply charged ions, though their role in ionized media is of importance, too. In particular, they represent a class of elementary collision processes in which large amounts of energy (20 eV or more) are typically transferred.

During the last decade there has been an increase of interest in studies of processes involving multiply-charged ions. The motivation came mainly from plasma physics, studies of ionosphere and astrophysical plasmas. This motivation determined also the atomic and molecular systems investigated (mostly atomic ion - atom processes). However, important achievements have been reached concerning both kinetics and dynamics of these processes which are of general character, and may form a guideline for studies of suitable, possibly more complicated systems of interest for the purposes of this conference.

Besides data on absolute total cross sections of charge transfer processes involving multiply charged ions, present experiments provide information on relative and absolute cross sections of electronic state-to-state processes which are of basic importance for full understanding of the ionization structure of fully or partly ionized systems.

In this contribution we will confine our attention to elementary processes of single-charge transfer (SCT) between atomic (A) and molecular (M) doubly-charged ions which, in principle, may be classified in the following way (AB, CD means a diatomic or a polyatomic molecule):

$A^{++} + C \rightarrow A^{+} + C^{+}$	A-A SCT	(1)
$AB^{++} + C \rightarrow AB^{+} + C^{+}$	non-dissociative M-A SCT	(2)
$AB^{++} + C \rightarrow A^{+} + B + C^{+}$	dissociative M-A SCT	(3)
$AB^{++} + C \rightarrow A^{+} + B^{+} + C$	collisional dissociation of M	(4)
$A^{++} + CD \rightarrow A^{+} + CD^{+}$	non-dissociative A-M SCT	(5)
$A^{++} + CD \rightarrow A^{+} + C^{+} + D$	dissociative A-M SCT	(6)
$AB^{++} + CD \rightarrow AB^{+} + CD^{+}$	non-dissociative M-M SCT	(7)
$AB^{++} + CD \rightarrow A^{+} + B + CD^{+}$ etc.	dissociative M-M SCT	(8)

Only some of the types of processes outlined above have been studied so far. The interest of atomic and plasma physicists concentrated most of the attention to process (1). Together with it, usually some simple molecular targets (H_2, N_2, NO, O_2) have been studied (process (5) and (6)), mostly at high collision energies. Collisional dissociation of polyatomic ions represents a specific area in mass spectrometry and will not be treated here. Quite recently,data are beginning to appear on molecular dication charge transfer, process (2). Practically no information exists or processes (8) and (9).

2. SOURCES OF DATA

Data on charge transfer of multiply-charged ions come from studies at very different collision energies:

- studies at collision energies of 10^2 - 10^4 eV represent a typical domain of atomic physics related to plasma physics. Earlier work has been summarized in monographies (e.g., ref.[1]). An excellent review of atomic processes involving multiply-charged ions has appeared recently[2]. The data concern mostly state-specific relative and absolute total cross sections of processes (1) obtained by the translational spectroscopy method in special instruments [3-6] or double-focusing mass spectrometers used in special arrangements[7]. Data on numerous atom ion- atom systems are available for this keV collision energy region;
- beam scattering studies at low collision energies (several eV or sub-eV)[8-10] provide information on relative total and differential cross sections of state-selected processes; some of the results will be discussed later on;
- data from swarm studies concern the region of thermal and hyperthermal energies (up to a few eV); selected-ion-flow-tube (SIFT) [11] and drift-tube [11,12] experiments have provided a wealth of data on absolute total cross sections and rate coefficients for many atomic processes of the type (1) involving doubly-charged ions; however,the data are only rarely state-selective: only if another competing process can be used to quench specifically a reactant excited state, selection of reactants is possible; state selection of products is difficult.

3. GENERAL FEATURES OF THE PROCESS

Charge transfer from doubly and multiply charged ions is a process in which large amount of energy is transferred to the target. Double ionization potentials of atoms and simple molecules lie at 35 - 45 eV and thus the energy exchanged in a single-charge transfer process, i.e. the difference between the double and single ionization potential of the projectile may be in excess of 20 eV, for multiply charged ions even higher.

Available data show a considerable variation in the total cross sections of these processes. In the range of thermal energies, the largest (not state specific) cross sections for atomic systems (e.g., Kr^{++}+ Kr, Ar^{++} + Ar, Ar^{++} + He [12,13]) attain values of 10 to 100 $Å^2$, in some cases thus approaching the Langevin limit. The energy dependence over a wide range of collision energies shows usually a slowly decreasing total cross section (as an example, see a summary of results for Ar^{++}+ He [13] in Fig. 1). State-to-state total cross sections exhibit a variation of several orders of magnitude (10^{-2} - 10 $Å^2$), depending on the exoergicity of the process. Endoergic channels appear only at high collision energies and their cross section is usually quite small. Clearly, this wide variation in state-selective cross sections is connected with the mechanism of the process.

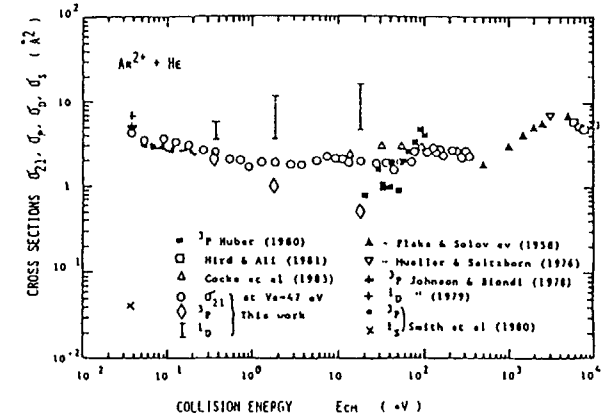

Fig.1: Total non-state-selective and state-selective cross section for Ar^{++} + He system (from ref. [13]).

A simple model was formulated which explains this variation in state-to-state total cross section [3,8,11,14,15]for atomic systems. Is is based on crossing of potential energy curves of the reactant and product pairs and assumes that the cross section is essentially determined by Landau-Zener type transitions in the vicinity of these crossings. The mechanism is illustrated in Fig. 2 for the Ar^{++} + He system. The slightly attractive, ion-induced dipole potential energy curves of the reactart systems Ar^{++} + He (V_{ID}) cross with the Coulombic repulsive curve of the product ions Ar^{+} + He^{+} (V_C). The crossing point, R_{CR}, occurs at different internuclear separations depending on the exoergicity of the process in question (3 eV, R_{CR}= 4.8 Å for $Ar^{++}(^3P)$, 4.74 eV, R_{CR}= 3.0 Å for $Ar^{++}(^1D)$). If the curve crossing occurs within a limited range of internuclear separations, 2 - 7 Å (corresponding to exoergicities about 7 - 2 eV), then there is a significant probability of a single electron transfer resulting in a fairly large charge transfer cross section of the particular reaction channel. This 'reaction window" concept car be applied over a wide range of collision energies. With increasing collision erergy the 'reaction window' moves to smaller internuclear separation in accordance with the changes in the Landau-Zener transition probability with energy. At high collision energies the system has to be treated in terms of the multiple-crossing concept.

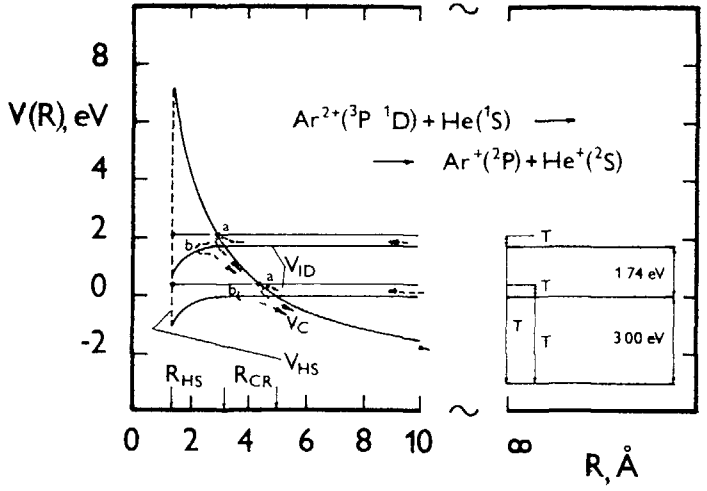

Fig. 2 Potential energy curves of the reactants and products in Ar^{++} + He (from ref. [8]).

For more complicated systems (atomic ion-molecule, molecular ion-atom) the' reaction window" concept is at least approximately applicable, too [16,17]. In case of the atomic ion- atom charge transfer process the exoergicity of the electronic state-to-state process appears as relative product translational energy. If molecular projectiles or targets are involved, excess energy may appear as internal (vibrational and rotational)excitation of the molecular product and more complicated crossings of potential energy surfaces are involved. Basic features of the treatment of atomic systems may be at least qualitatively used for molecular processes, too.

4. STATE-SELECTIVE RELATIVE CROSS SECTIONS FROM LOW ENERGY SCATTERING

State-to-state total cross sections are important in understanding the population of electronic states of particles in systems with high energy content. In the first approximation, high collision energy data on charge transfer of doubly charged ions can be used in description of systems treated in this meeting. Eventually, however, one would like to have thermal or near-thermal cross section data. Unfortunately,swarm experiments offer state-selected data only in some cases. We believe that low energy beam data (at eV and sub-eV energies)may serve as one of the possible sources of this information, though themain purpose of these studies is reaction dynamics. At low collision energies the products are usually scattered over an appreciable solid angle and thus the translational energy measurements in beam experiments have to be combined with angular measurements. It is, naturally, difficult and not practical to derive from crossed beam experiments information on absolute total cross sections, due to difficulties in determining target particle concentration in the neutral beam with sufficient accuracy, but relative state-selected data can be obtained. In the following we will describe several examples of exploiting results of crossed beam scattering experiments from our laboratory for this purpose.

The single-collision crossed beam scattering experiment in based on crossing a low energy (a few eV in the laboratory system) beam of a doubly charged ion, prepared by electron impact, with a thermal beam of the neutral target. Measurements of the angular distribution of a product ion and its translational energy distribution at a series of scattering angles makes it possible to obtain the scattering diagram of the product ion. Fig. 3 shows, as an example, the scattering diagram of the Ar^+ product ion from the charge transfer process

$$Ar^{++}(^3P,^1D) + He(^1S_o) \rightarrow Ar^{+}(^2P) + He^{+}(^2S_{1/2}) \qquad (9)$$

at the collision energy of 0.53 eV [8]. The two state-to-state processes are exoergic by 3.0 eV and 4.74 eV for the ground state $Ar^{++}(^3P)$ and excited metastable $Ar^{++}(^1D)$, respectively.

The two intensity ridges in the contour scattering diagram along the concentric circles correspond to Ar^+ formed in the two state-to-state processes (the $Ar^{++}(^1S)$ reactant has a negligible cross section). It can be seen from the figure that by measuring only at one scattering angle (e.g., ϑ= 0°) one would get an erroneous information on the ratio of state-selected cross sections. Only by appropriate integration of the annuli in the scattering diagram

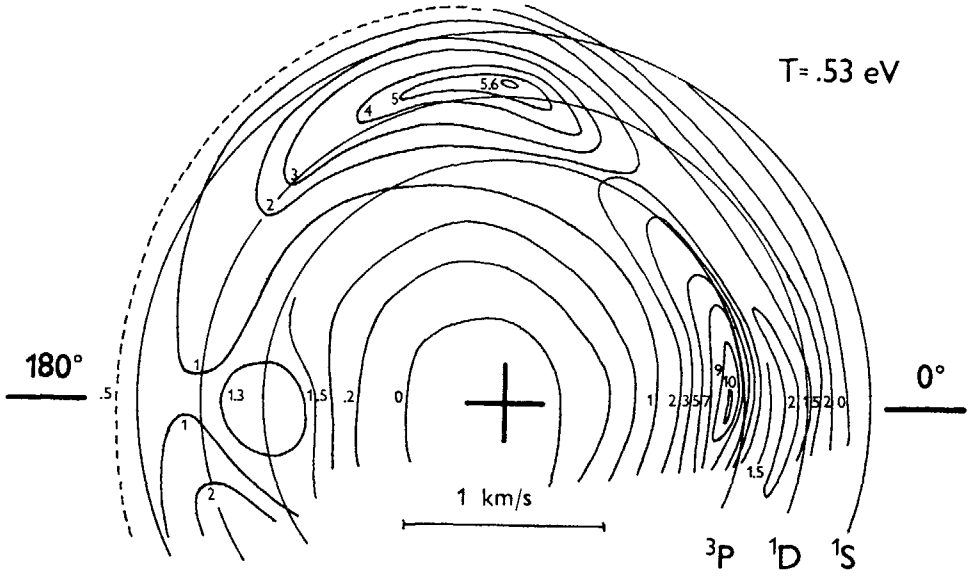

Fig. 3: Scattering contour diagram of Ar^+ from reaction (9) (from ref. [8]).

one arrives at meaningful ratios of the cross sections. In this case the result is $\sigma(^3P)/\sigma(^1D) = 0.32$. This value is based on the relative concentration of the two reactant states in the beam $Ar^{++}(^3P)$: $Ar^{++}(^1D) = 2 : 1$ known from other measurements [17,18].

In another study [10], we investigated the reaction system Kr^{++} + He and we were able to determine the ratio of state-to-state cross sections for the formation of the two spin-orbit states of the product Kr^+. The processes investigated were

$$Kr^{++}(^1S) + He(^1S_o) \rightarrow Kr^+(^2P_{3/2}) + He^+(^2S_{1/2}) \quad \Delta E = 4.07 \text{ eV} \quad (10a)$$

$$\searrow Kr^+(^2P_{1/2}) + He^+(^2S_{1/2}) \quad \Delta E = 3.42 \text{ eV} \quad (10b)$$

At the collision energies of 0.31 eV and 0.5 eV the ratio of state-to-state cross sections, $\sigma(3/2) / \sigma(1/2)$ was 1.1 and 1.0, respectively.

The third example concerns determination of the ratio of cross sections for the formation of the ground and excited state of the N^+ ion in the charge transfer process

$$N^{++}(^2P) + He(^1S_o) \rightarrow N^+(^3P) + He^+(^2S_{1/2}) \quad \Delta E = 5.02 \text{ eV} \quad (11a)$$

$$\searrow N^+(^1D) + He^+(^2S_{1/2}) \quad \Delta E = 3.12 \text{ eV} \quad (11b)$$

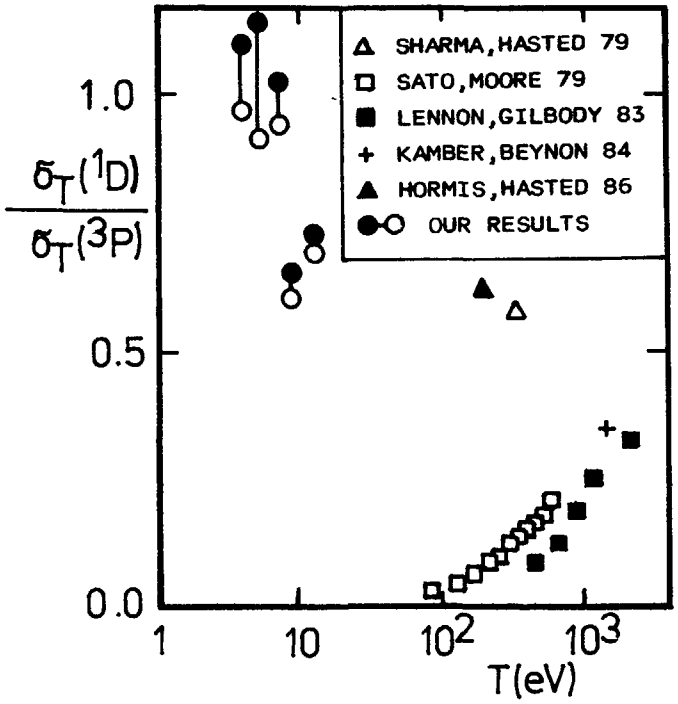

Fig. 4: Ratio of the total cross sections for the formation of ground and excited state of N^+ from reaction (11) in dependence on collision energy.

Only high energy data were available for this process and our low energy data showed that the ratio changes considerable in favour of the excited state [19]. Fig. 4 summarizes data from various sources over a wide collision energy range.

5. SUGGESTIONS FOR FUTURE RESEARCH

Most of the available data on charge transfer involving multiply charge ions concern processes which can be regarded, from the point of view of this meeting, as model processes only (rare gases, metal ions, hydrogen). The information need to be expanded, even for simplest systems, to studies of processes of doubly and multiply charged ions of biogenic elements and they should include molecular systems in particular. Some progress in this direction has been made (processes involving , e.g. CO^{++} [16], N_2^{++}, O_2^{++}, NO^{++} [20]).

Very little is known about polyatomic multiply charged projectiles and their charge transfer reactions. On the other hand, charge transfer between simple multiply charged ions and polyatomic molecules could provide new important data. We may expect also here that the "reaction window" concept will channel about 2 - 6 eV into the relative translational energy of the products, but the remaining transferred energy will be distributed to ionize the molecule and to excite the molecular ion; this means absorbing about 10 - 20 eV in excess of the ionization potential of the molecule. In a polyatomic molecular ion this will presumably lead to dissociation and the fragmentation patterns of molecular ions with unusually high internal energy content, easily achieved by charge transfer of this type, appear to be an interesting area of research to explore.

REFERENCES

1. J.B. Hasted, Physics of Atomic Collisions, Butterworths, 1972.
2. R.K. Janev, H. Winter, Physics Reports 117 (1985) 265, North-Holland, Amsterdam.
3. Y.Y. Makhdis, K. Birkinshaw, J.B. Hasted, J.Phys.B, At.Mol.Phys. 9 (1976) 111.
4. B.A. Huber, J.Phys.B, At.Mol.Phys. 13 (1980) 809.
5. M. Lennon, R.W. McCullough, H.B. Gilbody, J.Phys.B, At.Mol.Phys. 16 (1983) 443.
6. N.Kobayashi, T. Nakamura, Y. Kaneko, J.Phys.Soc.Japan 52(1983)2684.
7. R.P. Morgan, J.H.Beynon, R.H.Bateman, B.N.Green, Int. J. Mass Spectrom.Ion Processes 28 (1978) 171.
8. B. Friedrich, Z. Herman, Chem.Phys.Lett. 107 (1984) 375.
9. B.Friedrich, J.Vančura, M.Sadílek, Z.Herman, Chem.Phys.Lett. 120 (1985) 243.
10. B.Friedrich, J.Vančura, Z. Herman,Int. J. Mass Spetrom. Ion Processes 80 (1987) 177.
11. D. Smith, N.G.Adams, E.Alge, H.Villinger, Q.Lindinger, J.Phys.B, Atom.Mol.Phys. 13 (1980) 2787.
12. T. Koizumi, K.Okuno, Y.Kaneko, J.Phys.Soc. Japan 53 (1984) 567.
13. K.Okuno, Y.Kaneko, Atomic Collision Research in Japan 10 (1984) 59.
14. K.G.Spears, F.C.Fehsenfeld, M.McFarland, E.E.Ferguson, J.Chem. Phys. 56 (1972) 2562.
15. B.Friedrich, Š.Pick, L.Hládek, Z.Herman, E.E.Nikitin, A.I.Reznikov, S.Y. Umanskii, J.Chem.Phys. 84 (1986) 807.
16. Z. Herman, P.Jonathan, A.G.Brenton, J.H.Beynon,Chem.Phys.Lett. 141 (1987) 433.
17. K.Okuno, A. Fukuroda, N.Kobayashi, Y.Kaneko, Papers of the XVth ICPEAC, Brighton, 1987.
18. N.Kobayashi, Y. Kaneko, private communication.
19. J.Vančura, M.Sadílek, Z.Herman, to be published.
20. Z.Herman, P.Jonathan, A.G.Brenton, J.H.Beynon, Chem.Phys. (in print).

CROSS-SECTIONS FOR 0.025 eV-1 keV ELECTRONS AND 10 eV-1 keV PHOTONS

M. TERRISSOL, M.C. BORDAGE,
V. CAUDRELIER, P. SEGUR
Centre de physique atomique,
Université Paul Sabatier,
Toulouse, France

Abstract

We present total and differential cross-section for ionization and excitation of every atomic or molecular energy level, following electron or photon impact on gases relevant for radiotherapy studies such as H, N, O, He, Ar, H_2, N_2, O_2, CO_2, CH_4 or H_2O. For photons, we present here a method to obtain photoionization cross-sections for molecules. For electron after a review on all interaction processes, we show total, differential or momentum transfer cross-sections for elastic scattering and selected molecules. The methods used to obtain or derive from experimental data these cross-sections are quickly presented or discussed as well as all bibliographic references.

Introduction

Computer simulation of particle transport is an excellent way of investigation and its usefulness is not to improve. Whatever methods used, necessary basic data are cross-sections of all interactions and events along and around the path of the initial particle, until thermodynamic, chemical and biological equilibria are reached.

Simulation must be the most realistic possible : for instance, OH and H radicals have a great importance at the DNA level and the simulation must be able to follow their " whole life " . Particles such as electrons are active until and after their thermalization (0.025 eV) and aqueous and solvated electrons play an important part in chemical exchange. Also electronic reorganization of atoms and molecules in the irradiated media produces radiative (or not) processes with non negligible effects.

Theoretical and experimental studies of radiation interaction with biological material are not yet achieved and various stages (atoms-molecules-cells-) must be filled To bring a (little) contribution, we present here our recent development on molecular photoionization and electron cross-section for various species of biological interest

I- Molecular Photoionization.

Theoretical determination of photoionization cross-sections requires quantum mechanics technics by using final wave function of the photoelectron Methods using plan-wave approximation were first employed by RABALAIS et al (Ra-74), ELLISON (El-74) or DEWAR et al (De-75) Obtained results are partially incorrect because cross-sections are not well represented by this approximation More detailed calculations use the moments theory of Stieljes-Tchebycheff (WILLIAMS et al (Wi-79) and DIERCKSEN et al (Di-82)) or the one-centered technique of CACELLI et al (Ca-84))

Based on experimental results, some authors have developed simple chemical theories on photoionization intensity The experimental method used (ESCA) of SIEGBAHN et al (Si-69) allows to obtain full molecular spectra and gives orbital binding energies It allows also to bring informations on molecular structure and symmetrical nature of the orbits An model allowing to explain and calculate peaks intensities was proposed by GELIUS (Ge-72) The hypothesis says that the cross-section of one level is the sum of all atomic contributions to this level and that the intensity is proportional to the product of the cross-section by the electronic density This is explained as follows (Ba-72)

$$\sigma_j^{MO} = \sum_{A\lambda} P_{A\lambda j}\, \sigma_{A\lambda}^{AO} \qquad (1)$$

where σ_j^{MO} = cross-section of the molecular level j

$\sigma_{A\lambda}^{AO}$ = cross-section of the atomic shell $A\lambda$ in molecular level j

$P_{A\lambda j}$ = amount of atomic shell $A\lambda$ intervening in molecular level j

Usually, to obtain peaks intensities, it's more convenient to use a reference sub-level $A_0\lambda_0$ The level intensity is then proportional to

$$\sum_{A\lambda} P_{A\lambda j} \frac{\sigma_{A\lambda}^{O}}{\sigma_{A_0\lambda_0}^{AO}} \qquad (2)$$

Knowing the percentages of each atomic shell in a given molecule, the cross-sections ratio and atomic cross-sections taken in VEIGELE (Ve-73) , DUDZIAK (Du-70), MARR (Ma-76) and YEH (Ye-85), we can calculate the $P_{A\lambda j}$

Table 1 Electronic structures of stable molecules

Molecule	Structure	Reference
H_2O	$(1a_1)^2(2a_1)^2(1b_2)^2(3a_1)^2(1b_1)^2$	(Si-69)
CH_4	$(1a_1)^2\,(2a_1)^2\,(1t_2)^6$	(Se-83)
CO_2	$(1\sigma_g)^2(1\sigma_u)^2(2\sigma_g)^2(3\sigma_g)^2(2\sigma_u)^2$ $(4\sigma_g)^2(3\sigma_u)^2(1\pi_u)^4(1\pi_g)^4$	(Ki-86)
N_2	$(1\sigma_g)^2(1\sigma_u)^2(2\sigma_g)^2(2\sigma_u)^2(1\pi_u)^4$ $(3\sigma_g)^2$	(He-66)
O_2	$(1\sigma_g)^2(1\sigma_u)^2(2\sigma_g)^2(2\sigma_u)^2(3\sigma_g)^2$ $(1\pi_u)^4(1\pi_g)^2$	(He-66)

This theory of atomic weighted summations was taken by HUSH et al (Hu-79), and HILTON et al (Hi-79) who extended it with a plan-wave analysis of the diffraction effects between the molecule components

The complexity of molecular system make photoionization theory difficult to elaborate It seems interesting to take into account several mechanisms that goes with each molecule We have nevertheless adopted the summation theory of GELIUS, but we used as far as possible all the available experimental data

I-1 Molecular structures.

To apply GELIUS summations, we must know electronic structures of the stable molecules, those of interest are given in Table 1

These molecular structures allows to obtain $P_{A\lambda j}$ The weighting factors are then calculated for each molecule according to the number N_S of atomic electrons involved in the considered molecular level

I-2 Water molecule.

Following RABALAIS et al (Ra-74), the electronic structure of stable water molecule is

$$H_2O \quad (1a_1)^2(2a_1)^2(1b_2)^2(3a_1)^2(1b_1)^2 \qquad (3)$$

To know the binding energies of the ten electrons we have used SIEGBAHN et al (Si-69) data These authors gave each molecular level as weighted sum of atomic levels Weighting coefficients are given here by N_s in the Table 2

Table 2 H_2O levels

Molecular level	E_l(eV)	N_s	Atomic shell
$(1a_1)^2$	539 7	2 00	O1s
$(2a_1)^2$	32 2	0 50	H1s
		1 50	O2p
$(1b_2)^2$	18 5	0 82	H1s
		1 18	O2p
$(3a_1)^2$	14 7	0 34	H1s
		0 20	O2s
		1 46	O2p
$(1b_1)^2$	12 6	2 00	O2p

Then, for instance, total cross-section for the $(3a_1)^2$ level is given by

$$\sigma(3a_1)^2 = 0\,34\ \sigma(H1s) + 0\,20\ \sigma(O2s) + 1\,46\ \sigma(O2p) \qquad (4)$$

This type of calculation is then repeated for each level

In the outer shells, two electrons are from hydrogen and six from oxygen But the N_S sum (1 66) of H1s and that of O2s and O2p (6 34) are not in the expected ratio 2/6 That difference is due to the polarity of the O-H bond which grows the electronic density near the oxygen nucleus

Cross-sections obtained are in agreement with experimental results of TAN et al (Ta-78), TRUESDALE et al (Tr-82) and BANNA et al (Ba-86) These are also verified in partial energy ranges with theoretical values of WILLIAMS and LANGHOFF (Wi-79), and DIERCKSEN et al (Di-82) For the total cross section, in the range 12 62 eV-124 eV, a good agreement is obtained with experimental values of HADDAD and SAMSON (Ha-86)

I-3 Methane molecule.

The electronic configuration of stable methane molecule is

$$CH_4\ \ (1a_1)^2(2a_1)^2(1t_2)^6 \qquad (5)$$

The eight outer electrons lay on two levels and we took SENGER (Se-83) decomposition who used chemical hypothesis

Table 3 CH_4 levels

Molecular level	E_l(eV)	N_s	Atomic shell
$(1a_1)^2$	290 7	2 00	C1s
$(2a_1)^2$	23 1	0 25	C2s
		0 75	C2p
		1 00	H1s
$(1t_2)^6$	13 6	0 75	C2s
		2 25	C2p
		3 00	H1s

In this decomposition the N_s sums for H1s and C2s, C2p are in the expected ratio, because the C-H bond is not well polarized

For the methane there are few theoretical or experimental works In the medium energy range, there is a good agreement with experimental data of BACKX and VAN DER WIEL (Ba-75) and theoretical ones of DALGARNO (Da-52)

I-4 Nitrogen molecule.

It's a simple diatomic homonuclei molecule and for this type, calculations show a little difference with experiments (Ge-72) Nevertheless we adopt the same procedure The electronic configuration is

$$N_2\ (1\sigma_g)^2(1\sigma_u)^2(2\sigma_g)^2(2\sigma_u)^2(1\pi_u)^4(3\sigma_g)^2 \qquad (6)$$

With the use of relation (2) and peaks intensities of SIEGBAHN, we have determined atomic populations for each molecular level The obtained coefficients are

Table 4 N_2 levels

Molecular level	E_l(eV)	N_s	Atomic shell
$(1\sigma_g)^2$	409 9	2 00	N1s
$(1\sigma_u)^2$	409 9	2 00	N1s
$(2\sigma_g)^2$	37 3	0 456	N2s
		1 544	N2p
$(2\sigma_u)^2$	18 6	1 452	N2s
		0 548	N2p
$(1\pi_u)^4$	16 8	4 00	N2p
$(3\sigma_g)^2$	15 5	0 248	N2s
		1 752	N2p

Calculated cross-sections for $(2\sigma_u)^2$ and $(1\pi_u)^4$ levels are in very good agreement with experimental data of HAMNETT et al. (Ham-76) and PLUMMER et al. (Pl-77). For energies higher than 30 eV there is an excellent agreement with theoretical values of DAVENPORT (Da-76), RESCIGNO et al. (Re-79) and LUCCHESE et al. (Lu-82)2.

For the $(2\sigma_g)^2$ and $(3\sigma_g)^4$ levels, calculated values are valid above 50 eV. Below, we choose experimental data of KRUMMACHER et al. (Kr-80) verified by the theories of WIGHT et al. (Wi-76) and LANGHOFF et al. (La-81) for the $(2\sigma_g)^2$ level. For the $(3\sigma_g)^4$ level we have considered data of HAMNETT et al. (Ham-76) and PLUMMER et al. (Pl-77).

I-5 The carbon dioxide molecule.

The electronic configuration is a little more complex than the others molecules :

$$CO_2\ (1\sigma_g)^2(1\sigma_u)^2(2\sigma_g)^2(3\sigma_g)^2(2\sigma_u)^2(4\sigma_g)^2(3\sigma_u)^2(1\pi_u)^4(1\pi_g)^4 \qquad (7)$$

Table 5 : CO_2 levels.

Molecular level	E_l(eV)	N_s	Atomic shell
$(1\sigma_g)^2$	541.1	2.00	O1s
$(1\sigma_u)^2$	541.1	2.00	O1s
$(2\sigma_g)^2$	297.5	2.00	C1s
$(3\sigma_g)^2$	39.0	0.558 1.278 0.164	C2s O2s O2p
$(2\sigma_u)^2$	37.6	0.564 1.306 0.13	C2p O2s O2p
$(4\sigma_g)^2$	19.4	0.38 0.594 1.026	C2s O2s O2p
$(3\sigma_u)^2$	18.1	0.336 0.544 1.12	C2p O2s O2p
$(1\pi_u)^4$	17.6	1.508 2.492	C2p O2p
$(1\pi_g)^4$	13.8	4.00	O2p

Binding energies and atomic populations are given by ALLAN et coll. (Al-72) who realized a complete study of this molecule.

The binding energies levels have been measured by ESCA. The experimental spectrum shows only one peak for the levels $(3\sigma_g)^2$ and $(2\sigma_u)^2$. But preliminary calculations have shown an energy gap of 1.4 eV for these two levels. The calculations that give a very good agreement with experiments for the four outer levels, were adopted for this energy gap, though experimental spectrum does not show (Al-72).

When we compare GELIUS results with experiments, for energies higher than 50 eV, there is a good agreement. Also, sophisticated theories of SWANSON et al.(Sw-80), PADIAL et al.(Pa-81) and LUCCHESE and McKOY (Lu-82)1 confirm these experimental data. For lower energies, calculated cross-sections are under-estimated for the $(4\sigma_g)^2$,$(3\sigma_u)^2$ and $(1\pi_g)^4$ levels and we then used experimental data of CARLSON et al. (Ca-73), LEE et al. (Le-76), GUSTAFSSON et al. (Gu-78) and BRION and TAN (Br-79).

I-6 Oxygen molecule.

The electronic configuration is :

$$O_2\ (1\sigma_g)^2(1\sigma_u)^2(2\sigma_g)^2(2\sigma_u)^2(3\sigma_g)^2(1\pi_u)^4(1\pi_g)^2 \qquad (8)$$

Table 6 : O_2 levels.

Molecular level	E_l(eV)	N_s	Atomic shell
$(1\sigma_g)^2$	544.2	2.00	O1s
$(1\sigma_u)^2$	543.1	2.00	O1s
$(2\sigma_g)^2$	40.6	0.60 1.40	O2s O2p
$(2\sigma_u)^2$	26.6	1.76 0.24	O2s O2p
$(3\sigma_g)^2$	19.9	0.3 1.7	O2s O2p
$(1\pi_u)^4$	17.0	4.00	O2p
$(1\pi_g)^2$	13.1	0.16 1.84	O2s O2p

Figures 1 to 5 show the photoionization cross-sections variations for the five molecules studied. Energy is in eV and cross-sections in square Angstroems.

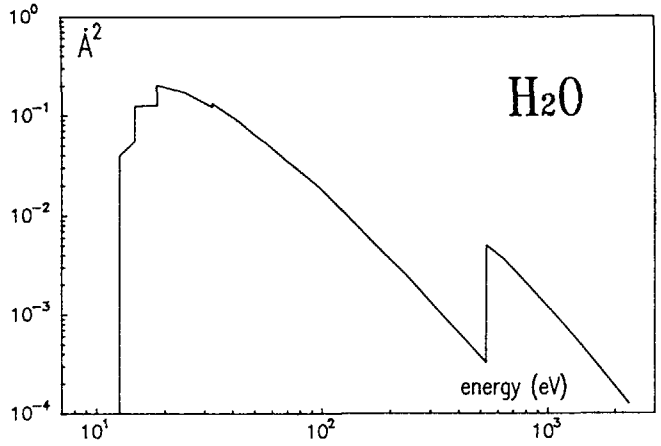

Fig 1 : Total photoionization cross-section.

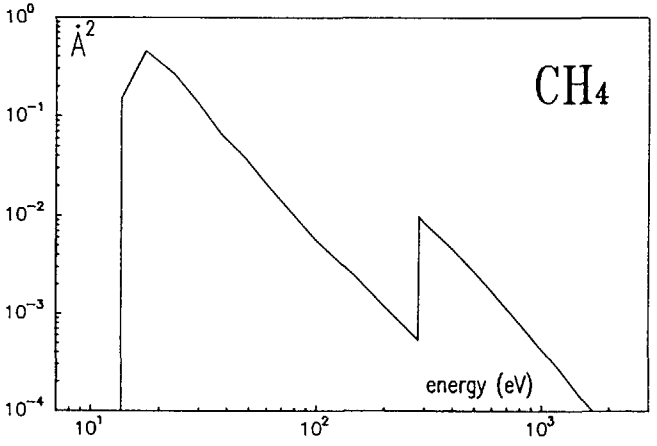

Fig 2 : Total photoionization cross-section.

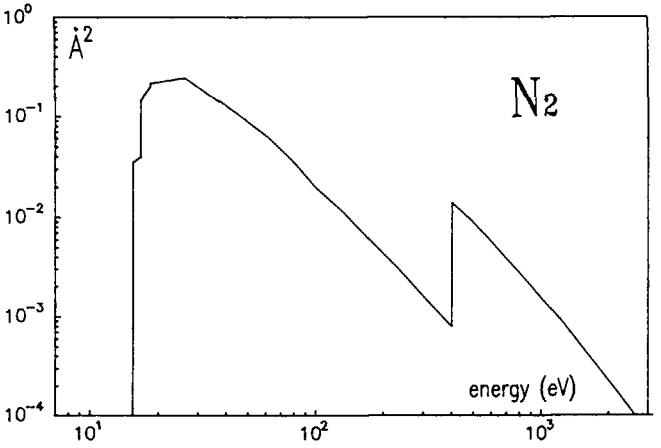

Fig 3 : Total photoionization cross-section.

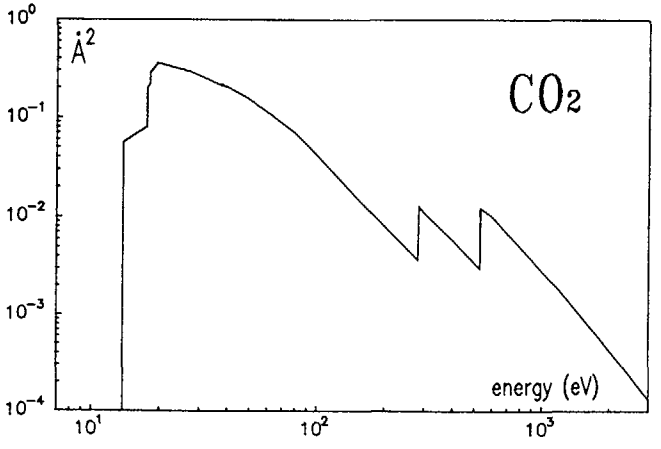

Fig 4 : Total photoionization cross-section.

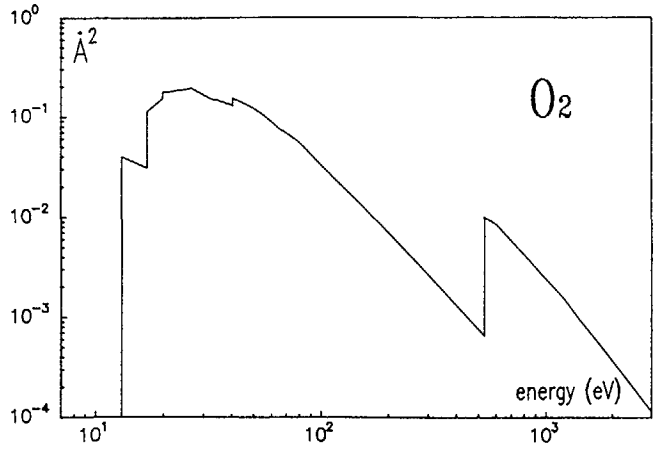

Fig 5 : Total photoionization cross-section.

II Electron scattering cross-sections.

Actually, no complete set of cross-sections is available in the literature in the energy range 0 025 eV - 1 keV for studied species Furthermore, for elastic cross sections, a lot of results exist but they are very dispersed We give the method used to obtain a full set of elastic differential cross-sections For inelastic cross sections, the employed semi-empirical formula are defined We detail the obtained main results for the elastic cross-sections for molecules

II-1 Ways and means used to determine elastic cross-sections.

In the energy range 0 025 eV-1 keV we can observe several domains where electron-molecule interaction mechanisms are different, and so the methods used to calculate the cross-sections

II-1-1 Very low energy electron (ε < 0.1 eV).

The main interaction potential is the induced dipole potential One can only take into account the global polarization of the target by the incident electron The motion is described by the Schrodinger equation The use of the modified effective range theory (Om-63) give simple expressions for the phase-shifts calculations (Ha-82) With the phase-shifts, it is relatively easy to obtain the differential, total (Q_0) and momentum-transfer (Q_m) cross-sections

In these expressions only four constants appear, and they can be determined with comparison between calculated values of Q_0 or Q_m and experimental ones found for several energies of the incident electron

II-1-2 Medium energy electron (0.1 eV < ε < 500 eV).

The incident electron energy is close to that of the bond electrons The spin-orbit coupling can be neglected, but we must now take into account exchange and polarization effects In this energy range experimental results are numerous

II-1-3 Intermediate energy electron (500 eV < ε < 1 keV).

The incident electron energy is greater than the bond electrons energy and here we can neglect the exchange and polarization but take into account the spin-orbit coupling (Mo-65 and Wa-70) The description of the electron motion is based on Dirac equation with a static potential In this energy range and above 1 keV various methods and formulas are collected in the paper of Motz and alii (Mo-64), who precise accuracy domains Below 1 keV, the only available results are the calculations of Fink (Fi-70) who used Dirac equation and neglect exchange and polarization Fink et al (Fi-70 and Fi-72) have calculated the elastic angular differential cross-section for various atoms in the energy range 100 eV - 1500 eV But no equivalence exists for molecules Using the independent scattering center theory of Massey (Ma-69, Te-78), the molecular differential cross-section is calculated from atomic cross-sections if the associated electron wave-length is lower than the inter-atomic distances in the molecule

Taking into account considerations above, a bibliographic study of experimental or theoretical works allows us to compare and then choose between the various available cross-sections Selected differential ones are integrated over angles to obtain total and momentum transfer cross-sections These values are then compared with the initial choice and allowed to improve some of them These two cross-sections (Q_0 and Q_m) are representative only of the first two moments in the differential cross-section integration, and irregularities may not appear So we have systematically developed the differential cross-sections in Legendre polynomial series and the ratios Q_l/Q_0 were plotted (Q_l is the l order component in the Legendre expansion)

$$Q_l = 2\pi \int dQ(v,\theta)/d\Omega \; P_l(\cos\theta) \; d\sin\theta \; d\theta \qquad (9)$$

A new comparison has then been done and a new set of cross-section elaborated It is easy to find the Q_l/Q_0 limits When the incident energy is zero, the cross-section is isotropic, and the ratio limit is zero For highest energies, the diffusion is mainly in the forward direction and the ratio limit is one The knowledge of these limits allows to complete data by interpolation between the

last known point and the limit Once the ratios Q_l/Q_0 are known, Q_l is for instance obtained with

$$Q_l = Q_m \frac{Q_l}{Q_0}\left\{1 - \frac{Q_1}{Q_0}\right\}^{-1} \qquad (10)$$

It is then possible to built the differential scattering cross-section from the Q_l with a Legendrè polynomial expansion A great care must be taken, because the ratios Q_l/Q_0 are calculated with a Gauss-Legendre method at an order at least equal to the highest one used in the Legendre series This order often lies between 40 and 50

II-2 Excitation cross-sections.

Precedent remarks concerning the incident electron energy for elastic collision are always valid We obtain total excitation cross-section for a given energy level Some angular differential ones are available, but for limited energy and angular ranges Most of the adopted relations are semi-empirical using the Born approximation, and at low energy the relations giving the cross-section are multiplied by a function The parameters of this function are calculated to fit experiments or quantum mechanics results For more details, see for instance the works of Jusick (Ju-67), Dalgarno (Da-69) or Drawin (Dr-67)

The relations use empirical formulas of Green (Gr-67), taken back recently by Bretagne (Br-86) and Slinker (Sl-88) These expressions have been determine to satisfy recents experimental and theoretic works

Three types of transitions are characterized

II-2-1 Optically allowed transitions:

$$Q_n = A_n\,(4\pi a_0^2 R^2 f_n/\varepsilon^2)((\varepsilon/\varepsilon_n)^{a}-1)^{b}\,\{\log[4C_n\varepsilon/\varepsilon_n]\} \qquad (11)$$

at higher energy the cross-section varies as $\log(\varepsilon)/\varepsilon$ A_n, C_n, a and b are adjustable parameters a_0 is the atom Bohr radius, ε is $mv^2/2$, m the electron rest mass, R is the Rydberg constant, ε_n the threshold energy and f_n is the oscillator strength

II-2-2 Optically forbidden transitions:

$$Q_n = A_n \frac{4\pi a_0^2 R^2}{(\varepsilon\varepsilon_n)^{a}}\left\{1 - \left[\frac{\varepsilon_n}{E}\right]^{b}\right\}^{c} \qquad (12)$$

at higher energy the cross section varies as $1/\varepsilon$ A_n, b and c are adjustable parameters

II-2-3 Rydberg series.

$$Q_n = C_n f_n \frac{4\pi a_0^2 R^2}{\varepsilon_n^2}\left\{1 - \frac{\varepsilon_n}{\varepsilon}\right\}^{c}\left[\frac{\varepsilon_n}{\varepsilon}\right]^{a} \qquad (13)$$

C_n, a and b are adjustable parameters For the Rydberg series, the oscillator strength is defined by

$$f_n = f^*/(n - \delta)^3 \qquad (14)$$

where δ the quantum defect and f^* the oscillator strength are constant for given series δ is obtain with

$$\varepsilon_n = \varepsilon_J - \{R/(n - \delta)^2\} \qquad (15)$$

II-3 Ionization cross-sections.

There is a lack of data on triple differential ionization cross-section (energy and angles after the interaction) due to the complexity of quantum calculations (actually limited to hydrogen (Wa-87) and helium) and the difficulty to do correct measurements (St-87) Simple or double differential cross-sections have been determined for other gazes than hydrogen and helium by Opal (Op-72 and Od-75) We present here, our search on total ionization cross-sections for inner shells and energy differential cross-sections

II-3-1 Total cross-section.

As for excitation, the Bethe theory works with the same restrictions for low energy The initial formula is modified, and depends on arbitrary constants obtained by comparison with experiments (for instance, see the papers of Rapp and Englander-Golden (Ra-65), and of Kieffer and Dunn (Ki-66)) We have nevertheless applied a formula proposed by Bell (Be-83), which fits very well the recent experimental data and verifies at high energy the asymptotic behavior predicted by the Bethe theory

II-3-2 Inner shells ionization cross-section.

With the same remarks on Bethe theory, we have adopted the semi-empirical formulation of Drawin (Dr-67 and Yo-85) The cross-section for one shell is given by

$$Q_{ion} = 2.66\,\pi\,a_0^2\,\xi_{ion}\frac{R}{\varepsilon_{ion}}\,f_1\frac{u - 1}{u^2}\,\log(1{,}25\,f_2\,u) \qquad (16)$$

ε_{ion} is the ionization threshold of the considered shell, ξ_{ion} is the effective number of electrons in that shell and $u = \varepsilon/\varepsilon_{ion}$ f_1 and f_2 are adjustable

parameters to fit experimental data. If no data is available, f_1 and f_2 are taken equal to one, giving appropriate results.

II-3-3 Energy differential cross-sections.

The mechanisms are very different according to the strength of the momentum transfer. The cross-section for weak interactions follows Bethe theory, while Mott cross-section (Mo-32 and Se-53) describes well strong ones. The reader may refer to the works of Khare (Kh-70), Dalgarno (Da-71), Kim (Ki-75), Oda (Od-75), Eggarter (Eg-75), Porter (Po-76), Jain (Ja-76), and Khare (Kh-87) who puts the two types of cross-sections in one semi-empirical formula.

We adopt the Jain and Khare formulation which allows to control the relative importance of the two collision types with only one parameter, chosen to fit experimental data.

$$
\begin{aligned}
&Q_{ion}(\varepsilon,T) = f_1(\varepsilon,T)\, Q_{BB}(\varepsilon,T) + f_2(\varepsilon,T)\, Q_M(\varepsilon,T)\\
&f_1(\varepsilon,T) = \frac{1}{1+\varepsilon_{ion}/\varepsilon}\left\{1 - \frac{T}{\varepsilon-\varepsilon_{ion}}\right\}\frac{\log(1+C_{ion}(\varepsilon-\varepsilon_{ion}))}{\log(C_{ion}\varepsilon)}\\
&f_2(\varepsilon,T) = \frac{T^3}{T^3 + \varepsilon_0{}^3}(1 - \varepsilon_{ion}/\varepsilon) \qquad (17)\\
&Q_{BB}(\varepsilon,T) = \frac{4\pi a_0{}^2 R^2}{\varepsilon}\frac{1}{W}\frac{df(W,0)}{dW}\log(C_{ion}\varepsilon)\\
&Q_M(\varepsilon,T) = \frac{4\pi a_0{}^2 R^2}{\varepsilon} N_{ion}\left\{\frac{1}{T^2} - \frac{1}{T(\varepsilon-T)} + \frac{1}{(\varepsilon-T)^2}\right\}
\end{aligned}
$$

Q_{BB} depends on the oscillator strength and hence on the photoionization cross-section and ε_0 has an arbitrary value which may be chosen in order to fit experimental values if available. We can then determine inner or outer shells cross-section if we know the associated photoionization cross-section.

II-4 Elastic scattering results :
Differential cross-section
Momentum transfer cross-section
Total elastic cross-section

We do not present here results on inelastic cross-sections. There is a great number of works on the excitation and ionization cross-sections. See for example, the papers of Green et al. (Gr-65, Gr-67, Wa-67, Po-76, St-67, Ol-72...), those of Phelps et al. (Ha-67, Ph-85 ...). All the details on excitation and ionization cross-sections are given in a report (Se-88). As for photons, we only present some results for molecules.

The elastic cross-sections obtained with the original method detailed before are presented. For differential elastic cross-section, we indicate the bibliographic references for the largest angular range determination.

To our knowledge, there is no experimental results for the momentum transfer cross-section for the studied molecules. The only available Q_m come from the calculations of Hayashi (Ha-80), and those of Phelps (Ph-85 for instance). This cross-section is obtained by analysis of swarm parameters (Hu-74). The other studies to obtain the momentum transfer cross section use the measurements or calculations of differential elastic scattering cross-sections. So, at the opposite of the rare gases that we also study, the comparison of the appropriated integration of differential cross-sections and the available Q_m values give less information.

II-4-1 Carbon dioxide molecule.

The elastic differential cross sections were measured by Register et al. (Re-80) between 4 and 50 eV, Iga et al. (Ig-84) from 500 to 1000 eV, by Shyn T.W., Sharp W.E. and Carigan G.R. (Sh-78) (3 to 90 eV) using a crossed beam method. Bromberg (Br-74) made experimental determination in the 2° to 45° range (300, 400 and 500 eV). Khare and Raj (Kh-82) used independent atom model (IAM) to obtain the differential cross sections at intermediate energies (50 to 500 eV). The atoms are represented by central potential (sum of the first order static and second order dynamic polarization potentials. Calculations were made with this model in the energy range 50-500 eV by Jain and Kayal (Ja-82). In IAM formulation, the short range static interaction potential between the incident electron and the molecule was considered as the sum of atomic potentials and therefore the molecular effects were neglected. In the renormalised multicenter potential model the electron molecule static potential is directly derived from the molecular wave-function. With that description, the electron-CO_2 scattering was studied from 20 to 1500 eV by Bothelo et al. (Bo-84). We used the independent scattering center theory of Massey (based on the knowledge of the elastic differential cross sections of C and O) to obtain the cross section from 100 eV.

Following the process defined before, the set of cross sections include the results of Register et al. between 4 and 40 eV, those of Bothelo et al. from 50 to 1000 eV. On this side of 4 eV, we use the interpolation of the ratios Q_I/Q_0 to obtain the differential cross sections represented in the figure 6.

Ferch et al. (Fe-81) determined the total elastic cross section in the energy range 0.07 eV - 4.5 eV with a time of flight spectrometer. Other recent measurements have been made by Kwan et al. (Kw-83) between 100 and 500 eV, by Hoffman et al. (Ho-82) from 2 and 50 eV. Hayashi (Ha-80) calculated the total elastic cross-sections as well as the momentum transfer cross-section for CO2, O_2, N_2.

Figure 7 shows the comparisons between experimental values of the total elastic cross sections with Hayashi's one and ours. The agreement is not as good as for the atoms (specially for rare gases).

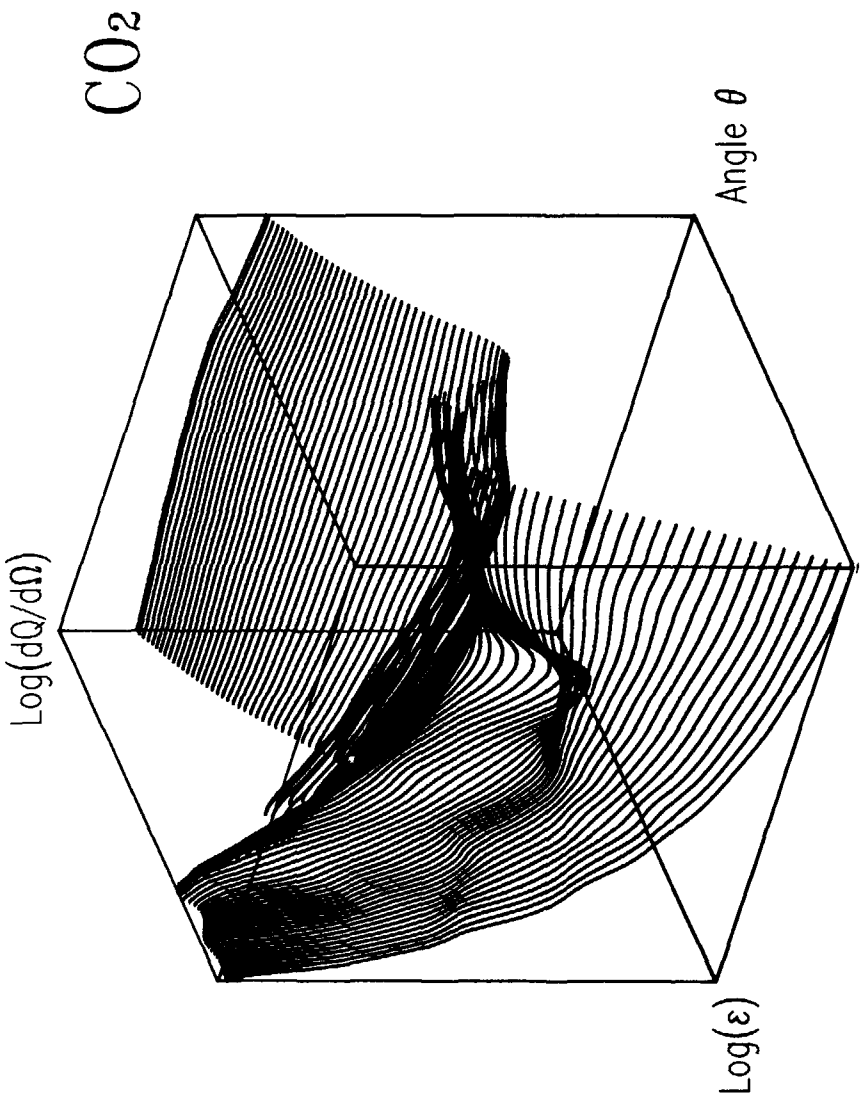

Fig 6 : Elastic differential cross-section for electron.
ε range 0.025 eV - 1 keV, θ range 0° - 180°.

II-4-2 Oxygen molecule.

Trajmar et al. (Tr-71) measured the differential cross sections in the 4 to 45 eV range. More recently, Shyn and Sharp (Sh-80) studied the 2-200 eV region and Bromberg (Br-74), like for CO_2, the low angles region for high energy elastic scattering (300,400 and 500 eV). The results of Daimon et al. (Da-82) include the 200-500 eV range. Electron energy loss spectra of O_2 were analyzed by Wakiya (Wa-78)for incident electron energies from 20 to 500 eV. Experimental results of Wakiya are compared with the theoretical calculations of Hayashi et al. (Hay-76). These calculations are based on the same model as that of Jain et al. for CO_2. Recent calculations between 20 and 200 eV were also made by Bhattacharyya (Bh-83) using the Glauber approximation.

The chosen elastic differential cross sections (figure 8) after the analysis of all the results are the experimental values of Shyn between 2 and 150 eV, those of Daimon (200-500 eV) and those obtained by the approximation of Massey from 500 eV. In the low energy range (.025-2 eV), the interpolation on the ratios Q_l/Q_0 is necessary since no data are available.

In the Wedde and Strand (We-74) paper, there is a comparison between experimental and theoretical values of the total elastic scattering cross sections. Measurements were made by Salop et Hakano (Sa-70) from 2.28 eV to

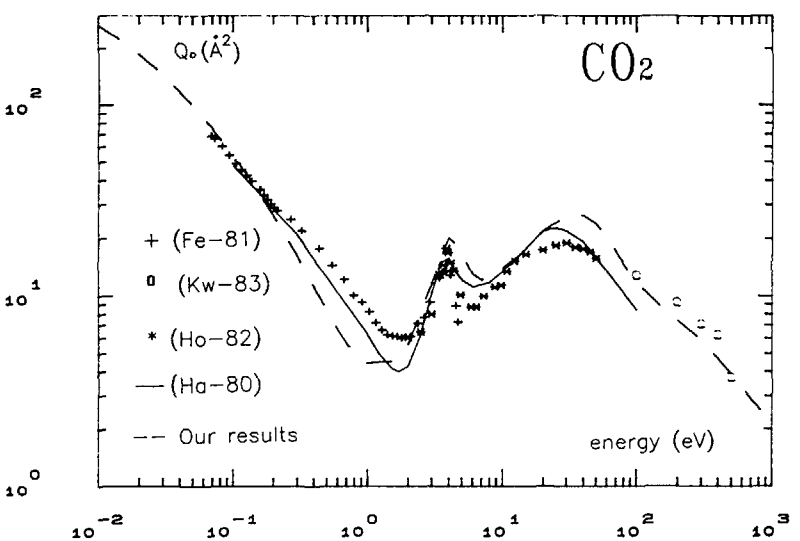

Fig 7 : Total elastic cross-section.

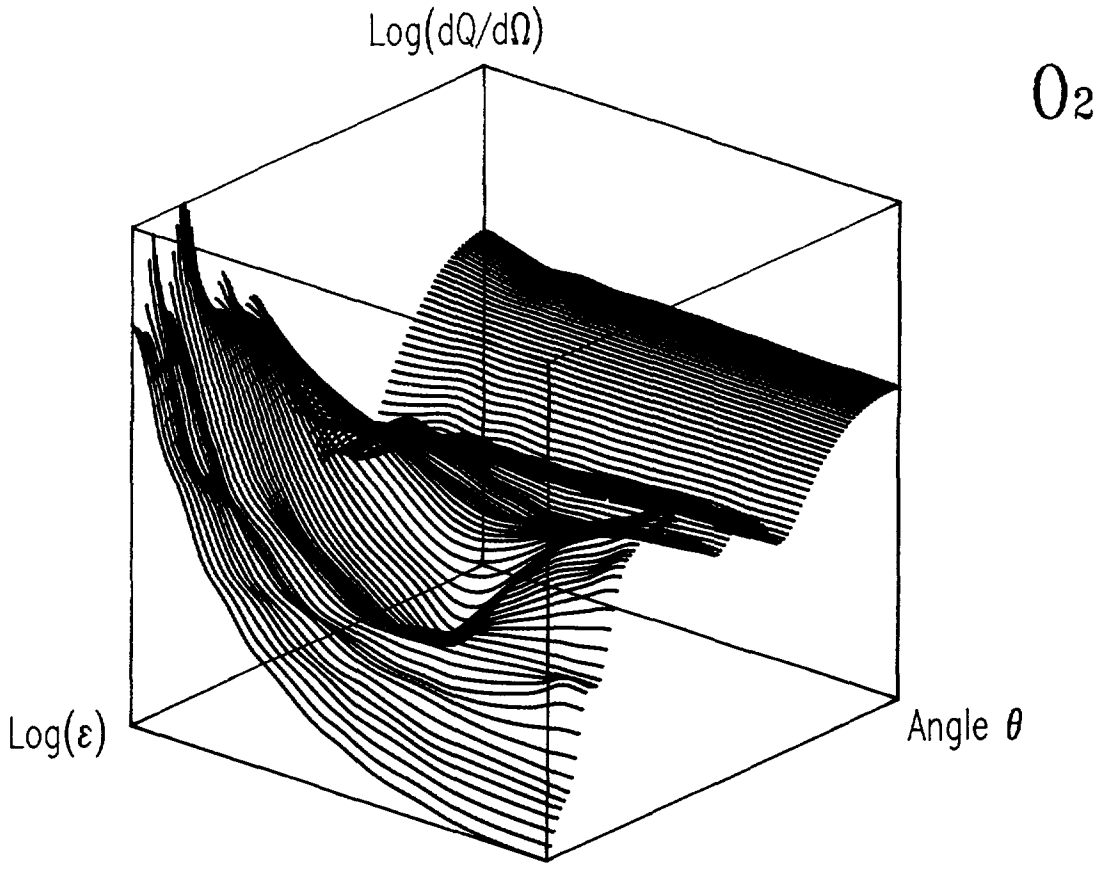

Fig 8 : Elastic differential cross-section for electron.
ε range 0.025 eV - 1 keV, θ range 0°- 180°.

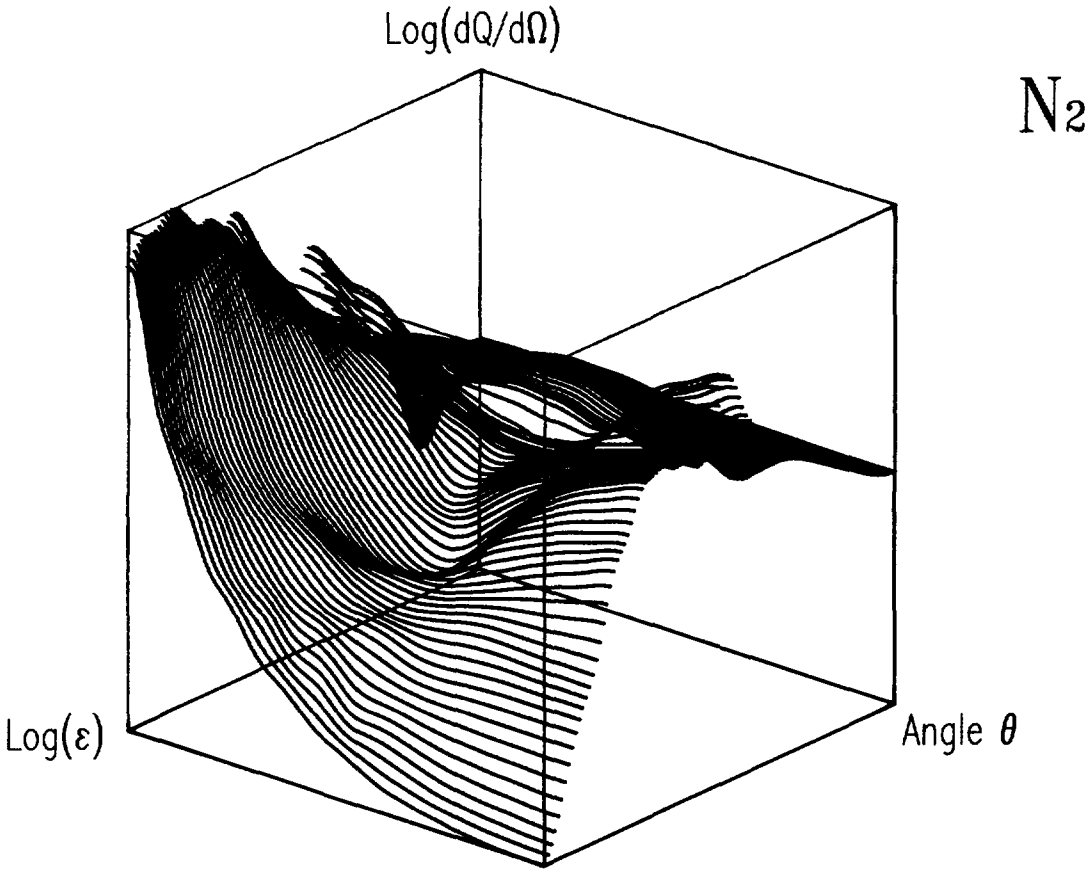

Fig 9 : Elastic differential cross-section for electron.
ε range 0.025 eV - 1 keV, θ range 0°- 180°.

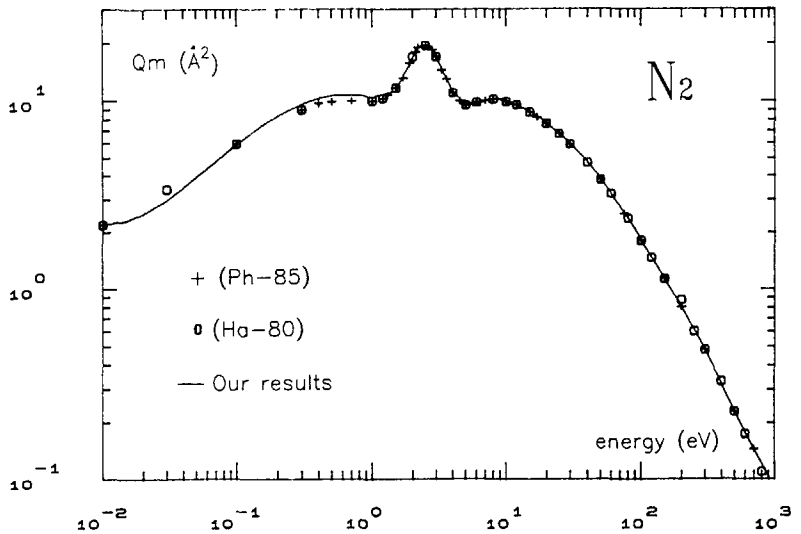

Fig 10 : Momentum transfer cross-section.

20 eV and more recently by Dalba et al (Da-80) from 100 to 1600 eV The agreement between these measurements and our results is good

II-4-3 Nitrogen molecule.

N_2 is one of the molecular specie which is the more studied Elastic differential cross sections have been measured by DuBois and Rudd (Du-76) between 20 and 800 eV, by Srivastava et al. (Sr-76) and more recently by Shyn et Carignan (Sh-80) from 5 to 90 eV Absolute differential cross sections were obtained by Bromberg (Br-70) in the same angular range and for the same values of energy Relative differential cross sections have been measured by Herrmann, Jost and Kessler (He-76) from 90 to 1000 eV They were normalized to absolute cross sections by theoretical calculations based on the independent atom model The calculations of Siegel et al (Si-78) in the 1 4-30 eV energy range are based on the multiple scattering method

Comparisons between the different sets of elastic differential cross sections, the momentum transfer cross sections, the total elastic cross sections, and the ratios Q_I/Q_0 are such that the cross sections chosen set (figure 9) is the following one between 1 5 and 400 eV the values of Shyn et al , and from 400 to 1000 eV those of Herrmann From 0 025 eV and 1 5 eV , the interpolation on Q_I/Q_0 was necessary

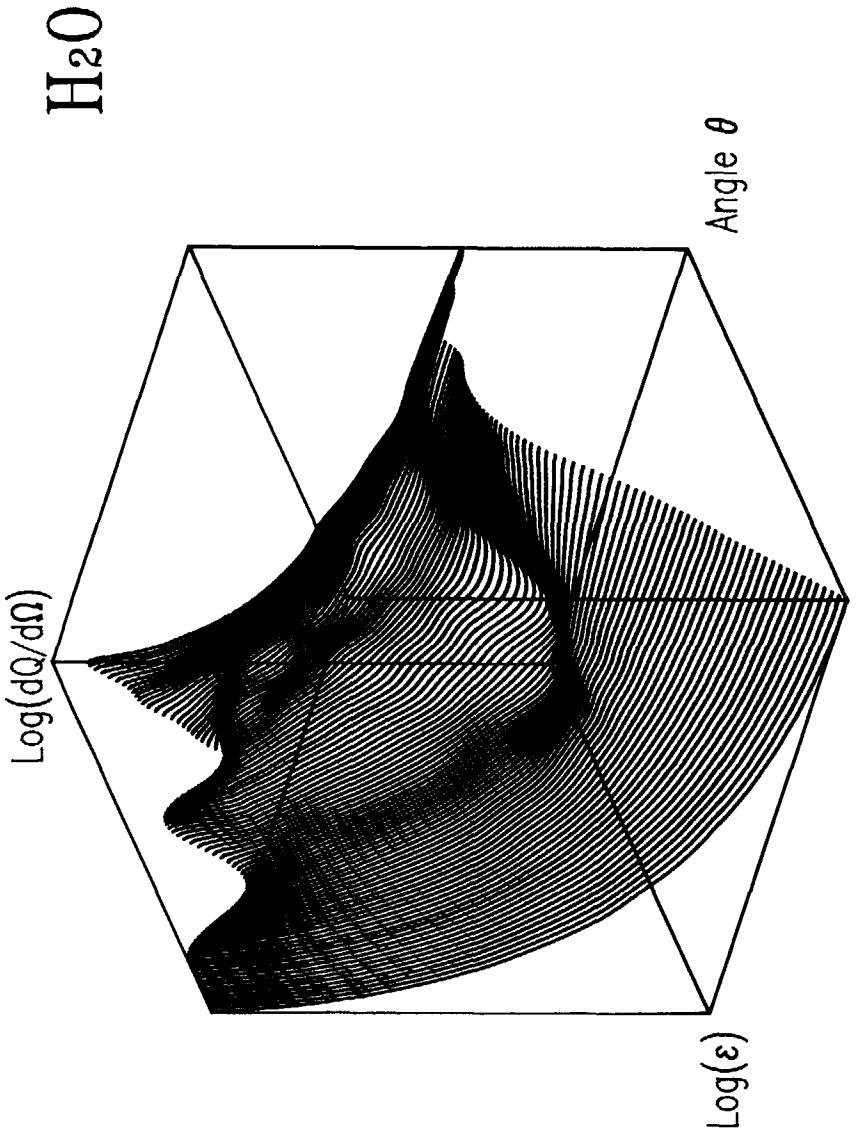

Fig 11 : Elastic differential cross-section for electron.
ε range 4 eV - 1 keV, θ range 0° - 180°.

The more recent measurements of the total cross-sections were made by Kennerly (Ke-80) from 0.519 eV and 51.33 eV, Blaauw et al. (Bl-80) (17.5 eV - 750 eV), Dalba et al. (Da-80) between 120 and 1600 eV and by Hoffman (Ho-82) in the energy range 2.2-700 eV. See also the Wedde and Strand paper (We-74). The figure 10 shows the very good agreement between the momentum transfer cross-sections of Hayashi (Ha-80), of Phelps (see for instance Ph-85) and this *obtained by integration of our differential set of cross-sections.*

II-4-4 Vapor water molecule.

There is relatively few studies on the elastic differential cross sections. the only set of cross sections (for a large angular range) was measured by Danjo and Nishimura (Da-85) from 4 to 200 eV. This set has been completed at high energy by the differential cross-sections calculated with those of O and H (figure 11). We were not able to determine the cross-sections at lower energy.

There are some discrepancies between the available results of the total elastic cross sections so they must be very carefully analyzed.

Conclusion

For the photoionization, the selected method allows to obtain each orbital cross-section for molecules, while verifying experimental data. With the use of the differential cross-section of RABALAIS (Ra-74, not explained here), it is then possible to simulate completely the photoelectric effect at these energies.

The results for electrons represent a first determination of the differential elastic cross sections by an original method to obtain a full set in a large energy range. This method of comparison and calculation allows to combine experimental and theoretical data, while physical mechanisms are kept. For inelastic processes, we use only semi-empirical formula and there are no many experimental results. It is also necessary to improve these sets of cross-sections. The calculation of the swarm parameters by the resolution of the Boltzmann equation will allow to compare them to the experimental values. An adjustment of the cross sections (so that the calculated coefficients are in a good agreement with the experimental values) may become a next stage. It is also useful to better define the low energy elastic differential cross sections. The application of the modified effective range theory must be undertaken.

REFERENCES

(Al-72) : Allan C., Gelius U., Allison D.A.,Johanson G.,Siegbahn G. and Siegbahn K.
J. Electron.Spectrosc., **1**, 131 (1972/73).

(Ba-72) : Baker A. D. and Betteridge D.
Photoelectron Spectroscopy .Vol 53 Pergamon Press (1972).

(Ba-75) : Backx C. and Van Der Wiel M.J.
J. Phys.B: At. Mol. Phys. **8**, 3020 (1975).

(Ba-86) : Banna M.S.,Mc Quaide B.H., Malutzki R. and Schmidt V.
J. Chem. Phys., **84**, 4739 (1986).

(Be-83) : Bell K. L., Gilbody J. G., Hughes J. G., Kingston A. E. and Smith F. J.
J. Phys. Chem. Ref. Data, **12**, 891 (1983).

(Bh-83) : Bhattacharyya P. K. and Goswami K. K.
Phys. Rev. A, **28**, 713 (1983).

(Bl-80) : Blaauw H. J., Wagenaar R. W., Barends D. H. and de Heer F. J.
J. Phys.B: At. Mol. Phys. **13**, 359 (1980).

(Bo-84) : Botelho L.F., Freitas L.C., Lee Mu-Tao, Jain A. and Tayal S.S.
J. Phys. B: Atom. Mol. Phys. **17**, L641 (1984).

(Br-70) : Bromberg J.P.
J. Chem. Phys., **52**, 1243 (1970).

(Br-74) : Bromberg J. P.
J. Chem. Phys., **60**, 1717 (1974).

(Br-79) : Brion A.D. and Tan K.H.J.
J. Electron Spectrosc.,**15**, 241 (1979).

(Br-86) : Bretagne J., Callede G., Legentil M.et Puech V.
J. Phys. D.: Appl. Phys. **19**, 761 (1986).

(Ca-84) : Cacelli L. and Moccia R.
Chem. Phys., **90**, 313 (1984).

(Da-52) : Dalgarno A
Proc. Phys. Soc. (LONDON).**A65**, 663 (1952).

(Da-69) : Dalgarno A., McElroy M. B. and Stewart A. I.
J. Atmos. Sci. **26**, 753 (1969).

(Da-71) : Dalgarno A. and Lejeune G.
Planet Space Sci **19**, 1653 (1971).

(Da-76) : Davenport J.W.
Phys. Rev. Lett.,**136**, 945 (1976).

(Da-80) : Dalba G., Fornasini R., Ranieri G. and Zecca A.
J. Phys.B: At. Mol. Phys. **13**, 4695 (1980).

(Da-82) : Daimon H., Hayashi S., Kondow T. and Kuchitsu J.
J. Phys. Soc. Japan **51**, 2641 (1988).

(Da-85) Danjo A and Nishimura H
J Phys Soc Japan **54**, 1224 (1985)

(De-75) Dewar M J S, Komornicki A and Thiel W
Chem Phys Lett , **31**, 286 (1975)

(Di-82) Diercksen G H F , Kraemer , W P , Rescigno T N , Bender C F , Mc KOY B V ,Langhoff S R and Langhoff P W
J Chem Phys , **76**, 1043 (1982)

(Dr-67) Drawin H W
Rapport Euratom-CEA, Ref Eur-CEA-FC-383, (1967)

(Du 67) Dudziak D J
Rapport UCLA n° LA-8301 (1967)

(Du-76) Dubois R D and Rudd M E
J Phys B Atom Mol Phys **9**, 2657 (1976)

(Eg-75) Eggarter E
J Chem Phys , **62**, 833 (1975)

(El 74) Ellison F O
J Chem Phys , **61**, 507 (1974)

(Fe 81) Ferch J , Masche C and Raith W
J Phys B Atom Mol Phys **14**, L97 (1981)

(Fi-70) Fink M and Yates A C
Atomic Data Tables, **1**, 385 (1970)

(Fi 72) Fink M and Yates A C
Atomic Data Tables, **4**, 129 (1972)

(Ge-72) Gelius U
Electron Spectroscopy D A Shirley (Ed) p311 (1972)

(Gr-65) Green A E S and Barth C A
J Geophys Res **70**, 1083 (1965)

(Gr 67) Green A E S and Dutta S K
J Geophys Res **72**, 3933 (1967)

(Gry 65) Gryzinski M
Phys Rev A, **138**, 336 (1965)

(Gry-73) Gryzinski M
Abstracts of papers, VIII ICPEAC, Belgrade, (1973)

(Gu-78) Gustaffson T , Plummer E W , Eastman D E and Gudat W
Phys Rev A, **17** 175 (1978)

(Ha-67) Hake R D and Phelps A V
Phys Rev **158,** 70 (1967)

(Ham-76) Hamnett A , Stoll W and Brion E
J Phys B At Mol Phys **9**, 675 (1976)

(Hay-76) Hayashi S and Kuchitsu K
Chem Phys Lett , **44**, 1 (1976)

(Ha-80) Hayashi M
Nagoya Institute of Technology Report N° IPPJ-AM-19 (1976)

(Ha-82) Haddad G N and O'Malley T F
Austr J Phys **35**, 35 (1982)

(Ha-86) Haddad G N and Samson J A
J Chem Phys , **84**, 6623 (1986)

(He 66) Herzberg G
Molecular spectra and molecular structure Spectra of diatomic molecules Von Nostrand Reinhold Company (1966)

(He-76) Herrmann D , Jost K and Kessler J
J Chem Phys , **64**, 1 (1976)

(Hi-79) Hilton P R , Nordholm S and Hush N S
Chem Phys Lett , **64**, 515 (1979)

(Ho-82) Hoffmann K R , Dabanbeh M S , Hsieh Y F , Kauppila W E , Pol V , Smart J H and Stein T S
Phys Rev A, **25,** 1393 (1982)

(Hu-74) Huxley L G H and Crompton R W
The Diffusion and Drift of Electrons in Gases, Wiley, New York, (1974)

(Hu-79) Hush N S ,Hilton P R and Nordholm S
J Electron Spectrosc Relat Phenom **15**, 101 (1979)

(Hu-84) Hunter S R , Christophorou L G
Electron-Molecule Interactions and their Applications, Christophorou Academic Press, Orlando, Floride, (1984)

(Ig-84) Iga I , Nogueira J C and Lee Mu-Tao
J Phys B Atom Molec Phys **17**, L185 (1984)

(Ja-76) Jain D K and Khare S P
J Phys B Atom Mol Phys **9**, 1429 (1976)

(Ja-82) Jain A and Tayal S S
J Phys B Atom Mol Phys **15**, L867 (1982)

(Ja-77) : Jackman C. H., Garvey R. H. and Green A. E. S.
J. Geophys. Res. **82**, 5081 (1977).

(Ju-67) : Jusick A. T., Watson C. E., Peterson L. R and Green A. E. S.
J. Geophys. Res. **72**, 3943 (1967).

(Ke-80) : Kennerly R. E.
Phys. Rev. A, **27**, 1328 (1983).

(Kh-70) : Khare S. P. and Padalia B. D.
J. Phys B: Atom. Mol. Phys. **3**, 1073 (1970).

(Kh-82) : Khare S.P. and Deo Raj
Indian J. of Pure & Applied Phys., **20,** 538-543, (1982).

(Kh-87) : Khare S. P., Tyagi R. and Meath W. J.
Abstracts of Papers, XV ICPEAC, Brighton, (1987).

(Ki-66) : Kieffer L. J. and Dunn G. H.
Rev. Mod. Phys. **38**, 1 (1966).

(Ki-75) : Kim Y. K.
Rad. Res. **64**, 205 (1975).

(Ki-86) : Kilcoyne D.A.L.,Nordholm S. and Hush N.S.
Chem. Phys., **107**, 225 (1986)

(Kr-80) : Krummacher S., Schmidt V. and Wuilleumier F.
J. Phys.B: At. Mol. Phys. **13**, 3993 (1980).

(Kw-83) : Kwan C. H., Hsieh Y.F., Kauppila W. E., Smith S. J.,
Stein T. S.and Uddin M. N.
Phys. Rev. A, **27**, 1328 (1983).

(La-81) : Langhoff P.W., Langhoff S.R., Rescigno T.N., Schirmer J.,
Lederbaum L.S.,Domcke W. and Von Niessen W.
Chem. Phys., **58**, 71,(1981).

(Le-76) : Lee L.C., Carlson R.W. and Judge D.L.
J. Phys.B: At. Mol. Phys. **9**, 855 (1976).

(Lu-82)1: Lucchese R.R. and Mc Koy V.
Phys. Rev. A, **26**, 1992 (1982).

(Lu-82)2: Lucchese R.R., Raseev G. and Mc Koy V.
Phys. Rev. A, **25**, 2572 (1982).

(Ma-69) : Massey H. S. W. and Burhop E. H. S.
Electronic and Ionic Impact Phenomena, Clarendon Press, Oxford, 1969.

(Ma-76) : Marr G.V. and West J.B.
Atomic Data Tables, **18,** 497 (1976).

(Mo-32) : Moller C.
Ann. Phys. **14**, 531 (1932).

(Mo-64) : Motz J. W., Olsen H. and Koch H. W.
Rev. Mod. Phys. **36**, 881 (1964).

(Mo-65) : Mott N. F. and Massey H. S. W.
The Theory of Atomic Collisions, Oxford University Press, London,1965.

(Od-75) : Oda N.
Radiat. Res. **64**, 80 (1975).

(Ol-72) : Olivero J.J., Stagat R.W. and Green A.E.S.
J. Geophys. Res. **77**, 4797, (1972).

(Om-63) : O'Malley T. F.
Phys. Rev. **130**, 1020 (1963).

(Op-72) : Opal C. B., Beaty E. C. and Peterson W. K.
Atomic Data Tables, **4**, 209 (1972).

(Pa-81) : Padial V., Csanak G., Mc Koy B.V. and Langhoff P.W.
Phys. Rev. A, **23**, 218 (1981).

(Ph-85) : Phelps A. V. and Pitchford L. C.
Phys. Rev. A, **31**, 2392 (1985).

(Pl-77) : Plummer E.W., Gustaffon T., Gudat W. and Eastman D.E.
Phys. Rev. A, **15**, 2339 (1977).

(Po-76) : Porter H. S., Jackman C. H. and Green A. E. S.
J. Chem. Phys., **65**, 154 (1976).

(Ra-65) : Rapp D. and Englander-Golden P.
J. Chem. Phys., **43**, 1464 (1965).

(Ra-74) : Rabalais J., Debies T.P., Berkosky J.L., Huang J.T. and Ellison F.O.
J. Chem. Phys. **61**, 516 (1974).

(Re-79) : Rescigno T.N., Gerwer A., Mc Koy B.V. and Langhoff P.W.
Chem. Phys. Lett., **66**, 116 (1979).

(Re-80) : Register D. F., Nishimura H. and Trajmar S.
J. Phys. B: Atom. Mol. Phys. **13**, 1651 (1980).

(Sa-70) : Salop A. and Nakano H. H.
Phys. Rev. A, **2**, 127 (1970).

(Se-53) Segre E
Experimental Nuclear Physics, Wiley and Sons, (1953)

(Se-83) Senger B
Thesis, Université Louis Pasteur, Strasbourg (1983)

(Se-88) Ségur P and Bordage M C
Internal report (1988)

(Sh-78) Shyn T W , Sharp W E and Carignan G R
Phys Rev A, **17**, 1855 (1978)

(Sh-80) Shyn T W and Carignan G R
Phys Rev A, **22**, 923 (1980)

(Si-69) Siegbahn K , Nordling C , Johansson G , Hedman J , Heden P F , Hamrin K , Gelius U , Bergmark T , Werne L O , Manne R et Baer Y
ESCA Applied to free molecules
Ed North Holland Publ Comp Amsterdam (1969)

(Si-78) Siegel J , Dill D and Dehmer J L
Phys Rev A **17**, 2106 (1978)

(Sl-88) Slinker S P , Taylor R D and Ali A W
J Appl Phys **63**, 1 (1988)

(Sr-76) Srivastava S K , Chutjan A and Trajmar S
J Chem Phys , **64**, 1340 (1976)

(St-67) Stolarski R S , Dulock V A , Watson C E and Green A E S
J Geophys Res **72**, 3933 (1967)

(St-87) Stefani G
Invited paper, XV ICPEAC, Brighton, 1987

(Sw-80) Swanson J R , Dill D R and Dehmer J L
J Phys B At Mol Phys **13**, L231 (1980)

(Ta-78) Tan K H , Brion C E , Van Der Leeuw P E and Van Der Wiel M J
Chem Phys , **29**, 299 (1978)

(Te-78) Terrissol M
Thesis n° 839, UPS Toulouse, 1978

(Tr-71) Trajmar S , Cartwright D C and Williams W
Phys Rev A, **4**, 1482 (1971)

(Tr-82) Truesdale C M , Southworth S , Kobrin P H , Lindle D W , Thornton G and Shirley D A
J Chem Phys , **76**, 860 (1982)

(Ve-73) Veigele W M J
Atomic Data Tables, **5**, 51 (1973)

(Wa-67) Watson C E , Dulock V A , Stolarski R S and Green A E S
J Geophys Res **72**, 3961 (1967)

(Wa-70) Walker D W
Adv Phys **20**, 257 (1970)

(Wa-78) Wakiya K
J Phys B Atom Mol Phys **11**, 3913 (1978)

(Wa-87) Walters H R J
Invited paper, XV ICPEAC, Brighton, (1987)

(We-74) Wedde T and Strand T G
J Phys B At Mol Phys **7**, 1091 (1974)

(Wi-76) Wight G R , Van Der Wiel M J and Brion C E
J Phys B At Mol Phys **9**, 675 (1976)

(Wi-79) Willams G R J and Langhoff P W
Chem Phys Lett , **60**, 201 (1979)

(Ye 85) Yeh J J and Lindau I
Atomic Data and Nuclear Data Tables, **32**, 1 (1985)

(Yo 85) Younger S M and Mark T D
Electron Impact Ionization, Mark and Dunn ed Springer-Verlag, Wien,1985

BACKGROUND INFORMATION

(Session III)

ATOMIC AND MOLECULAR DATA ACTIVITIES FOR FUSION IN THE IAEA NUCLEAR DATA SECTION

J.J. SMITH
Atomic and Molecular Data Unit,
Nuclear Data Section,
International Atomic Energy Agency,
Vienna

Abstract

This paper provides some brief background information on the efforts devoted to the generation, compilation and evaluation of atomic and molecular data which are required for an understanding and interpretation of fusion plasmas. In particular, the role of the atomic and molecular data center network in the international co-ordination of activities will be emphasised. A summary of the data needs for fusion is given and recent references which define the current extent of the atomic and molecular data base are provided.

1. INTRODUCTION

There is a need for a wide vareity of atomic and molecular (A+M) data required for the understanding, interpretation and design of fusion reactors. There is some overlap in data needs in the areas for fusion and radiotherapy, and the purpose of this paper is to briefly describe the international efforts which continue to be devoted towards the generation, compilation and evaluation of A+M data for fusion.

In both fields there are common needs for basic collisional cross sections for electron and heavy particle reactions and for detailed knowledge of the energy levels and emmission spectra of atoms, molecules and ions. Excluding complex systems (polymers, DNA, proteins) the species of interest are somewhat similar. For instance, oxygen based molecules (O_2, CO_2, H_2O ...) and hydrocarbons can be present in the edge plasma region in fusion devices. There seems to be a more urgent requirement in radiotherapy for differential cross sections than in fusion research and the energy range of interest, especially for particle induced therapy, can greatly exceed the energies relevant in fusion applications. It is obviously important that attention is paid to the basic experimental and theoretical research and compilation studies performed primarily for fusion.

Considering the tokamak configuration, the scope of requirements includes data defining the structure and emission spectra of the plasma atoms, ions and molecules, collision processes between these plasma constituents and also surface interactions of atoms, ions and molecules with the material of the containment vessel. Atomic and molecular data is required for plasma modelling studies, diagnostics, neutral beam production and penetration, impurity control and other physics and engineering studies. There are several extensive reviews [1-4] which provide information on the A+M requirements for fusion and describe the status of the relevant experimental and theoretical A+M physics areas.

The A+M Data Unit of the IAEA was created to coordinate international activities in the provision of A+M data for fusion. In the next section the programme of the Unit is described. As the major overlap of interest with radiotherapy involves collisional data, the atomic species pertinent to fusion are defined with the collision processes and energy ranges of interest. Finally, references are provided to the existing recommended and evaluated data base and to recent review articles defining the status of the A+M collision data.

2. ATOMIC AND MOLECULAR DATA ACTIVITIES

The A+M Data Unit was established within the Nuclear Data Section as part of the IAEA programme in 1977. The establishment of this unit derives from the recommendations of an IAEA advisory group meeting held in Culham [1] in 1976, which reviewed the requirements for A+M data for fusion research. It was concluded from this meeting that the needs for the development of fusion research and technology are so large that no single community could produce and diseminate the required data alone. It was agreed to create a network of data centres which would cooperate in the collection, evaluation and dissemination of A+M data and that the A+M Data Unit of the IAEA should coordinate these activities.

The programme of the A+M Data Unit of the IAEA can be described as,

1) To establish and maintain an international data library of evaluated/ recommended numerical data for fusion.

2) Devise ways of dissemination of evaluated numerical data to fusion laboratories and other users in machine readable form.

3) To co-ordinate and support international data compilation and evaluation efforts in developing the numerical data base, particularly within the A+M data centre network.

4) Establish and maintain an international bibliographic data base for fusion.

5) Promote and support production of A+M data for fusion.

6) Establish and maintain strong correlation between the atomic physics and fusion communities in the field of A+M data for fusion.

The national data centres co-operating within the data centre network are,

1) Controlled-Fusion Atomic Data Centre, Oak Ridge National Laboratory, USA

2) Atomic Spectroscopy and Atomic Transition Probabilities Data Centres, National Bureau of Standards, USA

3) Atomic and Molecular Data Centre, The Queen's University of Belfast, UK

4) Institute of Plasma Physics, Nagoya University, Nagoya, Japan

5) Japanese Atomic Energy Research Institute (JAERI), Tokai-mura, Japan

6) Kurchatov Institute of Atomic Energy, Moscow, USSR

7) GAPHYOR, Laboratoire de Physique des Gaz et des Plasmas, Orsay-Cedex, France.

8) Joint Institute for Laboratory Astrophysics (JILA), A+M Data Information Centre, Boulder, USA.

9) Institute of Atomic Energy, Beijing, Peoples Republic of China.

The following comments provide some details on the recent progress and ongoing activities involving the A+M Data Unit.

In the last few years there has been a significant improvement in the available data base of recommended and evaluated data. The choice of a data structure and system which could be used for storage and dissemmination of such data was addressed at a recent IAEA meeting [5]. A labelled atomic data interface system (ALADDIN) [6], which has the capability and flexibility of accomodating data covering the structure and spectra of atoms, ions and molecules and collisional and surface interaction data was accepted as the means of international exchange. The ALADDIN system provides a standard structure for storing diverse types of data. The physical parameters definning a particular process are held as labels and these can be used as keys to interactively search and retreive data. All types of numerical data formats including data tables and analytic fitting functions can be represented. Comments and references can also be included. As the computer software is written in Fortran 77, the system can be run on a range of computers from PC's to a Cray. As the ALADDIN system does not have any application constraints built into it, the system may also be used in other data processing applications. It should be considered when compiling and exchanging A+M or nuclear data for radiotherapy.

Several approaches have been employed to stimulate the production and compilation of A+M data for fusion. Co-ordinated research programmes (CRP's) can be initiated by the Nuclear Data Section to focus international efforts in areas where there is an essential need for data and the status of the experimental and theoretical base is lacking. The number of ongoing CRP's at any time is however limited by the Agency's ability to offer funds. A recent CRP has been initiated devoted to need for low energy (plasma temperature $\lesssim$ 500 eV) A+M collision data for plasma edge studies. A review of a completed CRP on Collision data for diagnostics of magnetic fusion plasmas has recently been published [7]. For projects of a smaller scope, the data centre network is employed to compile and evaluate data, where necessary expertise outside of the network is also used. An example of this type of project is the recent recommended data compilation for collisions involving iron ions [8]. Currently underway is an internationally co-ordinated study to review and generate data for collisions involving carbon and oxygen atoms and ions with the primary plasma species and impurities [9]. Emphasis is being placed on providing data for as complete a range of collision processes as possible, including electron recombination processes and state selective electron capture for which there are presently no recommended data available.

Since 1977, the A+M Data Unit has regularly published the International Bulletin on Atomic and Molecular Data for Fusion [10], which provides an index to references to journal, report and book articles which contain data covering the fields of structure and spectra, collisions and surface interactions. The input for the bulltin is taken from references supplied through the data centre network and is supplemented by additional references added by the A+M Data Unit. The bulletin is published bi-annually and is distributed free of charge to over 1000 recipients world-wide. The IAEA has also published two comprehensive indexes to the literature on A+M collision data relevant to fusion research (CIAMDA Series) [11].

3. A+M COLLISION DATA REQUIREMENTS FOR FUSION

The diversity of the species and processes for which collision data are required is reflected in the temperature and density ranges and the structural material base of current and planned fusion reactors. In the hot central plasma core, low and medium-Z impurities are completely stripped and only heavy impurities have attached electrons. The number of A+M processes affecting the radial distribution of the ionized species is relatively small, primarily electron-ion impact ionization and radiative and dielectronic recombination. This can be contrasted with the situation in the cool plasma edge, where atoms and ions are in low stages of ionization and molecular neutral and ionized species are present in significant quantities. Data are needed for molecular collision processes with electrons, basic plasma components and impurities. The generation and use of neutral beams for heating and application of active and passive diagnostics widens the scope of requirements. The most important collision processes for which data are needed in fusion research are, for electron impact:

- excitation, ionization, and dielectronic, radiative and dissociative recombination

and for heavy particle interactions involving atoms, molecules and ions:

- charge exchange, exciation, ionization, dissociation and interchange reactions.

where for molecular excitation electronic, vibrational and rotational transistions are included and for ionization and charge exchange collisions where a molecule/molecular ion is involved, both a knowledge of the cross sections for the dissociative and non-dissociative channels is required. Other important processes which change the ionization and excited state distributions in the plasma are transfer ionization and transfer excitation.

The primary species of interest for fusion are:

- H, D, and T and their molecules (form the basic plasma components)
- He (from the fusion of D-T)
- Be, B, C, Al, Si, Ti, Cr, Fe, Ni, Mo, Ta and W (main structural materials)
- O, O_2, H_2O, CO, CO_2 C_mH_n (impurities released from the containment vessel by collisional, chemical or other processes)

- Li, Ne, Ar, Ga, Kr and Xe (diagnostics and/or also used in cooling of the plasma edge)

- Na, Mg and Cs (beam production)

It is also useful to have data for other elements not included in the above list as scaling rules can be applied for some reactions, in appropriate conditions, to provide estimates for required species.

For electron collisions the maximum energy range of interest is of the order of 100 keV. For heavy particles, excluding helium, the upper energy range can be taken as 500 keV. For collisions of helium atoms and ions the upper limit of the collision energy can be set at 3.5 MeV.

As well as total cross sections and reaction rate coefficients, normally generated by taking cross section averaged over some maxwellian particle distributions, angular and energy single differential cross sections are required for modelling and diagnostics.

4. DATA AVAILABILITY

In the last few years there have been increasing efforts devoted to providing the fusion community with handbooks and reports of recommended and evaluated A+M data. In the majority of these, analytic fits are provided to the best available experimental and theoretical data for ease of incorporation of the data into computer codes. Two recent reviews of the available A+M data base for diagnostics of fusion plasmas [7] and for plasma edge studies [12] provide extensive references to the existing recommended and evaluated data. In the following references will be provided to only the most comprehensive data compendia which have been published or are in preparation.

For collisions of carbon and oxygen ions with electrons, H, H_2 and He, cross sections and reaction rate coefficients are given [13] for electron-impact excitation and ionization and for heavy particle reactions total charge exchange and ionization. Also near to completion from the Oak Ridge Atomic Data Centre is a compendia of recommended data covering collisions of H, H_2, He and Li atoms and ions with atoms and molecules [14]. Recommended data on atomic collisions involving iron and its ions [8] contains electron impact excitation and ionization reaction rate coefficients and charge transfer cross sections of iron ions with H, H_2 and He. For electron impact ionisation there are a series of recommendations for cross sections and reaction rate coefficients from the Queen's University of Belfast group, which have been published or are in preparation. These are for atoms and ions for hydrogen through oxygen [15], fluorine through nickel [16], and for high-Z species of interest in fusion research [17]. Also underway is a critical survey of electron impact ionization data for selected molecules [18]. This survey covers both dissociative and non-dissociative ionization processes.

For electron impact excitation of atomic ions, as well as the recommended data for C, O and Fe ions mentioned above, a very recent compilation gives recommended values for the excitation reaction rate coefficients of helium atoms and helium-like ions [19], and evaluated compilations covering other species are contained in Refs. [20] and [21].

A comprehensive data compendia covering all inelastic reactions involving electrons, atomic and molecular hydrogen and atomic helium has recently been published [22]. As well as cross sections and reaction rate coefficients, the survey also contains brief descriptions of the energetics for each reaction. For some reactions involving hydrocarbons a compilation of data can be found in Ref. [23].

REFERENCES

[1] Atomic and molecular data for controlled fusion, Invited papers at IAEA Advisory Meeting, Vienna, 1976, Phys. Rep. 37, (2) (1978)

[2] DRAWIN, H.W., KATSONIS, K. (Eds.), Atomic and molecular data for fusion, Phys. Scr. 23 (1981).

[3] McDOWELL, M.R.C., FERENDECI, A.M. (Eds.), Atomic and Molecular Processes in Controlled Thermonuclear Fusion, Plenum Press, New York, (1980)

[4] JOACHAIN, C.J., POST, D.E. (Eds.), Atomic and Molecular Physics of Controlled Thermonuclear Fusion, Plenum Press, New York, (1983)

[5] IAEA Consultants' Meeting on 'Atomic and Molecular Data Base and Fusion Applications Interface' held in Vienna, 9-11 May 1988, Summary report in preparation

[6] HULSE, R.A., 'A labelled Atomic Data Interface for Fusion Applications', presented at [5]

[7] JANEV, R.K., KATSONIS, K., Nucl. Fusion 27 (1987) 1493

[8] BOTTCHER, C. et al., Nucl. Fusion Special Supplement 1987

[9] IAEA Specialists' Meeting on 'Carbon and Oxygen Data for Fusion Plasma Research', held in Vienna, 12-13 May 1988, Summary report in preparation

[10] SMITH, J.J. (Ed.), International Bulletin on Atomic and Molecular Data for Fusion (IAEA, Vienna)

[11] CIAMDA-80 and CIAMDA-87, Indexes to the Literature on Atomic and Molecular Collision Data Relevant to Fusion Research, (IAEA, Vienna). (CIAMDA-80 covers period from 1950-1980, CIAMDA-87 continues from CIAMDA-80 coverage to mid 1986).

[12] JANEV, R.K., HARRISON, M.F.A., DRAWIN, H.W., Atomic and Molecular Data Base for Fusion Plasma Edge Studies, to be submitted for publication.

[13] PHANEUF, R.A., JANEV, R.K., PINDZOLA, M.S., Collisions of Carbon and Oxygen Ions with Electrons, H, H_2 and He. Report ORNL-6090, Vol. 5 (Oak Ridge, 1987)

[14] BARNETT, C.F., Atomic Data for Fusion: Collisions of H, H_2, He and Li Atoms with Atoms and Molecules. ORNL-6086, Vol. 1 (Oak Ridge Natl. Lab., Oak Ridge, 1988)

[15] BELL, K.L., GILBODY, H.B., et al. J. Phys. Chem. Ref. Data 12 (1983) 891 (Recommended Data on Electron Impact Ionization of Light Atoms and Ions. From H to O)

[16] LENNON, M.A., BELL, K.L., et al. "Recommended Cross Sections and Rates for Electron Ionization of Atoms and Ions: Fluorine to Nickel", UKAEA Report CLM-270, (Culham, 1986) (to be published in J. Phys. Chem. Ref. Data)

[17] LENNON, M.A., BELL, K.L., et al. "Recommended Cross Sections and Rates for Electron Ionization of Atoms and Ions for high-Z Species: Cu-U" (to be published in J. Phys. Chem. Ref. Data)

[18] LENNON, M.A., et al. Critical Survey of Electron Impact Ionisation Data for Selected Molecules. Report of Dept. Computer Sci., Queen's Univ. Belfast (1987)

[19] KATO, T., NAKAZAKI, S., "Recommended Data for Excitation Rate *Coefficients of Helium Atoms and Helium-like Ions by Electron Impact*", Report IPPJ-AM-58 (1988) (Inst. Plasma Phys., Nagoya Univ., 1988)

[20] GALLAGHER, J.W., PRADHAN, A.K., An Evaluated Compilation of Data for Electron Impact Excitation of Atomic Ions. JILA Data Center Report No. 30 (1985) (Joint Inst. for Lab. Astrophys., Boulder, Colorado, 1985)

[21] AGGARVAL, K., BERRINGTON, K., et al. Report on Recommended Data for Electron Impact Excitation (Atomic Data Workshop, Daresbury, 1985)

[22] JANEV, R.K., et al. "Elementary Processes in Hydrogen-Helium Plasmas" (Springer-Verlag, Springer Series on Atoms and Plasmas, Vol. 4, Berlin-Heidelberg-New York, 1987)

[23] EHRHARDT, A.B., LANGER, W.D., Collision Processes of Hydrocarbons in Hydrogen Plasmas. Report PPPL-2477 (1987) (Plasma Phys. Lab., Princeton Univ., 1987)

LIST OF PARTICIPANTS

AUSTRIA

P. Bauer
Universität Linz
Abteilung Atom und Kernphysik
A-4040 Linz

N. Getoff
Institute für Theoretische Chemie u. Strahlenchemie der Universität Wien
Währinger Strasse 38
A-1090 Wien

T. Märk
Institut für Ionenphysik der Universität Innsbruck
Technikerstrasse 25
A-6020 Innsbruck

H. Paul
Johannes Kepler Universität
A-4040 Linz

BELGIUM

P. Pihet
Service de Radiotherapie
Cliniques Universitaires St-Luc
UCL St-Luc 4753
Avenue Hippocrate 10
B-1200 Brussels

A. Wambersie
Université Catholique de Louvain
Faculté de Médicine
Unité de Radiotherapie et de Radioprotection
Avenue Hippocrate 54
B-1200 Brussels

CZECHOSLOVAKIA

Z. Herman
J. Heyrovsky Institute of Physical Chemistry and Electrochemistry
Dolejskova 3
182 28 Prague 8

GERMANY, FED. REP.

G. Kraft
Gesellschaft für Schwerionenforschung
Planckstrasse 1
D-6100 Darmstadt

P. Olko
Institut für Medizin
Kernforschungsanlage Jülich GmbH
Postfach 1913
D-5170 Jülich

H.G. Paretzke (Co-Chairman)
GSF Inst. for Radiation Protection
Ingolstädter Landstrasse 1
D-8042 Neuherberg bei München

E. Waibel
Physikalish-Technische
Bundesanstalt
Bundesallee 100, P.O. Box 3345
D-3300 Braunschweig

JAPAN

Y. Hatano
Department of Chemistry
Tokyo Institute of Technology
12-1 O-Okayama, 2-Chome
Meguro-ku, Tokyo 152

U.S.S.R.

I.G. Kaplan
L. Ya. Karpov Institute of
Physical Chemistry
Ul. Obukha 10
107120 Moscow, B-120

U.S.A.

M. Inokuti (Chairman)
Environmental Research Division
Argonne National Laboratory
Bldg. 203
9700 South Cass Avenue
Argonne, Illinois 60439

L.H. Toburen
Battelle Northwest Laboratory
P.O. Box 999, P8-47
Richland, Washington 99352

S. Trajmar
MS-183-601
Jet Propulsion Laboratory
California Institute of Technology
4800 Oak Grove Drive
Pasadena, California 91109

YUGOSLAVIA

D. Srdoc
Rudjer Boskovic Institute
P.O. Box 1016
YU-41001 Zagreb
tel. (041)424 239 (direct) (or (041)425 809)
telex 21383 irb yu zq

INTERNATIONAL ATOMIC ENERGY AGENCY

RILS: Y. Skoropad
RIPC: D. Gandarias Cruz
K. Okamoto (Scientific Secretary)
J.J. Schmidt
J.J. Smith